ADVANCING MEMBRANE CHROMATOGRAPHY PROCESSES FOR THE PURIFICATION OF THERAPEUTIC VIRUSES

ADVANCING MEMBRANE CHROMATOGRAPHY PROCESSES FOR THE PURIFICATION OF THERAPEUTIC VIRUSES

By KARINA KAWKA, B.Eng.

A Thesis Submitted to the School of Graduate Studies in Partial Fulfilment of the Requirements of the Degree Doctor of Philosophy

McMaster University DOCTOR OF PHILOSOPHY (2021) Hamilton, Ontario (Chemical Engineering)

TITLE: Advancing membrane chromatography processes for the purification of therapeutic viruses

AUTHOR: Karina Kawka, B.Eng. (Federal University of Paraná, Brazil)

CO-SUPERVISORS: Professor Dr. David R. Latulippe and Professor Dr. Raja Ghosh

PAGES: xxx, 239

Lay Abstract

Certain viruses can be used for human benefit and there are now more than a dozen approved therapies worldwide that use a virus as the main therapeutic agent or as the vector to instruct the patient's cells to fight cancer and other diseases. The area keeps growing as thousands of other clinical trials continue to be conducted. One of the main challenges that can inhibit patient access to these ground-breaking new options is related to difficulties in producing and purifying enough virus. This study tackles the virus purification challenge by applying and improving membrane chromatography (MC), a promising and scalable technique where virus and impurities are separated based on how differently they interact with a membrane. Different experimental and modelling and simulation tools were applied to optimize MC and other directly-related steps of the production process. The findings in this study can contribute to the development of new virus-based therapeutics so they can reach patients in safe, effective, and affordable ways.

Abstract

Viruses have emerged as a new class of biotherapeutics used as vectors in gene and cell therapies, vaccines, and as oncolytic agents in novel cancer immunotherapies. While these new and potentially curative new therapies bring great promise for patients, the large-scale purification of viruses is hampered by complicated unit operations, poor overall yields, and high costs. Membrane chromatography (MC) is one of the most ideal options for the removal of host-cell impurities in virus manufacturing. Centred on developing and improving MC processes for virus purification, this thesis focuses on different aspects of downstream processes that are directly related to MC.

It describes the development of the first hydrophobic interaction MC process for the purification of vesicular stomatitis virus as a scalable method for the removal of host-cell protein and DNA. It also describes the development of MC for adenovirus purification, and how device design and membrane type impact the resolution; here, the novel laterally-fed membrane chromatography (LFMC) was proven to provide higher resolution than conventional MC devices, and allowed for the first direct comparison between the most popularly used membranes in virus manufacturing – Sartobind Q and Mustang Q. Beyond MC, this thesis also addresses how other downstream unit operations contribute to the final purity. Through an integrated study optimizing clarification, DNA digestion, and MC simultaneously, significant improvement in adenovirus purity was obtained. Finally, the collection of experimental results was used to model complete adenovirus production processes using BioSolve Process and determine the cost-of-goods (COG) of

manufacturing for clinical applications. Through simulations of multiple scenarios, critical process parameters were identified and can serve as a guide for future process development decisions. It is anticipated that the contributions herein described will help address critically outstanding questions related to virus purification and thus enable the development of the economical processes for various manufacturing scales.

Acknowledgements

It is incredible how so many pieces had to come together to culminate in this thesis which not only includes the findings of more than four years of research but contains influences from people who have been inspiring me throughout my life. I am thankful to God for surrounding me with people who are the best at what they do and for allowing my story to have been unfolding the way it has been.

Education has the power to transform. And I am fortunate to have my parents, Irene and Domingos, in my life. You have been my constant supporters and always did everything to give me what was essential. You have done it with mastery, and I will forever be grateful. This thesis, as well as any of my achievements, are not only mine; they are ours. I am also thankful to have my little brother, Matheus, with whom I am lucky to always share a beautiful and special connection. May your entrepreneurial spirit continue guiding you to great achievements and I will always be here for you.

I am extremely thankful to my co-advisor, Dr David Latulippe, for being a fantastic mentor and a friend. I am proud to be a part of your team, and of the discoveries and ideas we had together, and I will carry your example as a person, a leader, and a teacher for life. I am also grateful to my second co-advisor, Dr Raja Ghosh, whose work I admired well before meeting him in person when I was an undergraduate student and first got interested in bioseparations. Now I am honoured to have worked alongside a role model who has provided me with brilliant mentorship. To both my co-advisors, thank you for

allowing me to develop a research project so well aligned with my aspirations and I look forward to when the future brings us opportunities to develop new collaborations together.

I would also like to express my gratitude to Dr Boyang Zhang and Dr Jonathan Bramson, members of my supervisory committee, for first having agreed to be part of this journey and for all the great advice they have given me. I am thankful for having had the opportunity to collaborate with Dr Maria Medina, Dr Brian Lichty, and Dr Prashant Mhaskar, who played essential roles on my project and whose multidisciplinary backgrounds have greatly enriched my experience. I would also like to thank Dr Yuki Abe and Nicholas Graham from Biopharm Services for the great collaboration that resulted in Chapter 6 of this thesis.

I am grateful to Dr Shabnam Shoaebargh and Dr Pedram Madadkar for having laid the groundwork on virus purification and membrane chromatography, respectively, from which I built my research. I am extremely happy to have met and worked alongside an amazing team of co-op and summer students. Noelle, Nicole, Anushree, Eric, Shayna, Alexandra, and Sarah, thank you for your help on different projects, for your motivation, support, and for everything each one of you have taught me. I am also grateful to have directly worked with Evan, Uma, Ian, Ana, and Claire who are brilliant fellow graduate students.

I would like to thank the technical staff who are essential in allowing research and science to be conducted. From the McMaster Immunology Research Centre, I would like to thank Natasha and Uma, who have taught me a great deal about virus analytical assays.

From the Department of Chemical Engineering, I would like to express my gratitude to Michelle, Linda, Kristina, Paul, Doug, and Tim for their efficiency and care.

I would also like to recognize the people who have been supporting me throughout my life, and that were essential to my career. Thank you, uncle Mariano and aunt Ivone for inspiring me to pursue education since I was little, and for the extraordinary gesture of having me at your house during my time in Curitiba for my undergrad. Thank you also to uncle João, aunt Marisia, Claudia, and Renata who are my special supporters and role models in my family. To all my family, my most sincere thank you for the encouragement, prayers, care, and love you have always gifted me with.

I am grateful to all my incredible friends who were a part of this adventure. You all bring meaning to my life and thank you for letting me be a part of yours. Special thanks to my childhood friends, Daniel, Letícia, and Franciele, to my friends from university, Rafaele, Bianka, and Elisiane, and to the great friends I met in Canada, Nina, Felipe, Daniela, Ryan, Evan, Patrick, Abhishek, Melissa, Blake, and Reza, who I am always happy to share conversations and special moments with. I am especially thankful to my boyfriend, Indranil, who has been a strong encourager throughout this journey and has always motivated me to give my best. I feel lucky to have such a like-minded advocate to count on.

I could not possibly have mentioned all the important people who are a part of this accomplishment in the few lines above. So, I would like to express my sincere appreciation to all my extended family, all members of the Latulippe and Ghosh Labs, all my teachers

from the Rocha Pombo and Garcez schools who have prepared me for life, my Professors at the Federal University of Paraná and graduate students who I had the pleasure to learn from, all my friends from Arapongas and Curitiba, the people I met through church in Canada, especially Fr Todd, Sr Mary, and Karen. Finally, I want to thank the people from Gleba Orle, the community of farmers I was born in and where I learned the meaning of dedication and hard work, which has shaped who I am today.

Agradecimentos

(This is a Portuguese translation of the acknowledgements)

É incrível como tantas peças tiveram que se juntar para culminar nesta tese, que não apenas contém descobertas de mais de quatro anos de pesquisa, mas também contém influências de pessoas que vêm me inspirando durante minha vida. Eu agradeço a Deus por me cercar de pessoas que são as melhores naquilo que fazem e por permitir que minha história se desenrole deste jeito.

A educação tem o poder de transformar. E eu sou afortunada por ter meus pais, Irene e Domingos, em minha vida. Vocês são meu suporte e sempre fizeram de tudo para me dar o que era essencial. Vocês fizeram tudo com maestria e eu serei eternamente grata. Esta tese, assim como quaisquer outras conquistas, não são apenas minhas; são nossas. Também sou grata pelo meu irmão mais novo, Matheus, com quem eu tenho a sorte de sempre ter compartilhado uma conexão muito bonita e especial. Que o seu espírito

empreendedor continue te guiando rumo à grandes conquistas e eu sempre estarei aqui por você.

Eu sou extremamente agradecida ao meu co-orientador, Dr. David Latulippe, por ser um fantástico mentor e um amigo. Tenho orgulho de fazer parte do seu time e das descobertas e ideias que desenvolvemos juntos. Levarei seu exemplo como pessoa, líder, e professor por toda a vida. Também sou grata ao meu segundo co-orientador, Dr. Raja Ghosh, cujo trabalho eu já admirava muito antes de conhecê-lo pessoalmente, quando eu ainda estava na graduação e comecei a me interessar por biosseparações. Agora eu tenho a honra de ter trabalhado ao junto de um ícone que me orientou de forma briliante. A ambos meus co-orientadores, obrigada por me deixar trabalhar em um projeto de pesquisa tão alinhado com minhas aspirações e eu não vejo a hora do futuro nos trazer oportunidades para trabalhar em novas colaborações juntos.

Eu gostaria de expressar minha gratidão ao Dr. Boyang Zhang e ao Dr. Jonathan Bramson, membros do meu comitê de supervisão de doutorado, por terem concordado em ser parte desta jornada e por todos os ótimos conselhos que recebi deles. Sou grata por ter tido a oportunidade de colaborar com Drª. Maria Medina, Dr. Brian Lichty e Dr. Prashant Mhaskar, que tiveram papéis essenciais no meu projeto e cujas formações multidisciplinares contribuíram para enriquecer minha experiência. Também gostaria de agradecer a Drª. Yuki Abe e o Nicholas Graham da Biopharm Services, pela ótima colaboração que resultou no capítulo 6 desta tese.

Gostaria ainda de agradecer a Drª. Shabnam Shoaebargh e o Dr. Pedram Madadkar por terem alicerçado o trabalho em purificação de vírus e cromatografia de membrana, sobre o qual eu construí minha pesquisa. Sou extremamente feliz por ter conhecido e trabalhado junto de um time incrível de estagiários: Noelle, Nicole, Anushree, Eric, Shayna, Alexandra e Sarah, obrigada pela sua ajuda com diversos projetos, pela sua motivação, suporte e por tudo o que cada um de vocês me ensinou. Também sou grata por ter trabalhado diretamente com Evan, Uma, Ian, Ana e Claire que são colegas brilhantes.

Eu gostaria de agradecer à equipe técnica que é essencial para a execução das pesquisas. Do Centro de Imunologia da McMaster, eu gostaria de agradecer a Natasha e Uma, que me ensinaram muito sobre análise de vírus, e do Departamento de Engenharia Química, eu gostaria de expressar meus agradecimentos a Michelle, Linda, Kristina, Paul, Doug e Tim pela eficiência e cuidado que eles têm para conosco.

Também quero reconhecer as pessoas que têm me dado suporte ao longo da minha vida e que foram essenciais para minha carreira. Obrigada, Tio Mariano e Tia Ivone por terem me inspirado a estudar desde que eu era pequena, e pelo gesto extraordinário de me receber na sua casa durante o tempo que fiquei em Curitiba para a faculdade. Obrigada, Tio João, Tia Marisia, Claudia e Renata, por serem meus especiais torcedores e exemplos na família. A toda à minha família, meu mais sincero obrigada por todo encorajamento, pelas orações, carinho e amor que vocês sempre me deram de presente.

Sou grata a todos os meu incríveis amigos que foram parte desta aventura. Vocês todos trazem sentido à minha vida e obrigada por me deixarem fazer parte das suas.

Agradecimentos especiais aos amigos de infância, Daniel, Letícia e Franciele, às minhas amigas da faculdade, Rafaele, Bianka e Elisiane, e a todos os grandes amigos que eu conheci no Canadá: Nina, Felipe, Daniela, Ryan, Evan, Patrick, Abhishek, Melissa, Blake e Reza, com quem é sempre bom compatilhar conversas e momentos especiais. Sou especialmente grata ao meu namorado, Indranil, que tem sido um forte encorajador durante esta jornada e sempre me motiva a dar o meu melhor.

Eu não poderia ter mencionado todas as pessoas que são parte desta conquista nas poucas linhas acima. Portanto, eu gostaria de expressar minha sincera apreciação à toda a minha família, todos os membros dos grupos de pesquisas dos professores Latulippe e Ghosh, todos os meus professores da Escola Rocha Pombo e do Colégio Garcez, que me prepararam para a vida, meus professores da Universidade Federal do Paraná e pós graduandos com quem tive o prazer de aprender, todos os meus amigos de Arapongas e de Curitiba, as pessoas que conheci na igreja no Canadá, especialmente o Pe. Todd, a Irmã Mary e a Karen. Finalmente, eu quero agradecer a todos da Gleba Orle, a comunidade de agricultores onde eu nasci e onde eu aprendi o significado de dedicação e trabalho árduo, que moldou quem eu sou hoje.

Table of Contents

Lay Abstract iii
Abstract iv
Acknowledgements vi
Table of Contents xiii
List of Figures xviii
List of Tables xxiv
Declaration of Academic Achievement xxviii
1. Introduction 2
1.1. Therapeutic viruses 2
1.1.1. Gene therapy 2
1.1.2. Oncolytic viruses 4
1.1.3. Cell therapy 6
1.2. Virus manufacturing processes 8
1.2.1. Upstream processing 8
1.2.2. Downstream processing 10
1.2.2.1. Harvest and clarification 11
1.2.2.2. Removal of host-cell protein and DNA 12
1.2.2.3. Concentration and sterile filtration 14
1.3. Objectives and thesis outline 15
1.4. References 18
2. Purification of therapeutic adenoviruses using laterally-fed membrane chromatography 25
2.1. Abstract 25
2.2. Introduction 26
2.3. Materials and Methods 29
2.3.1. Virus production and sample preparation 29
2.3.2. Membrane chromatography devices 30
2.3.3. CFD simulations 33
2.3.4. Chromatography experiments 33

2.3.5. Analytical methods 35
2.4. Results and Discussion 37
2.4.1. CFD simulation and tracer experiments 37
2.4.2. Purification of adenoviruses via gradient elution strategy 39
2.4.3. Purification of adenoviruses via stepwise elution strategy 46
2.5. Conclusions 50
2.6. Acknowledgements 52
2.7. References 52
3. A direct comparison of anion exchange membranes for virus purification applications 56
3.1. Abstract 56
3.2. Introduction 57
3.3. Materials and Methods 61
3.3.1. Membrane chromatography devices 61
3.3.2. Chromatography experiments 62
3.4. Results and discussion 65
3.4.1. Hydrodynamic characterization of Mustang Q and Sartobind Q LFMC devices 65
3.4.2. Chromatography runs with single-component feed materials: DNA, protein and purified adenovirus standard 68
3.4.3. Chromatography runs with cell lysates containing adenovirus 73
3.5. Conclusions 78
3.6. Acknowledgements 80
3.7. References 80
4. Integrated development of enzymatic DNA digestion and membrane chromatography processes for the purification of therapeutic adenoviruses 84
4.1. Abstract 84
4.2. Introduction 85
4.3. Materials and Methods 91
4.3.1. Adenovirus production 91
4.3.2. Cell disruption and enzymatic DNA digestion 91
4.3.3. High-throughput screening of membrane chromatography process 92

4.3.4. Laterally-fed membrane chromatography (LFMC) process 94
4.3.5. Analytical methods 96
4.4. Results and Discussion 99
4.4.1. Optimization of the DNA digestion step that precedes the membrane chromatography 99
4.4.2. High-throughput screening of membrane chromatography performance using Sartobind Q 96-well filter plate 107
4.4.3. Laterally-fed membrane chromatography purification of adenovirus sample 110
4.5. Conclusions 115
4.6. Acknowledgements 116
4.7. References 117
5. Purification of vesicular stomatitis virus (VSV) using hydrophobic interaction membrane chromatography 122
5.1. Abstract 122
5.2. Introduction 123
5.3. Materials and Methods 125
5.3.1. Preparation of VSV cultures 125
5.3.2. Chromatography runs 126
5.3.3. Analysis of virus infectivity, total protein, and DNA in chromatography fractions 128
5.4. Results and Discussion 130
5.4.1. Effect of buffer pH and ammonium sulfate concentration on the purification of VSV using hydrophobic interaction membrane chromatography 130
5.4.2. Scale-up of hydrophobic interaction membrane chromatography runs for VSV purification 134
5.5. Conclusions 137
5.6. Acknowledgements 138
5.7. References 138
6. Economic analysis of adenovirus manufacturing processes for gene therapy clinical applications 143
6.1. Abstract 143
6.2. Introduction 144

6.3. Model construction and analysis 149
6.4. Results and Discussion 156
6.4.1. Estimated COG for MA and resin base scenarios assuming dosages of 1×10^{12} and 1×10^{13} PT/dose 156
6.4.2. COG breakdown for MA base scenarios assuming dosages of 1×10^{12} and 1×10^{13} PT/dose 157
6.4.3. Effect of target throughput on COG for MA and resin scenarios assuming dosages of 1×10^{12} and 1×10^{13} PT/dose 161
6.4.4. Sensitivity analysis for the MA and Resin models to produce 2,000 doses/year for dosages of 1×10^{12} or 1×10^{13} PT/dose 162
6.4.5 Quantifying savings from using Denarase as an alternative to Benzonase for DNA digestion in MA and resin scenarios targeting the production of 2,000 doses/year assuming a dosage of 1×10^{13} PT/dose 166
6.5. Conclusions 167
6.6. Acknowledgements 168
6.7. References 168
7. Conclusions and recommendations for future work 175
7.1. Conclusions 175
7.2. Recommendations for future work 181
7.2.1. Development of novel membrane adsorber materials and ligands for virus purification 181
7.2.2. High-throughput screening platforms 184
7.2.3. Advanced analytical tools for the characterization of product and impurities 185
7.2.3.1. Virus analytical tools 185
7.2.3.2. Accurate detection of host-cell DNA concentration and fragment sizes using qPCR methods 185
7.3. References 190
Appendix A: Optimization and scale-up of laterally-fed membrane chromatography (LFMC) for adenovirus purification using the Sartobind Q membrane 193
A1. Optimization of membrane loading conditions for adenovirus purification using 1 mL LFMC devices 193
A2. Scale-up of adenovirus purification using 1 mL LFMC devices 196
A3. Scale-up of adenovirus purification using 10 mL LFMC devices 199

Appendix B: Supplemental information for Chapter 4 203
Appendix C: Supplemental information for Chapter 5 210
C1. VSV purification using Sartobind Q anion-exchange membrane chromatography 210
C2. VSV purification Sartobind Sulfated Cellulose (SC) pseudo-affinity membrane chromatography 211
Appendix D: A critical evaluation of the fifty percent tissue culture infective dose ($TCID_{50}$) assay for the titration of vesicular stomatitis virus (VSV) 213
D1. Abstract 213
D2. Introduction 214
D3. Materials and methods 216
D4. Results and Discussion 219
D4.1. Frequency of occurrence of skipped wells during titration of VSV using $TCID_{50}$ 219
D4.2. Effect of skipped wells on the calculated recovery of VSV chromatography runs 220
D4.3. Variability of the $TCID_{50}$ and plaque assays for VSV titration 221
D5. Conclusions 223
D6. Acknowledgements 223
D7. References 224
Appendix E: Supplemental Information for Chapter 6 225
Appendix F: Standard operating procedure (SOP) for determining DNA fragment size via qPCR assay 235

List of Figures

Figure 2.1. Details of the construction of the LFMC device and scanning electron microscopy (SEM) of the Sartobind Q membrane. A: external view of the LFMC device, B: blow-out diagram showing the different parts of the device, C: cross-section side view of the device. D: SEM image of the top/bottom surface of the Sartobind Q membrane, E: SEM image of the cross-section of the Sartobind Q membrane. 32

Figure 2.2. Residence time distribution comparing the LFMC device (solid line) and the radial flow device (dashed line) results for the CFD simulations (top panel) and acetone tracer experiments (bottom panel), at a 5 mL/min flow rate. 39

Figure 2.3. UV absorbance (280 nm) and conductivity profiles for the duplicate chromatography runs using the LFMC device and gradient elution strategy. The dashed-dotted line indicates the percentage of buffer B with values given on the secondary y-axis. 41

Figure 2.4. Chromatograms for adenovirus purification via gradient elution strategy with the LFMC device (top panel) and the radial flow device (bottom panel). The dashed line indicates the percentage of buffer B (which correlates to the NaCl concentration), the dotted line indicates the conductivity, and the solid line indicates the UV absorbance at 280 nm (refer to the secondary axis). The 3D bar charts display the amount of adenovirus (front solid red bars), total protein (middle hatched yellow bars), and total DNA (back striped green bars) within each fraction as a percentage of the amount in the injected feed sample. 44

Figure 2.5. Chromatograms for adenovirus purification via stepwise elution strategy with the LFMC device (top panel) and the radial device (bottom panel). The dashed line indicates the percentage of buffer B (which correlates to the sodium chloride concentration), the dotted line indicates the conductivity, and the solid line indicates the UV absorbance at 280 nm (refer to the secondary axis). The 3D bar charts display the amount of adenovirus (front red bars), total protein (middle yellow bars), and total DNA (back green bars) within each fraction as a percentage of the amount in the injected feed sample. 49

Figure 3.1. External view of the LFMC device; B: Blow-out diagram showing the different parts of the LFMC device; C: Top view SEM image (1500× magnification) of the Mustang Q membrane; D: Top view SEM image (1500× magnification) of the Sartobind Q membrane. 62

Figure 3.2. Acetone tracer experiment with a Mustang Q and a Sartobind Q LFMC devices. Tests were performed using equilibration buffer containing 10 mM HEPES, 4% sucrose,

360 mM NaCl, pH 7.4, and by injecting a pulse of 100 µL of a 2% acetone solution in equilibration buffer. 68

Figure 3.3. UV absorbance (280 nm) and conductivity profiles for BSA protein standard (1.6 mg/mL) chromatography runs using the Mustang Q (panel A) and Sartobind Q (panel D) LFMC devices. UV absorbance (255 nm) and conductivity profiles for pre-purified adenovirus standard (6.7×10^9 IFU/mL) chromatography runs using the Mustang Q (panel B) and Sartobind Q (panel E) LFMC devices. UV absorbance (260 nm) and conductivity profiles for 1 Kb Plus DNA ladder (10 µg/mL) chromatography runs using the Mustang Q (panel C) and Sartobind Q (panel F) LFMC devices. 72

Figure 3.4. UV absorbance (255 nm) profiles and amounts of virus (solid red bars) and DNA (striped green bars) in each fraction of adenovirus cell lysate chromatography runs using the Mustang Q (A) and Sartobind Q (B) LFMC devices. The first peaks indicate the flow-through elution of unbound biomolecules (primarily host-cell protein); the second peaks indicate the elution adenovirus followed by DNA. The same gradient elution profiles shown in Figure 3.3 were applied in this experiment; conductivity and buffer B profiles were omitted for simplicity. Expanded view of UV absorbance (255 nm) in elution volume range (12 to 20 mL) for Mustang Q and Sartobind Q (C). 77

Figure 4.1. Schematic of the process steps used to produce the adenovirus feed samples used for the membrane chromatography studies described in Sections 4.3.3 and 4.3.4....96

Figure 4.2. Comparison of Process Sequence and enzyme type on levels of DNA (two top panels) and adenovirus (two bottom panels). Panels A and B correspond to Process Sequence #1: freeze-thaw → DNA digestion → centrifugation; panels C and D correspond to Process Sequence #2: freeze-thaw → centrifugation → DNA digestion. The same enzyme concentration (10 U/mL) was used for the different enzymes, and the same incubation condition (1 hour at 37°C) was used for all samples. The two vertical bars for each condition correspond to the duplicate tests that were performed, and the error bars correspond to the standard deviation from either the duplicate measurements of amount of DNA, or the triplicate measurements of adenovirus levels. 101

Figure 4.3. Agarose gel electrophoresis (using 1% agarose in TAE buffer, run for 45 min at 100 V, stained with Red Safe, and imaged using via a ChemiDoc™ system) of samples from Process Sequence #1 (centrifugation followed by DNA digestion) and Process Sequence #2 (DNA digestion followed by centrifugation). Samples were prepared using the DNA Clean and Concentrator™ kit (Zymo Research) to isolate DNA. The linear DNA ladder in the first and last lanes was the '1 kb Plus DNA ladder' (Invitrogen). 103

Figure 4.4. Comparison of the effect of DNA digestion time (at 37 °C) and enzyme concentration on final DNA concentration (panels A and C) and virus infectivity (panels B and D panels) in samples prepared according to Process Sequence #2. Panels A and B

correspond to Benzonase, and panels C and D correspond to Denarase. The average value obtained from the duplicate experiments is shown for each condition. Error bars correspond to the standard deviation from either the duplicate measurements of DNA concentration (i.e., n = 4) or the triplicate measurements of virus concentration (i.e., n = 6). The raw average virus and DNA concentrations in each sample in this figure are shown in Table B1 in Appendix B. 107

Figure 4.5. Chromatogram for adenovirus purification run using an LFMC device containing 1 mL of Sartobind Q membrane, a linear gradient elution step (initiated at 12 mL mark to ramp from 18% Buffer B to 50% Buffer B over 10 mL), and a feed sample that was pre-processed according to Process Sequence #2, with the DNA digestion step conducted using 10 U/mL of Denarase and 4 hours of incubation at 37 °C. The solid line indicates the UV absorbance profile at 255 nm (mAU), while the dashed line indicates the solution conductivity profile (mS/cm). The 3D bar chart indicates the amount of virus (front pink solid bars), protein (middle yellow striped bars), and DNA (back green dotted bars) within the middle of each of the 15 fractions, as a percentage of the amount in the injected feed sample. 113

Figure 5.1. Calibration curves used to estimate the DNA concentration in fractions of chromatography runs using the Picogreen assay, using lambda-DNA standard diluted in buffer containing different concentrations of AS as indicated by the different markers. Each point represents the average of duplicate tests. Dashed lines along each set of points correspond to their linear regression model. 129

Figure 5.2. Results of chromatography Run #4 (top panel, using pH 7.4) and Run #2 (bottom panel, using pH 8.0). Solid lines and short-dashed lines correspond to the UV absorbance (mAU) at 280 nm and 260 nm, respectively; long-dashed lines correspond to the buffer conductivity (mS/cm); front solid pink bars correspond to the amount of virus ($\times 10^7$ $TCID_{50}$) in each fraction; middle yellow bars correspond to the amount of protein ($\times 10^2$ μg) in each fraction; and green dotted bars correspond to the amount of DNA (ng) in each fraction. The bars are aligned with the centre of each fraction. 132

Figure 5.3. Results of HIMC for Run #11. Solid lines and short-dashed lines correspond to the UV absorbance (mAU) at 280 nm and 260 nm, respectively; long-dashed lines correspond to the buffer conductivity (mS/cm); front solid pink bars correspond to virus recovery respective to the amount in the feed; middle yellow bars correspond to residual protein; and green dotted bars correspond to residual DNA in each fraction. The bars are aligned with the centre of each fraction. 135

Figure 6.1. Process sequence and unit operation details used in the model. The MA base scenario used membranes in the two chromatography steps, while the resin base scenario used resins in the two chromatography steps. 152

Figure 6.2. Overall COG breakdown for the MA scenario targeting the production of 2,000 doses/year and dosages of 1×10^{12} PT/dose (left) and 1×10^{13} PT/dose (right). 159

Figure 6.3. COG per-batch breakdown for MA scenario assuming a dose size of 1×10^{12} PT/dose (top panel) and 1×10^{13} PT/dose (bottom panel) and a production target of 2,000 doses/year. The per-batch COG is presented for all the unit operations (listed at bottom) based on the five major different cost types (i.e., capital, materials, consumables, labour, and other) indicated by the different colors. 160

Figure 6.4. COG/dose as a function of target throughput (doses produced per year) for MA (solid lines) and resin (dashed lines) scenarios assuming a dosage of 1×10^{12} PT/dose (black lines) and 1×10^{13} PT/dose (gray lines).....161

Figure 6.5. Tornado plots showing the sensitivity analysis results for the MA scenario assuming 1×10^{12} PT/dose (top left panel); the MA scenario assuming 1×10^{13} PT/dose (top right panel); the resin scenario assuming 1×10^{12} PT/dose (bottom left panel); and the resin scenario assuming 1×10^{13} PT/dose (bottom right panel). All scenarios use a production target of 2,000 doses/year. The black bars indicate the percent change in COG in the worst-case scenario in relation to the base scenario, and the light gray bars indicate the percent change in COG in the best-case scenario in relation to the base scenario, as shown in Table 6.3.....165

Figure 7.1. qPCR amplification data using for standard human genomic DNA targeting regions that generate 254 bp amplicons (panel A) and 123 bp amplicons (panel B), displaying the fluorescence normalized reporter value (ΔRn) as a function of cycle number. C: qPCR assay calibration curves with standard human genomic DNA, for the 123 bp (grey triangles) and 254 bp (black circles) amplicons. Dashed lines represent the respective linear regression for each of the calibration curves. 188

Figure A1. Chromatograms for adenovirus purification via stepwise elution strategy with a 1 mL LFMC device for membrane loading buffer containing 0.40 M NaCl (top panel), 0.36 M NaCl (middle panel), and 0.30 M NaCl (bottom panel). The dashed line indicates the conductivity, and the solid line indicates the UV absorbance at 280 nm (refer to the secondary axis). The 3D bar charts display the amount of adenovirus (front red bars), total protein (middle yellow bars), and total DNA (back green bars) within each fraction as a percentage of the amount in the 1 mL injected feed sample..... 195

Figure A2. Chromatograms for adenovirus purification via stepwise elution strategy with a 1 mL LFMC device using feed lysates prepared from 50 mL of cell culture (top panel), 100 mL of culture (middle panel), and 200 mL of culture (bottom panel). The dashed line indicates the conductivity, and the solid line indicates the UV absorbance at 280 nm (refer to the secondary axis). The 3D bar charts display the amount of adenovirus (front red bars), total protein (middle yellow bars), and total DNA (back green bars) within each fraction as a percentage of the amount in the feed sample. 198

Figure A3. LFMC devices containing 1 mL (left) and 10 mL (right) of the Sartobind Q membrane. 199

Figure A4. Chromatograms for adenovirus purification via stepwise elution strategy with a 10 mL LFMC device using feed lysates prepared from 200 mL of cell culture (top panel), 400 mL of culture (middle panel), and 800 mL of culture (bottom panel). The dashed line indicates the conductivity, and the solid line indicates the UV absorbance at 280 nm (refer to the secondary axis). The 3D bar charts display the amount of adenovirus (front red bars), total protein (middle yellow bars), and total DNA (back green bars) within each fraction as a percentage of the amount in the feed sample. 201

Figure B1. DOE conditions for DNA digestion time and enzyme concentration for the different studies described. All DNA digestion experiments were conducted at 37°C. Circles: all DNA digestion conditions tested with Benzonase and Denarase. Diamonds: DNA digestion conditions with Denarase used before MC in a 96-well format. Square: DNA digestion conditions with Denarase used before LFMC runs. 203

Figure C1. Chromatogram for VSV purification via gradient elution with a 1 mL Sartobind Q LFMC device. The dashed line indicates the conductivity, and the solid line indicates the UV absorbance at 280 nm (refer to the secondary axis). The 3D bar charts display the amount of VSV (front red bars), total protein (middle yellow bars), and total DNA (back green bars) within each fraction as a percentage of the amount in the 1 mL injected feed sample. 211

Figure C2. Chromatograms for VSV purification via gradient elution with a 1 mL Sartobind Sulfated Cellulose LFMC device. A: using HEPES-based buffers and B: using citric acid-based buffers. The dashed line indicates the conductivity, and the solid line indicates the UV absorbance at 280 nm (refer to the secondary axis). The 3D bar charts display the amount of VSV (front red bars), total protein (middle yellow bars), and total DNA (back green bars) within each fraction as a percentage of the amount in the 1 mL injected feed sample. 212

Figure D1. A typical well plate used in the titration of VSV expression GFP through the $TCID_{50}$ assay. Each row corresponds to repeats of a given serial dilution. The first 6 columns are repeats of sample 1 and the last 6 rows are repeats of sample 2. Black wells correspond to infected cells (i.e. presenting green fluorescence) and light grey wells correspond to uninfected cells. Skipped wells are indicated, where there is a negative response between two positive responses. 216

Figure D2. Frequency of skipped wells in historical raw data from an analysis of images of 96-well plates for VSV titration via the $TCID_{50}$ assay. 219

Figure D3. VSV titer estimated by $TCID_{50}$ (30 independent replicates, using three different approaches for interpreting skipped wells), and by plaque assay (6 independent replicates). 222

Figure E1. COG per batch breakdown for MA scenario assuming a dosage of 1×10^{12} PT/dose (top panel) and 1×10^{13} PT/dose (bottom panel) targeting the production of 2000 doses/year. The COG per batch is presented for all the unit operations indicated at the bottom for the different types of costs (capital, materials, consumables, labour, and other), indicated by the different colours..... 225

List of Tables

Table 1.1. List of approved gene therapies based on viral vectors. 3

Table 1.2. List of approved oncolytic viruses for cancer treatment. 5

Table 1.3. Approved cell therapies that are based on viral vectors. 7

Table 2.1. Comparison of the total sample volume effect on recovery of virus, total protein, and total DNA for the LFMC and radial flow devices using a gradient elution strategy; the percentages are reported with respect to the amounts of each component in the feed sample. The error bars are based on propagation of error analysis from triplicate testing (for virus titer) or duplicate testing (for protein and DNA) on duplicate runs. 46

Table 2.2. Comparison of the total sample volume effect on recovery of virus, total protein, and total DNA for the LFMC and radial flow devices using a stepwise elution strategy; the percentages are reported with respect to the amounts of each component in the feed sample. The error bars are based on propagation of error analysis from triplicate testing (for virus titer) or duplicate testing (for protein and DNA) on duplicate runs. 49

Table 3.1. A review of the various bioprocessing applications in which the relative performance of Mustang Q and Sartobind Q membranes was studied. MV: membrane volume.....60

Table 3.2. Average pressure as a function of flow rate for the NGC chromatography system without an LFMC device attached, and for three LFMC devices containing Mustang Q and three LFMC devices containing Sartobind Q. The displayed averages and standard deviation were calculated over the pressures obtained with the three devices with each membrane. 66

Table 3.3. Summary of peak characteristics (retention time, width at half height, and asymmetry) obtained with the Mustang Q and Sartobind Q membranes. Avg: averages of runs 1 and 2. 71

Table 3.4. Comparison of the composition of selected fractions from adenovirus cell lysate chromatography runs using Mustang Q and Sartobind Q LFMC devices 78

Table 4.1. Composition of feed and elute (i.e., E1 fraction) samples for the MC runs performed with the 96-well filter plate. The two rows for each set of DNA digestion conditions correspond to the duplicate MC experiments that were performed, each using independently digested lysates. The amount of DNA and protein were normalized and expressed on a per virus dose basis using 10^{10} IFU per dose. Process Sequence #2 was used to generate the feed samples. Refer to Table A3 for the corresponding concentrations of

virus (IFU/mL), DNA (ng/mL), and protein (μg/mL) that were used to generate the results shown. BDL: below detection limit. 110

Table 4.2. Comparison of process conditions and results for adenovirus purification via LFMC from this study and our previous study. The amounts of adenovirus and DNA after LFMC correspond to the amounts found in the 2 mL fractions containing most of the virus eluted during each run. † Based on 10^{10} IFU/dose. 115

Table 5.1. Total amount of virus, protein and DNA in the flow-through and elution fractions of HIMC runs investigating the effects of buffer pH and AS concentration in the binding buffer. Virus amounts and their standard deviations were calculated using the Spearman Karber method, protein and DNA averages and standard deviations were calculated based on duplicate measurements of each sample. BDL: below the detection limit. 134

Table 5.2. Total amount of virus, protein and DNA in the different fractions of HIMC scale-up runs where 300 mL of VSV lysate was purified using a 3 mL Sartobind Phenyl Nano device. Virus amounts and their standard deviations were calculated using the Spearman Karber method, protein and DNA averages and standard deviations were calculated based on duplicate measurements of each sample. BDL: below the detection limit. 136

Table 6.1. General input parameters for the base-scenarios created on BioSolve. 149

Table 6.2. Model unit operation input parameters and quality control tests. 153

Table 6.3. Parameters used for sensitivity analysis of MA and resin scenarios to produce 2,000 doses/year for dose sizes of 1×10^{12} PT/dose or 1×10^{13} PT/dose. 155

Table 6.4. COG per dose estimated to produce 2,000 or 20,000 doses/year using the MA or resin models for dose sizes of 1×10^{12} PT/dose or 1×10^{13} PT/dose. 157

Table 6.5. COG for the MA and resin scenarios, assuming a dosage of 1×10^{13} PT/dose and a production target of 2,000 doses/year. 167

Table 7.1. Affinity chromatography mechanisms used for virus purification. Adapted from elsewhere.[12] 182

Table 7.2. DNA amounts based on the qPCR assay for the determination of fragment size. Lysates were digested for 4 h and 24 h either in the absence of enzyme (Controls) or with 10 U/mL of Benzonase. DNA amounts for each amplicon were calculated based on calibration curves generated using standard human genomic DNA. 189

Table A1. Percent amount of virus, protein and DNA with respect to the amount in the feed in the different fractions of LFMC runs using different NaCl concentrations in the loading buffer. BDL: below the detection limit. 196

Table A2. Percent amount of virus, protein and DNA with respect to the amount in the feed in the different fractions of LFMC runs using different amounts of feed lysate. BDL: below the detection limit. 198

Table A3. Percent amount of virus, protein and DNA with respect to the amount in the feed in the different fractions of 10 mL LFMC runs using different amounts of feed lysate. BDL: below the detection limit. 202

Table B1. Results of the 3^2 full factorial DOE using Benzonase and Denarase. 203

Table B2. Results of the linear models for Log (DNA concentration) and Log (Virus concentration) as functions of the transformed parameters enzyme concentration (E, calculated using Equation B1) and digestion time (D, calculated using Equation B2) for Denarase and Benzonase using R (RStudio). 207

Table B3. Virus, DNA, and protein concentrations in the fractions obtained during MC using a 96-well format. Results are shown for each set of duplicate MC runs under each DNA digestion condition. 209

Table D1. Calculated titers in the feed and elution samples from run 5 (Chapter 5), according to the 3 different approaches for treating the skipped wells in the titration of VSV via the $TCID_{50}$ assay. 221

Table E1. Technical specifications and costs of commercially available membrane chromatography devices 226

Table E2. COG per batch breakdown for MA scenario assuming dosage of 1×10^{12} PT/dose 228

Table E3. COG per batch breakdown for MA scenario assuming dosage of 1×10^{13} PT/dose 229

Table E4. COG per batch breakdown for resin scenario assuming dosage of 1×10^{12} PT/dose 230

Table E5. COG per batch breakdown for resin scenario assuming dosage of 1×10^{13} PT/dose 231

Table E6. COG/dose as a function of target throughput for MA and resin scenarios at the dosages of 1×10^{12} and 1×10^{13} PT/dose 232

Table E7. Sensitivity analysis results for the MA scenario targeting the production of 2,000 doses/year 233

Table E8. Sensitivity analysis results for the resin scenario targeting the production of 2,000 doses/year..... 234

Declaration of Academic Achievement

This Ph.D. thesis has been prepared as a sandwich thesis containing work previously published or prepared for publishing, as listed below.

- Chapter 2: K. Kawka, P. Madadkar, U. Umatheva, S. Shoaebargh, M. F. C. Medina, B. D. Lichty, R. Ghosh, D. R. Latulippe. Purification of therapeutic adenoviruses using laterally-fed membrane chromatography. Journal of Membrane Science, 579 (2019) 351–358. https://doi.org/10.1016/j.memsci.2019.02.056
- Chapter 3: K. Kawka, A. N. Wilton, E. J. Redmond, M. F. C. Medina, B. D. Lichty, R. Ghosh, D. R. Latulippe. A direct comparison of anion exchange membranes adsorbers for virus purification applications. Prepared for Journal submission.
- Chapter 4: K. Kawka, A. N. Wilton, P. Madadkar, M. F. C. Medina, B. D. Lichty, R. Ghosh, D. R. Latulippe. Integrated development of enzymatic DNA digestion and membrane chromatography processes for the purification of therapeutic adenoviruses. Separation and Purification Technology, 254 (2021) 117503. https://doi.org/10.1016/j.seppur.2020.117503
- Chapter 5: K. Kawka, A. N. Wilton, M. F. C. Medina, R. Ghosh, D. R. Latulippe. Purification of vesicular stomatitis virus (VSV) using hydrophobic interaction membrane chromatography. Prepared for Journal submission.

- Chapter 6: K. Kawka, S. Earle, I. Gough, N. Graham, Y. Abe, M. F. C. Medina, D. R. Latulippe. Economic analysis of adenovirus manufacturing processes for gene therapy applications. Prepared for Journal submission.
- Appendix D: K. Kawka, E. Wright, A. N. Wilton, M. F. C. Medina, D. R. Latulippe. A critical evaluation of the fifty percent tissue culture infective dose ($TCID_{50}$) assay for the titration of vesicular stomatitis virus (VSV). Prepared for Journal submission.

The work was performed under the supervision of Professors Dr. David R. Latulippe and Dr. Raja Ghosh. Most of the work was conducted, planned, interpreted, and written by me, Karina Kawka, but it would not have been possible without the significant contributions of my colleagues that have supported the work the following ways:

- Pedram Madadkar fabricated the laterally-fed membrane chromatography (LFMC) devices used in Chapter 2 and assisted with part of the experiments. He also provided inputs on LFMC experimental planning for Chapters 2 and 4.
- Umatheny Umatheva modelled the LFMC fluidics and ran the computational fluid dynamics simulations for Chapter 2.
- Shabnam Shoaebargh provided training and assisted with the adenovirus lysate preparation and LFMC runs for Chapter 2.
- A. Noelle Wilton assisted with LFMC device fabrication, experiment planning, execution, and writing of Chapter 3. She also provided experimental support to Chapter 4 and conducted part of chromatography runs and analysis for Chapter 5.

- Eric Redmond assisted with data analysis and with creating figures for Chapter 3.
- Shayna Earle assisted with the construction of the BioSolve models and running simulations and analysis for Chapter 6. She also assisted with planning the qPCR method for DNA analysis described in Chapter 7 and Appendix F.
- Ian Gough assisted with the construction of the BioSolve model for Chapter 6 and has created Table E1 in Appendix E with technical and pricing details of commercially available membrane adsorber modules.
- Evan Wright assisted with performing the experiments for evaluating the $TCID_{50}$ assay for virus titration presented in Appendix D.

Chapter 1

Introduction

1. Introduction

1.1. Therapeutic viruses

1.1.1. Gene therapy

Gene therapy has been rising as a promising new alternative with the potential to cure certain diseases, often after a single dose of the therapeutic agent.[1] In the treatment of genetic diseases, this is achieved by correcting non-working genes by silencing, replacing, or delivering a new functional gene to the patient's cells.[2] To do so, different types of vectors can be used, with viruses being the most widely used option.[3] Oncolytic viruses that are able to treat cancer by selectively infecting and killing tumour cells, are often classified as being within the gene therapy space.[4] However, due to their particularities, they will be discussed in more detail in their dedicated Section 1.1.2 of this thesis.

To date, there are at least 5 gene therapy products based on viral vectors approved around the world as shown in Table 1.1. All these drugs act by delivering a functional gene to the patients' cells, as a replacement of deficient genes such as Glybera, Luxturna, and Zolgensma, or encoding for proteins that targets and suppress tumours in the case of Gendicine and Rexin-G. The major downside of these new therapies is their price, that can surpass millions of dollars per dose and is mostly driven by development and manufacturing costs.[5] Table 1.1 features two of the most expensive drugs in the world: Glybera, which has been withdrawn from markets in Europe due to the high price and low demand, and Zolgensma, that holds the title of most-expensive drug in the world.[2]

Table 1.1. List of approved gene therapies based on viral vectors.

Drug	Indication	Gene delivered	Viral vector	First approval (location/ year)	Price per dose	Ref.
Gendicine (SiBiono Gene Tech Co.)	Head and neck squamous cell carcinoma	p53 (tumour-suppressing)	Adeno-virus	China/2003	-	[6–8]
Rexin-G (Epeius Biotech)	Soft tissue sarcoma, osteosarcoma, pancreatic cancer	Cytocidal cyclin G1	Retro-virus	Philippines/ 2007	-	[1,9]
Glybera * (Uniqure)	Lipoprotein lipase (LPL) deficiency	Lipoprotein lipase	AAV-1	Europe/2012	$ 1,200,000	[2,10]
Luxturna (Spark Therapeutics)	Leber's congenital amaurosis or retinitis pigmentosa	Retinoid isomero-hydrolase RPE65	AAV-2	USA/2017	$ 425,000	[2]
Zolgensma (Novartis)	Spinal muscular atrophy (SMA)	Survival motor neuron SMN1	AAV-9	USA and Japan/2019	$ 2,100,000	[2]

* Glybera was withdrawn from markets due to high cost and low demand.[2] AAV: adeno-associated virus.

In addition to approved therapies, there are currently more than 3,700 gene therapy clinical trials underway around the world.[1] Adenoviruses, adeno-associated viruses (AAV), and lentiviruses are currently the most popular types of vectors used in these clinical trials.[2] Other types of vectors of clinical interest include rhabdoviruses, vaccinia viruses, poxviruses, herpes viruses, Newcastle disease viruses, and others.[3,11] All these vectors present unique properties that make them ideal for different therapeutic applications.

Adenoviruses are currently the leading type of vector in gene therapy clinical trials,[2] and will be the one of the main subjects of this thesis. They are non-enveloped, icosahedral viruses with a DNA-based genome,[12] and of sizes in the range of 70 to 90 nm.[13]

Their advantages include the fact that they are well characterized, safe, relatively easy to produce, and have the ability to infect different types of cells.[12] Adenoviruses are therefore used in a variety of applications not only for gene delivery in gene therapies and as oncolytic viruses, but also as vaccine vectors.[12] They became essential during the current COVID-19 pandemic, as a few of the most important vaccines being administered globally, including the AstraZeneca-Oxford, Janssen, and Sputnik V vaccines, are based on different serotypes of adenoviral vectors.[14]

1.1.2. Oncolytic viruses

Often classified within the realm of gene therapy, oncolytic viruses are a particular class of viruses capable of selectively infecting and killing cancer cells while triggering immune responses against the tumour.[4] Their mechanisms of action are broader and more complex than that of viral vectors delivering tumour-supressing genes as discussed above for Gendicine and Rexin-G. Oncolytic viruses are replication-competent viruses able to cause an infection at the tumour site, triggering local inflammation.[15] One of the proposed explanations for their mechanism of action in conjunction with the immune system involve the fact that when cancer cells are killed by the virus, tumour antigens are released and the immune system starts to recognize and clear tumours systematically at different sites of the body, even those far away from the original virus injection site.[15] Recent studies have also been exploring intravenous administration of oncolytic viruses.[11]

Table 1.2 lists the different oncolytic viruses already approved for use in humans around the world. Imlygic was the first oncolytic virus approved by the FDA in 2015 and

is currently available for use in the treatment of melanoma.[1] Adenoviruses, important vectors in gene therapy and vaccines in general as discussed in Section 1.1.1, are also used for oncolytic applications; a drug based on a recombinant oncolytic adenovirus called Oncorine is approved in China for the treatment of head and neck cancer since 2005.[11] There is currently an extensive list of phase I-III clinical trials being conducted using oncolytic adenoviruses for the treatment of melanoma, prostate, bladder, brain, and pancreatic cancers, melanoma and other solid tumours.[16]

Table 1.2. List of approved oncolytic viruses for cancer treatment.

Drug	Indication	Viral vector	First approval (location/ year)	Price per dose	Ref.
Rigvir (Rigvir Group)	Melanoma	Picornavirus	Latvia/2004	-	[11]
Oncorine (Shanghai Sunway Biothec)	Head and neck cancer	Adenovirus-5	China/2005	-	[11]
T-VEC/Imlygic (Amgen)	Melanoma	Herpes simplex virus	USA/2015	$ 65,000	[11,17]
Delytact (Daiichi Sankyo/University of Tokyo's Institute of Medical Science)	Malignant glioma	Herpes simplex virus	Japan/2021	-	[18]

Rhabdoviruses are a promising type of virus for oncolytic applications and are one of the main focuses of this thesis. They are enveloped, bullet-shaped, single-stranded RNA viruses with sizes ranging from 100-180 nm in length and 45-100 nm in width.[19] Vesicular stomatitis virus (VSV) and Maraba virus (developed in Canada) are the most studied types of rhabdoviruses for oncolytic applications.[11] They present a series of advantages including the lack of pre-existing immunity against these viruses in humans and the relative ease to

modify and cultivate them.[20] Clinical trials are currently underway with oncolytic Maraba virus for the treatment of solid tumours and non-small cell lung cancer, and a variety of therapeutic approaches using Maraba and VSV are currently in development.[20]

Now, with the rise of combination therapies where oncolytic viruses are used in conjunction with traditional chemotherapeutics, antibodies,[16,21] and even cell therapies,[22,23] there are endless possibilities to be explored for applying oncolytic adenoviruses, rhabdoviruses, and other promising vectors in the search for novel alternatives for cancer patients.

1.1.3. Cell therapy

Viral vectors are also an essential tool in novel cell therapies such as those based on chimeric antigen receptor T cells (CAR-T cell therapies) in use for cancer treatment that has been presenting ground-breaking outcomes with complete cancer remission reported in many cases.[24] In this new type of therapy, viruses are used to transfer the CAR's genetic information into T cells harvested from a patient ex vivo; next, the CAR-T cells that now programmed to fight the cancer are propagated in the lab and transfused back into the patient.[24] In the last years, a considerable number of new cell therapies have been developed and approved worldwide as shown in Table 1.3. Yescarta, Kymriah, Zynteglo, Tecartus, Breyanzi, Abecma, and Relma-cel are all CAR-T cell therapies, while Strimvelis and Libmeldy are used to modify CD34+ cells from the patient ex vivo by adding genes to human adenosine deaminase (ADA) and arylsulphatase A enzymes respectively, and Skysona is used to deliver a gene for the adrenoleukodystrophy protein to immature bone

marrow cells of the patient.[25] So far, lentiviruses and retroviruses are the preferred type of vector for ex-vivo modifications in novel cell therapies, as indicated in Table 1.3. However, AAV vectors have recently been gaining more interest for this application.[26] With all these advances in the field of gene and cell therapy and oncolytic viruses and the approval of at least 5 therapies during the course of this year alone, it is undeniable that viruses will continue to have an essential role in the development of powerful and potentially curative future new therapies.

Table 1.3. Approved cell therapies that are based on viral vectors.

Drug	Indication	Viral vector	First approval (location/ year)	Price per dose	Ref.
Yescarta (Kite Pharma)	Large B cell lymphoma	Gamma retrovirus	USA/2017	$ 373,000	[27,28]
Kymriah (Novartis)	Acute lymphoblastic leukemia (ALL)	Lentivirus	USA/2017	$ 475,000	[27,28]
Zynteglo (Bluebird bio)	Beta-thalassemia	Lentivirus	Europe/2019	$ 1,800,000	[9,29]
Tecartus (Kite Pharma)	Mantle cell lymphoma (MCL)	Gamma retrovirus	USA/2020	$ 373,000	[28]
Breyanzi (Brystol Myers Squibb)	Large B cell lymphoma (LBCL)	Lentivirus	USA/2021	$ 410,300	[30–32]
Abecma (Brystol Myers Squibb, Bluebird bio)	Multiple myeloma	Lentivirus	USA/2021	$ 419,500	[31,33]
Relma-cel (JW Therapeutics)	Large B cell lymphoma	Lentivirus	China/2021	-	[34]
Strimvelis (GlaxoSmith-Kline)	Severe combined immuno-deficiency	Retrovirus	Europe/2016	€ 594,000	[9,17]

Libmeldy (Orchard Therapeutics)	Metachromatic leukodystrophy (MLD)	Lentivirus	Europe/2020	-	[25]
Skysona (Bluebird bio)	Cerebral adrenoleuko-dystrophy	Lentivirus	Europe/2021	-	[25]

1.2. Virus manufacturing processes

1.2.1. Upstream processing

With all the promise of novel virus-based therapeutics, there is a still a need for the development of advanced manufacturing processes that can keep up with the demand in the years to come.[35] Effective manufacturing processes also contribute to decreasing the high cost of new virus-based therapeutics. Bioprocesses typically involve multiple unit operations that are separated into upstream (operations that lead to and include the production of the target product, typically in a bioreactor), and downstream (operations that involve product recovery and purification).

Viruses for therapeutic applications are typically produced in adherent or suspension mammalian cell cultures.[36] Adherent cells are cultivated in cell stacks, roller bottles or fixed-bed bioreactors, while suspension cells use stirred-tank or wave bioreactors.[37] Processes using suspension cell cultures are usually easier to scale-up, while adherent cultures need to be scaled-out.[36] However, recent advances and the development of modern fixed-bed bioreactors such as the Pall iCELLis bioreactor are bringing promising new solutions for adherent cultures.[38] In either culture system, once the desired cell density

is achieved, cells are transfected or infected to generate the viral particles. To generate lentiviruses and AAV, transient transfection is typically used, where cells are transfected with vector and helper/packaging plasmids.[36] Another option is to use stable producer cell lines that were transduced to express the different parts of the vector of interest upon induction.[36] Finally, direct infection of cells can be done using a small amount of vector as it is often done with adenoviruses[36] and rhabdoviruses,[39] both subjects of this thesis.

Advances in the development of cell culture media have also been contributing to improved upstream processes. Serum is a traditional additive in cell culture media, however due to being a component from animal source, it presents variability, risk for contamination, and can difficult the purification process to be completely removed.[40] Therefore, serum-free media is typically preferred for biomanufacturing applications and now, there exists a variety of composition-defined cell culture media especially optimized for different types of cells.[40] The type of media can significantly affect cell growth; as an example, the specific growth rate of HEK-293 cells (a popular cell line for the production of adenoviruses, AAV and other vectors) can be more than doubled depending on the cell culture media used.[41] This translates in increased cell densities in short periods of time and the potential for better viral vector yields.

With the above-mentioned advances and the rise of new technologies, such as viral sensitizers – a class of small molecules able to increase the replication of viruses in cells by as high as 1000-fold,[42] upstream processes are currently at a critical point, with promise to continue increasing virus productivity. Downstream processes, on the other hand, are

still considered the bottleneck of virus manufacturing[43] and need significant development in order to keep up with the progress and yields arising from upstream processes, as it will be discussed on the next section.

1.2.2. Downstream processing

The role of downstream processes in virus manufacturing is to remove process-related impurities, includes components from the host-cell (debris, protein, DNA), plasmids used in the transfection stage, culture media components, reagents, etc.; and product-related impurities such as virus aggregates, empty and/or defective particles.[44] These need to be removed by a series of multiple unit operations and there are regulatory requirements for purity that need to be satisfied.[44] It is in the downstream phase that significant product losses occur and where most production costs are spent.[45,46]

The unique physicochemical properties of each virus type make them versatile for the development of new drugs, but they also impose a great challenge for the development of downstream processes. It is not possible to design a universal process that would work for all virus types, and therefore processes typically need to be developed exclusively for a given vector.[45] Generally, large-scale downstream process typically starts with a harvest step to recover the product from the bioreactor.[45] Depending on the vector, a cell disruption step is required to release viral particles from the host-cells and a DNA digestion using endonucleases such as Benzonase is typically employed.[47] Next, a clarification step is used to remove large debris before the material is sent to chromatography for the removal of host-cell protein and DNA. A second round of chromatography for polishing purposes is

often required. Tangential-flow filtration is also typically employed at different stages of the process to concentrate the product or to exchange buffers. Finally, the process ends with a sterile filtration step.[45,47,48] The drug substance can then be stored and/or sent to aseptic fill and finish operations. The next sections will explore the different unit operations more in-depth.

1.2.2.1. Harvest and clarification

At the end of the production step in the bioreactor, viruses can be either present intracellularly, extracellularly, or both, depending on the type of vector. For example, adenoviruses and rhabdoviruses, the focuses of this thesis, are predominantly intracellular and extracellular, respectively, at the end of the culturing step. For intracellular products, a cell harvest step can be conducted via microfiltration or centrifugation.[49,50] This is an interesting strategy to reduce volumes early in the process, but different studies skip this step and proceed to the cell disruption step in the bioreactor itself.[51]

For the cell disruption step, mechanical or chemical methods can be used. This step is not required for vectors that can disrupt the cells by the end of the production process. At small-scale, cycles of freezing and thawing is an effective strategy that can be easily implemented. However, for large scales, microfluidization of cells at high pressures using specialized equipment or the addition of detergents able to disrupt the cellular membrane are typically used.[52] Up until recently, Triton X-100 was the most popularly used detergent in cell disruption, but it has been prohibited by regulatory agencies due to

environmental concerns.[53] Alternatives such as polysorbate 20 are now being further explored and have been presenting promising results.[53]

Finally, a clarification step aims to mainly remove host-cell debris and decrease the turbidity of the product[54] Scalable techniques to achieve this include the use of microfilters, either in dead-end or tangential flow filtration (TFF) formats, depth filters in dead-end mode, or centrifugation.[54] Depth filtration is an interesting technology where impurities are retained by adsorption throughout the filter matrix, in addition to conventional size-based separation. The active portion of a depth filter is typically made of diatomaceous earth or charged resins to which impurities bind through different types of interactions.[55] Depth filtration has been largely used for the clarification of viruses, but caution should be taken since the product has the potential to bind to the filter along with impurities, decreasing the yield of the process.[54]

1.2.2.2. Removal of host-cell protein and DNA

According to guidelines from the FDA for gene therapy products, residual levels of host-cell DNA should be below 10 ng/dose with fragments shorter than 200 base pairs;[44] for host-cell proteins, commonly accepted levels are in the range of 1-100 ng/mg.[56] To facilitate the removal of host-cell DNA specifically, an enzymatic DNA digestion step using endonucleases such as Benzonase is often employed.[52]

Density gradient ultracentrifugation is largely applied at small scales for the purification of different types of viruses and is an effective strategy, where separation is

based on the buoyancy of each molecule. However, this method is very complex to scale up[45] and therefore chromatography is often adopted as the scalable alternative.[57] Most chromatographic methods applied for virus purification rely on anion-exchange (AEX) or cation-exchange (CEX) interactions depending on the charge of the vector. However, other types of interactions have been explored such as size-exclusion, hydrophobic interaction, affinity, pseudo-affinity and multimodal chromatography.[58]

Conventional chromatography resins present sub-optimal characteristics for the purification of large biomolecules as is the case of viruses. Large molecules cannot access and diffuse inside the small pores of most traditional resins, and therefore binding is limited to the surface of the resin beads, which corresponds to only a small fraction of the binding capacity of these materials.[59] Newer chromatography matrices based on monoliths and membranes offer a solution to these challenges by presenting large and accessible pores, convective mass transfer, low-pressure drops and resistance.[60] More recently, cellulose nanofibre-based matrices have emerged[58] (originally developed by Puridify and called FibroSelect, now acquired by Cytiva and commercialized under the trademark of Fibro), adding to the list of advanced materials suitable for virus purification.

Added to the advantages described above, membrane adsorbers possess ideal characteristics for single-use applications, which eliminates the need for the tedious column packing and cleaning procedures required with conventional resins.[61] The market of membrane adsorbers is currently dominated by Sartorius with the Sartobind membranes, Pall with the Mustang membranes, and Millipore Sigma with the Natrix membranes.

However, novel solutions have been arising from start-ups such as Purilogics, the developer of the Purexa membranes available in different chemistries. Table E1 in Appendix E provides a list of the membrane adsorbers commercially available, along with their base materials, ligand chemistries, device sizes, and pricing.

1.2.2.3. Concentration and sterile filtration

Ultrafiltration membranes in TFF mode are typically employed to concentrate virus particles and/or exchange buffers through diafiltration.[45] In this process, the virus is retained in the permeate while buffer and impurities are transmitted through the membrane; this can therefore assist as a polishing step to remove residual impurities that remained until this stage.[45]

The final step of the production of virus drug substances is a sterile filtration step. This consists in passing the solution containing the virus through a sterile filter, where the virus should be transmitted and any potential bacteria, retained. Although typically rated as a 0.22 µm filter, the definition of a sterile filter is broader than that and consists in the ability to retain *Brevundimonas diminuta*,[62] small bacteria measuring approximately 0.3 – 0.4 µm by 0.6 – 1.0 µm.[63] This size is close to the size of larger viruses of clinical interest such as rhabdoviruses that measure approximately 0.05 – 0.10 µm by 0.10 – 0.18 µm.[19] Given the distribution of pore sizes in sterile filter membranes, it is common that significant amounts of virus stay retained in the filter. Depending on product attributes and buffer conditions, losses in the sterile filtration alone can be as high as more than 90%,[64] however the selection of the ideal type of membrane for each virus, and careful optimization of

buffer conditions can improve recovery.[64] In the event a sterile filtration cannot be performed with satisfactory recoveries, the complete manufacturing process then needs to be performed in aseptic conditions,[4] which can increase overall manufacturing processes.

1.3. Objectives and thesis outline

Although significant advances have been made with regards to upstream virus manufacturing, the downstream phase is currently considered the bottleneck of the process and it can account for 70% of the production costs.[45] Typical overall yields in downstream virus processes are in the order of 10 – 30%,[29,65] and therefore there is a need to increase these recoveries so they are comparable with those obtained with more traditional biotherapeutics such as monoclonal antibodies (mAbs), where overall recoveries can be greater than 70%.[66] This thesis aims to contribute to the improvement of virus downstream processes by advancing membrane chromatography technologies and addressing related unit operations. By considering the strong co-dependence and integration between upstream and the diverse unit operations in the downstream processes, experimental and modelling tools were applied to develop and improve virus purification processes.

Chapter 2 describes the development of MC processes for the purification of adenoviruses and investigates the impact of device format on the performance of the separation. To address a common drawback of MC, the low resolution caused by inefficient device designs,[67] the laterally-fed membrane chromatography (LFMC) technology[68] was

implemented and compared against a conventional radial flow-based MC device, both containing 1 mL of the same AEX membrane. The performance of both devices was evaluated in terms of the flow distribution through tracer experiments and computational fluid dynamics simulations (CFD), as well as the removal of host-cell protein and DNA in the purification of adenovirus lysates.

Chapter 3 was idealized upon the critical impact device design had on the performance of the purification of adenoviruses as described in Chapter 2, and focuses on comparing two of the most popularly used AEX membrane adsorbers in biomanufacturing (Sartobind from Sartorius and Mustang from Pall) using the LFMC device. Surprisingly, although interchangeably used in the literature, these two membranes had never been compared directly using the same device format. The performance of the two membranes was compared through a series of comprehensive runs using single-component feed materials containing purified protein, DNA, or virus. Finally, proof-of-concept experiments were conducted for the purification of adenovirus lysates.

Chapter 4 presents an integrated approach for process development, where different unit operations of the adenovirus downstream process were optimized in conjunction. The conditions of the clarification, DNA digestion, and MC steps were optimized aiming to improve the host-cell DNA removal and overall product purity. The study involved the selection of an alternative enzyme to Benzonase, the investigation of how the order of the unit operations clarification and DNA digestion affected DNA removal, and design-of-experiments (DoE) addressing the impact of enzyme type,

concentration, and digestion time. The DoE was extended to high-throughput MC experiments using 96-well filter plates containing the Sartobind Q membrane to determine optimal DNA digestion conditions that enable maximum DNA removal during MC. Finally, the best conditions were applied in proof or concept MC experiments using LFMC.

Chapter 5 focuses on a different vector, the vesicular stomatitis virus, and had as the main goal the development of an MC step for its purification. Preliminary studies evaluated different types of membranes and hydrophobic interaction membrane chromatography (HIMC) presented the greatest potential. Therefore, a HIMC process using the Sartobind Phenyl membrane was designed to harvest, concentrate, and purify VSV directly from cell culture. Effect of buffer pH and salt concentrations were investigated in small volume runs purifying 1 mL of lysate. The best conditions were applied in scale-up experiments targeting the purification of 300 mL of lysate.

Chapter 6 takes the investigation of the interactions between different process steps seen in Chapter 4 to a different level by applying modelling and simulation tools to understand and improve processes. A complete adenovirus production process was modelled using the collection of results from previous chapters as well as literature information, using the software BioSolve. With the model, hundreds of scenarios were run and compared in terms of the cost-of-goods (COG) of production to identify the major cost drivers and understand the contribution of each unit operation to the final COG. The use of membranes or resins in the chromatography step was evaluated in financial terms to determine the most cost-effective option, and the effect of switching the types of enzymes

in the DNA digestion step was addressed. Finally, sensitivity analyses were performed to identify critical process parameters.

1.4. References

1. Goswami, R. *et al.* Gene Therapy Leaves a Vicious Cycle. *Front. Oncol.* **9**, 1–25 (2019).
2. Bulcha, J. T., Wang, Y., Ma, H., Tai, P. W. L. & Gao, G. Viral vector platforms within the gene therapy landscape. *Signal Transduct. Target. Ther.* **6**, (2021).
3. Ginn, S. L., Amaya, A. K., Alexander, I. E., Edelstein, M. & Abedi, M. R. Gene therapy clinical trials worldwide to 2017 - an update. *J. Gene Med.* e3015 (2018). doi:10.1002/jgm.3015
4. Ungerechts, G. *et al.* Moving oncolytic viruses into the clinic: clinical-grade production, purification, and characterization of diverse oncolytic viruses. *Mol. Ther. - Methods Clin. Dev.* **3**, 16018 (2016).
5. Gene therapy's next installment. *Nat. Biotechnol.* **37**, 697–697 (2019).
6. Chen, K. Da *et al.* Process optimization for the rapid production of adenoviral vectors for clinical trials in a disposable bioreactor system. *Appl. Microbiol. Biotechnol.* **102**, 6469–6477 (2018).
7. Fett-Conte, A. C. & Salles, A. B. C. F. The importance of the p53 gene in human carcinogenesis. *Rev. Bras. Hematol. Hemoter.* **24**, 85–89 (2002).
8. Wirth, T., Parker, N. & Ylä-Herttuala, S. History of gene therapy. *Gene* **525**, 162–169 (2013).
9. Tang, R. & Xu, Z. Gene therapy: a double-edged sword with great powers. *Mol. Cell. Biochem.* **474**, 73–81 (2020).
10. Wang, D., Tai, P. W. L. & Gao, G. Adeno-associated virus vector as a platform for gene therapy delivery. *Nat. Rev. Drug Discov.* **18**, 358–378 (2019).
11. Russell, L. & Peng, K.-W. The emerging role of oncolytic virus therapy against cancer. *Chinese Clin. Oncol.* **7**, 16–16 (2018).
12. Wold, W. & Toth, K. Adenovirus Vectors for Gene Therapy, Vaccination and Cancer Gene Therapy. *Curr. Gene Ther.* **13**, 421–433 (2014).

13. Yang, L. & Yamamoto, T. Quantification of virus particles using nanopore-based resistive-pulse sensing techniques. *Front. Microbiol.* **7**, (2016).

14. Kamen, A. A. Vectored-Vaccine Platforms Enabled Rapid Development of Safe and Effective Vaccines in Response to COVID-19 Pandemic Situation. *Vaccines* **9**, (2021).

15. Russell, S. J. & Peng, K. W. Oncolytic Virotherapy: A Contest between Apples and Oranges. *Mol. Ther.* **25**, 1107–1116 (2017).

16. Cervera-Carrascon, V., Havunen, R. & Hemminki, A. Oncolytic adenoviruses: a game changer approach in the battle between cancer and the immune system. *Expert Opin. Biol. Ther.* **19**, 443–455 (2019).

17. Sinclair, A., Islam, S. & Jones, S. Gene therapy: an overview of approved and pipeline technologies. in *CADTH Issues in Emerging Health Technologies* (2018).

18. Zeng, J. *et al.* Oncolytic Viro-Immunotherapy: An Emerging Option in the Treatment of Gliomas. *Front. Immunol.* **12**, 1–24 (2021).

19. Swenson, S. L., Mead, D. G. & Kinker, D. R. Rhabdoviruses. in *Diseases of Swine* 733–739 (Wiley, 2019). doi:10.1002/9781119350927.ch45

20. Felt, S. A. & Grdzelishvili, V. Z. Recent advances in vesicular stomatitis virus-based oncolytic virotherapy: A 5-year update. *J. Gen. Virol.* **98**, 2895–2911 (2017).

21. Martin, N. T. & Bell, J. C. Oncolytic Virus Combination Therapy: Killing One Bird with Two Stones. *Mol. Ther.* **26**, 1414–1422 (2018).

22. Watanabe, K. *et al.* Pancreatic cancer therapy with combined mesothelin-redirected chimeric antigen receptor T cells and cytokine-armed oncolytic adenoviruses. *JCI Insight* **3**, 1–17 (2018).

23. Burchett, R., Walsh, S., Wan, Y. & Bramson, J. L. A rational relationship: Oncolytic virus vaccines as functional partners for adoptive T cell therapy. *Cytokine Growth Factor Rev.* **56**, 149–159 (2020).

24. Miliotou, A. N. & Papadopoulou, L. C. CAR T-cell Therapy: A New Era in Cancer Immunotherapy. *Curr. Pharm. Biotechnol.* **19**, 5–18 (2018).

25. Federico, A. & de Visser, M. New disease modifying therapies for two genetic childhood-onset neurometabolic disorders (metachromatic leucodystrophy and adrenoleucodystrophy). *Neurol. Sci.* **42**, 2603–2606 (2021).

26. Moço, P. D., Aharony, N. & Kamen, A. Adeno-Associated Viral Vectors for Homology-Directed Generation of CAR-T Cells. *Biotechnol. J.* **15**, 1–6 (2020).

27. Zheng, P.-P., Kros, J. M. & Li, J. Approved CAR T cell therapies: ice bucket

challenges on glaring safety risks and long-term impacts. *Drug Discov. Today* **23**, 1175–1182 (2018).

28. Labbé, R. P., Vessillier, S. & Rafiq, Q. A. Lentiviral Vectors for T Cell Engineering: Clinical Applications, Bioprocessing and Future Perspectives. *Viruses* **13**, 1–22 (2021).

29. Comisel, R. M., Kara, B., Fiesser, F. H. & Farid, S. S. Lentiviral vector bioprocess economics for cell and gene therapy commercialization. *Biochem. Eng. J.* **167**, 107868 (2021).

30. Ilic, D. & Liovic, M. Industry updates from the field of stem cell research and regenerative medicine in June 2021. *Regenerative Medicine* (2021). doi:10.2217/rme-2020-0208

31. Comisel, R. M., Kara, B., Fiesser, F. H. & Farid, S. S. Gene therapy process change evaluation framework: transient transfection and stable producer cell line comparison. *Biochem. Eng. J.* **Pre-proof**, 108202 (2021).

32. Pagliarulo, N. & Fidler, B. Bristol Myers finally wins FDA approval for cancer cell therapy. *Biopharma Dive* (2021). Available at: https://www.biopharmadive.com/news/bristol-myers-liso-cel-fda-approval-car-t/594660/.

33. Pagliarulo, N. FDA Approves CAR T-Cell Therapy for Multiple Myeloma. *Biopharma Dive* (2021). Available at: https://www.biopharmadive.com/news/fda-car-t-multiple-myeloma-approval-bristol-myers-bluebird/597438/.

34. Ying, Z. *et al.* Relmacabtagene autoleucel (relma-cel) CD19 CAR-T therapy for adults with heavily pretreated relapsed/refractory large B-cell lymphoma in China. *Cancer Med.* **10**, 999–1011 (2021).

35. Moleirinho, M. G., Silva, R. J. S., Alves, P. M., Carrondo, M. J. T. & Peixoto, C. Current challenges in biotherapeutic particles manufacturing. *Expert Opin. Biol. Ther.* **20**, 451–465 (2020).

36. van der Loo, J. C. M. & Wright, J. F. Progress and challenges in viral vector manufacturing. *Hum. Mol. Genet.* **25**, R42–R52 (2016).

37. Grein, A. T., Weidner, T. & Czermak, P. Concepts for the production of viruses and viral vectors in cell cultures. in *New Insights into Cell Culture Technology* 1–15 (2020).

38. Cameau, E., Pedregal, A. & Glover, C. Cost modelling comparison of adherent multi-trays with suspension and fixed-bed bioreactors for the manufacturing of gene therapy products. *Cell Gene Ther. Insights* **5**, 1663–1674 (2019).

39. Ausubel, L. J. *et al.* Current Good Manufacturing Practice Production of an

Oncolytic Recombinant Vesicular Stomatitis Viral Vector for Cancer Treatment. *Hum. Gene Ther.* **22**, 489–497 (2011).

40. Arora, M. Cell Culture Media: A Review. *Mater. Methods* **3**, 1–14 (2013).

41. Lorenzo, E. *et al.* Plasticity of the HEK-293 cells, related to the culture media, as platform to produce a subunit vaccine against classical swine fever virus. *AMB Express* **9**, 139 (2019).

42. Diallo, J.-S. *et al.* A High-throughput Pharmacoviral Approach Identifies Novel Oncolytic Virus Sensitizers. *Mol. Ther.* **18**, 1123–1129 (2010).

43. Terova, O., Soltys, S., Hermans, P., De Rooij, J. & Detmers, F. Overcoming Downstream Purification Challenges for Viral Vector Manufacturing: Enabling Advancement of Gene Therapies in the Clinic. *Cell Gene Ther. Insights* **4**, 101–111 (2018).

44. FDA & CBER. Chemistry, Manufacturing, and Control (CMC) Information for Human Gene Therapy Investigational New Drug Applications (INDs) - Guidance for Industry. (2020).

45. Nestola, P. *et al.* Improved virus purification processes for vaccines and gene therapy. *Biotechnol. Bioeng.* **112**, 843–857 (2015).

46. Wolff, M., Reichl, U. & Opitz, L. Method for the preparation of sulfated cellulose membranes and sulfated cellulose membranes. (2012).

47. Vellinga, J. *et al.* Challenges in Manufacturing Adenoviral Vectors for Global Vaccine Product Deployment. *Hum. Gene Ther.* (2014). doi:10.1089/hum.2014.007

48. Valkama, A. J. *et al.* Development of Large-Scale Downstream Processing for Lentiviral Vectors. *Mol. Ther. - Methods Clin. Dev.* **17**, 717–730 (2020).

49. Kalbfuss, B. *et al.* Harvesting and concentration of human influenza A virus produced in serum-free mammalian cell culture for the production of vaccines. *Biotechnol. Bioeng.* **97**, 73–85 (2007).

50. Grieger, J. C., Soltys, S. M. & Samulski, R. J. Production of recombinant adeno-associated virus vectors using suspension HEK293 cells and continuous harvest of vector from the culture media for GMP FIX and FLT1 clinical vector. *Mol. Ther.* **24**, 287–297 (2016).

51. Robert, M. A. *et al.* Manufacturing of recombinant adeno-associated viruses using mammalian expression platforms. *Biotechnol. J.* **12**, (2017).

52. Clément, N. & Grieger, J. C. Manufacturing of recombinant adeno-associated viral vectors for clinical trials. *Mol. Ther. - Methods Clin. Dev.* **3**, 16002 (2016).

53. Moleirinho, M. G. *et al.* Clinical-Grade Oncolytic Adenovirus Purification Using Polysorbate 20 as an Alternative for Cell Lysis. *Curr. Gene Ther.* **18**, 366–374 (2018).

54. Cherradi, Y. *et al.* Filter-based clarification of viral vaccines and vectors. *Bioprocess Int.* **16**, 48–53 (2018).

55. Roush, D. J. & Lu, Y. Advances in primary recovery: Centrifugation and membrane technology. *Biotechnol. Prog.* **24**, 488–495 (2008).

56. Zhu-Shimoni, J. *et al.* Host cell protein testing by ELISAs and the use of orthogonal methods. *Biotechnol. Bioeng.* **111**, 2367–2379 (2014).

57. Forsberg, N. *et al. Key Considerations in Gene Therapy Manufacturing for Commercialization*. *Cell Culture Dish* (2018).

58. Junter, G. & Lebrun, L. Polysaccharide-based chromatographic adsorbents for virus purification and viral clearance. *J. Pharm. Anal.* (2020). doi:10.1016/j.jpha.2020.01.002

59. Ljunglöf, A., Bergvall, P., Bhikhabhai, R. & Hjorth, R. Direct visualisation of plasmid DNA in individual chromatography adsorbent particles by confocal scanning laser microscopy. *J. Chromatogr. A* **844**, 129–135 (1999).

60. Orr, V., Zhong, L., Moo-Young, M. & Chou, C. P. Recent advances in bioprocessing application of membrane chromatography. *Biotechnol. Adv.* **31**, 450–465 (2013).

61. Zydney, A. L. New developments in membranes for bioprocessing – A review. *J. Memb. Sci.* **620**, 118804 (2021).

62. Meltzer, T. H. & Jornitz, M. W. The sterilizing filter and its pore size rating. *Am. Pharm. Rev.* (2003).

63. American Society for Testing and Materials (ASTM). Standard test method for determining bacterial retention of membrane filters utilized for liquid filtration - F838-15a. (2015).

64. Shoaebargh, S. *et al.* Sterile filtration of oncolytic viruses: An analysis of effects of membrane morphology on fouling and product recovery. *J. Memb. Sci.* **548**, 239–246 (2018).

65. Pettit, S., Glover, C., Hughes, J., Madsen, J. & Jaluria, P. Downstream Manufacturing of Gene Therapy Vectors. in *Key considerations for gene therapy manufacturing for commercialization* (2018).

66. Gomis-Fons, J., Andersson, N. & Nilsson, B. Optimization study on periodic counter-current chromatography integrated in a monoclonal antibody downstream process. *J. Chromatogr. A* **1621**, 461055 (2020).

67. Gagnon, P. The emerging generation of chromatography tools for virus purification. *BioProcess Int* 24–30 (2008).

68. Madadkar, P., Wu, Q. & Ghosh, R. A laterally-fed membrane chromatography module. *J. Memb. Sci.* **487**, 173–179 (2015).

Chapter 2

Purification of therapeutic viruses using laterally-fed membrane chromatography

2. Purification of therapeutic adenoviruses using laterally-fed membrane chromatography

Karina Kawka, Pedram Madadkar, Umatheny Umatheva, Shabnam Shoaebargh, Maria Fe C. Medina, Brian D. Lichty, Raja Ghosh, David R. Latulippe

Published work at the Journal of Membrane Science. Reprinted with permission.

 https://doi.org/10.1016/j.memsci.2019.02.056

2.1. Abstract

Viruses are an emerging class of biotherapeutics with the potential to treat cancer, genetic, cardiovascular, and other diseases. Their commercial success depends on cost-effective purification processes. Membrane chromatography processes offer great potential for virus purification, however conventional devices are known to suffer from issues related to resolution and sample dilution. Laterally-fed membrane chromatography (LFMC) overcomes these issues by minimizing the dead-volume and establishing a uniform flow distribution pattern within the device. While the efficiency of LFMC has been previously demonstrated for protein purification studies, here we present a direct comparison of the performance of a LFMC device and a conventional radial flow device (both containing 1 mL of the same strong anion-exchange membrane) for the purification of adenoviruses. Using a gradient elution strategy, a 74% virus recovery with 4% of residual amount of total protein and 1% residual amount of total DNA was obtained using the LFMC device; for

the radial flow device, only 20% virus recovery was achieved for a similar level of purity. Using a stepwise elution strategy, close to 100% virus recovery with 10% residual protein and DNA was achieved with both devices. However, the product was at least 50% more dilute with the radial flow device. Overall, this study demonstrates the considerable benefits to using LFMC over conventional membrane chromatography devices for purifying virus-based biotherapeutics.

2.2. Introduction

There is a great research and commercial interest in the use of viruses for therapeutic purposes. In addition to the common usage of vaccines against viral diseases, increasing interest has been given to the area of gene therapy, where viruses play an important role as vectors to deliver therapeutic genes. In 2017 there were approximately 1800 clinical trials worldwide involving virus-based gene therapies, most of them targeting the treatment of cancer and genetic diseases.[1] Oncolytic viruses are yet another class of therapeutic viruses have attracted significant attention for their ability to selectively kill cancer cells. The first oncolytic virus therapeutic was approved by the FDA in 2015 for the treatment of melanoma cancer[2] and various oncolytic virus candidates were tested in over 40 different clinical trials in 2016.[3] Adenoviruses have been used in 20% of clinical trials for gene therapy[1] and certain adenovirus strains have been shown to possess oncolytic activity.[2] The widespread use of adenoviruses for therapeutic purposes is mostly due to the broad knowledge available about their structure and replication cycle, their ease for genetic modifications, and their high stability.[2]

In order to enable the commercialization of virus therapeutics, considerable advances in upstream manufacturing capacity have been made such as the selection of 'producer cells' that are ideal for large-scale cultivation and the development of advanced bioreactor systems.[4] Additionally, there is growing interest in the development of 'viral sensitizers' that are capable of significantly increasing production capacities by maximizing virus titers in cell cultures.[5] Adenovirus production requires a cell lysis step and thus host-cell proteins and host-cell DNA must be sufficiently removed in the subsequent downstream separation steps. Conventional ion exchange chromatography resins that were developed for the production of recombinant proteins and monoclonal antibodies have been used for virus purification,[6-8] however the large size of viruses limits binding just to the external surface of the resin beads and demands the use of low flow rates.[9] The last step of virus production usually includes a sterile-filtration step to ensure product sterility.[6] Overall, the downstream purification of viruses is currently a bottleneck in the manufacturing process that can account for up to 70% of the total production costs.[7]

New chromatography matrixes and process formats such as monolithic column chromatography (MCC) and membrane chromatography (MC) have the potential to overcome the aforementioned issues in virus purification due to the presence of a network of large interconnected pores that allow for operation at higher flow rates.[10,11] The advantages of MC over MCC include lower pressure drops and the possibility to be used in single-use (disposable) format and thus eliminate the need for cleaning procedures and GMP validation. Currently, most commercially available MC devices are based on a radial-flow configuration which has been shown to result in higher degrees of sample dilution

(due to non-uniform flow distribution) and lower peak resolutions (due to peak broadening).[10] Current radial flow devices are usually available in sizes ranging from 1 mL to 5 L of membrane. The Sartobind® Cassettes (Sartorius) are another format commercially available, which have the advantage of being highly scalable from 0.8 L to 100 L of membrane and therefore are suitable for large-scale applications.

Laterally-fed membrane chromatography (LFMC) is a new purification method based on an improved MC device with low dead-volume and uniform flow distribution properties.[12] LFMC was originally developed to overcome the limitations of conventional stacked-disc MC devices that are typically used for small-scale purification applications;[12] it has also been shown to perform better than radial-flow MC devices for the separation of multicomponent protein mixtures,[13] PEGylated proteins,[14] and monoclonal antibody charge variants.[15] Based on those recent works, we felt that the LFMC method could be ideally suited for the purification of therapeutic viruses. In this study, we compare the purification of adenovirus from actual cell lysates (i.e. removal of protein and DNA) using a commercial radial-flow MC device and an LFMC device. Both these devices contained the exact same type and amount of anion exchange membrane. Additionally, we compared the performance of the two MC devices using computational fluid dynamics (CFD) simulations. The radial format was selected for this comparison, as opposed to the cassettes, based on the available small sizes (i. e. 1 mL of membrane), which are suitable for process development studies.

2.3. Materials and Methods

2.3.1. Virus production and sample preparation

Suspension 293 cells were provided by the Robert E. Fitzhenry Vector Laboratory at McMaster University and were cultured in CDM4HEK293 media (Hyclone) supplemented with 200 mM L-glutamine (BioShop) and 10 mM HEPES (Gibco), both prepared at the McMaster Immunology Research Centre media kitchen. Cells were seeded at 3×10^5 cell/mL and passaged every 3-4 days when they reached a cell density of 1×10^6 cell/mL. To prepare the infected cell cultures, cells were resuspended in fresh media at a cell density of 4×10^5 cell/mL and infected with a human Adenovirus 5 vector (provided by the Fitzhenry Vector Laboratory) at a multiplicity of infection of 5. Infected cells were harvested after 48 h at 37°C by centrifugation at 1460 × g for 15 min. The supernatant was discarded and the infected cell pellets were stored at -80°C.

Cell pellets originally from 50 mL cultures were thawed and resuspended with 100 µL of 10 mM Tris buffer pH 8 (Sigma), and then the viruses were released by disrupting the cells through three freeze-thaw cycles. The cell lysates were treated with Benzonase® (Novagen EMD Millipore) at 0.001 U/µL in 10 mM Tris buffer pH 8 (using a total of 0.1 U per pellet) and incubated in a 37°C water bath for 30 min to enzymatically degrade the DNA. Afterwards, the lysate was centrifuged at 1460 × g for 15 min then the supernatant (approximately 500 µL) was collected and diluted with two volumes of buffer containing 10 mM HEPES, 4% sucrose (BioShop), and 0.4 M NaCl (BioShop). The resulting solution was clarified by passing it through a 0.45 µm pore size PVDF Acrodisc® syringe filter (Pall). At this stage, the virus concentration of the clarified cell lysate was on the order of

1010 infectious units (IFU) per mL, the concentration of total protein was approximately 1.7 mg/mL, and the concentration of total DNA was approximately 38 µg/mL.

2.3.2. Membrane chromatography devices

Two MC devices were used in this study. The first one device being the Sartobind Nano capsule (Sartorius) which features a radial-flow configuration and thus will be hereafter referred to as the 'radial flow device', and the second one being the LFMC device. Both devices contained 1 mL of Sartobind® Q membrane (Sartorius), a strong anion-exchange membrane constructed of reinforced cellulose functionalized with quaternary-ammonium groups. Scanning electron microscopy (SEM) images acquired using a Vega II LSU Tescan electron microscope are shown in Figure 2.1, panels D and E, which highlight the structure of the top/bottom surface and the cross-section of the membrane, respectively.

The features of the LFMC device are shown in Figure 2.1. Note that this particular design has fewer parts than that described in previous studies[15,16] and thus is easier to fabricate. A blow-out schematic of the internal design is shown in Figure 2.1. An identical top and bottom plate containing an O-ring groove and lateral channels sandwiched the middle frame in which the membrane stack was housed. Each plate was provided with seven male pins of hexagonal cross-section that aligned with their corresponding circumscribed circle (6 mm diameter) female feature. A small droplet of medical grade 4902 instant glue (Loctite) was put on each pin and then the device was clamped overnight to seal the device. The plates were fabricated in Formlabs Standard resin using Form 2 3D printer (Formlabs). The rectangular portion of the lateral channels had the same length and width as the membrane stack and was tapered at both ends to two threaded ports (for

standard PEEK connectors), with one taper being a bit longer than the other. The longer port on the top plate was used as the feed inlet, while the longer port on the bottom plate was used as the permeate outlet. The two remaining ports were used as vents to 'prime' the device. The depth of the lateral channels was 0.5 mm. An array of pillars was etched on each lateral channel to enhance flow distribution and to support the membrane stack. The exact arrangement of the 15 rows of pillars with an alternating arrangement of 3 and 4 pillars per row was determined based on CFD simulations using COMSOL Multiphysics 5.3a (results not shown). Each pillar was a truncated cone (circular bevelled) having a diameter of 2 mm at the base and 0.6 mm at the contact point with the membrane. The membrane frame was made of 1085 polyurethane (Freeman) using a customized moulding technique.[17] The membrane stack (ten sheets of 38 mm × 10 mm membranes stacked to a bed height of 2.75 mm) was held in place in a silicon rubber mould (V-330 mixed in 10:1 ratio with CA-45, Freeman) using an aligner which was then enclosed by removing the aligner and adding another silicone mould on the top. The polyurethane elastomers (i.e. the resin and the hardener) were mixed in 1:1 ratio. The mixture which did not require degassing was poured in the mould via the embedded through-holes in the top mould. The polyurethane membrane frame was cured for 2 h and this fused the membranes in-place within the frame. The cross-sectional side view of the LFMC device along with idealized flow-paths are shown in Figure 2.1-C. The feed enters the device at the inlet, the liquid flows in the top lateral channel, goes through the membrane, emerges in the bottom lateral channel, flows towards the outlet, and exits the device.

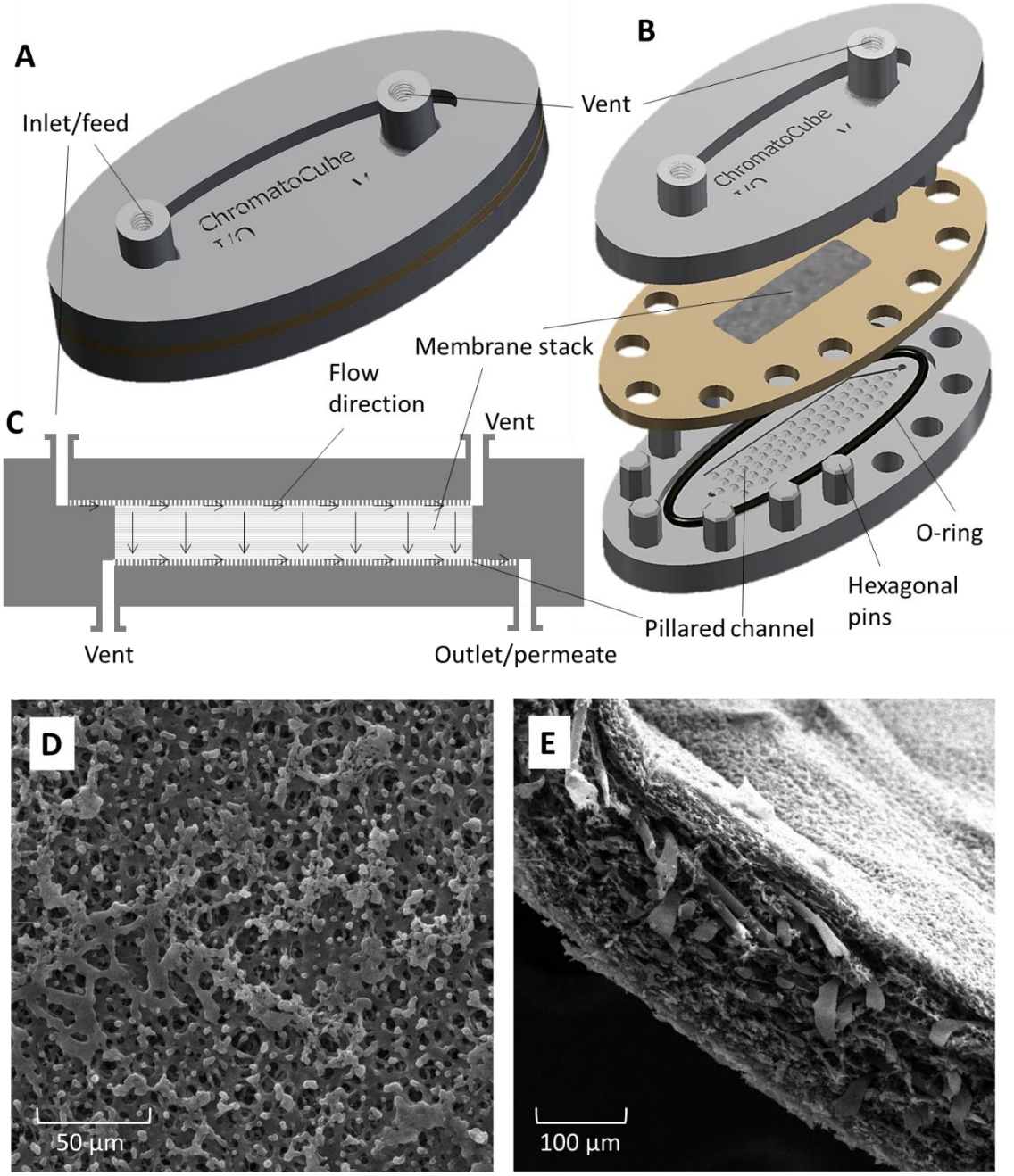

Figure 2.1. Details of the construction of the LFMC device and scanning electron microscopy (SEM) of the Sartobind Q membrane. A: external view of the LFMC device, B: blow-out diagram showing the different parts of the device, C: cross-section side view of the device. D: SEM image of the top/bottom surface of the Sartobind Q membrane, E: SEM image of the cross-section of the Sartobind Q membrane.

2.3.3. CFD simulations

CFD simulations were performed using the approach described in detail in an earlier publication.[18] Briefly, models of the two devices based on actual internal dimensions and experimental conditions were created using COMSOL Multiphysics software and solved using the Brinkman equations with Transport of Diluted Species in Porous Media and Particle Tracing for Fluid Flow package. Residence time distributions (RTD) studies were performed for both devices using COMSOL Multiphysics 5.3a.

2.3.4. Chromatography experiments

An NGC™ medium-pressure liquid chromatography system (BioRad) with an in-line conductivity meter and UV detector (260 and 280 nm) was used to characterize the performance of the two MC devices. A flow rate of 5 mL/min (i.e. 12 s residence time) was used for all experiments, in order to operate below the maximum pressure rating (400 kPa) for the Sartobind Q membrane. At this flow rate, the BioRad NGC system pressure was similar for both the LFMC device and the radial device and ranged from 282 kPa to 296 kPa. In the absence of either device, the system pressure was approximately 269 kPa.

Tracer experiments were performed by injecting 100 µL of a 10% solution of acetone in Milli-Q water. For virus purification runs, a 100 µL sample of the clarified cell lysate (as prepared according to section 2.3.1) was injected. The ChromLab™ software was used to maintain a constant flow rate of 5 mL/min and to automatically adjust the proportion of Buffer A (10 mM HEPES, 4% sucrose) and Buffer B (10 mM HEPES, 4% sucrose, 2 M NaCl) according to the two elution strategies (linear gradient and stepwise) that were evaluated for both MC devices. Based on early testing with the radial flow device, it was

observed that it can take up to 6 membrane volumes (i.e. 6 mL) for the signal of the 'flow-through' peak to return to baseline (results not shown). Therefore, a total of 6 mL was collected (in 3 fractions of 2 mL each) between the start of the run and the first increase in salt concentration in all experiments.

For the gradient elution strategy, a linear increase from 0.4 M NaCl (20% Buffer B) to 1 M NaCl (50% Buffer B) was done over 4 mL and then another 6 mL was run at 1 M NaCl with 1 mL fractions continuously collected. Including the 'flow-through' fractions, a total of 13 fractions were collected for each gradient elution run. For the stepwise elution strategy, a step change from 0.4 M NaCl (20% Buffer B) to 0.6 M NaCl (30% Buffer B) was done and held for 3 mL, then from 0.6 M NaCl to 1 M NaCl for 8 mL. The stepwise elution conditions were defined based on results from the gradient elution strategy and on a set of early optimization experiments which results are not shown. Again 1 mL fractions were collected continuously for a total of 14 fractions per stepwise elution run. A solution of 50% glycerol (Caledon Laboratory Chemicals) in Milli-Q water was added to each fraction (in 20% v/v proportion) and then they were stored temporarily at -80°C.

Between runs, the MC devices and NGC chromatography system were 'cleaned-in-place' following the instructions of the membrane manufacturer. A 1 M NaOH solution (BioShop) was passed through the system for 30 min at 1 mL/min flow rate, followed by a 1 M NaCl solution (BioShop) for 3 minutes at 5 mL/min flow rate. Finally, the system was re-equilibrated with Buffer A.

2.3.5. Analytical methods

2.3.5.1. Virus infectivity assay

The amount of infectious adenovirus was determined in triplicate for each fraction using the procedure based on hexon staining.[19] A 500 µL aliquot of a suspension of adherent 293 cells (3×10^5 cell/mL) in Minimum Essential Media with Earle's salts (Gibco, Life Technologies) supplemented with 10% fetal bovine serum (FBS; Gibco, Life Technologies) and 1% L-glutamine (MIRC media kitchen) were seeded in each well of a 24-well plate (Corning) and incubated for 24 hours at 37°C and 5% CO_2. Then, a dilution series of the collected fraction was prepared using the same culture media. A 250 µL aliquot from each diluted fraction sample was added to the individual wells and the plates were incubated at 37°C and 5% CO_2. After 48 h, the culture media was removed, then the cells were fixed by adding ice-cold methanol to the wells, and the plates were stored in a freezer for 10 min. Each well was then washed three times with 500 µL of 1% bovine serum albumin (BSA) solution (Equitech-Bio) in phosphate-buffered saline (PBS) solution (MIRC media kitchen) prior to the addition of 250 µL of a murine anti-hexon primary antibody (prepared at the MIRC) diluted 40,000 times with 1% BSA in PBS solution. The plates were then stored at 37°C on a rocker platform for 1 h. Next, the wells were washed three times with 500 µL of 1% BSA in PBS solution and followed by the addition of 250 µL of a goat anti-mouse secondary antibody conjugated with horseradish peroxidase (HRP) enzyme (Santa Cruz Biotechnology) diluted 5,000 times with 1% BSA in PBS solution. The plates were again stored at 37°C for 1 h, washed three times with 1% BSA in PBS solution, and then 250 µL of 1× diaminobenzidine (DAB) substrate (Roche) was added.

After a 10 min incubation at room temperature, the DAB substrate was removed and 500 µL of PBS solution was added. Finally, the cells were visualized under the microscope using a 10× objective, to count the number of infected cells (coloured dark brown) and the total titer (in IFU/mL) was calculated with consideration of the sample dilution factors.

2.3.5.2. Protein assay

The total protein concentration in each fraction was determined in duplicates using the micro BCA™ Protein Assay Kit (Thermo Scientific) following the protocol provided by the manufacturer. A 120 µL aliquot of each fraction was mixed with an equal volume of working reagent in a 96-well transparent microplate (Corning) and incubated at 37°C for 2 hours. The absorbance at 562 nm was measured using a SpectraMax i3 (Molecular Devices) plate reader and the concentration was calculated from calibration curves of concentration (range from 2 to 40 µg/mL) versus absorbance for the recommended standard (BSA).

2.3.5.3. DNA assay

The total DNA concentration in each fraction was determined in duplicate using Quant-iT™ PicoGreen® dsDNA Kit (Invitrogen) following the protocol provided by the manufacturer. A 60 µL aliquot of each fraction sample was mixed with an equal volume of working reagent in a half-area 96-well black microplate (PerkinElmer) and incubated for five minutes at room temperature while protected from light. The fluorescence was measured (520 nm emission, 480 nm excitation) using a SpectraMax i3 (Molecular Devices) plate reader and the concentration was calculated from calibration curves of

concentration (range from 1 to 1000 ng/mL) versus fluorescence for the recommended standard (Lambda-DNA).

2.4. Results and Discussion

2.4.1. CFD simulation and tracer experiments

The RTDs obtained by CFD simulations at 5 mL/min flow rate are compared in the top panel of Figure 2.2. There is a clear difference in the predicted behaviour of the two MC devices. With the LFMC device, the incipient unbound tracer breakthrough time (defined as the moment when the tracer particle count was 1% of the peak height) was 15 seconds, which was 2.3 times lower than the corresponding value for the radial flow device (35 seconds). Also, the flow-through tracer profile obtained with the radial flow device was broad and skewed, i.e. had a significant tailing, with a peak height being approximately 2.4 times smaller than the corresponding value for the LFMC device. The sharper, narrower and more symmetric peak obtained with the LFMC device showed that it had significantly better hydrodynamic attributes than the radial flow device. These simulation results predicted that the LFMC device would yield sharper and better resolved chromatographic peaks than the radial flow device during a bind and elute mode of operation. For further details on the interpretation of the results of such simulation studies, the reader is directed to an earlier publication.[18]

In order to confirm the accuracy of the above CFD simulation results, a set of tracer experiments were performed with the NGC chromatography system by injecting 100 μL ‘pulses’ of a 10% acetone solution and monitoring the UV absorbance signal. Acetone

was chosen because it does not interact with the Sartobind Q membrane. The resulting UV absorbance profiles (at 280 nm) are shown in the bottom panel of Figure 2.2. Note that these displayed profiles were obtained by shifting the actual profiles by 0.6 mL, which was the volume associated with the internal parts (tubing, valves, etc.) of the NGC chromatography system. This correction volume was determined by running acetone tracer experiments without any MC device connected to the system. While the experimental results do not exactly match the simulation results, there was a good agreement in the trends obtained with the two MC devices. For example, the experimental incipient unbound tracer breakthrough time for the LFMC and radial flow devices were 6 and 27 seconds respectively, i.e. the offset with the theoretical data were similar. A possible reason for the difference between the theoretical and experimental results was that while the CFD simulation was based entirely on convective solute transport, given the small size of acetone it is expected to undergo a significant amount of diffusional transport within the MC devices, resulting in peak broadening. Quite interestingly, the acetone tracer tests showed that for the radial flow device, the UV signal had not returned to the baseline condition after running the pulse test for 140 seconds (i.e. after running approximately 12 column volumes of Buffer A through the device).

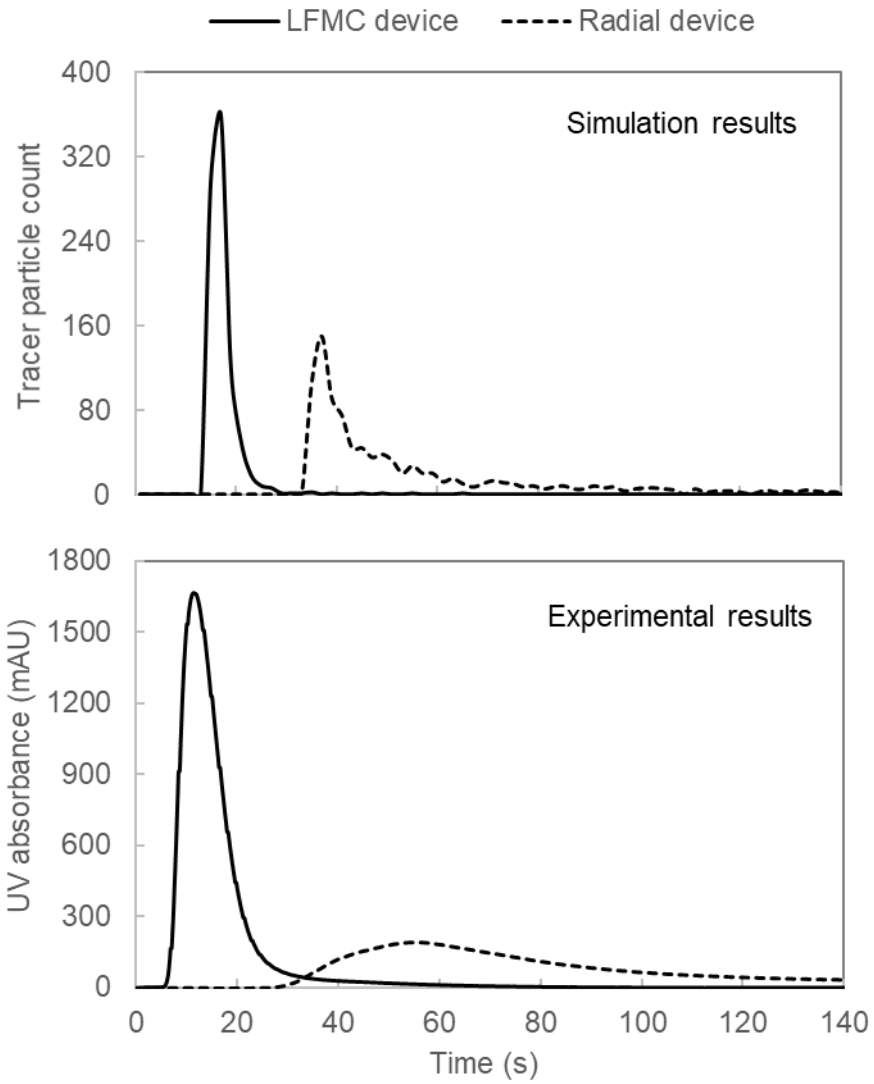

Figure 2.2. Residence time distribution comparing the LFMC device (solid line) and the radial flow device (dashed line) results for the CFD simulations (top panel) and acetone tracer experiments (bottom panel), at a 5 mL/min flow rate.

2.4.2. Purification of adenoviruses via gradient elution strategy

In order to evaluate the reproducibility of the conditions and procedures that were used to both prepare the lysates and conduct the chromatography runs, the four

experimental combinations (two MC devices and two elution conditions) were run in duplicate. The UV absorbance at 280 nm and conductivity signals from the duplicate runs for the LFMC device operated according to the gradient elution strategy are displayed in Figure 2.3. It is evident that there is very good agreement between the two runs in terms of UV absorbance and conductivity profiles. The first large peak observed in the 'flow-through' corresponded to any biomolecules that did not adsorb to the membrane at the loading conditions of 0.4 M NaCl (i.e. 20% Buffer B). The plateau observed at approximately the 2 mL mark is related to a disturbance in the UV detection cell caused by a sudden change in pressure when the sample loop is closed after the sample was injected. The first eluted peak appeared approximately 2.5 mL after the linear gradient was initiated (at the 6 mL mark) and coincided with the moment when the conductivity started to increase as a response to the higher NaCl concentration. A second eluted peak appeared shortly afterwards around the 10.5 mL mark and finally, the signal gradually returned to baseline. The same high degree of similarity was seen between the duplicate runs for the other three chromatography conditions (results not shown).

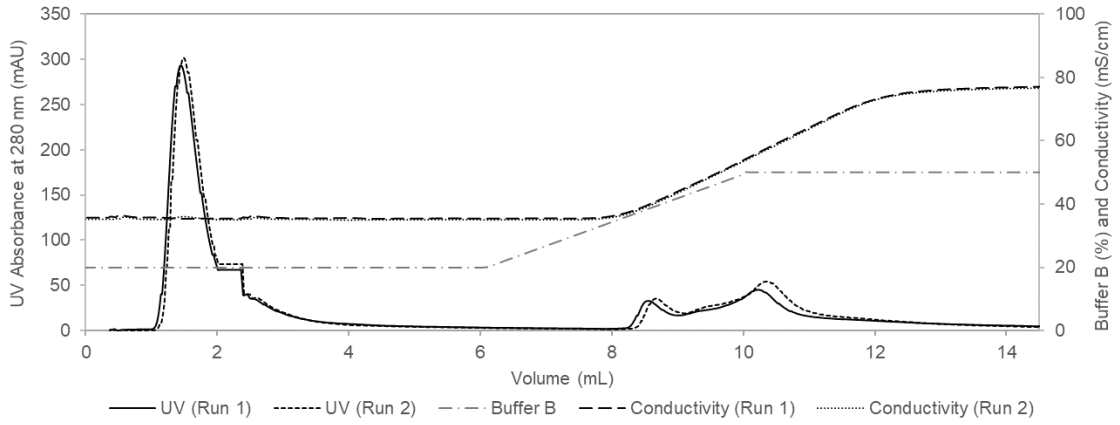

Figure 2.3. UV absorbance (280 nm) and conductivity profiles for the duplicate chromatography runs using the LFMC device and gradient elution strategy. The dashed-dotted line indicates the percentage of buffer B with values given on the secondary y-axis.

While the UV absorbance signal does indicate the relative separation behaviour of the MC device, it was not possible to determine the concentration of each component given the complex nature of the feed sample. Thus, for this study, we were required to run separate assays to determine the virus titer, protein concentration, and DNA concentration (as described above in section 2.3.5) for each of the 13 fractions that were collected during the gradient elution chromatography runs. The results from this analysis for the LFMC device are shown in the top panel of Figure 2.4. Only one of the duplicate runs under this condition is shown (corresponding to Run 1 from Figure 2.3), given the good reproducibility of the duplicate runs. The 3D bar chart displays the amount of virus (front solid red bars), protein (middle hatched yellow bars), and DNA (back striped green bars) within each fraction as a percentage of the amount in the injected feed sample. The large UV absorbance peak that appeared in the ‘flow-through’ (corresponding to 20% Buffer B

and NaCl concentration of 0.4 M) contained 88% of the total amount of protein in the feed sample, 1.7% of the total amount of DNA in the feed sample, and less than 0.01% of the total amount of virus in the feed sample. The first elution peak, which appeared approximately 2.5 mL after the linear gradient was initiated, contained mostly virus and a small amount of detectable protein and DNA; a detailed description of the composition of the fractions for the first elution peak is presented in Table 2.1. The second elution peak contained mostly DNA. No further increase in NaCl concentration beyond 1 M (i.e. 50% Buffer B) was used because it was observed in some of our early studies that no detectable level of biomolecules were eluted at NaCl concentrations higher than 1 M NaCl (results not shown).

The gradient elution strategy was run partly in order to provide an understanding of the required solution conditions to elute the virus and DNA from the anion-exchange Sartobind Q membrane. Based on the conductivity profile, it was determined that the elution of adenoviruses happened at a NaCl concentration of approximately 0.6 M while the elution of DNA occurred at NaCl concentration between 0.8 M and 1 M. These values were determined using the chromatography runs with the LFMC device, given its faster conductivity response to NaCl concentration increase and lower degree of back-mixing compared with the radial flow device. Our results are in good agreement with a previous study of adenovirus purification using the Sartobind Q membrane that reported the virus eluted at a NaCl concentration of 0.65 M and the DNA eluted at a NaCl concentration of 1 M for a solution pH of 8.[20]

The same set of results for the radial flow device are shown in the bottom panel of Figure 2.4. It is readily apparent that the UV absorbance profiles for the two MC devices run at the same conditions are significantly different. For example, the 'flow-through' peak for the radial flow device started at the 2.5 mL mark while that for the LFMC device started at the 1 mL mark; this observation is in good agreement with the results shown in Figure 2.3. Also, the peak for the radial flow device was nearly four times broader (based on the peak width at the peak half height value) than that for the LFMC device. In accordance with Figure 2.3, the disturbance plateau around the 2 mL mark caused by the closing of the sample loop also appeared in the runs using the radial flow device but it was almost not detectable given the very different UV absorbance profile. For the radial flow device, the large peak that appeared in the 'flow-through' (corresponding to 20% Buffer B and NaCl concentration of 0.4 M) contained 80% of the total amount of protein in the feed sample, 1% of the total amount of DNA in the feed sample, and less than 0.01% of the total amount of virus in the feed sample. A single peak appeared approximately 5 mL after the linear gradient was initiated. As shown by the assay results, that peak contained a mixture of virus and DNA. For the exact same conditions, the LFMC device was able to resolve the eluted biomolecules into two separate peaks due to the better hydrodynamic attributes than the radial flow device.

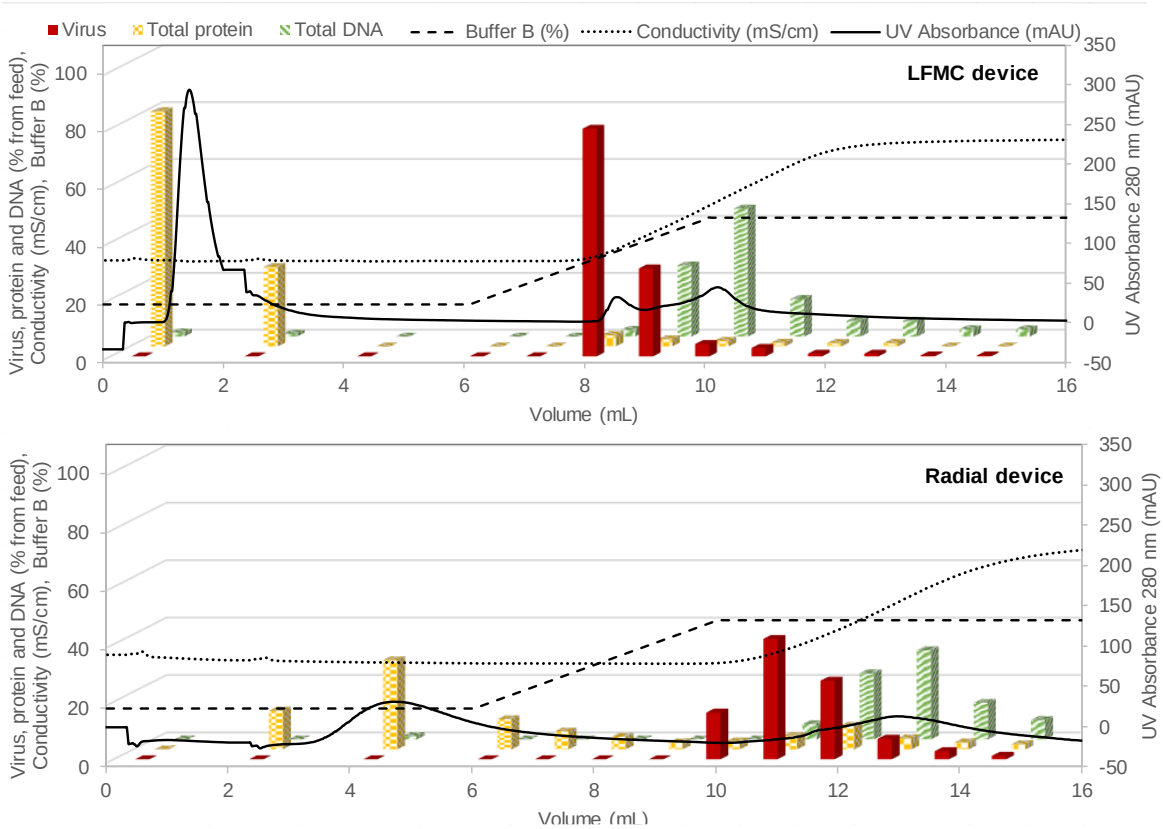

Figure 2.4. Chromatograms for adenovirus purification via gradient elution strategy with the LFMC device (top panel) and the radial flow device (bottom panel). The dashed line indicates the percentage of buffer B (which correlates to the NaCl concentration), the dotted line indicates the conductivity, and the solid line indicates the UV absorbance at 280 nm (refer to the secondary axis). The 3D bar charts display the amount of adenovirus (front solid red bars), total protein (middle hatched yellow bars), and total DNA (back striped green bars) within each fraction as a percentage of the amount in the injected feed sample.

Based on the collection of results displayed in Figure 2.4, it is apparent that the degree of virus purification is strongly dependent on the design of the MC device. A detailed comparison of the effect of the total fraction size on the virus recovery and purity is given in Table 2.1. The first fraction to be displayed on Table 2.1 was selected based on the criteria of containing at least 1% of the initial amount of virus after the gradient was started. The reported results are averages of the composition of fractions from the duplicate runs that were performed at each condition. Additionally, each fraction for one of the

independent runs was analysed in triplicate for virus amount and duplicate for protein and DNA amounts. The error bars were calculated by propagating the standard deviations of the values obtained from the duplicate runs performed at each condition. The large error bars and accompanying virus recoveries larger than 100% that are listed in Table 2.1 are due to the limitations of the hexon staining assay that was used to determine the virus infectivity of the feed and fractions. While there are other methods that give more precise estimates of the total amount of virus particles (e.g. q-PCR), those methods do not distinguish between active and inactive virus particles which is a critical concern in this study. It was found that 100% of the virus eluted in a 2 mL fraction with the LFMC device while a 4 mL fraction was needed to recover a comparable amount of virus for the radial flow device. The requirement to use larger volumes with the radial flow device is undesirable because clinical virus doses have high titers usually in the order of magnitude of 10^{10} IFU/mL.[6] For the LFMC device, the 2 mL fraction contained 7.2% of the initial amount of protein and 25% of the initial amount of DNA. For the radial flow device, the 4 mL fraction contained much higher amounts of both protein (17%) and DNA (56%). In terms of virus purity, it was found that 74% of the initial virus, 4.1% of the initial protein, and 1.1% initial DNA was obtained in the 1 mL fraction for the LFMC device; these values correspond to approximately 10^{9} IFU/mL of virus, 6.8 µg/mL of protein and approximately 38 ng/mL of DNA. Although a significant amount of contaminants have been removed, the need for a subsequent polishing step will depend on the dose and application of the therapeutic virus, and regulatory requirements. The concern is specially related to the amount of host-cell DNA, which should be below 10 ng per dose according to FDA

standards.[7] A similar degree of purity could be achieved with the radial flow device in a 1 mL fraction, however the recovery of the virus was over three times lower than that obtained with the LFMC device.

Table 2.1. Comparison of the total sample volume effect on recovery of virus, total protein, and total DNA for the LFMC and radial flow devices using a gradient elution strategy; the percentages are reported with respect to the amounts of each component in the feed sample. The error bars are based on propagation of error analysis from triplicate testing (for virus titer) or duplicate testing (for protein and DNA) on duplicate runs.

Device	**LFMC**				**Radial Flow**			
Fraction size	1 mL [a]	2 mL [b]	3 mL [c]	4 mL [d]	1 mL [e]	2 mL [f]	3 mL [g]	4 mL [h]
Virus (% of initial)	74±9	102±13	108±14	112±15	20±2	61±5	90±7	97±9
Protein (% of initial)	4.1±0.1	7.2±0.2	9.7±0.3	11±1	2.8±0.1	7.1±0.1	13±3	17±4
DNA (% of initial)	1.1±0.1	25±1	74±3	89±4	0.34±0.03	5.7±0.2	28±1	56±3

[a] Corresponds to the fraction at the 8 mL mark in the top panel of Figure 2.4
[b] Corresponds to the fractions at the 8 and 9 mL marks in the top panel of Figure 2.4
[c] Corresponds to the fractions at the 8, 9, and 10 mL marks in the top panel of Figure 2.4
[d] Corresponds to the fractions at the 8, 9, 10, and 11 mL marks in the top panel of Figure 2.4
[e] Corresponds to the fraction at the 10 mL mark in the bottom panel of Figure 2.4
[f] Corresponds to the fractions at the 10 and 11 mL marks in the bottom panel of Figure 2.4
[g] Corresponds to the fractions at the 10, 11, and 12 mL marks in the bottom panel of Figure 2.4
[h] Corresponds to the fractions at the 10, 11, 12, and 13 mL marks in the bottom panel of Figure 2.4

2.4.3. Purification of adenoviruses via stepwise elution strategy

Based on the knowledge gained during the gradient elution tests, a stepwise elution strategy was designed for the purification of adenoviruses. Similarly to the gradient elution strategy, the run was started at a 0.4 M NaCl concentration (i.e. 20% Buffer B) in order to remove most of the protein in the run 'flow-through'; next a step change to 30% Buffer B (i.e. 0.6 M NaCl) was made followed by a step change to 50% Buffer B (i.e. 1 M NaCl). The experimental results for one of the duplicate runs with the LFMC device are shown in the top panel of Figure 2.5. As previously mentioned for Figure 2.4, the 3D bar chart displays the amount of virus (front solid red bars), protein (middle hatched yellow bars),

and DNA (back striped green bars) within each fraction as a percentage of the amount in the injected feed sample. The large UV absorbance peak that appeared in the 'flow-through' (corresponding to 20% Buffer B and NaCl concentration of 0.4 M) contained mostly protein and small amounts of the virus (less than 0.01% of that in the feed) and DNA (approximately 3% of that in the feed). The first elution peak, which appeared approximately 2 mL after the step change to 0.6 M NaCl was made, contained mostly virus and a small amount of protein and DNA; a detailed description of the composition of the fractions is presented in Table 2.2. The second elution peak contained mostly DNA (approximately 76% of that in the feed) and a slight tailing effect was observed with the very last fraction (at the 16 mL mark) containing approximately 2% of the initial amount of DNA.

The same set of results for the radial device are shown in the bottom panel of Figure 2.5. Again, there was a large difference in the UV absorbance profiles and distribution of biomolecules within the collected fractions for the two devices. After the first step increase in NaCl concentration, it took approximately 2 mL for the peak corresponding to the virus elution to appear for the LFMC device, while for the radial device it took around 4 mL. Moreover, this peak was twice as broad (based on the peak width at the peak half height value) for the radial device (1.72 mL) in comparison to the LFMC device (0.83 mL). The large UV absorbance peak that appeared in the 'flow-through' again contained most of the protein in the feed sample. A very small elution peak appeared approximately 4 mL after the step change to 30% Buffer B (i.e. 0.6 M NaCl) was made. The corresponding fractions for that peak contained most of the virus and some

protein and DNA; the exact percentages are given in Table 2.2. The second elution peak after the step change to 50% Buffer B (i.e. 1 M NaCl) was made contained mostly DNA. In agreement with all the previous results, a large tailing effect was observed.

Similarly to what was observed using the gradient elution strategy, the results shown in Figure 2.5 indicate that the design of the MC device is a critical parameter on the performance of virus purification. A comparison of the effect of the total fraction size on the recovery and purity of the virus samples is shown in Table 2.2. The values reported in Table 2.2 were obtained following the same calculations used in Table 2.1. The dilution effect was once again quite pronounced in the radial flow device. While 93% of virus was recovered in a 2 mL fraction containing 8% of the initial amount of protein and 9% of DNA using the LFMC device, a 3 mL fraction was required to recover 88% of virus with 10% of the initial amount of protein and 8% of DNA using the radial flow device. Considering these two fractions (2 mL for the LFMC and 3 mL for the radial flow device), the amount of protein and DNA are not significantly different, therefore there was no difference between the two devices in terms of purity.

Focusing just on the LFMC device, a distinct difference in separation performance was found for the two elution strategies. A virus recovery of 74% and high purity was obtained in the 1 mL fraction for the gradient elution strategy (Table 2.1); approximately 100% virus recovery was possible in a 2 mL fraction but there was a greater amount of DNA (25% of initial amount). The stepwise elution mode provided more balanced virus recovery versus purity results; for the 2 mL fraction, the recovery of virus was 93% with less than 10% of both protein and DNA.

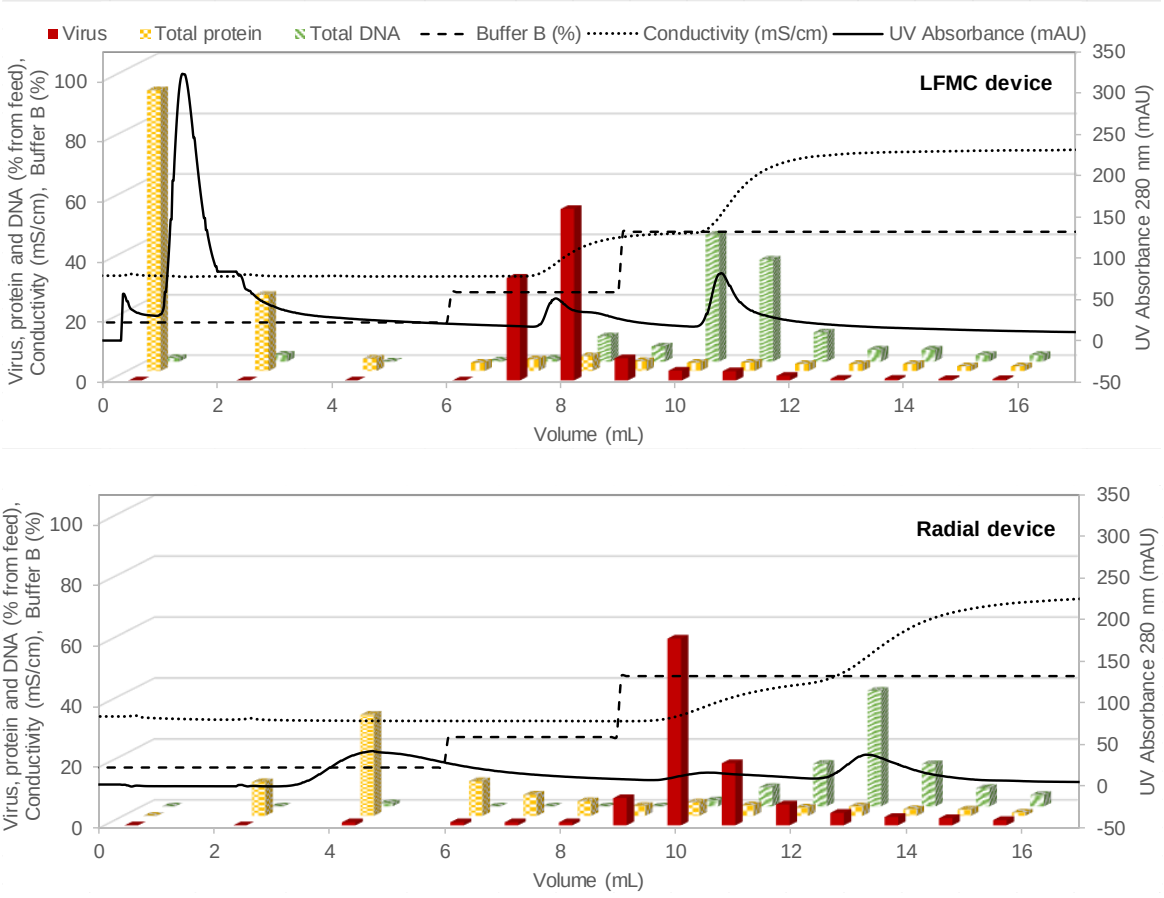

Figure 2.5. Chromatograms for adenovirus purification via stepwise elution strategy with the LFMC device (top panel) and the radial device (bottom panel). The dashed line indicates the percentage of buffer B (which correlates to the sodium chloride concentration), the dotted line indicates the conductivity, and the solid line indicates the UV absorbance at 280 nm (refer to the secondary axis). The 3D bar charts display the amount of adenovirus (front red bars), total protein (middle yellow bars), and total DNA (back green bars) within each fraction as a percentage of the amount in the injected feed sample.

Table 2.2. Comparison of the total sample volume effect on recovery of virus, total protein, and total DNA for the LFMC and radial flow devices using a stepwise elution strategy; the percentages are reported with respect to the amounts of each component in the feed sample. The error bars are based on propagation of error analysis from triplicate testing (for virus titer) or duplicate testing (for protein and DNA) on duplicate runs.

Device	**LFMC**				**Radial Flow**			
Fraction size	1 mL [a]	2 mL [b]	3 mL [c]	4 mL [d]	1 mL [e]	2 mL [f]	3 mL [g]	4 mL [h]
Virus (% of initial)	35±4	93±10	101±10	104±11	10 ± 1	57±6	88±8	100±10
Protein (% of initial)	3.5±0.3	8.0±0.4	11±1	14±1	3.0 ± 0.4	6.8±0.5	10±1	13±1
DNA (% of initial)	0.67±0.01	8.9±0.4	14±1	53±2	0.29±0.02	2.6±0.1	8.2±0.4	22±1

[a] Corresponds to the fraction at the 7 mL mark in the top panel of Figure 2.5
[b] Corresponds to the fractions at the 7 and 8 mL marks in the top panel of Figure 2.5
[c] Corresponds to the fractions at the 7, 8, and 9 mL marks in the top panel of Figure 2.5

[d] Corresponds to the fractions at the 7, 8, 9, and 10 mL marks in the top panel of Figure 2.5
[e] Corresponds to the fraction at the 9 mL mark in the bottom panel of Figure 2.5
[f] Corresponds to the fractions at the 9 and 10 mL marks in the bottom panel of Figure 2.5
[g] Corresponds to the fractions at the 9, 10, and 11 mL marks in the bottom panel of Figure 2.5
[h] Corresponds to the fractions at the 9, 10, 11, and 12 mL marks in the bottom panel of Figure 2.5

Future work in this area includes further optimization of the process parameters (e.g. buffer pH and elution profile) in order to maximize virus recovery and purity in step-elution mode, which is the most-used strategy for large-scale processes. Additionally, the LFMC device will be scaled-up to accommodate more membrane volumes, targeting sizes comparable with the commercially available radial devices (i.e. 1 mL to 5 L of membrane). A systematic approach will be used to evaluate the other steps of the downstream in order to stablish a full scalable process. For example, other scalable techniques for cell lysis such as cell homogenization and use of detergents will be tested and their potential effects in the chromatography step will be evaluated. Finally, the performance of the purification of other types of therapeutic viruses will be addressed; for example, the rhabdovirus Maraba is of particular interest to us given its strong oncolytic activity and its ability to stimulate an immune response against tumours.[21]

2.5. Conclusions

The LFMC device has been shown to have several advantages over radial flow devices for the purification of adenoviruses. Using a linear gradient elution strategy resulted in virus recoveries near 100% of the total amount in the feed sample for both devices. However, the LFMC device provided better overall purities, given that the peaks corresponding to virus and DNA respectively were overlapped when the radial device was

used. Additionally, the sample dilution effect was at least 50% higher for the radial flow device. Using a stepwise elution strategy resulted in improved purity of the virus fractions. Virus recoveries of 100% with less than 10% of the initial amount of protein and DNA were possible using both devices. The radial flow device resulted in similar purities as the LFMC because the elution strategy was designed in such a way that time enough was allowed for all the peaks to be completely resolved from each other, avoiding the overlapping that occurred during the gradient elution experiments. Despite the comparable performance in terms of purity, a 50% higher sample dilution effect was again observed for the radial flow device. This suggests that the purification can be done in a shorter interval of time using the LFMC, saving buffer and time while maintaining similar separation performance.

The virus purification results were in good agreement with the CFD simulations and acetone tracer experiments of the LFMC and radial flow devices. The peaks resulting from the LFMC device were higher and narrower in comparison with the radial flow device indicating that a more uniform flow distribution was obtained using the LFMC device.

The faster response of the LFMC to changes in buffer conditions makes it a more accurate way to determine the best elution conditions for different types of viruses and biomolecules during the development of purification processes. Based on the results presented herein, the Sartobind Q membrane is effective for the purification of adenoviruses independent of the format it is applied. In this paper, it is shown that the LFMC device provides an enhanced performance for the purification of adenoviruses for 1

mL membrane volume devices. Its advantages are in terms of minimizing sample dilution, allowing shorter chromatography runs with a removal of at least 90% of contaminants.

2.6. Acknowledgements

Funding was provided by the ‘Alliance for Biotherapeutics Manufacturing Innovation’ project that was supported by the Ontario Research Fund-Research Excellence program, an Idea to Innovation Grant from the Natural Sciences and Engineering Research Council of Canada, and the Mitacs Accelerate program. From the Chemical Engineering Department at McMaster University, the authors thank Paul Gatt for his assistance in designing and fabricating the LFMC device, Carlos Filipe for his particularly insightful contributions to the study, and Reza Pazouki for acquiring the SEM images of the Sartobind Q membrane. From the Faculty of Health Sciences at McMaster University, the authors thank Natasha Kazhdan and Uma Sankar (Department of Pathology and Molecular Medicine) for providing valuable insights about the adenovirus titer assay.

2.7. References

1. Ginn, S. L., Amaya, A. K., Alexander, I. E., Edelstein, M. & Abedi, M. R. Gene therapy clinical trials worldwide to 2017 - an update. J. Gene Med. e3015 (2018). doi:10.1002/jgm.3015
2. Ungerechts, G. et al. Moving oncolytic viruses into the clinic: clinical-grade production, purification, and characterization of diverse oncolytic viruses. Mol. Ther. - Methods Clin. Dev. 3, 16018 (2016).
3. Lawler, S. E., Speranza, M.-C., Cho, C. F. & Chiocca, E. A. Oncolytic viruses in cancer treatment. JAMA Oncol. 3, 841 (2017).
4. van der Loo, J. C. M. & Wright, J. F. Progress and challenges in viral vector manufacturing. Hum. Mol. Genet. 25, R42–R52 (2016).
5. Diallo, J.-S. et al. Compositions and methods for viral sensitization. 1, (2018).

6. Vellinga, J. et al. Challenges in Manufacturing Adenoviral Vectors for Global Vaccine Product Deployment. Hum. Gene Ther. (2014). doi:10.1089/hum.2014.007

7. Nestola, P. et al. Improved virus purification processes for vaccines and gene therapy. Biotechnol. Bioeng. 112, 843–857 (2015).

8. Eglon, M. N., Duffy, A. M., O'Brien, T. & Strappe, P. M. Purification of adenoviral vectors by combined anion exchange and gel filtration chromatography. J. Gene Med. 10, 610–618 (2008).

9. Morenweiser, R. Downstream processing of viral vectors and vaccines. Gene Ther. 12, S103–S110 (2005).

10. Gagnon, P. The emerging generation of chromatography tools for virus purification. BioProcess Int 24–30 (2008).

11. Orr, V., Zhong, L., Moo-Young, M. & Chou, C. P. Recent advances in bioprocessing application of membrane chromatography. Biotechnol. Adv. 31, 450–465 (2013).

12. Madadkar, P., Wu, Q. & Ghosh, R. A laterally-fed membrane chromatography module. J. Memb. Sci. 487, 173–179 (2015).

13. Madadkar, P. & Ghosh, R. High-resolution protein separation using a laterally-fed membrane chromatography device. J. Memb. Sci. 499, 126–133 (2016).

14. Madadkar, P., Nino, S. L. & Ghosh, R. High-resolution, preparative purification of PEGylated protein using a laterally-fed membrane chromatography device. J. Chromatogr. B Anal. Technol. Biomed. Life Sci. 1035, 1–7 (2016).

15. Sadavarte, R., Madadkar, P., Filipe, C. D. & Ghosh, R. Rapid preparative separation of monoclonal antibody charge variants using laterally-fed membrane chromatography. J. Chromatogr. B Anal. Technol. Biomed. Life Sci. 1073, 27–33 (2018).

16. Madadkar, P., Sadavarte, R., Butler, M., Durocher, Y. & Ghosh, R. Preparative separation of monoclonal antibody aggregates by cation-exchange laterally-fed membrane chromatography. J. Chromatogr. B Anal. Technol. Biomed. Life Sci. 1055–1056, 158–164 (2017).

17. Ghosh, R. & Madadkar, P. Laterally-fed membrane chromatography device. 1–33 (2017).

18. Umatheva, U., Madadkar, P., Selvaganapathy, P. R. & Ghosh, R. Computational fluid dynamic (CFD) simulation of laterally-fed membrane chromatography. Chem. Eng. Res. Des. 137, 412–420 (2018).

19. Bewig, B. & Schmidt, W. E. Accelerated titering of adenoviruses. Biotechniques 28, 871–873 (2000).

20. Peixoto, C., Ferreira, T. B., Sousa, M. F. Q., Carrondo, M. J. T. & Alves, P. M. Towards purification of adenoviral vectors based on membrane technology. Biotechnol. Prog. 24, 1290–1296 (2008).

21. Pol, J. G. et al. Maraba virus as a potent oncolytic vaccine vector. Mol. Ther. 22, 420–429 (2014).

Chapter 3

A direct comparison of anion exchange membranes for virus purification applications

3. A direct comparison of anion exchange membranes for virus purification applications

Karina Kawka, A. Noelle Wilton, Eric J. Redmond, Maria Fe C. Medina, Brian D. Lichty, Raja Ghosh, David R. Latulippe

Prepared for Journal submission

3.1. Abstract

Viruses are an emerging class of biotherapeutics with great potential to treat a breadth of diseases. Ion-exchange membrane chromatography is commonly used for virus purification in either bind-and-elute or flow-through modes. Two of the most widely used ion-exchange membranes are the Mustang Q (from Pall) and the Sartobind Q (from Sartorius) – both are strong anion-exchangers functionalized with amine ligands. While previous studies have attempted to compare the performance of these two membranes, those efforts have been hindered mostly because they are not available commercially in equivalent formats. In this work, we fabricated laterally-fed membrane chromatography (LFMC) devices containing the equivalent amount (1 mL) of the Mustang Q or Sartobind Q membranes and then compared their performance based on residence time distributions, the elution patterns of pre-purified biomolecules, and the ability to purify adenovirus from a clarified cell lysate. The key differences between the membranes were found in regards to the adenovirus elution patterns. For the same linear gradient pattern, the elution of pre-

purified adenovirus appeared approximately one membrane volume earlier from Sartobind Q than Mustang Q. The same effect was found in purification experiments with clarified cell lysate which resulted in the Sartobind Q device being able to remove 48% more DNA impurities compared with Mustang Q; importantly the same level of adenovirus recovery was found for devices made from both membranes. The results from this study are important in that they include a comprehensive comparison of two widely used membrane adsorbers for virus manufacturing and also because it establishes the LFMC device as a useful method for evaluating true membrane performance.

3.2. Introduction

Virus-based therapeutics have now become a key sector of the biopharmaceutical industry – they are used as vaccines against viral diseases, as vectors to deliver therapeutic genes, and as oncolytic agents in immunotherapies. Adenoviruses have been used in a good portion of the many clinical trials both completed and in progress due to a multitude of reasons including their broad cell tropism in quiescent and non-quiescent cells, their inability to integrate into the host genome, their well-understood structure and replication cycle, and their high capacity for therapeutic gene integration.[1-3]

Recent advances in the manufacturing of adenoviral vectors. In general, this involves virus propagation in producer cell cultures capable of yielding high titers,[3] followed by cell lysis, which releases the virus and impurities such as host cell proteins and DNA, which must be removed by the subsequent steps to meet FDA standards. Anion-exchange chromatography is commonly used for adenovirus separations because of the

acidic isoelectric point of this virus, which will cause it to interact with the chromatography medium reversibly, depending on the solution conditions.[4] Packed-bed chromatography has been used for the purification of adenoviruses in place of less scalable alternatives, such as density gradient ultracentrifugation, but are still subject to several major limitations.[5,6] With packed-bed chromatography, the pressure drop across the bed is typically high, and often increases throughout a run due to bed deformation or pore blockage; scale-up is very difficult, and these columns must be extensively validated for adequate cleaning. Additionally, packed-bed chromatography relies on diffusive mass transfer, which limits the binding of large particles to the surface of the stationary phase as they are too large to diffuse inside the beads.[4,7,8] Given this, traditional packed-bed chromatography is not the ideal platform for the capture of large particles such as viruses. Membrane chromatography (MC) utilizes microporous or macroporous membranes as a support material for ligands with selective binding affinity for different molecules. In MC processes, the transport of solutes to their binding sites occurs through convection, which reduces process time and volume. Additionally, membranes have binding capacity independent of flow rate, lower pressure drops, and can be applied in a single-use format.[8,9] These features address many of the limitations of packed-bed chromatography and make MC a promising platform for virus purification.

Traditionally, the biopharmaceutical industry has considered viruses as product impurities and, therefore, has used anion-exchange chromatography as a polishing step to remove these particles.[10-12] This typically utilizes a flow-through modality, where viruses and other impurities bind to the stationary phase, and the protein product flows through.

However, in gene therapy applications, where the virus is the therapeutic product, anion-exchange membranes can be used in bind-elute mode to perform separation from product impurities such as host cell proteins (HCPs) and DNA.[13] Mustang Q (Pall) and Sartobind Q (Sartorius) are two of the most popular commercially available strong anion-exchange membranes used for the purification of viruses (e.g. Adenovirus,[13] AAV,[19] MVM,[12] MuLV,[10,12,18] PRV[12]). According to the manufacturers, Mustang Q consists of a polyethersulfone membrane with a nominal pore size of 0.8 µm, and Sartobind Q consists of a base regenerated cellulose membrane, with a nominal pore size of 3 µm. Additionally, both membranes are reported by the manufacturers to have polymer ligands containing quaternary ammonium groups grafted to their surface, which are the most commonly used anionic chemistry applied in biopharmaceuticals.[14-16] However, the results of XPS spectra for nitrogen for these membranes indicates the presence of a primary amine (400 eV) peak for the Mustang Q membrane in addition to the expected quaternary amine (402 eV) peak. This is assumed to be the result of the monomer and linker/coupler chemistry used.[17]

As shown in Table 3.1, several studies have compared the performance of devices containing Mustang Q and Sartobind Q membranes in various bioprocessing applications. However, all of these studies used the commercially-available chromatography devices which unfortunately are different in both their flow patterns and the amount of membrane volume. For example, one study compared the performance of a radially-fed device containing 5 mL of Mustang Q membrane to that of a stacked-disc device containing 0.08 mL of Sartobind Q membrane.[14] Thus, there has not been any studies to date that resolve

the effect of device geometry and directly compare the performance of anion-exchange membranes.

Table 3.1. A review of the various bioprocessing applications in which the relative performance of Mustang Q and Sartobind Q membranes was studied. MV: membrane volume.

Application	Mustang Q (Format / MV)	Sartobind Q (Format / MV)
MAb purification (HCP clearance)[21]	Stacked discs / 0.18 mL	Stacked discs / 0.08 mL
MAb purification (DNA clearance)[14]	Radial / 5 mL	Stacked discs / 0.08 mL
Virus clearance[17]	Stacked discs / 0.35 mL	Radial / 1 mL
MAb purification (virus, HCP and DNA clearance)[20]	Stacked discs / 0.35 mL	Radial / 1 mL
Virus purification (recombinant baculovirus of AcMNPV)[22]	Stacked sheet / 0.54 mL	Stacked sheet / 0.46 mL
MAb purification (endotoxin removal)[25]	Stacked discs / 0.18 mL	Syringe Filter / 0.41 mL
Protein purification (dynamic binding capacity, virus reduction, HCP and DNA removal)[24]	Stacked discs / 0.18 mL	Syringe Filter / 0.41 mL
Impurity binding performance (DNA and endotoxin removal)[23]	Stacked discs / 0.35 mL	Radial / 1 mL

LFMC is a fairly new chromatography device that was specifically designed to have an ultra-low dead-volume and uniform flow distribution properties.[26] It has been shown that the LFMC device performs significantly better than radial-flow MC devices for the separation of therapeutic viruses and other biomolecules as discussed in Chapter 2 and in the literature.[13,27-29] In this study, we made LFMC devices with Mustang Q or Sartobind Q membranes which eliminated any device geometry effects and thus allows for a direct comparison of how just the membranes themselves affect separation performance.

3.3. Materials and Methods

3.3.1. Membrane chromatography devices

Laterally fed membrane chromatography (LFMC) devices containing 1 mL of either the Mustang Q (Pall) or Sartobind Q (Sartorius) membrane were assembled as shown in panels A and B of Figure 3.1. A total of six devices were fabricated for this study – three with the middle layer containing 20 layers of Mustang Q (reported thickness = 0.138 mm) and three with the middle layer containing 10 layers of Sartobind Q (reported thickness = 0.275 mm). A comprehensive list of the LFMC device materials and assembly procedures method can be found in Chapter 2.[13] Both the Mustang Q and Sartobind Q membranes are described as strong anion-exchangers functionalized with quaternary ammonium groups. However, as shown by the scanning electron microscopy (SEM) images in panels C and D of Figure 3.1, the two membranes have very different structures. The Mustang Q membrane is made from polyethersulfone (PES) with a reported nominal pore size of 0.8 μm; the Sartobind Q membrane is made from regenerated cellulose with a reported nominal pore size greater than 3 μm.

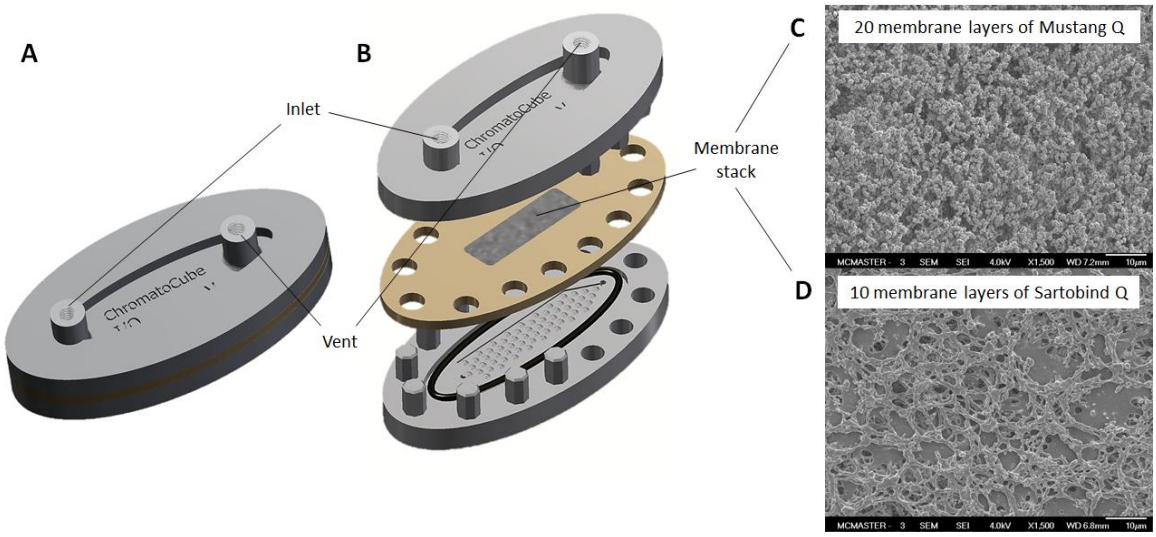

Figure 3.1. External view of the LFMC device; B: Blow-out diagram showing the different parts of the LFMC device; C: Top view SEM image (1500× magnification) of the Mustang Q membrane; D: Top view SEM image (1500× magnification) of the Sartobind Q membrane.

3.3.2. Chromatography experiments

A NGC^{TM} medium-pressure liquid chromatography system (BioRad) with an in-line UV detector module and conductivity meter was used to perform all the device characterization and performance tests. The resulting UV absorbance profiles were analyzed using the built-in tools of the NGC system's ChromLab software. Between tests, the LFMC devices were cleaned in place according to the membrane manufacturer's instructions. Specifically, the Mustang Q device was cleaned by passing a 1 M NaOH solution (BioShop) for 30 minutes at 1 mL/min, followed by a solution of 0.9 M NaCl (BioShop) and 0.1 M NaOH for 5 minutes at 1 mL/min; the Sartobind Q device was cleaned by passing a 1 M NaOH solution for 30 minutes at 1 mL/min, followed by a 1 M solution of NaCl for 3 minutes at 5 mL/min, and finally a 20% ethanol solution for 10 minutes at 2

mL/min. When not in use the NGC system was stored in a solution of 20% ethanol and Milli-Q water.

Tracer experiments were performed by running equilibration buffer (10 mM HEPES, 4% sucrose, 0.36 M NaCl, pH 7.4) at a flow rate of 5 mL/min for 10 membrane volumes (MV) followed by the injection of a pulse of 100 µL of 2% acetone in equilibration buffer and a wash step for 10 MV of equilibration buffer. The composition of equilibration buffer was based on our earlier study of adenovirus purification, which is presented in Chapter 4.[30]

Chromatography experiments were also performed at a flow rate of 5 mL/min and started by passing at least 10 MV of equilibration buffer through the membranes followed by the injection of 1 mL of the following four solutions:

- Bovine serum albumin (BSA) protein standard (Thermo Scientific) at a concentration of 1.6 mg/mL in equilibration buffer. The wavelength for the in-line UV detector module was set at 280 nm.
- 1 Kb Plus DNA ladder (Invitrogen) at a concentration of 10 µg/mL in equilibration buffer; this ladder was selected as it contains DNA fragments between 100 bp and 15,000 bp and thus captures the diverse range of fragment sizes commonly found in adenovirus lysates (Chapter 4).[30] The wavelength for the in-line UV detector module was set at 260 nm.

- Purified adenovirus 5 stock (Robert E. Fitzhenry Vector Laboratory) at a concentration of 6.7×10^9 IFU/mL. The wavelength for the in-line UV detector module was set at 255 nm.
- Clarified cell lysate containing adenovirus 5 (approximately 6.2×10^9 IFU/mL), proteins (approximately 245 µg/mL), and DNA (approximately 689 ng/mL). The cell lysate containing adenovirus was produced from infected suspension 293 cells cultured in CDM4HEK293 media (Hyclone) using spinner flasks as described in detail in Chapters 2 and 4.[13,30] Briefly, centrifugation was used to harvest the cells from culture media, followed by a cell disruption step using three freeze-thaw cycles. The lysate was then clarified by centrifugation and subjected to a DNA digestion step using 100 U/mL of Denarase (c-LEcta) enzyme for 4 hours at 37 °C in 10 mM Tris (BioShop) buffer pH 8, containing 2 mM $MgCl_2$. Finally, the lysate was diluted 6 times in equilibration buffer and further clarified by filtration using Acrodisc syringe filters with 0.45 µm Supor membranes (Pall). The wavelength for the in-line UV detector module was set at 255 nm.

A wash step was then performed by passing 10 MV of equilibration buffer. Next, a linear gradient increase in salt concentration from 0.36 M to 1 M NaCl was performed over 10 MV through the ChromLab software automatically adjusting the proportions of Buffer A (10 mM HEPES, 4% sucrose, pH 7.4) and Buffer B (10 mM HEPES, 4% sucrose, 2 M NaCl, pH 7.4). This higher salt concentration was held for an additional 6 MV. The run duration was approximately 5 minutes with 26 mL of sample collected in total; initially, two 5 mL fractions were collected, followed by ten 1 mL fractions and three 2 mL fractions.

For the runs using adenovirus lysate, all fractions were collected and a solution of 50% glycerol (Caledon Laboratory Chemicals) in equilibration buffer was added (for a final 10% glycerol) before samples were stored at -80 °C until further virus, protein, and DNA analysis. Fractions collected during the runs using adenovirus lysate were analysed for the presence of adenovirus and DNA using the hexon staining and PicoGreen assays, respectively, as previously described in Chapter 2.[13,30]

3.4. Results and discussion

3.4.1. Hydrodynamic characterization of Mustang Q and Sartobind Q LFMC devices

The required pressures to operate the NGC^{TM} system with either the Mustang Q or Sartobind Q LFMC devices at three different flow rates of equilibration buffer are displayed in Table 3.2. This demonstrated that Mustang Q devices yielded overall higher pressures than Sartobind Q devices, with the difference being more noticeable at increasing flow rates. For example, at 1 mL/min, the baseline pressure of the NGC system without any device attached was 20.7 kPa while it was an average of 26.8 kPa with Mustang devices and 21.6 kPa with Sartobind devices; at 5 mL/min (flow rate used in the remaining experiments discussed in this study) the baseline pressure of the NGC system was 89.6 kPa, 117.8 kPa with Mustang devices and 98.2 kPa with Sartobind devices. The higher pressures observed with Mustang devices are likely due to the smaller nominal pore size of the membrane, as well as the requirement of 20 membrane layers in this device (as opposed to the 10 layers in the Sartobind Q device), which is understood to decrease the "effective" pore size of the membrane.[17] Moreover, the membranes are composed of different base materials, which might affect their respective permeabilities. These results indicate that it

is possible to operate below the maximum pressure ratings of commercially available Mustang Q and Sartobind Q devices (550 kPa and 400 kPa, respectively) at the selected flow rate of 5 mL/min used across the chromatography runs presented in this study. Based on the results, a flow rate of 5 mL/min was selected for the chromatography experiments since this flow rate allowed operation at pressures below the maximum suggested by the membrane manufacturers of 550 kPa and 400 kPa for Mustang Q and Sartobind Q, respectively.

Table 3.2. Average pressure as a function of flow rate for the NGC chromatography system without an LFMC device attached, and for three LFMC devices containing Mustang Q and three LFMC devices containing Sartobind Q. The displayed averages and standard deviation were calculated over the pressures obtained with the three devices with each membrane.

Flow rate	**1 mL/min**	**5 mL/min**	**9 mL/min**
		Pressure (kPa)	
NGC system	20.7	89.6	164.1
Sartobind Q	21.6 ± 1.4	98.2 ± 7.7	176.9 ± 11.9
Mustang Q	26.8 ± 1.4	117.8 ± 1.9	211.1 ± 6.2

Two of the LFMC devices discussed above, one containing Mustang Q (LMQ 2) and one containing Sartobind Q (LSQ 3), were randomly selected to be used in the remaining experiments in this study. Initially, the hydrodynamics of the two devices were evaluated via acetone tracer experiments by injecting 100 µL pulses of 2% acetone solution in equilibration buffer and monitoring the UV absorbance at 280 nm. Acetone was selected for these experiments because it does not interact with either of these anion-exchange membranes. As shown in Figure 3.2, the profiles from the duplicate runs on each device are indistinguishable and the peaks for both devices started at approximately the same volume (1.2 mL for Mustang Q and 1.1 mL for Sartobind Q).

and thus have similar void volumes; this observation indicated to us that the variations between our ‘in-house’ assembled devices were minimal. This observation eliminates the concern of device-to-device variability introduced in the fabrication process and enables comparisons solely on membrane characteristics. The average areas under the peaks were also similar for both devices, being 225 mL·mAU for Mustang Q and 237 mL·mAU for Sartobind Q. The main difference between the devices resides in the fact that Mustang yielded slightly sharper peaks with an average height of 388 mAU and width at half height of 0.44 mL compared with Sartobind which had an average height of 321 mAU and width at half height of 0.55 mL. Peak asymmetry was also slightly lower for Mustang Q (3.9) than that for Sartobind Q (4.4). The difference observed between the two membranes can be attributed to their different structures and pore sizes. Mustang Q, having smaller pore size and a more compact nature as indicated by the SEM images in Figures 3.1C and 3.1D, contributed to sharper peaks to be obtained in the tracer experiments. Moreover, the greater uniformity of pore sizes for the Mustang membrane as Figure 3.1C suggests could also be contributing to more uniform flow distribution within the membrane given the dispersion effects resulting from lower variability in path length.

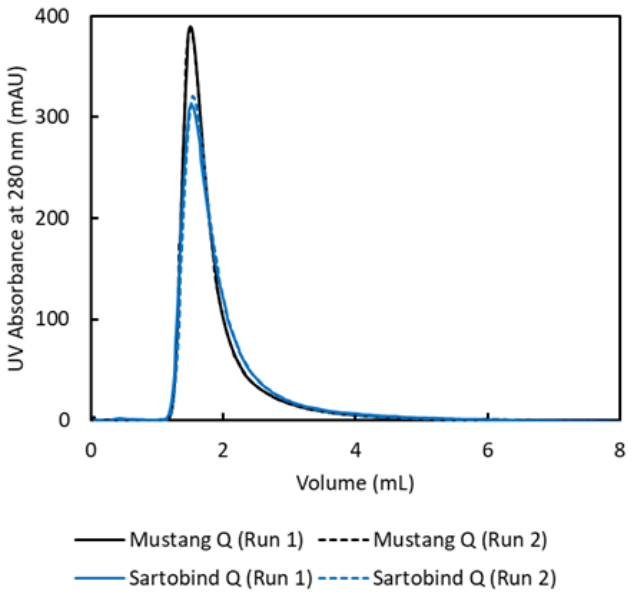

Figure 3.2. Acetone tracer experiment with a Mustang Q and a Sartobind Q LFMC devices. Tests were performed using equilibration buffer containing 10 mM HEPES, 4% sucrose, 360 mM NaCl, pH 7.4, and by injecting a pulse of 100 µL of a 2% acetone solution in equilibration buffer.

3.4.2. Chromatography runs with single-component feed materials: DNA, protein and purified adenovirus standard

Runs were performed with single component feed samples to assess individual interactions with each membrane type, free of competitive interferences – therefore enabling comparison of Mustang Q and Sartobind Q based on individual interactions of protein, virus, and DNA. To ensure reproducibility of the preparation and purification conditions and procedures, each experimental condition was conducted in duplicate. The elution strategy outlined in Section 3.3.2 was used for both the Mustang Q and Sartobind Q membranes. The UV absorbance and conductivity signals from the duplicate runs are displayed in Figure 3.3, with panels displaying the BSA protein standard, pre-purified

adenovirus, and 1 Kb Plus DNA ladder experiments for both the Mustang Q and Sartobind Q membranes. The retention volume, peak width at half height and asymmetry values are summarized in Table 3.3. These results indicate that, in general, there is a very good agreement between the two runs for all samples.

For both membranes, the protein standard elution (Figure 3.3A/D) is observed in the 'flow-through, indicating that these molecules did not adsorb to the membranes at the loading conditions of 18% Buffer B (0.36 M NaCl). This is consistent with observations of most of the host-cell (HEK-293) protein interactions with Sartobind Q made in Chapters 2 and 4.[13,30] The peak from the Mustang Q membrane eluted after 2.05 mL with asymmetry of 2.54 and peak width at half-height of 1.09 mL. Similarly, the peak eluted from the Sartobind Q device after 1.98 mL with asymmetry of 2.60 and peak width at half-height of 1.14 mL. Additionally, for both membranes, the sample was cleared well before the beginning of the gradient elution, which is desirable from a downstream perspective. Therefore, in terms of protein elution, the membranes perform comparably.

Differences in membrane performance are first notable in the elution profile of the pre-purified adenovirus (Figure 3.3B/E). The asymmetry and peak width at half-height of the virus peak was 4.09 and 0.44 mL for the Mustang Q membrane, and 5.73 and 0.54 mL for the Sartobind Q membrane. Additionally, the virus peak is delayed by almost 1 mL (retention volume = 15.6 mL) for the Mustang Q membrane compared to what is observed for the Sartobind Q membrane (retention volume = 14.8 mL). This result is significant because, in such a gradient elution, later elution is associated with a higher NaCl concentration or conductivity (approximately 46.4 mS/cm for Mustang and 40.4 mS/cm for

Sartobind), which can introduce additional challenges in downstream operations (i.e. desalting before polishing or formulation). This shift is hypothesized to primarily be the result of the difference in pore size between the two membranes, where the overall smaller effective pore size of the Mustang Q membrane bed results in increased retention volume. Additionally, the slightly different membrane chemistries may be interfering with the binding, as it has been shown that the Mustang Q membranes have both primary and quaternary amine groups bound to the core matrix, where Sartobind Q only have a quaternary amine group.[17] From this, the Sartobind Q membrane would appear to have superior performance; however, the elution of DNA and the resolution between the virus and DNA peaks will impact this conclusion.

The elution profiles of the 1 Kb Plus DNA ladder (Figure 3.3C/F) were also observed to differ between the two membranes. The elution from the Mustang Q device had an asymmetry value of 3.0 and a peak width at half-height of 0.63 mL. Unlike the elution from the Mustang Q device, the DNA elution produced using the Sartobind Q device is observed to have a leading ‘shoulder’. Asymmetry and peak width at half-height were hence only calculated for the main peak eluted from the Sartobind Q membrane, which were determined to be 2.79 and 0.7 mL, respectively. Similarly to what was observed previously for the pre-purified virus elution, the retention volume for the DNA standard is shifted back by approximately 0.5 mL with the Mustang Q membrane (retention volume = 20.53 mL) compared to the Sartobind Q membrane (retention volume = 20.05 mL). When considering these results alongside the results of the pre-purified adenovirus runs, there is slightly reduced separation of the virus and DNA peaks for the Mustang Q membrane

(approximate difference of 5 mL in retention volume, compared to 5.3 mL for Sartobind Q). While this difference is can be assumed insignificant in these experiments, it is possible that the reduced separation between the virus and DNA peaks eluted from the Mustang Q membrane may be exacerbated when performing more complex separations (i.e. with both DNA and virus particles present in the same feed solution). This hypothesis will be explored in the following section.

Table 3.3. Summary of peak characteristics (retention time, width at half height, and asymmetry) obtained with the Mustang Q and Sartobind Q membranes. Avg: averages of runs 1 and 2.

Biomolecule	**Membrane**	**Retention volume (mL)**			**Peak width at half height (mL)**			**Asymmetry**		
		Run 1	**Run 2**	***Avg***	**Run 1**	**Run 2**	***Avg***	**Run 1**	**Run 2**	***Avg***
BSA protein standard	Mustang Q	2.05	2.05	*2.05*	1.11	1.06	*1.09*	2.82	2.54	*2.68*
	Sartobind Q	1.95	2.00	*1.98*	1.15	1.13	*1.14*	3.10	2.60	*2.85*
Purified adenovirus	Mustang Q	15.60	15.55	*15.58*	0.45	0.43	*0.44*	3.47	4.71	*4.09*
	Sartobind Q	14.75	14.80	*14.78*	0.55	0.53	*0.54*	5.92	5.54	*5.73*
1 Kb Plus DNA ladder	Mustang Q	20.50	20.55	*20.53*	0.64	0.62	*0.63*	3.13	2.86	*3.00*
	Sartobind Q	20.00	20.10	*20.05*	0.67	0.72	*0.70*	2.87	2.71	*2.79*

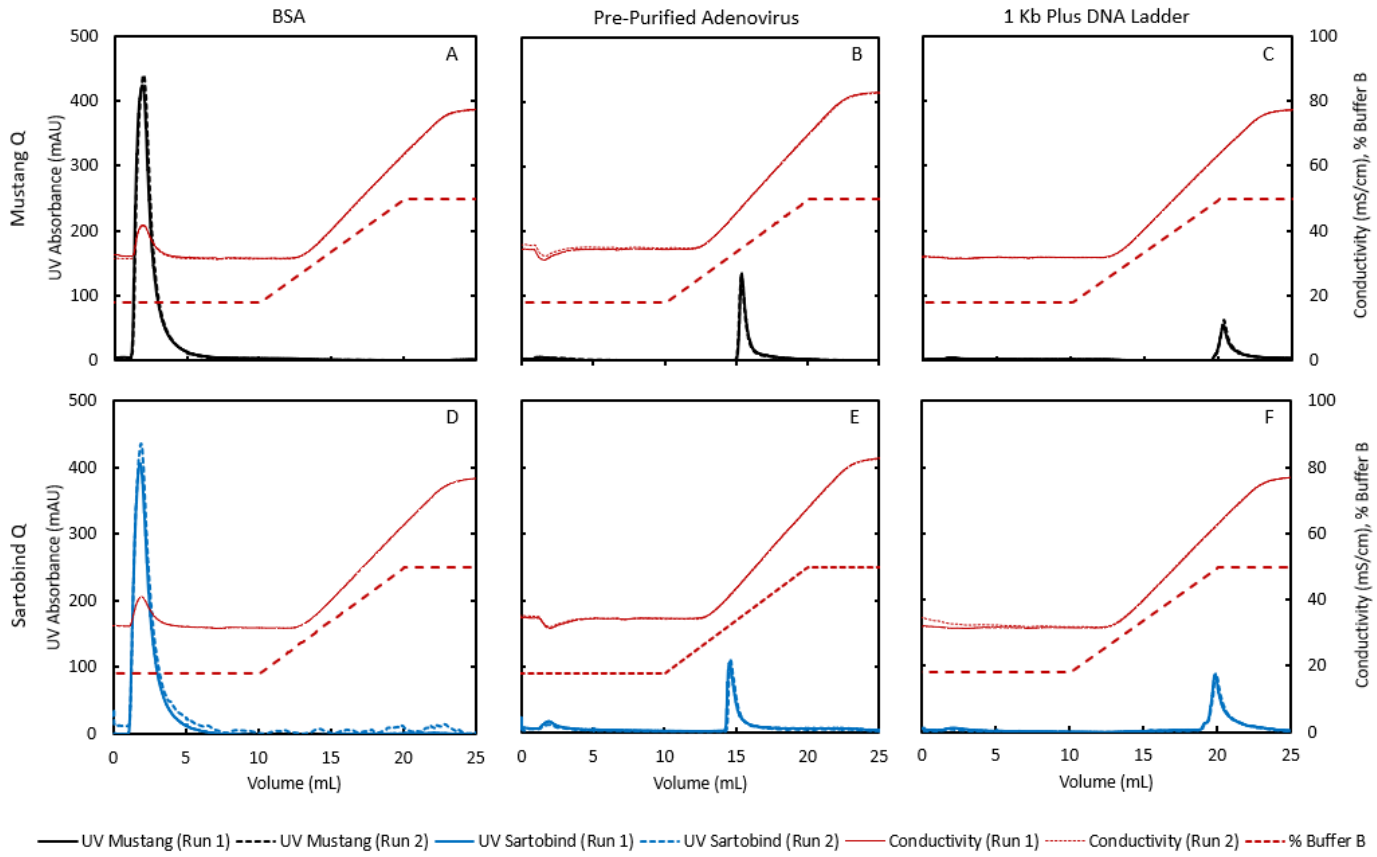

Figure 3.3. UV absorbance (280 nm) and conductivity profiles for BSA protein standard (1.6 mg/mL) chromatography runs using the Mustang Q (panel A) and Sartobind Q (panel D) LFMC devices. UV absorbance (255 nm) and conductivity profiles for pre-purified adenovirus standard (6.7×10^{9} IFU/mL) chromatography runs using the Mustang Q (panel B) and Sartobind Q (panel E) LFMC devices. UV absorbance (260 nm) and conductivity profiles for 1 Kb Plus DNA ladder (10 µg/mL) chromatography runs using the Mustang Q (panel C) and Sartobind Q (panel F) LFMC devices.

3.4.3. Chromatography runs with cell lysates containing adenovirus

To confirm the results found for the Mustang Q and Sartobind Q membranes in the previous section for a realistic feed solution, adenovirus cell lysate was purified using the same experimental conditions on both membrane devices. A 1 mL aliquot of the lysate was injected into the devices using a sample loop, and it contained an average of 6.3×10^{9} ± 1.1×10^{9} IFU of adenovirus, 245 ± 55 μg of protein, and 689 ± 30 ng of DNA in total. Figure 3.4 displays the UV absorbance at 255 nm and the amounts of virus and DNA in each. The first large peak in the flow-through corresponds to unbound biomolecules, which based on previous studies, are mostly proteins (Chapter 2),[13,30] along with small amounts of DNA (39 ± 2 ng for Mustang and 44 ± 3 ng for Sartobind) and very small amounts of virus (8.2×10^{4} ± 5.0×10^{4} IFU for Mustang and 1.1×10^{5} ± 2.3×10^{4} IFU for Sartobind) in the fractions between the 1 and 5 mL marks. The retention volume, width at half-height, and asymmetry values for the first peak (using UV absorbance at 280 nm to enable comparison with the BSA runs) were 2.00 mL, 1.18 mL, and 3.32, respectively, for Mustang and 2.07 mL, 1.26 mL, and 2.50, respectively, for Sartobind. These values are very close to what was predicted by the single-component runs using BSA as the model protein, shown in Table 3.3. Although the intensity (height) of the first peaks were distinct in comparison with the BSA runs due to differences in the concentrations and the presence of small amounts of virus and DNA in the run with lysate, the agreement between peak parameters indicates that BSA was a suitable molecule to predict the behaviour of the mixture of unbound molecules in the runs with adenovirus lysates for both membranes.

As seen in Figure 3.4C, for the Mustang Q device, the peak corresponding to the adenovirus (considering UV at 255 nm) started at the 15.4 mL mark, while for Sartobind Q, the elution peak started at approximately 1 mL before that, at the 14.3 mL mark. These results are in good agreement and follow the same trend predicted by the runs with purified adenovirus shown in Table 3.3, confirming that adenoviruses elute earlier from the Sartobind Q device when the same elution gradient is applied. This fact is further quantitatively demonstrated in Table 3.4, where the average conductivity over the fractions containing most of the virus is given and demonstrate the elution at lower conductivities from Sartobind Q. The reason for this observation is unclear, but as was stated in the previous section, is likely related to a combination of different membrane chemistries and effective pore size. The Mustang Q membrane was shown to have primary and quaternary amine functional groups while Sartobind Q only has quaternary amine groups,[17] which could impact the interactions happening between virus and membrane. Additionally, the smaller pore size (0.8 μm) and increased number of membrane layers (20) in the LFMC device for Mustang Q (as opposed to 3 μm and 10 layers for Sartobind Q, respectively), could cause greater resistance to the permeation of large molecules such as adenovirus (approximately 0.1 μm in diameter). Further investigation is needed to fully understand the mechanisms behind the difference in retention volumes for Mustang Q and Sartobind Q. In practical terms, the elution at lower salt concentrations as the one achieved with the Sartobind Q is advantageous because it facilitates the desalting step commonly employed after the chromatography in adenovirus manufacturing.[5] The adenovirus UV at 255 nm peaks obtained in these runs were slightly lower and broader, with width at half heights of

0.63 mL and 0.61 mL for Mustang and Sartobind, respectively, as compared with the results obtained with purified adenovirus shown in discussed in Section 3.4.2. On the other hand, these peaks were more symmetric (2.08 for Mustang and 2.68 for Sartobind) as compared with those obtained with pure adenovirus. These differences can be attributed to the presence of impurities, mostly DNA as discussed below, that co-eluted with the virus in the runs with lysate. Apart from the differences in retention volumes, no significant difference was observed in terms of virus recovery for the two membranes as indicated by Table 3.4. Considering the 3 mL fractions were most of the virus eluted from each device, a total of $3.7\times10^{9} \pm 7.0\times10^{8}$ IFU was recovered with Mustang and $3.8\times10^{9} \pm 7.1\times10^{8}$ IFU was recovered with Sartobind; these numbers correspond to approximately 59% and 60% of the average amount of virus in the feed, respectively.

There was a notable difference between the two membranes in terms of the UV profile that followed the main virus peaks highlighted in Figure 3.4C. While a flat tail followed the virus peak with Sartobind up to past the 18 mL mark, for the Mustang device, an additional small peak appeared after the virus peak. In both cases, the fractions right after the virus elution contained mostly DNA as shown in Figures 3.4A and 3.4B. Analysis of the DNA content in the fractions containing most of the virus as shown in Table 3.4 and Figures 3.4A and 3.4B indicated that more DNA impurities co-eluted with the virus with the Mustang Q membrane compared to the Sartobind Q membrane. The 3 mL fraction containing most of the virus had an average of 155 ng of DNA for the runs with Mustang and 105 ng for the runs with Sartobind. These numbers correspond to approximately 22% and 15% of the amount of DNA in the feed lysate, respectively. Finally, the level of protein

impurities that co-eluted with the virus were below 100 µg/mL. This is in good agreement with the observations made in Section 3.4.2, where, based on the single component runs, it was predicted that there may be reduced separation between the virus and DNA eluate for the Mustang Q membrane.

Overall, the results obtained with model molecules as discussed in Section 3.4.2 provided a good prediction of the performance of the two membranes for the purification of complex mixtures such as adenovirus lysates. The exception was in terms of the degree of separation of virus and DNA. While good resolution was demonstrated based on the fully resolved peaks for purified virus and DNA ladder observed in Figure 3.3, small amounts of DNA did co-eluted with the virus. The two membranes presented very similar performance with Sartobind Q being slightly advantageous under the conditions used in this study, as it allowed virus elution at lower salt concentrations and provided approximately 32% greater DNA removal. Other membrane characteristics such as dynamic binding capacity, cost, and durability, were not addressed in this study but can be critical parameters when selecting appropriate materials for a given application.

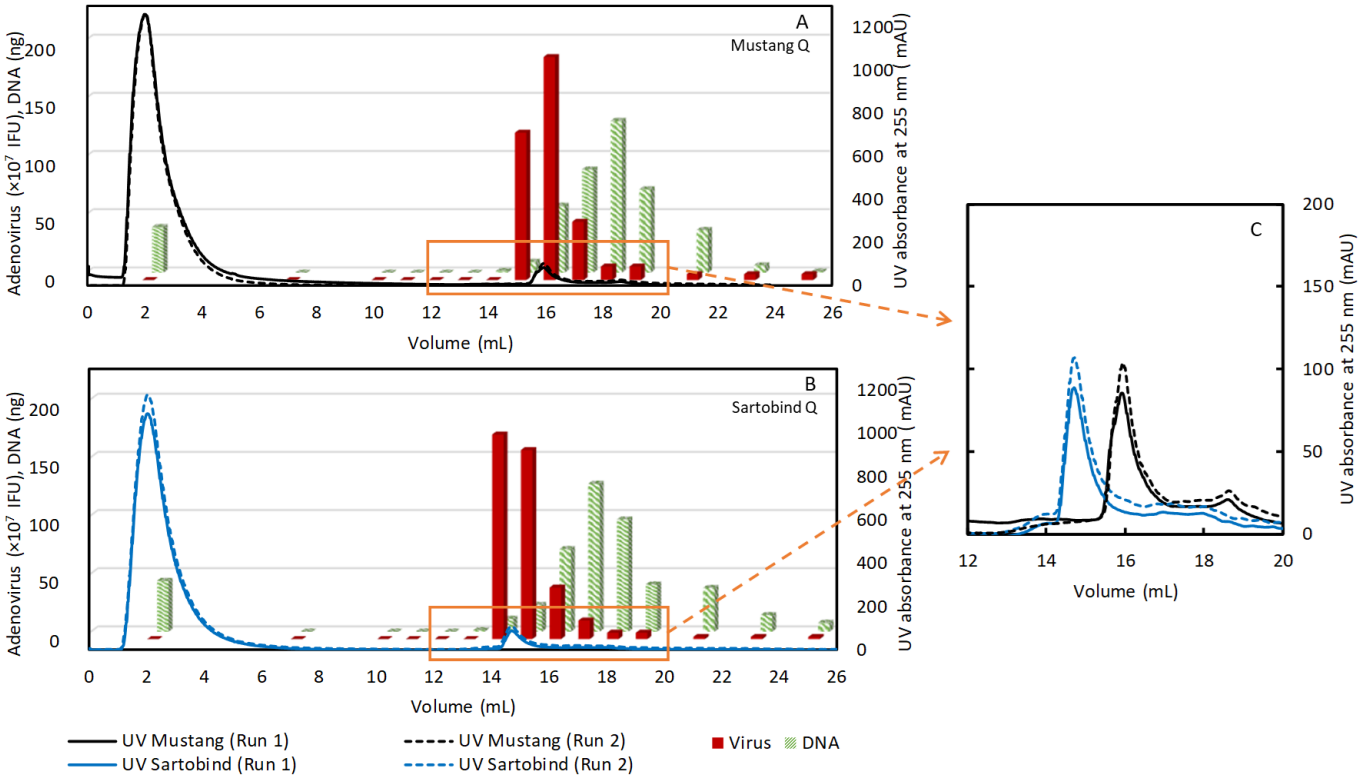

Figure 3.4. UV absorbance (255 nm) profiles and amounts of virus (solid red bars) and DNA (striped green bars) in each fraction of adenovirus cell lysate chromatography runs using the Mustang Q (A) and Sartobind Q (B) LFMC devices. The first peaks indicate the flow-through elution of unbound biomolecules (primarily host-cell protein); the second peaks indicate the elution adenovirus followed by DNA. The same gradient elution profiles shown in Figure 3.3 were applied in this experiment; conductivity and buffer B profiles were omitted for simplicity. Expanded view of UV absorbance (255 nm) in elution volume range (12 to 20 mL) for Mustang Q and Sartobind Q (C).

Table 3.4. Comparison of the composition of selected fractions from adenovirus cell lysate chromatography runs using Mustang Q and Sartobind Q LFMC devices

Membrane	**Mustang Q**			**Sartobind Q**		
Fraction volume	1 mL[a]	2 mL[b]	3 mL[c]	1 mL[d]	2 mL[e]	3 mL[f]
Conductivity (mS/cm)	46.5 ± 1.5	49.0 ± 2.9	51.5 ± 4.4	41.3 ± 1.3	43.7 ± 2.8	46.1 ± 4.2
Virus (IFU)	$1.3\times10^9 \pm 2.7\times10^8$	$3.2\times10^9 \pm 5.8\times10^8$	$3.7\times10^9 \pm 7.0\times10^8$	$1.8\times10^9 \pm 4.0\times 10^8$	$3.4\times10^9 \pm 6.4\times10^8$	$3.8\times10^9 \pm 7.1\times10^8$
DNA (ng)	9.4 ± 0.8	66.9 ± 4.0	155.6 ± 8.4	11.2 ± 0.9	34.2 ± 6.9	105.2 ± 16.4

[a] Corresponds to the volume eluted between the 15 and 16 mL marks in Figure 3.4 from the Mustang Q device.
[b] Corresponds to the volume eluted between the 15 and 17 mL marks in Figure 3.4 from the Mustang Q device.
[c] Corresponds to the volume eluted between the 15 and 18 mL marks in Figure 3.4 from the Mustang Q device.
[d] Corresponds to the volume eluted between the 14 and 15 mL marks in Figure 3.4 from the Sartobind Q device.
[e] Corresponds to the volume eluted between the 14 and 16 mL marks in Figure 3.4 from the Sartobind Q device.
[f] Corresponds to the volume eluted between the 14 and 17 mL marks in Figure 3.4 from the Sartobind Q device.

3.5. Conclusions

The Mustang Q and Sartobind Q membranes have been compared through several works due to their similar applications in the biopharmaceutical industry. However, these membranes are not available for purchase at the same scale or format, which has prevented direct comparison of their separation performance. Through the application of the LFMC technology, this work was able to perform a never before published head-to-head comparison on the performance of these two membranes in the presence of a variety of feed solutions typical of gene-therapy manufacturing applications.

Tracer experiments demonstrated comparability between the Mustang Q and Sartobind Q devices based on active membrane area and hold up volume. Pressure drop experiments were used to confirm appropriate flow rates and demonstrate further that the devices prepared were done in such a reproducible way, thus eliminating the concern that the observations made in this study were confounded with device interferences. Through chromatography runs performed on a BioRad NGC system, the membranes were found to have comparable performance in protein separation, both with the BSA standard and the host cell protein separation in experiments using cell lysates. However, the characteristics of the virus and DNA separations differed slightly between the two membranes. In both the single-component and virus lysate experiments, the virus was observed to elute earlier with the Sartobind Q membrane. This is of advantage over the Mustang Q membrane, as lower salt has benefits in further downstream processing and formulation. Additionally, analysis of fractions collected from the virus lysate experiments demonstrated that the Sartobind Q membrane provided approximately 48% greater DNA removal over the Mustang Q membrane. These proved to be the two main advantages of Sartobind Q, as there was no statistical difference in virus recovery between the two membranes. Therefore, this work was able to conclude that the Sartobind Q membrane is preferable for the purification of adenovirus. Furthermore, these results can conclude that in general, while these membranes may appear equivalent based on chemistry and are often used interchangeably in industry, the differences in pore size and chemistry are relevant and have effects on their separation performance.

3.6. Acknowledgements

Funding was provided by: Ontario Research Fund-Research Excellence program; BioCanRx, a Networks of Centres of Excellence program, in the form of a Summer Studentship Award to ANW; Natural Sciences and Engineering Research Council of Canada (NSERC) in the form of a Discovery Grant (to DRL) and Undergraduate Student Research Award (to EJR). The authors thank Mr. Paul Gatt from the Department of Chemical Engineering at McMaster University for his assistance in fabricating the LFMC device, Ms. Natasha Kazhdan from the McMaster Immunology Research Centre (Department of Pathology and Molecular Medicine) for her assistance with culturing adenovirus batches, and Mr. Ryan LaRue for acquiring the SEM images of the membranes.

3.7. References

1. Ginn, S. L., Amaya, A. K., Alexander, I. E., Edelstein, M. & Abedi, M. R. Gene therapy clinical trials worldwide to 2017 - an update. J. Gene Med. e3015 (2018). doi:10.1002/jgm.3015
2. Dormond, E., Perrier, M. & Kamen, A. From the first to the third generation adenoviral vector: What parameters are governing the production yield? Biotechnol. Adv. 27, 133–144 (2009).
3. Ungerechts, G. et al. Moving oncolytic viruses into the clinic: clinical-grade production, purification, and characterization of diverse oncolytic viruses. Mol. Ther. - Methods Clin. Dev. 3, 16018 (2016).
4. Miesegaes, G. R., Lute, S. C., Read, E. K. & Brorson, K. A. Viral clearance by flow-through mode ion exchange columns and membrane adsorbers. Biotechnol. Prog. 30, 124–131 (2014).
5. Vellinga, J. et al. Challenges in Manufacturing Adenoviral Vectors for Global Vaccine Product Deployment. Hum. Gene Ther. (2014). doi:10.1089/hum.2014.007
6. Bo, H. et al. Chromatographic purification of adenoviral vectors on anion-exchange resins. Eur. J. Pharm. Sci. 67, 119–125 (2015).

7. Ljunglöf, A., Bergvall, P., Bhikhabhai, R. & Hjorth, R. Direct visualisation of plasmid DNA in individual chromatography adsorbent particles by confocal scanning laser microscopy. J. Chromatogr. A 844, 129–135 (1999).

8. Ghosh, R. Protein separation using membrane chromatography: Opportunities and challenges. J. Chromatogr. A 952, 13–27 (2002).

9. Curling, J. & Gottschalk, U. Process Chromatography: Five Decades of Innovation. BioPharm Int. 20, 70–94 (2007).

10. Knudsen, H. L., Fahrner, R. L., Xu, Y., Norling, L. A. & Blank, G. S. Membrane ion-exchange chromatography for process-scale antibody purification. J. Chromatogr. A 907, 145–154 (2001).

11. Van Reis, R. & Zydney, A. Membrane separations in biotechnology. Curr. Opin. Biotechnol. 12, 208–211 (2001).

12. Zhou, J. X. & Tressel, T. Basic concepts in Q membrane chromatography for large-scale antibody production. Biotechnol. Prog. 22, 341–349 (2006).

13. Kawka, K. et al. Purification of therapeutic adenoviruses using laterally-fed membrane chromatography. J. Memb. Sci. 579, 351–358 (2019).

14. Stone, M. C., Borman, J., Ferreira, G. & Robbins, P. D. Effects of pH, conductivity, host cell protein, and DNA size distribution on DNA clearance in anion exchange chromatography media. Biotechnol. Prog. 34, 141–149 (2018).

15. Sartorius Stedim Biotech. Operating Instructions: Sartobind® Q and S Membrane Adsorbers for 4 and 8 mm bed height. (2016). doi:10.1038/cddis.2011.143

16. Pall Biotech. Mustang ® Q XT Chromatography Capsules Meeting Process Demands for Scalability and Economy.

17. Weaver, J., Husson, S. M., Murphy, L. & Wickramasinghe, S. R. Anion exchange membrane adsorbers for flow-through polishing steps: Part I. clearance of minute virus of mice. Biotechnol. Bioeng. 110, 491–499 (2013).

18. McNally, D. J., Darling, D., Farzaneh, F., Levison, P. R. & Slater, N. K. H. Optimised concentration and purification of retroviruses using membrane chromatography. J. Chromatogr. A 1340, 24–32 (2014).

19. Pall Biotech. Scalable Purification of High Yield Adeno-Associated Virus and Lentivirus Gene Therapy Vectors Using Membrane Chromatography. (2019).

20. Weaver, J., Husson, S. M., Murphy, L. & Wickramasinghe, S. R. Anion exchange membrane adsorbers for flow-through polishing steps: Part II. Virus, host cell protein, DNA clearance, and antibody recovery. Biotechnol. Bioeng. 110, 500–510 (2013).

21. Trnovec, H., Doles, T., Hribar, G., Furlan, N. & Podgornik, A. Characterization of membrane adsorbers used for impurity removal during the continuous purification of monoclonal antibodies. J. Chromatogr. A 1609, 460518 (2020).

22. Grein, T. A., Michalsky, R., Vega López, M. & Czermak, P. Purification of a recombinant baculovirus of Autographa californica M nucleopolyhedrovirus by ion exchange membrane chromatography. J. Virol. Methods 183, 117–124 (2012).

23. Woo, M. et al. A novel primary amine-based anion exchange membrane adsorber. J. Chromatogr. A 1218, 5386–5392 (2011).

24. Shirataki, H., Sudoh, C., Eshima, T., Yokoyama, Y. & Okuyama, K. Evaluation of an anion-exchange hollow-fiber membrane adsorber containing γ-ray grafted glycidyl methacrylate chains. J. Chromatogr. A 1218, 2381–2388 (2011).

25. Serdakowski London, A., Kerins, B., Tschantz, W. R. & Mackay, K. Endotoxin removal and prevention for pre-clinical biologics production. Biotechnol. J. 7, 1509–1516 (2012).

26. Madadkar, P., Wu, Q. & Ghosh, R. A laterally-fed membrane chromatography module. J. Memb. Sci. 487, 173–179 (2015).

27. Madadkar, P. & Ghosh, R. High-resolution protein separation using a laterally-fed membrane chromatography device. J. Memb. Sci. 499, 126–133 (2016).

28. Madadkar, P., Sadavarte, R., Butler, M., Durocher, Y. & Ghosh, R. Preparative separation of monoclonal antibody aggregates by cation-exchange laterally-fed membrane chromatography. J. Chromatogr. B Anal. Technol. Biomed. Life Sci. 1055–1056, 158–164 (2017).

29. Sadavarte, R., Madadkar, P., Filipe, C. D. & Ghosh, R. Rapid preparative separation of monoclonal antibody charge variants using laterally-fed membrane chromatography. J. Chromatogr. B Anal. Technol. Biomed. Life Sci. 1073, 27–33 (2018).

30. Kawka, K. et al. Integrated development of enzymatic DNA digestion and membrane chromatography processes for the purification of therapeutic adenoviruses. Sep. Purif. Technol. 254, 117503 (2021).

Chapter 4

Integrated development of enzymatic DNA digestion and membrane chromatography processes for the purification of therapeutic adenoviruses

4. Integrated development of enzymatic DNA digestion and membrane chromatography processes for the purification of therapeutic adenoviruses

Karina Kawka, A. Noelle Wilton, Pedram Madadkar, Maria Fe C. Medina, Brian D. Lichty, Raja Ghosh, David R. Latulippe

Published work at Separation and Purification Technology (Special Issue: Innovation and Perspectives in the Bioseparations Field). Reprinted with permission.

 https://doi.org/10.1016/j.seppur.2020.117503

4.1. Abstract

High titer and purity levels are key requirements for virus-based cancer and gene therapy biopharmaceuticals. However, the task of removing enough host-cell DNA from therapeutic viruses in order to comply with the FDA's 10 ng/dose limit is particularly challenging. In a previous study, we demonstrated the advantages of using laterally-fed membrane chromatography (LFMC) for adenovirus purification. Although this approach achieved >90% DNA removal, significant amounts of DNA remained in the product due to the poor performance of a pre-LFMC DNA digestion step. In the present study, we attempt to improve upon this outcome by employing an integrated approach to process development that examines the interactions between different downstream steps (i.e., clarification, enzymatic DNA digestion, and membrane chromatography (MC)). First, we

identified the most efficient process sequence involving a clarification step followed by a DNA digestion step, as well as three endonucleases (Benzonase®, Denarase®, and Turbonuclease™) that perform similarly with respect to DNA digestion. Next, a factorial design of experiments (DOE) was used to evaluate how enzyme (Benzonase and Denarase) concentration and time impact DNA and virus concentrations after DNA digestion. Since Denarase showed slightly better efficiency, it was used along with a subset of the DOE conditions to evaluate the removal of DNA via MC with Sartobind Q 96-well filter plates. The lowest amount of DNA per dose was achieved using MC in conjunction with feed that had been digested with 10 U/mL of Denarase for 4 hours; as such, this approach was used to prepare lysates, which were then purified using an LFMC device containing 1 mL of Sartobind Q membrane. This process enabled a virus-recovery rate of 73%, and residual DNA levels of 77 ng/dose. Ultimately, the proposed integrated process development approach resulted in an approximately 80-fold improvement in DNA removal.

4.2. Introduction

Human adenoviruses are ubiquitous icosahedral, non-enveloped viruses that commonly cause asymptomatic or mild diseases in infected hosts.[1] Due to their broad cell tropism and high capacity for integrating therapeutic genes into host-cells, some adenoviruses have garnered considerable attention as potential vectors in gene therapy.[2] In fact, adenoviruses are currently used in approximately 20% of clinical trials related to gene therapy.[3] Moreover, there are also numerous studies aimed at reducing the immunogenicity of adenoviruses—thereby, expanding their possible applications—currently in the development stage.[4] Thus, it is expected that adenoviruses will have a strong, long-term

presence in the field of gene therapy. One particularly promising area of adenovirus research is the use of adenoviruses that present oncolytic activity in cancer treatments. For example, a phase I clinical trial conducted by Lang et al.[5] produced promising results regarding the use of oncolytic adenoviruses to treat recurrent malignant glioma. Additionally, researchers have also explored the effectiveness of using oncolytic adenoviruses in combination immunotherapies; for example, a recent phase II clinical trial yielded promising preliminary results regarding the combined use of an oncolytic adenovirus and a monoclonal antibody (Pembrolizumab) for the treatment of glioma.[6] This recent surge in the use of different types of viruses to develop new biotherapeutics highlights the need for efficient, high-yield, scalable, and cost-effective downstream purification processes.

The removal of host-cell DNA is a well-known challenge in the large-scale manufacturing of viruses. The U.S. Food and Drug Administration (FDA) specifies that the final product cannot contain more than 10 ng/dose of host-cell DNA, and that DNA fragments must not exceed 200 base-pairs (bp) in length.[7] The removal of DNA is typically achieved through a combination of two processes: an enzymatic digestion step using recombinant endonucleases, and a separation step using a variety of technologies. A number of endonucleases have been reported to have broad activity with respect to the non-specific cleaving of both DNA and RNA. Benzonase® (Merck KGaA), a recombinant endonuclease produced in Escherichia coli, is commonly used in various bioprocessing applications to remove host-cell DNA[8,9] and/or plasmid DNA.[10] The manufacturer of Benzonase reports that this enzyme is capable of digesting all nucleic acids into short

oligonucleotides (less than 10 base pairs) under optimum processing conditions.[11] Other notable recombinant endonucleases include Denarase® (c-LEcta), which is expressed in Bacillus sp. and has been used in the downstream purification of Influenza A virus,[12,13] and Turbonuclease™ (Accelagen), which is expressed in Serratia marcescens and has been used in the downstream purification of adeno-associated viruses.[14,15]

It is known that the exact conditions used in the DNA digestion step will vary depending on the final application of the virus, with a wide range of endonuclease concentrations (from 1 U/mL to as high as 1000 U/mL) having been reported for virus production.[16-19] Multiple studies have shown that the use of manufacturer-recommended endonuclease concentrations results in the incomplete removal of DNA during the production of lentivirus[10] and influenza A and B viruses;[20] this outcome is most likely due to the fact that virus lysates are complex in nature and do not reflect the ideal conditions under which manufacturers assess the performance of their enzymes. This is a concern because, as other researchers have pointed out, the use of high concentrations of endonuclease significantly increases production costs.[8] Furthermore, given safety concerns related to the presence of residual endonuclease in the final virus product, it is considered good practice to add them in early stages of the process so they can be removed during the subsequent downstream purification steps.[11] With regards to incubation time, endonuclease manufacturers typically report enzyme activity in terms of the amount of DNA that is completely digested after 30 minutes of incubation at 37 °C. However, much longer incubation times have been used in bioprocessing. For example, incubation times of 4 hours[13] and 12 hours[12] were used in two separate studies related to the production of

influenza vaccine. While this approach may be suitable for producing inactivated viral vaccines, there are concerns regarding the impact of long incubation periods at elevated temperatures on the potency of viruses (i.e., infectious titer) intended for use in gene therapy and oncolytic therapy applications.

If DNA is to be removed successfully, it is important to consider the capacity of the post-digestion separation step. For very small-scale production, density gradient ultracentrifugation is widely used to separate the degraded DNA from the virus product; however, while this technique is very effective, it is also highly laborious, time-intensive, and not amenable to scale-up.[21] Conversely, tangential flow filtration is an alternative method that is both scalable and capable of partially removing host-cell DNA during virus concentration via ultrafiltration membranes.[22,23] In addition, chromatography processes have also been widely used for the large-scale purification of recombinant proteins, which makes them another attractive option for virus purification. The relatively large size of virus particles poses problems for conventional packed-bed chromatography, particularly in the form of low capacity and throughput;[21] as such, monoliths and membrane-based chromatography materials have emerged as preferred alternatives, as these materials feature large pore-sizes that enable convective-based mass transfer, and thus, the use of high flow rates. Another concern is that commercially available chromatographic membrane devices (e.g. Mustang® (Pall), Sartobind® (Sartorius)) are manufactured using either stacked disk or radial flow geometries. As recent studies have shown, these geometries result in poor flow distribution inside the device, which in turn affects the separation resolution and degree of sample dilution.[24]

Recent research has demonstrated that laterally-fed membrane chromatography (LFMC) devices are able to overcome the resolution issues inherent to conventional MC devices.[24] The homogenous hydraulic path lengths and residence time in the LFMC device enables high separation resolution and results that are comparable to resin-based chromatography.[25] In a previous study, we demonstrated that LFMC devices outperform conventional radial-flow devices (both containing 1 mL of the Sartobind® Q anion-exchange membrane (Sartorius)) in terms of both resolution and sample dilution for adenovirus purification as discussed in Chapter 2.[16] In that study, we used the endonuclease manufacturer's recommended DNA digestion conditions, which surprisingly resulted in residual DNA amounts of over 20 µg per dose (considering 10^{10} adenovirus infectious units (IFU) per dose) following the digestion step. This high level of impurity in the feed significantly affected the LFMC device's separation performance, which made it clear that the entire purification process needed to be optimized.

Traditionally, the development of biotherapeutics production processes is performed in a 'stepwise' fashion wherein each unit operation is optimized without consideration of their interaction with other unit operations.[26] However, it has been shown that this approach results in overall sub-optimal performance conditions when the various operations are strongly related.[27] One alternative strategy is to use an 'integrated' approach that considers the relevant interactions between all the operations in the purification process. Rathore et al.[26] employed such an approach in their research on therapeutic glycoprotein purification, and were able to increase product yield by 6% as a result of considering the interactions between the protein refolding conditions and the multimodal

chromatography steps. In the field of monoclonal antibody processing, Liu et al.[28] were able to reduce the average manufacturing cost of goods by as much as 50% by employing an integrated approach that sought to optimize the upstream and downstream conditions. In the field of therapeutic viruses, Cruz et al.'s[29] use of an integrated approach that considered upstream and downstream conditions enabled them to identify an important interaction between the specific ultrafiltration area (downstream) and the perfusion rate and time in the bioreactor (upstream).

In this study, we use an integrated approach that considers both the enzymatic DNA digestion step and the membrane chromatography step in order to address the insufficient DNA removal on adenovirus purification presented in Chapter 2.[16] To this end, we used a variety of process improvement tools, including design-of-experiments (DOE) and high-throughput membrane chromatography in a 96-well filter plate format. Ultimately, the identified best process conditions were implemented for adenovirus purification using a scalable MC technology. Briefly, a full-factorial DOE was used to evaluate how two endonucleases (Benzonase and Denarase) at various concentrations and incubation times impacted the final amount of DNA and adenovirus titer after DNA digestion. Next, a subset of the DOE conditions was tested in MC runs the Sartobind Q membrane adsorber in 96-well filter plate format. Finally, the best conditions identified from the 96-well filter plate MC tests were then translated into a purification process based on the LFMC device.

4.3. Materials and Methods

4.3.1. Adenovirus production

An adenovirus stock was produced in suspension 293 cells according to the method detailed in Chapter 2.[16] Briefly, the cells were diluted up to 4×10^5 cell/mL in spinner flasks containing CDM4HEK293 media (Hyclone) and supplemented with 200 mM L-glutamine (BioShop) and 10 mM HEPES (Gibco). Next, the cells were infected with human adenovirus type 5 (multiplicity of infection = 5) and then cultured for 48 h at 37°C. Aliquots of the cell culture were then transferred into 50 mL conical tubes and centrifuged at 1430×g and 4°C for 15 minutes. After centrifugation, the supernatant was discarded and the obtained cell pellets were stored at -80°C.

4.3.2. Cell disruption and enzymatic DNA digestion

The cell pellets obtained from the process described in Section 4.3.1 were thawed in a warm water bath (~37°C) and then combined with 100 µL of enzyme buffer (10 mM Tris (BioShop) and 2 mM of MgCl2 (Sigma), pH 8). Lysing was achieved by subjecting the re-suspended 293 cells to three consecutive ‘freeze-thaw’ cycles using an ethanol-dry ice bath (~-78°C) and a warm water bath (37°C). For a select number of experiments, the lysates from the freeze-thaw step were used directly in the DNA digestion step (conditions are described below) and then clarified via centrifugation at 2060×g and 4°C for 15 minutes. This sequence of steps will be referred to as ‘Process Sequence #1’. For all of the membrane chromatography tests, the lysates from the freeze-thaw step were clarified via centrifugation at 2060×g and 4°C for 15 minutes, with the resulting supernatant being transferred to a clean microcentrifuge tube for the DNA digestion step. This sequence of

steps will be referred to as ‘Process Sequence #2’. Three different enzymes were used in this study: Benzonase (Millipore), Denarase (c-LEcta), and Turbonuclease (Accelagen). For all DNA digestion experiments, the enzymes were pre-diluted in enzyme buffer, which was then added to the cell lysate in equal proportions (i.e., 100 µL of the pre-diluted enzyme for 100 µL of cell lysate). The final mixture was then incubated at 37°C. A 32 full factorial DOE with either Benzonase or Denarase was used to investigate how enzyme concentration (1, 10, and 100 U/mL) and digestion time (1, 4, and 24 h) impact adenovirus and DNA concentrations after digestion. Following digestion, a second round of clarification was performed to further remove cellular debris. This round of clarification was performed via centrifugation at 1430×g and 4°C for 15 minutes, with the resulting supernatant being collected and stored at -80°C to be later used as feed samples in the chromatography runs performed with the 96-well filter plate.

4.3.3. High-throughput screening of membrane chromatography process

Sartobind® Q (Sartorius), a strong anion-exchange reinforced cellulose membrane (pore size range of 3 to 5 µm) functionalized with quaternary ammonium groups, was implemented in a 96-well filter plate format to run 12 MC experiments in parallel. These 12 experiments corresponded to independent duplicate testing of 6 enzymatic digestion conditions: 5 corresponding to the DOE setup conditions described in Section 4.3.2, and one corresponding to a control run with undigested lysate. The 96-well filter plate format is ideal for running high-throughput screening studies, especially when only small amounts of feed sample are available, as the volume of membrane in each filter-plate well is 19 µL, which is over 50 times lower than the that of the smallest Nano capsule radial-flow device

(Sartorius). Additionally, all the equilibrating, binding, washing, and eluting steps described below were performed by centrifuging the 96-well filter plate at 924×g for 2 minutes and collecting the flow-through in a standard round-bottom 96-well microplate. As noted in the literature, such miniaturized formats are ideal for overcoming limitations related to the large number of experiments required for typical process development studies.[30]

The membranes in each filter plate well were first equilibrated through 5 'wash' cycles with a solution consisting of 200 µL of equilibration buffer (10 mM HEPES (Gibco), 4% sucrose (BioShop), and 360 mM NaCl (BioShop) (pH 7.4). The exact composition of this solution was determined through a fairly extensive optimization study on the binding of adenovirus to the Sartobind Q membrane which details are discussed in Appendix A. In summary, adenovirus present in lysates prepared from 50 mL of cell culture could successfully bind to the membrane when the equilibration buffer had 300 mM or 360 mM NaCl; but it was not able to completely bind at 400 mM NaCl. Each feed sample was prepared by diluting 33.3 µL of a digested lysate (see Figure B1 in Appendix B for the exact digestion conditions for Denarase) or a non-digested lysate (for the control run) with 66.7 µL of the same equilibration buffer. A 38 µL aliquot of the diluted feed solution (i.e., two times the volume of membrane in each well) was loaded into each well, and the plate was then centrifuged (924×g for 2 minutes) to elute the sample. The collected eluate was then set aside, and two more 'wash' cycles were performed according to the above-described conditions. The three eluate samples from each well were pooled together (total volume of 438 µL) and designated as the Sample 'flow-through' (FT). Next, two elution

steps were performed. The first elution (identified as Sample E1) corresponded to the pooled eluates from two 'wash' cycles with a solution consisting of 200 µL of 10 mM HEPES, 4% sucrose, and 600 mM NaCl (pH 7.4). The second elution (identified as Sample E2) corresponded to the pooled eluates from two 'wash' cycles with a solution consisting of 200 µL of 10 mM HEPES, 4% sucrose, and 1000 mM NaCl (pH 7.4). The three samples from each MC experiment (i.e., FT, E1, and E2) were sub-divided into two aliquots. One aliquot was frozen 'as-is' at -80 °C to later be used for the determination of protein and DNA concentrations. The other aliquot was used for the determination of infectious adenovirus titer; as such, it was spiked with 50% glycerol solution (Caledon) until a glycerol concentration of 10% (v/v) was achieved. This solution was then frozen at -80 °C.

4.3.4. Laterally-fed membrane chromatography (LFMC) process

An LFMC device containing 1 mL of Sartobind® Q membrane (Sartorius) was connected to an NGC™ system (Bio-Rad) equipped with an in-line conductivity meter and a UV detector set at a wavelength of 255 nm, as it was observed that purified adenovirus has greater UV absorbance at this wavelength than at 260 nm or 280 nm (data not shown). A schematic of the LFMC system is provided in Figure 2.1 (Chapter 2), while extensive details regarding the fabrication of the LFMC device and the basic operation of the NGC™ system are provided in Chapter 2.[16] The LFMC device was cleaned-in-place on the NGC™ system by first passing 30 membrane volumes (MV) of 1 M NaOH solution through it at a rate of 1 mL/min, followed by 10 MV of 1 M NaCl solution at a rate of 5 mL/min. Next, the device was equilibrated by passing at least 10 MV of a solution consisting of 10 mM HEPES, 4% sucrose, and 360 mM NaCl (pH 7.4) (conductivity ~32 mS/cm) through it at

a rate of 5 mL/min. This was achieved by automatically adjusting the proportions of Buffer A (10mM HEPES, 4% sucrose) and Buffer B (10 mM HEPES, 4% sucrose, 2 M NaCl) using the Chromlab™ software.

As shown in Figure 4.1, the feed sample for the LFMC device was prepared via 'Process Sequence #2' using a Denarase concentration of 10 U/mL and a digestion time of 4 hours. After the digestion step, the sample was diluted 4.5 times (to a final volume of ~1.7 mL) using a solution consisting of 10 mM HEPES, 4% sucrose, and 360 mM NaCl (pH 7.4), before being further clarified by filtration through an Acrodisc® syringe filter with a 0.45 µm Supor® membrane (Pall). A small aliquot of the filtered feed sample was collected for future analysis, while the remaining amount was manually loaded into the 1 mL sample loop on the NGC™ system and then automatically injected into the system while the NaCl concentration was maintained at 360 mM (corresponding to 72% Buffer A and 18% Buffer B). After the membrane was washed with a total of 10 MV of buffer, a linear gradient elution over 10 MV was started by increasing the NaCl concentration from 360 mM (72% Buffer A and 18% Buffer B) to 1000 mM (50% Buffer A and 50% Buffer B). Finally, a 'hold' step with 1000 mM NaCl was maintained for an additional 6 MV before the end of the run. A total of 15 sample fractions were collected during the entire run: two 5 mL 'flow-through' fractions were collected after the sample injection step, ten 1 mL fractions were collected immediately after the linear gradient elution started, and three 2 mL fractions were collected during the final 'hold' step. As described in Section 4.3.3, all of the collected fractions and corresponding feed samples were split into two

aliquots and stored at -80 °C, either 'as-is' or spiked with enough 50% glycerol (Caledon) solution to achieve a 10% (v/v) glycerol concentration.

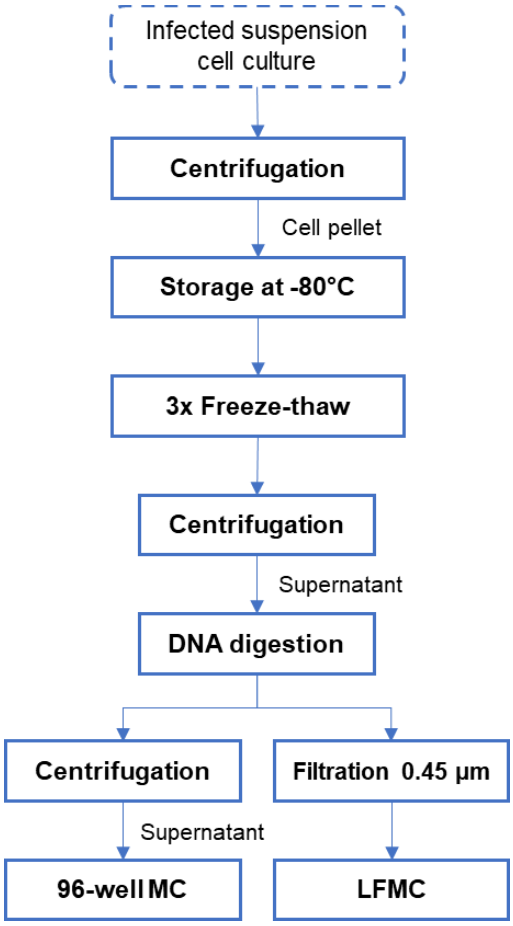

Figure 4.1. Schematic of the process steps used to produce the adenovirus feed samples used for the membrane chromatography studies described in Sections 4.3.3 and 4.3.4.

4.3.5. Analytical methods

4.3.5.1. Virus infectivity assay

Adenovirus infectious titer was determined using the hexon staining assay described in detail in our previous work.[16] In brief, adherent 293 cells grown in 24-well

plates (Corning) were infected with virus samples. The infected cells were then serially-diluted in Minimum Essential Media with Earle's salts (Gibco), supplemented with 10% fetal bovine serum (Gibco) and 1% L-glutamine (BioShop), and then incubated at 37 °C and 5% CO_2 for 48 h. The cells were then fixed and incubated three more times: once in the presence of a murine anti-hexon primary antibody; once with a secondary anti-mouse antibody that had been conjugated with horseradish peroxidase enzyme (Santa Cruz Biotechnology); and once with diaminobenzidine (DAB) substrate solution (Roche). After the final incubation period, the cells were visualized under an optical microscope, and the infectious titer (in IFU/mL) was determined with consideration of the corresponding dilution factor by counting the brown-stained plaques corresponding to cells infected with adenovirus.

4.3.5.2. Protein assay

The total amount of protein was measured using either the Pierce™ Micro BCA assay (Thermo Scientific) or the conventional Pierce™ BCA assay (Thermo Scientific). Samples were diluted at least two times in Buffer A, with assays being run in accordance with the manufacturer's instructions, using clear, flat-bottomed 96-well microplates (Corning), and in duplicate for each sample. Absorbance signals were measured at 562 nm using a SpectraMax i3 plate reader (Molecular Devices). Finally, varying the NaCl concentration from 0 to 500 mM did not significantly affect the absorbance readings; therefore, the corresponding protein concentrations for each sample were determined based on a calibration curve prepared from standard solutions containing known amounts of bovine serum albumin in the absence of NaCl.

4.3.5.3. DNA assay

The total amount of DNA was measured using the Quanti-iT™ PicoGreen™ dsDNA assay (Invitrogen) in half-area black 96-well microplates (PerkinElmer) as per the manufacturer's instructions. Assays were run in duplicate for each sample, with fluorescence signals (excitation at 480 nm and emission at 520 nm) being measured using a SpectraMax i3 plate reader. The samples were pre-diluted as necessary with Tris-EDTA buffer (Fisher Bioreagents) for two reasons: first, some samples contained DNA concentrations that fell outside of the PicoGreen assay's linear range; and second, some samples contained high concentrations of NaCl, which is known to affect the fluorescence signal. Thus, multiple calibration curves corresponding to different NaCl concentrations in Tris-EDTA buffer were prepared from standard solutions containing known amounts of lambda-DNA.

4.3.5.4. Agarose gel electrophoresis (AGE)

The digested lysate samples were first processed using a DNA Clean and Concentrator™ kit (DCC-25; Zymo Research). First, a 20 µL aliquot of each sample was mixed with 100 µL of the provided 'binding buffer' before being loaded into the spin column and centrifuged at 10,000×g for 30 s. Next, two wash steps were performed using 200 µL of the provided 'washing buffer'. Finally, 25 µL of warm (~80°C) TE buffer (Fisher Scientific) was carefully added to the spin column matrix. Following a 5-minute incubation period at room temperature, the eluent was collected in a clean microcentrifuge tube via centrifugation at 10,000×g for 1 min. An aliquot of the DCC-25 processed samples was

then mixed with a gel loading dye (Invitrogen) at a ratio of 1:10 and loaded into 1% agarose (Invitrogen) gel that had been prepared in TAE buffer containing Red Safe (Intron Biotechnology). The '1 kb Plus DNA ladder' (Invitrogen) was used as the electrophoresis standard, with the gels being run at 100 V for 45 min before being imaged via a ChemiDoc™ system (Bio-Rad).

4.4. Results and Discussion

4.4.1. Optimization of the DNA digestion step that precedes the membrane chromatography

Our initial study of DNA digestion conditions and their effect on the composition of the feed sample used in the membrane chromatography step focused on two parameters: the order of the unit operations, that is, DNA digestion followed by clarification via centrifugation (i.e., Process Sequence #1) and vice-versa (i.e., Process Sequence #2); and the specific type of enzyme. The same enzyme buffer (containing 10 mM Tris, 2 mM Mg^{2+} and a pH of 8 for optimal enzymatic activity) and incubation conditions (1 hour at 37 °C) were used for each digestion experiment. In Chapter 2,[16] the enzyme, Benzonase, was used with Process Sequence #1 to digest the DNA in the feed sample for the LFMC experiments. Following the completion of that study, we discovered that the samples that had been prepared using only centrifugation contained significantly lower amounts of DNA (data not shown). It is interesting to note that, for Process Sequence #1 (Figure 4.2-A), the DNA concentration for the control run without enzymes was almost 2 times lower compared to the runs performed with any of the selected enzymes. We hypothesize that this result is due to the enhanced removal by centrifugation of large DNA fragments that are complexed with cellular debris in the feed sample; once these fragments have been released from the

complexes by the action of the enzyme, they can no longer be removed by centrifugation. This hypothesis is supported by the fact that we obtained lower DNA concentrations using Process Sequence #2. For example, the percentage of DNA in the samples digested with Benzonase using Process Sequence #1 and Process Sequence #2 was 69% and 32%, respectively. As has been detailed in the literature, batch centrifugation steps can be used to simultaneously remove partially denatured genomic DNA and cell debris during plasmid DNA isolation from bacterial lysates.[31] As shown in Figure 4.2-C, no significant difference in DNA concentration was observed for any of the three enzymes when used in Process Sequence #2. In addition, Figures 4.2-B and 4.2-D show no significant difference in the amount of infectious adenovirus in the test samples obtained using the different enzymes and Process Sequences.

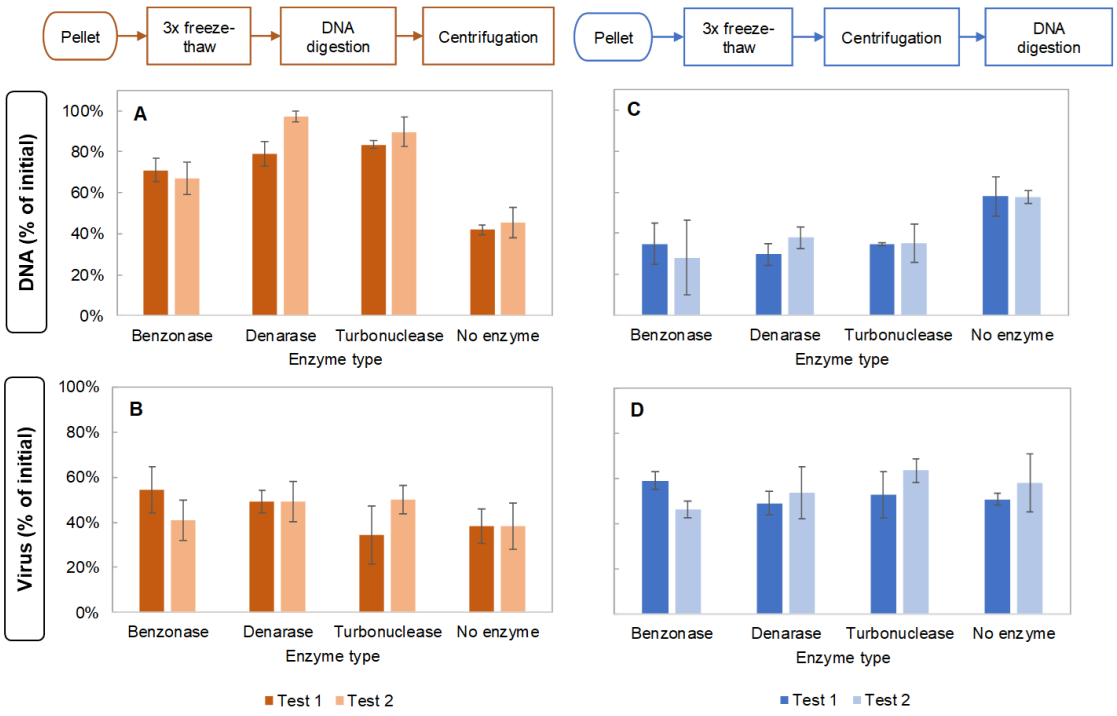

Figure 4.2. Comparison of Process Sequence and enzyme type on levels of DNA (two top panels) and adenovirus (two bottom panels). Panels A and B correspond to Process Sequence #1: freeze-thaw → DNA digestion → centrifugation; panels C and D correspond to Process Sequence #2: freeze-thaw → centrifugation → DNA digestion. The same enzyme concentration (10 U/mL) was used for the different enzymes, and the same incubation condition (1 hour at 37°C) was used for all samples. The two vertical bars for each condition correspond to the duplicate tests that were performed, and the error bars correspond to the standard deviation from either the duplicate measurements of amount of DNA, or the triplicate measurements of adenovirus levels.

As shown in Figure 4.3, analysis via agarose gel electrophoresis revealed that all eight samples (corresponding to the eight conditions in Figure 4.2) contained DNA fragments ranging between 200 and 4000 bp in length, with the brightest intensities being observed for the fragments in the 650 to 1000 bp range. Notably, no significant difference was observed between the three enzymes with respect to the range of DNA fragment sizes, which suggests that all three have similar levels of activity. The distribution of DNA fragment sizes (Figure 4.3) may have been affected by the use of the DNA Clean and Concentrator™ kit, as the percent recovery of DNA in such kits is known to decrease as

DNA fragments increase in length. Nonetheless, it was absolutely essential for us to perform this step for two reasons: first, we found that the kit completely removed any amount of adenovirus (results not shown), which was necessary to run the gel tests and to image the gel with the available equipment; and second, it was necessary to concentrate the amount of DNA for detection at the limits of the AGE technique.

Initially, we were quite surprised by the large fragments of DNA in the digested samples, as the various endonuclease manufacturers claim that optimum digestion conditions will result in DNA fragments in the size range of a few base pairs.[11] Although an early study by Janning et al.[32] is often cited in the literature to support this claim, that study was performed using pre-purified calf-thymus DNA, a combination of Benzonase (25 U/mg of DNA) and alkaline phosphatase (1.75 U/mg of DNA), and an overnight incubation step. Conversely, our results with respect to residual DNA levels after using Benzonase on an unpurified sample of adenovirus are in good agreement with those reported by Weigel et al.[20] for influenza virus. Given this, one possible direction for future research into improving the efficiency of DNA digestion would be to explore the use of a combination of different types of enzymes, perhaps in immobilized form. This approach has already been employed in the field of small-scale DNA analytics wherein a cascade capillary bioreactor containing three different enzymes immobilized in series was shown to digest at least 99.5% of purified genomic DNA in 10 minutes.[33]

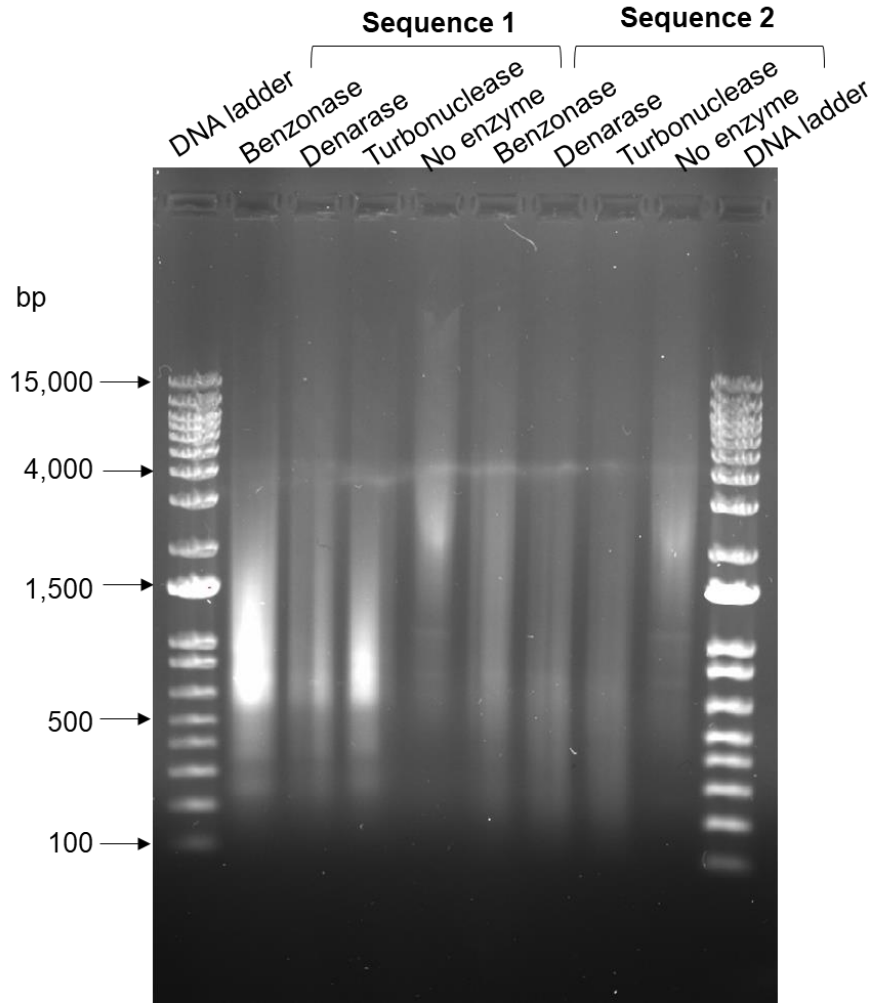

Figure 4.3. Agarose gel electrophoresis (using 1% agarose in TAE buffer, run for 45 min at 100 V, stained with Red Safe, and imaged using via a ChemiDoc™ system) of samples from Process Sequence #1 (centrifugation followed by DNA digestion) and Process Sequence #2 (DNA digestion followed by centrifugation). Samples were prepared using the DNA Clean and Concentrator™ kit (Zymo Research) to isolate DNA. The linear DNA ladder in the first and last lanes was the '1 kb Plus DNA ladder' (Invitrogen).

To develop a better understanding of how DNA digestion conditions impact the subsequent downstream purification operations, a 32 full-factorial DOE study was designed to evaluate the effects of enzyme concentration (1, 10, and 100 U/mL) and digestion time (1, 4, and 24 h) for Benzonase and Denarase. Digestion was carried out at a

temperature of 37 °C, using a pH 8 enzyme buffer; these parameters were fixed and defined based on the optimal conditions suggested by the manufacturers of Benzonase and Denarase. The third enzyme, Turbonuclease, was excluded from the rest of our study for two reasons. The first reason was that we were limited in the number of digestion experiments that could be run for a single batch of adenovirus, and we wanted to avoid any confounding effects associated with batch-to-batch variations. The second reason was that Benzonase and Denarase have been more widely used individually in virus manufacturing studies, but, to the best of our knowledge, there are no previous studies that compare their performance in the context of virus purification processes. In addition, based on the results presented in Figure 4.2, Process Sequence #2 (i.e., centrifugation followed by DNA digestion) was used for this and all subsequent parts of the study described herein.

Statistical analysis of the DOE data was performed in R language using RStudio version 1.3.959 to generate linear models of the transformed variables. This process is discussed in detail in the Appendix B. As shown in Table B2, enzyme concentration and digestion time had statistically significant (P-value < 0.05) effects on the virus concentration after digestion with Denarase or Benzonase. Furthermore, both these factors, as well as the interaction between them, had statistically significant effects on the DNA concentration after digestion with either enzyme.

As shown in Figures 4.4-A and 4.4-C, the final DNA concentration decreased dramatically with increasing enzyme concentration for both the 1 h and 4 h digestion times. For example, the final DNA concentration for the 1-hour digestion decreased by 96% (from 42.8 ± 12.6 µg/mL to 1.8 ± 0.2 µg/mL) when the Benzonase concentration was increased

from 1 to 100 U/mL. Similarly, the final DNA concentration for the 4-hour digestion decreased by 65% (from 3.1 ± 0.4 µg/mL to 1.06 ± 0.09 µg/mL) when the Benzonase concentration was increased from 1 to 100 U/mL. These results are attributable to the abundance of DNA in the feed and the fact that, in this case, enzymatic digestion is limited by the amount of enzyme present; thus, when the enzymes are present in higher concentrations, more DNA will be digested. No significant difference in DNA concentrations was observed at 1 and 10 U/mL (average of 0.75 µg/mL) of Benzonase for the 24-hour digestion time; however, there was a slight decrease in DNA concentration (0.46 µg/mL of DNA) at the highest enzyme concentration. Similarly, Denarase amounts ranging from 1 to 100 U/mL (average of 0.2 µg/mL of DNA) also did not significantly affect DNA concentrations during the 24-hour digestion time. For all conditions tested, the final DNA concentrations in samples digested with Denarase were lower than in those digested with Benzonase. Indeed, the use of Denarase yielded DNA concentrations ranging from 35% (for 4-hour digestion with 10 U/m) to 73% (for 24-hour digestion with 1 U/mL) lower than those achieved with Benzonase.

The results also indicated that the digestion conditions also affected the final amount of infectious adenovirus (Figure 4.4-B and Figure 4.4-D), with incubation time having the strongest effect on the virus titer. For example, the infectious titer decreased by over two orders of magnitude (from $4.5\times10^{10} \pm 4.5\times10^{9}$ IFU/mL to $3.6\times10^{8} \pm 6.2\times10^{7}$ IFU/mL) when the digestion time with 1 U/mL of Benzonase was increased from 1 to 24 hours. A similar effect was also observed in the tests run with Denarase. In an attempt to minimize lentiviral inactivation during an ‘overnight’ DNA digestion step (no specific time

given) with Benzonase, Merten et al.[17] used an incubation temperature of 4 °C. Despite this low temperature, they were able to achieve an 85% reduction in the amount of host cell DNA. It is particularly interesting to note that infectious titer was also affected by enzyme concentration. For example, for the 4-hour incubation, infectious titer was reduced by 68% (from $2.4\times10^{10} \pm 3.1\times10^{9}$ IFU/mL to $7.7\times10^{9} \pm 3.5\times10^{9}$ IFU/mL) when the amount of Benzonase was increased from 1 to 100 U/mL. Similarly, increasing the amount of Denarase from 1 to 100 U/mL under the same conditions reduced the infectious titer by 73% (from $1.6\times10^{10} \pm 2.4\times10^{9}$ IFU/mL to $4.4\times10^{9} \pm 1.3\times10^{9}$ IFU/mL). While the exact cause of this effect is not known, a previous study[34] has proposed that adenovirus capsids could allow the permeation of foreign material. In our study, it is possible that the likelihood of enzyme permeation in the capsid (and consequent virus inactivation) increased with higher enzyme concentrations. In addition, it is also possible that this effect may be driven by long incubation times at elevated temperatures. Another possible explanation is that residual amounts of endonuclease may have affected the cells used for the virus infectivity assay, thus resulting in a lower virus titer. However, this hypothesis is unlikely given the significant serial dilutions (at least 10^{6}-fold) of virus samples in culture media prior to the assay. Thus, a more comprehensive study is needed to assess these hypotheses. Regardless, the results of this study are in good agreement with Sastry et al.'s[10] findings regarding the effects of Benzonase on infectious titers of lentiviral vectors. Despite this agreement, it is important to note that Sastry et al.'s[10] study was limited to just two enzyme concentrations (15 and 50 U/mL) and a single short incubation time (15 mins at 37 °C).

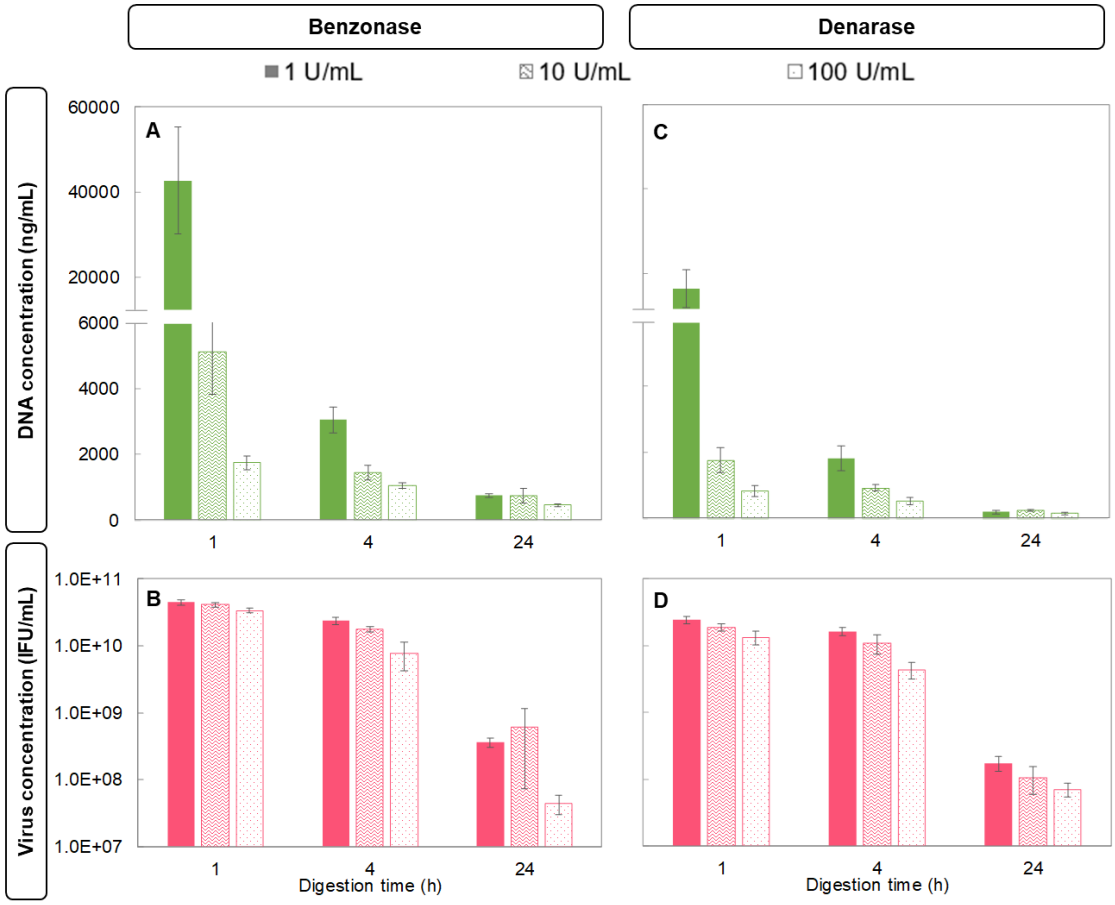

Figure 4.4. Comparison of the effect of DNA digestion time (at 37 °C) and enzyme concentration on final DNA concentration (panels A and C) and virus infectivity (panels B and D panels) in samples prepared according to Process Sequence #2. Panels A and B correspond to Benzonase, and panels C and D correspond to Denarase. The average value obtained from the duplicate experiments is shown for each condition. Error bars correspond to the standard deviation from either the duplicate measurements of DNA concentration (i.e., n = 4) or the triplicate measurements of virus concentration (i.e., n = 6). The raw average virus and DNA concentrations in each sample in this figure are shown in Table B1 in Appendix B.

4.4.2. High-throughput screening of membrane chromatography performance using Sartobind Q 96-well filter plate

The DNA digestion results presented in Figure 4.4 indicate that Denarase was slightly more effective in reducing the DNA concentration; therefore, we exclusively used Denarase for the remainder of this study. The MC runs with the Sartobind Q 96-well filter

plate were conducted using a subset consisting of 5 of the 9 DNA digestion conditions from the DOE and one control (i.e., only enzyme-free buffer added and then placed in -80 °C freezer) using adenovirus lysates. This subset of DNA digestion conditions was selected for three main reasons: first, it was not practical to consider all 9 conditions and an undigested control, as such an approach would produce a very large number of samples to later be analysed; second, two of the conditions using 24-hour digestion times were excluded, as such long digestion times resulted in high virus inactivation (>99%) during DNA digestion; and finally, the digestion conditions using 1 U/mL for 1 hour and 100 U/mL for 1 hour were not considered because they resulted in digested lysates with a similar composition to that of the undigested control lysate and the lysates prepared using 10 U/mL of Denarase for 4 h, respectively. The relationship between the conditions used in the DOE study and the MC runs with the 96-well filter plate is illustrated in Figure B1 in Appendix B.

A comparison of the feed and eluate sample compositions (i.e., virus, DNA, and protein concentrations) used in the six MC runs in duplicate is given in Table 4.1. The two rows for each digestion condition correspond to the duplicate tests using the independently prepared feed samples. As Table 4.1 shows, the results for the duplicate MC runs using feed material digested under the same conditions showed good overall reproducibility. The control samples without digestion had the highest amount of virus in the feed, with an average of 6.5×10^{8} IFU. A considerably lower virus concentration was observed in the feed of the samples digested with 10 U/mL of Denarase for 24 h, with an average of 2.7×10^{6} IFU. This is in good agreement with the results shown in Figure 4.4: compared to 1-hour

digestion period, the 24-hour digestion period resulted in an over 99% decrease in the amount of virus. The runs with the lowest amount of virus in the feed also yielded the lowest virus recovery rate from the eluate at only 14%; higher virus recoveries were achieved for the remaining runs, varying between 42% and 79%.

In Table 4.1, the amounts of protein and DNA are reported as a ratio of the amount of virus in the sample in order to represent the total amount per dose (with a dose defined as 10^{10} IFU). Note that the amounts of DNA and protein per dose shown in Table 4.1 have been normalized based on the infectious titer in each sample; the virus (IFU/mL), DNA (ng/mL), and protein (µg/mL) concentrations that were used for the calculations can be found in Table B3 in Appendix B. The amounts of protein per dose in the eluate ranged from 3% to 19% of the amounts in the feed. The only MC runs that were able to achieve DNA levels below the FDA's target specification of 10 ng/dose were those wherein the feed sample was pre-digested with 10 U/mL of Denarase for 24 hours. Although these conditions were able to meet the FDA's threshold, they also resulted in the loss of more than 99% of the infectious adenovirus during the DNA digestion step. For the other five digestion conditions, the amount of DNA in the eluate ranged from 137 ng/dose to 1517 ng/dose. Interestingly, the MC runs using the undigested lysate had the highest percentage of DNA removal, with only approximately 15% of the initial amount of DNA remaining in the eluate. The lowest absolute amount of DNA (average of 144 ng/dose) in the elution was obtained via the MC runs conducted with feed samples that had been pre-digested with 10 U/mL of Denarase for 4 hours. Table B3 provides the compositions of the feed, flow-through (FT), and first and second elution Samples (E1 and E2, respectively) used to obtain

the results in Table 4.1. As Table B3 shows, the most protein was eluted in the Sample FT (containing 360 mM NaCl in Buffer A), while the most virus was eluted in Sample E1 (containing 600 mM NaCl in Buffer A). Finally, the most DNA was eluted in Samples E1 and E2 (containing when 600 mM and 1000 mM NaCl in Buffer A, respectively).

Table 4.1. Composition of feed and elute (i.e., E1 fraction) samples for the MC runs performed with the 96-well filter plate. The two rows for each set of DNA digestion conditions correspond to the duplicate MC experiments that were performed, each using independently digested lysates. The amount of DNA and protein were normalized and expressed on a per virus dose basis using 10^{10} IFU per dose. Process Sequence #2 was used to generate the feed samples. Refer to Table B3 for the corresponding concentrations of virus (IFU/mL), DNA (ng/mL), and protein (µg/mL) that were used to generate the results shown. BDL: below detection limit.

DNA digestion conditions		**Virus amount (IFU)**		**DNA amount (ng/10^{10} IFU)**		**Protein amount (µg/10^{10} IFU)**	
[Denarase] (U/mL)	**Time (h)**	**Feed**	**Eluate**	**Feed**	**Eluate**	**Feed**	**Eluate**
1	4	2.8×10^{8}	1.4×10^{8}	844	231	4860	441
1	4	3.7×10^{8}	1.5×10^{8}	339	BDL	2001	146
10	1	5.2×10^{8}	3.1×10^{8}	386	186	2406	230
10	1	6.2×10^{8}	3.5×10^{8}	329	181	1611	122
10	4	3.5×10^{8}	2.6×10^{8}	342	137	3210	157
10	4	3.4×10^{8}	2.7×10^{8}	375	150	3391	143
10	24	2.5×10^{6}	3.7×10^{5}	17544	BDL	402452	77119
10	24	2.9×10^{6}	4.0×10^{5}	14826	BDL	316014	42342
100	4	1.2×10^{8}	5.7×10^{7}	663	478	10542	938
100	4	1.2×10^{8}	8.9×10^{7}	740	297	10080	332
0	0	6.3×10^{8}	4.5×10^{8}	9925	1255	2233	159
0	0	6.7×10^{8}	3.8×10^{8}	8272	1517	1844	197

4.4.3. Laterally-fed membrane chromatography purification of adenovirus sample

In order to demonstrate the usefulness of our detailed approach to optimizing the DNA digestion conditions, the final part of this study focused on translating the best operating conditions identified in the high-throughput screening study (Section 4.4.2) into a scalable membrane chromatography device. An LFMC device containing 1 mL of the same Sartobind Q membrane used in the 96-well MC experiments was evaluated using the NGC system and a feed sample prepared from 50 mL of adenovirus cell culture. The exact

feed-sample preparation sequence is shown in Figure 4.1. Based on the results shown in Table 4.1, it was decided that the DNA digestion step would be performed using 10 U/mL of Denarase, with a 4-hour incubation at 37 °C. It is worth noting that this amount of enzyme is much lower than that used in prior research on adenovirus production.[8] The relationships between the digestion conditions used in all parts of our study are illustrated in Figure B1 in Appendix B.

As shown in Figure 4.5, the UV absorbance profile for the run displayed two prominent peaks. The first peak (with a maximum that occurs around the 2 mL mark) corresponds to all components in the feed sample that did not bind to the Sartobind Q membrane at the given conditions (i.e., 360 mM NaCl). The second peak (with a maximum at around the 15.5 mL mark) occurs at the beginning of the linear gradient from 360 mM NaCl (solution conductivity of approximately 32 mS/cm) to 1000 mM NaCl (solution conductivity of approximately 77 mS/cm). To resolve the relative contributions of DNA, protein, and virus to the UV signal, the results from the individual assays on each fraction are presented in the vertical bar series. The first UV peak was mostly comprised of protein (approximately 85% of the amount in the feed), a small amount of DNA (approximately 3% of the amount in the feed), and a very small amount of adenovirus (<0.001% of the amount in the feed). The second UV peak, corresponding to the 4th and 5th 1 mL elution fractions, consisted of mostly adenovirus (73% of the initial amount in the feed was eluted in the combined 2 mL fraction) and a small amount of DNA (approximately 6% of the amount in the feed). The majority of the DNA eluted at solution conditions corresponded to higher NaCl concentrations, while the elution fraction with the highest amount of DNA

corresponded to a solution conductivity of approximately 70 mS/cm (~900 mM NaCl). In good agreement with Chapter 2,[16] the DNA eluted as a broad peak and the amount of DNA in each fraction was so low that it was not detected in the UV absorbance signal. The reproducibility of the LFMC device was verified in a duplicate run under the exact same conditions (results not shown).

Overall, the results from the LFMC run are in good agreement with those from the MC runs with the 96-well filter plate. Specifically, both runs showed that residual amounts of DNA co-eluted with the virus. The amount of DNA in the feed solution used for the LFMC run (856 ng/dose) was higher than the amount of DNA in the feed for the 96-well filter plate MC runs (359 ng/dose), even though both lysates were prepared under the same digestion conditions (10 U/mL Denarase for 4 hours). This difference is likely due to variations in the cell pellets that were used to generate the lysates, and possibly to the increase in scale required to prepare lysates for the LFMC runs. Despite the differences in the feed, the results obtained with the LFMC showed improved DNA removal compared to the outcomes of the small-scale MC in 96-well plate format using the same DNA digestion conditions. This is not surprising given the use of a linear gradient in salt concentration in the LFMC experiment as opposed to the two step changes in salt concentration that were used for the 96-well filter plate MC experiments.

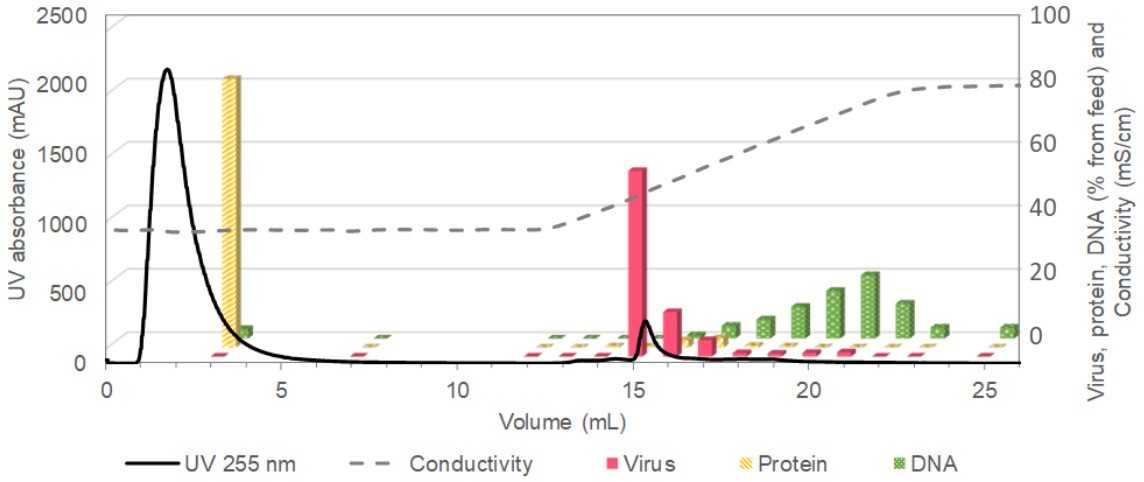

Figure 4.5. Chromatogram for adenovirus purification run using an LFMC device containing 1 mL of Sartobind Q membrane, a linear gradient elution step (initiated at 12 mL mark to ramp from 18% Buffer B to 50% Buffer B over 10 mL), and a feed sample that was pre-processed according to Process Sequence #2, with the DNA digestion step conducted using 10 U/mL of Denarase and 4 hours of incubation at 37 °C. The solid line indicates the UV absorbance profile at 255 nm (mAU), while the dashed line indicates the solution conductivity profile (mS/cm). The 3D bar chart indicates the amount of virus (front pink solid bars), protein (middle yellow striped bars), and DNA (back green dotted bars) within the middle of each of the 15 fractions, as a percentage of the amount in the injected feed sample.

Table 4.2 provides a comparison of the chromatography runs performed with the LFMC devices in this study and those performed in Chapter 2.[16] There are some key differences between the two processes that were used. In our previous study, we used Process Sequence #1 with a lower concentration (1 U/mL) of Benzonase and a shorter incubation time (0.5 hours), which resulted in a feed sample that contained a very large amount of DNA (22 520 ng/dose). In this study, for the various reasons cited above, Process Sequence #2 was used with 10 U/mL of Denarase and an incubation period of 4 hours, which resulted in a feed sample with 26-times less DNA (856 ng/dose). This substantial decrease in DNA concentration meant that up to 10 times more feed sample could be

injected onto the LFMC device compared to our previous study. In addition, the starting NaCl concentration was reduced to 360 mM in this study in order to induce stronger virus binding to the membrane during sample application. Finally, the rate of the linear gradient increase in salt concentration to elute the bound components on the Sartobind Q membrane was decreased in this study, such that it occurred over 10 MV. Overall, the optimum processing conditions identified in this integrated study (i.e., the sequence of operations, DNA digestion conditions, and LFMC parameters) led to a substantial decrease in the amount of DNA in the 2 mL elution fraction containing the majority of the adenovirus sample; specifically, the amount of DNA per infectious virus was reduced by over 80 times. In this study, we achieved a virus recovery rate of 73%; by comparison, a previous study on adenovirus purification using the same Sartobind Q membrane reported a recovery rate of 62%.[22] This reduction in DNA levels is directly related to the new carefully adjusted downstream processing conditions. First, we changed the sequence of unit operations to enable the partial removal of DNA during the clarification step prior to digestion. Next, our use of new DNA digestion conditions—namely, the use of a different enzyme at a higher concentration for a longer period of time (Table 4.2)—provided a higher degree of DNA fragmentation. In addition, this new digestion protocol also reduced the concentration of DNA measured with the Picogreen assay, which is known to have a binding site to DNA duplexes of at least 4 base pairs.[35] Finally, the lower DNA concentration and smaller fragment sizes contributed to a lower final DNA concentration after separation with the LFMC device. Despite these improvements, it is important to note that the amount of residual DNA in this study (77 ng/dose) is still 8-fold the FDA's mandated level of 10

ng/dose. Given the limitations of MC in reducing low residual DNA amounts—as seen in the 96-well MC and LFMC studies—an additional polishing step might be necessary, for example, salt tolerant membrane chromatography, which has been used in the production of influenza A virus.[36]

Table 4.2. Comparison of process conditions and results for adenovirus purification via LFMC from this study and our previous study. The amounts of adenovirus and DNA after LFMC correspond to the amounts found in the 2 mL fractions containing most of the virus eluted during each run. † Based on 10^{10} IFU/dose.

Condition	This study	Previous study[16]
LFMC device	1 mL of Sartobind Q	1 mL of Sartobind Q
DNA digestion enzyme	Denarase 10 U/mL	Benzonase 1 U/mL
DNA digestion time	4 hours	0.5 hour
Feed volume	1 mL	0.1 mL
Amount of adenovirus in the feed	$1.4\times10^{10} \pm 2.1\times10^{9}$ IFU	$1.4\times10^{9} \pm 1.1\times10^{8}$ IFU
Amount of DNA in the feed†	856 ± 159 ng/dose	22 520 ng/dose
[NaCl] in equilibration buffer	360 mM	400 mM
Elution strategy	Linear gradient over 10 MV	Linear gradient over 4 MV
Volume of eluate containing virus	2 mL	2 mL
Amount of adenovirus after LFMC	$1.0\times10^{10} \pm 1.2\times10^{9}$ IFU	1.4×10^{9} IFU ± 1.5×10^{8} IFU
Amount of DNA after LFMC†	77 ± 3 ng/dose	6507 ± 187 ng/dose

4.5. Conclusions

In this paper, we presented the development of a process sequence predicated on the removal of cell debris via centrifugation before DNA digestion, and the integrated optimization of enzymatic DNA digestion and membrane chromatography. As a result, we were able to reduce the level of residual DNA per dose of adenovirus by over 80-fold compared to the results of Chapter 2.[16] Specifically, the presented process sequence enabled residual DNA to be reduced from 6507 ng/dose to 77 ng/dose after LFMC.

The results presented in this study demonstrate the considerable advantage of using an integrated approach towards optimizing adenovirus purification processes. First, we highlight the importance of the sequence of events, particularly with respect to performing a clarification step (i.e., the removal of cell debris by centrifugation) prior to DNA digestion. A certain amount of DNA, probably large fragments associated with cell debris, was removed in the centrifugation step, favouring lower DNA concentrations after digestion. Second, a higher percentage of DNA was removed via MC when the initial sample was not previously digested with endonuclease. Moreover, although a 24-hour digestion period resulted in an enormous reduction in DNA levels, regardless of the amount or type of enzyme used, the high degree of virus inactivation (99%) that results from such long incubation periods makes this option unfeasible. By comparison, a 1-hour digestion period using 1 U/mL of Denarase resulted in a virus inactivation rate of approximately 47%. Finally, the experiments in the 96-well plate format proved to be a good predictor of the membrane's separation performance in the LFMC format. When one of the best conditions was implemented for an actual LFMC run using a device containing 1 mL of the Sartobind Q membrane and a linear gradient elution strategy, high virus recovery (73%) and good DNA removal (93%) were obtained. These results were superior to those predicted by the small-scale MC experiment, most likely due to flexibility in terms of operation and elution strategy design during an actual LFMC run.

4.6. Acknowledgements

Funding was provided by the Ontario Research Fund-Research Excellence program and the Natural Sciences and Engineering Research Council of Canada.

Additional funding was provided by BioCanRx, a Networks of Centres of Excellence program, in the form of a Summer Studentship Award to A. Noelle Wilton. The Sartobind Q 96-well plates were generously provided by Sartorius; the Denarase and Turbonuclease were generously provided by c-LEcta and Accelagen, respectively. The authors thank Mr. Kevin Dunn from DSM (Netherlands) for his assistance with the statistical analysis of the DOE; Mr. Paul Gatt from the Department of Chemical Engineering at McMaster University for his assistance in fabricating the LFMC device; and Ms. Natasha Kazhdan from the McMaster Immunology Research Centre (Department of Pathology and Molecular Medicine) for her assistance with culturing adenovirus batches.

4.7. References

1. Wold, W. & Toth, K. Adenovirus Vectors for Gene Therapy, Vaccination and Cancer Gene Therapy. Curr. Gene Ther. 13, 421–433 (2014).
2. Dormond, E., Perrier, M. & Kamen, A. From the first to the third generation adenoviral vector: What parameters are governing the production yield? Biotechnol. Adv. 27, 133–144 (2009).
3. Ginn, S. L., Amaya, A. K., Alexander, I. E., Edelstein, M. & Abedi, M. R. Gene therapy clinical trials worldwide to 2017 - an update. J. Gene Med. e3015 (2018). doi:10.1002/jgm.3015
4. Sharon, D. & Kamen, A. Advancements in the design and scalable production of viral gene transfer vectors. Biotechnol. Bioeng. 115, 25–40 (2018).
5. Lang, F. F. et al. Phase I study of DNX-2401 (delta-24-RGD) oncolytic adenovirus: replication and immunotherapeutic effects in recurrent malignant glioma. J. Clin. Oncol. 36, 1419–1427 (2018).
6. Kiyokawa, J. & Wakimoto, H. Preclinical and clinical development of oncolytic adenovirus for the treatment of malignant glioma. Oncolytic Virotherapy Volume 8, 27–37 (2019).
7. FDA & CBER. Chemistry, Manufacturing, and Control (CMC) Information for Human Gene Therapy Investigational New Drug Applications (INDs) - Guidance for Industry. (2020).

8. Vellinga, J. et al. Challenges in Manufacturing Adenoviral Vectors for Global Vaccine Product Deployment. Hum. Gene Ther. (2014). doi:10.1089/hum.2014.007

9. Merten, O. W., Hebben, M. & Bovolenta, C. Production of lentiviral vectors. Mol. Ther. - Methods Clin. Dev. 3, 16017 (2016).

10. Sastry, L., Xu, Y., Cooper, R., Pollok, K. & Cornetta, K. Evaluation of Plasmid DNA Removal from Lentiviral Vectors by Benzonase Treatment. Hum. Gene Ther. 15, 221–226 (2004).

11. Gousseinov, E., Kools, W. & Pattnaik, P. Nucleic acid impurity reduction in viral vaccine manufacturing. Bioprocess Int. 12, 59–68 (2014).

12. Marichal-Gallardo, P., Pieler, M. M., Wolff, M. W. & Reichl, U. Steric exclusion chromatography for purification of cell culture-derived influenza A virus using regenerated cellulose membranes and polyethylene glycol. J. Chromatogr. A 1483, 110–119 (2017).

13. Fortuna, A. R. et al. Use of sulfated cellulose membrane adsorbers for chromatographic purification of cell cultured-derived influenza A and B viruses. Sep. Purif. Technol. 226, 350–358 (2019).

14. Cecchini, S., Virag, T. & Kotin, R. M. Reproducible high yields of recombinant adeno-associated virus produced using invertebrate cells in 0.02-to 200-liter cultures. Hum. Gene Ther. 22, 1021–1030 (2011).

15. Wang, Q. et al. Identification of an adeno-associated virus binding epitope for AVB sepharose affinity resin. Mol. Ther. - Methods Clin. Dev. 2, 15040 (2015).

16. Kawka, K. et al. Purification of therapeutic adenoviruses using laterally-fed membrane chromatography. J. Memb. Sci. 579, 351–358 (2019).

17. Merten, O. W. et al. Large-scale manufacture and characterization of a lentiviral vector produced for clinical Ex vivo gene therapy application. Hum. Gene Ther. 22, 343–356 (2011).

18. Bandeira, V. et al. Downstream processing of lentiviral vectors: Releasing bottlenecks. Hum. Gene Ther. Methods 23, 255–263 (2012).

19. Vyas, G. N. et al. Derivation of non-infectious envelope proteins from virions isolated from plasma negative for HIV antibodies. Biologicals 40, 15–20 (2012).

20. Weigel, T. et al. A flow-through chromatography process for influenza A and B virus purification. J. Virol. Methods 207, 45–53 (2014).

21. Nestola, P. et al. Improved virus purification processes for vaccines and gene therapy. Biotechnol. Bioeng. 112, 843–857 (2015).

22. Peixoto, C., Ferreira, T. B., Sousa, M. F. Q., Carrondo, M. J. T. & Alves, P. M. Towards purification of adenoviral vectors based on membrane technology. Biotechnol. Prog. 24, 1290–1296 (2008).

23. Hensgen, M. I., Czermak, P., Carlson, J. O. & Wickramasinghe, S. R. Purification of Minute Virus of Mice using high performance tangential flow filtration. Desalination 250, 1121–1124 (2010).

24. Madadkar, P., Wu, Q. & Ghosh, R. A laterally-fed membrane chromatography module. J. Memb. Sci. 487, 173–179 (2015).

25. Ghosh, R., Madadkar, P. & Wu, Q. On the workings of laterally-fed membrane chromatography. J. Memb. Sci. 516, 26–32 (2016).

26. Rathore, A. S., Pathak, M. & Godara, A. Process development in the QbD paradigm: Role of process integration in process optimization for production of biotherapeutics. Biotechnol. Prog. 32, 355–362 (2016).

27. Cruz, P. E., Maranga, L. & Carrondo, M. J. T. Integrated process optimization: Lessons from retrovirus and virus-like particle production. J. Biotechnol. 99, 199–214 (2002).

28. Liu, S., Farid, S. S. & Papageorgiou, L. G. Integrated Optimization of Upstream and Downstream Processing in Biopharmaceutical Manufacturing under Uncertainty: A Chance Constrained Programming Approach. Ind. Eng. Chem. Res. 55, 4599–4612 (2016).

29. Cruz, P. E., Gonçalves, D., Almeida, J., Moreira, J. L. & Carrondo, M. J. T. Modeling retrovirus production for gene therapy. 2. Integrated optimization of bioreaction and downstream processing. Biotechnol. Prog. 16, 350–357 (2000).

30. Vicente, T., Mota, J. P. B., Peixoto, C., Alves, P. M. & Carrondo, M. J. T. Rational design and optimization of downstream processes of virus particles for biopharmaceutical applications: Current advances. Biotechnol. Adv. 29, 869–878 (2011).

31. Holmes, D. S. & Quigley, M. A rapid boiling method for the preparation of bacterial plasmids. Anal. Biochem. 114, 193–197 (1981).

32. Janning, P., Schrader, W., Linscheid, M. & Baillie, T. A. A new mass spectrometric approach to detect modifications in DNA. Rapid Commun. Mass Spectrom. 8, 1035–1040 (1994).

33. Yin, J., Chen, S., Zhang, N. & Wang, H. Multienzyme Cascade Bioreactor for a 10 min Digestion of Genomic DNA into Single Nucleosides and Quantitative Detection of Structural DNA Modifications in Cellular Genomic DNA. ACS Appl. Mater. Interfaces 10, 21883–21890 (2018).

34. Konz, J. O., Lee, A. L., Lewis, J. A. & Sagar, S. L. Development of a purification process for adenovirus: Controlling virus aggregation to improve the clearance of host cell DNA. Biotechnol. Prog. 21, 466–472 (2005).

35. Dragan, A. I. et al. Characterization of PicoGreen interaction with dsDNA and the origin of its fluorescence enhancement upon binding. Biophys. J. 99, 3010–3019 (2010).

36. Weigel, T. et al. A membrane-based purification process for cell culture-derived influenza A virus. J. Biotechnol. 220, 12–20 (2016).

Chapter 5

Purification of vesicular stomatitis virus (VSV) using hydrophobic interaction membrane chromatography

5. Purification of vesicular stomatitis virus (VSV) using hydrophobic interaction membrane chromatography

Karina Kawka, A. Noelle Wilton, Maria Fe C. Medina, Raja Ghosh, David R. Latulippe

Prepared for Journal submission

5.1. Abstract

Vesicular stomatitis virus (VSV) is an enveloped, RNA-based type of rhabdovirus, that has been gaining significant biopharmaceutical interest for applications as oncolytic viruses in cancer immunotherapy and as vectors for vaccines. Although significant progress has been made in terms of upstream process development, VSV purification for the removal of host-cell proteins and DNA often rely on non-scalable and labour-intensive techniques such as density gradient ultracentrifugation. Membrane chromatography (MC) is a scalable and promising alternative for the purification of large biomolecules and entities such as viruses. Its large flow pores allow easy access to the binding sites, and convective mass transfer allows operation at high flow rates. The goal of this study was to develop an MC process to remove process- and product-related impurities including host-cell and cell culture media components (i.e. phenol-red). Initial attempts using Sartobind Q, which is an anion-exchange membrane widely used for virus purification resulted in poor virus recoveries (below 10%). Attempts to purify VSV with Sartobind Sulfated Cellulose (SC), a pseudo-affinity membrane, were also unsuccessful as discussed in Appendix C. However, very promising initial results were obtained with hydrophobic interaction membrane

chromatography (HIMC) using the Sartobind Phenyl membrane (3 mL Nano capsule). In HIMC, binding is induced in the presence of high concentrations of kosmotropic salts; in this study, buffers containing ammonium sulfate (AS) were used during membrane equilibration, loading, and washing, while elution was performed using a salt-free buffer in a step-change mode. In low-volume separation experiments (i.e. 1 mL of VSV feed) carried out at pH 7.4, VSV bound to the membrane in the AS concentrations range of 0.7 M to 1.0 M, with the average overall recovery being 67%. Separation at pH 8.0 resulted in only 23% recovery, indicating a significant effect of pH on virus stability. Finally, the volume of sample was scaled up to 300 mL (i.e. 100 membrane volumes) and the separation was carried out at pH 7.4 and 1.0 M AS. VSV was concentrated into a 6 mL eluate fraction with up to 78% recovery. Most impurities were removed in the flow-through, and so only <1% and approximately 10% of the initial amounts of host-cell protein and DNA, respectively, remained in the eluate. Moreover, phenol-red that was initially present in the cell culture media was removed. To the best of our knowledge, this is the first study to use HIMC for VSV purification, and one of the firsts for viruses in general. In only one process step, VSV was successfully harvested from culture media, concentrated more than 50-fold, and purified. This study demonstrates the potential of HIMC as a method for large-scale purification of VSV, and potentially other types of viruses

5.2. Introduction

Vesicular stomatitis virus (VSV) is an enveloped, RNA-based type of rhabdovirus that has been used as the vector for the development of vaccines (e.g. against HIV,[1] Ebola virus,[2] and coronavirus[3]) and novel cancer therapeutics.[4] The success of VSV for

therapeutic purposes depends on the development of efficient manufacturing processes. Recently, substantial progress has been made in terms of upstream, with the use of new bioreactor designs that maximize virus production in adherent cultures,[5] the development of suspension serum-free cultures,[6,7] and the optimization of upstream process parameters.[2] However, there is a limited number of studies related to the purification of VSV. The removal of host-cell proteins and DNA typically relies on density gradient ultracentrifugation for small-scale applications,[2] or different combinations of anion-exchange chromatography and/or tangential flow filtration (TFF) for large scale applications.[8–10] A downstream process for the purification of clinical-grade VSV was described by Ausubel, et al.[8], and involved a series of steps including clarification of the cell culture supernatant, enzymatic DNA digestion, anion-exchange chromatography, TFF, diafiltration, and sterile filtration. Although the method was shown to be robust, there is room for process simplification and improvement with the use of alternative and scalable technologies.

Hydrophobic interaction chromatography (HIC) is a widely used technique in the field of protein purification at different scales,[11] and a limited number of studies have also addressed this alternative for virus purification. The few reports found in the literature focused on the purification of vaccinia, influenza and foot-and-mouth disease viruses using resins and monoliths with different hydrophobic ligand chemistries, and presented promising results with high virus yields (>70%).[12–16]

For the purification of large molecules, such as viruses, membrane chromatography (MC) presents a series of advantages over conventional resins. These

include large pore sizes, more accessible binding sites, and convective mass transfer allowing high operating flow rates,[17] and ultimately contributing towards more economical processes.[18] These membranes are currently available in a variety of materials and chemistries for different applications such as anion and cation exchange, affinity, and hydrophobic interaction.[17] Hydrophobic interaction membrane chromatography (HIMC) has been successfully applied in flow-through mode for the capture of aggregates from monoclonal antibody preparations,[19–22] and in bind-and-elute mode for the purification of therapeutic proteins[17,18,23–25] and plasmid DNA.[26–28] Despite its potential, HIMC has only been applied very recently in the purification of a short list of viruses, including adeno-associated viruses (AAV),[29] lentiviruses,[30] and Orf virus,[31] with good recoveries and purities being reported. In this study, the application of HIMC for virus purification is further examined by evaluating its performance for the purification of VSV from cell culture using the Sartobind Phenyl membrane. Important process parameters, such as buffer pH and the salt concentration in the binding buffer have been addressed and the scalability of the process was demonstrated in experiments where 300 mL of virus lysate were purified using a 3 mL HIMC device.

5.3. Materials and Methods

5.3.1. Preparation of VSV cultures

Vero cells were grown in culture plates or 1720 cm² Hyperflaks® (Corning®) using Dulbecco's Modified Eagle's medium (DMEM, Gibco™) supplemented with 10% fetal bovine serum (FBS, Gibco™) and 1% L-glutamine (BioShop). The media contained phenol red, a pH indicator commonly used in cell culture and an important process-related impurity

that needed to be removed. At approximately 90% cell confluency, the culture media was removed, cells were gently rinsed with phosphate-buffered saline (PBS) and infected with VSV expressing green fluorescent protein (GFP) resuspended in FBS-free DMEM, using a multiplicity of infection of 0.1. After 24 hours, the supernatant containing virus was harvested and clarified by centrifugation for 15 min at 1430×g and 4°C, followed by filtration with a 0.45 µm bottle top filter (Nalgene®), before being aliquoted and stored at -80 °C.

5.3.2. Chromatography runs

For HIMC runs, the clarified VSV lysate was thawed and mixed with a high-salt buffer of pH 7.4 or 8.0 containing 10 mM HEPES (Gibco™), 4% sucrose (BioShop) and 2.6 to 3.6 M ammonium sulfate (AS, Sigma-Aldrich), for final AS concentrations of 0.7 or 1.0 M. A Sartobind® Phenyl Nano 3 mL (Sartorius) device connected to an NGC™ medium-pressure chromatography system (BioRad) was used to perform chromatography runs at a flow rate of 9 mL/min. Although the laterally-fed membrane chromatography (LFMC) device can provide better separation resolution than the radial flow-based Sartobind Nano capsule as discussed in detail in Chapter 2, the Sartobind Phenyl membrane was not commercially available in flat sheet format to be used to fabricate LFMC devices at the time this study was conducted. Therefore, the Sartobind Phenyl Nano 3 mL device was used as supplied by Sartorius. Before each run, the Sartobind Phenyl device was equilibrated with at least 10 membrane volumes (MV) of binding buffer (10 mM HEPES, 4% sucrose, 0.7 or 1.0 M AS, pH 7.4 or 8.0). A small aliquot of the feed lysate sample was taken for analysis and the remaining was loaded into the Sartobind Phenyl device. Two

types of experiments were performed: low-volume runs using 1 mL of feed for evaluating the effect of pH and AS concentration in the loading phase, and scale-up runs using 300 mL of feed as discussed in the Results section. In either case, a wash step with binding buffer was conducted after samples loading. Finally, a step-change to elution buffer (10 mM HEPES, 4% sucrose, pH 7.4 or 8.0) in the absence of AS was implemented. Fractions were collected throughout each run and immediately stored in an ice bath. The fractions were used in the virus infectivity assay immediately after the chromatography runs to avoid interferences and losses of infectivity during storage. Later, the samples were stored at -80 °C for future protein and DNA analysis.

Following each run, the Sartobind Phenyl device was cleaned in place. First, a 1 M NaOH (BioShop) solution was passed through the system for 30 min at a 3 mL/min flow rate, followed by Milli-Q water for 3 minutes at a 9 mL/min flow rate. Next, the Sartobind Phenyl membrane was regenerated by passing a 70% ethanol solution through the system at 1 mL/min for 1 hour. The device was stored in 20% ethanol at 4°C between runs.

Although this study focuses on HIMC using the Sartobind Phenyl membrane, early experiments were performed using Sartobind Q and Sartobind Sulfated Cellulose (SC) membranes using the method previously reported for the purification of adenoviruses.[32] For runs with Sartobind Q, VSV lysates prepared as described above were either used directly or mixed with buffer containing 10 mM HEPES (Gibco™), 4% sucrose (BioShop), 2 M NaCl (BioShop) for final NaCl concentrations of 0.36 M before being loaded onto the membrane. Similarly, for runs with Sartobind SC, the sample was diluted in 10 mM HEPES

(Gibco™), 4% sucrose (BioShop) buffer without NaCl before being loaded onto the membrane.

5.3.3. Analysis of virus infectivity, total protein, and DNA in chromatography fractions

VSV infectivity was determined using the fifty-percent tissue culture infective dose ($TCID_{50}$) assay adapted from Roldão et al.[33] as described in Appendix D and the titer was calculated using the Spearman-Karber method.[34]

Total protein concentration was determined in duplicate using the BCA™ Protein Assay Kit (Thermo Scientific), following the manufacturer's instructions. It was observed that the presence of AS in the samples significantly reduced the sensitivity of the BCA assay, mainly when the 96-well plate format of the assay was used. Thus, an adapted version of the enhanced test-tube BCA protocol was used. In summary, a 950 µL aliquot of the BCA working reagent was mixed with 50 µL of sample in a microcentrifuge tube and incubated for 1 hour at 60 °C using a heat block. After incubation, the tubes were transferred to an ice bath for 5 minutes and the absorbance at 562 nm was measured using a Biophotometer (Eppendorf), using Milli-Q water as the blank sample. Since the presence of AS affected the sensitivity of the assay, three different calibration curves with known amounts of bovine serum albumin (BSA, Thermo Scientific) standard diluted in buffer A containing different concentrations of AS were prepared in parallel with each round of tests.

Total DNA concentration was measured in duplicate using Quanti-iT™ Picogreen® dsDNA kit (Invitrogen) with the reactions being conducted in black half-area 96-well microplates (PerkinElmer). Similar to what was observed for the BCA protein

assay, the sensitivity of the Picogreen assay was also reduced in the presence of increasing concentrations of AS. Therefore, multiple calibration curves were prepared (Figure 5.1) with known amounts of lambda-DNA (Roche) standard in buffer containing AS concentrations between 0 and 0.5 M of AS, and the DNA concentration in the sample was estimated based on the calibration curve with the corresponding amount of AS, or the interpolation between the two closest calibration curves. For the assay, all samples were diluted 1:1 in Tris-EDTA buffer (Fisher Bioreagents), except Fractions #1 and Feed samples, which were diluted 1:5 and 1:10, respectively. Fluorescence with excitation at 480 nm and emission at 520 nm was measured using a SpectraMax i3 plate reader.

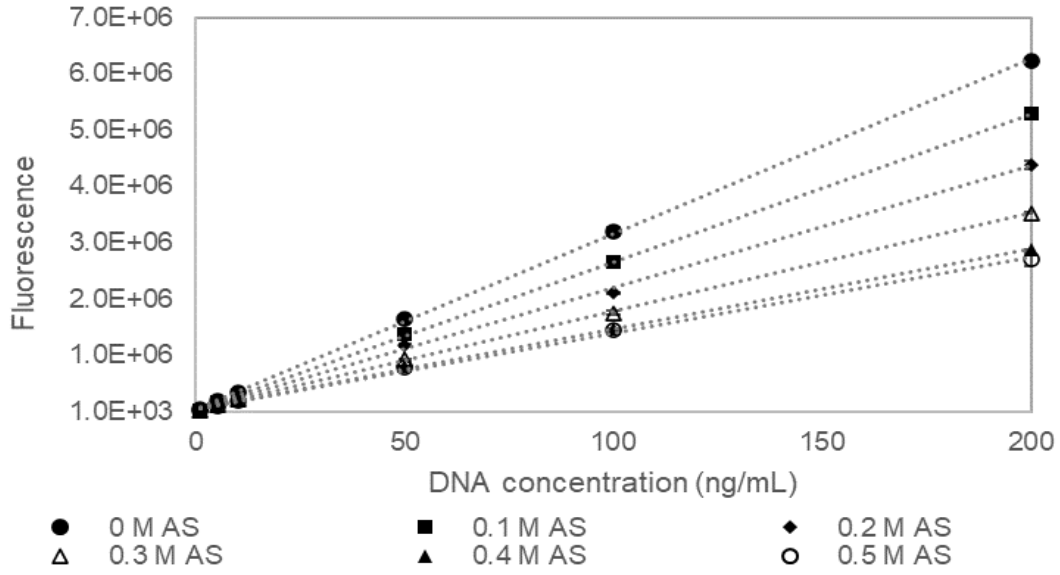

Figure 5.1. Calibration curves used to estimate the DNA concentration in fractions of chromatography runs using the Picogreen assay, using lambda-DNA standard diluted in buffer containing different concentrations of AS as indicated by the different markers. Each point represents the average of duplicate tests. Dashed lines along each set of points correspond to their linear regression model.

5.4. Results and Discussion

5.4.1. Effect of buffer pH and ammonium sulfate concentration on the purification of VSV using hydrophobic interaction membrane chromatography

Briefly, before the HIMC runs are discussed, the results of initial attempts of using Sartobind Q were unsuccessful with only less than 10% of the virus being recovered in the eluate (Appendix C). This is consistent with previous reports of low recoveries of VSV from Sartobind Q anion-exchange membrane.[9] Attempts to purify VSV with Sartobind SC, a pseudo-affinity membrane to which certain viruses can bind, were also unsuccessful since VSV did not bind to this membrane and simply flowed through along with impurities (Appendix C).

A total of ten runs using 1 mL of diluted VSV lysate were conducted to investigate the effect of buffer pH on virus recovery and purity, and the effect of the concentration of AS in the binding buffer. The VSV feed material used for these ten runs were all from the same batch and contained an average VSV titer of $2.41\times10^{9} \pm 1.71\times10^{9}$ $TCID_{50}$/mL, 6797 ± 1466 µg/mL of protein, and 142 ± 39 ng/mL of DNA.

Although pH is not a parameter commonly considered during the optimization of HIC processes, it is known to affect the dynamic binding capacity of columns during protein purification;[35] pH is also an important factor for virus stability. For rhabdoviruses, the pH used in different stages of the downstream process typically ranges between 6.5 and 7.8.[2,8-10,36] In this part of the study, the effect of pH (7.4 or 8.0) was investigated for runs starting with binding buffer containing 1.0 M AS. Figure 5.2 shows the results of one of

the duplicate runs performed for each pH condition (Runs #4 and #2 as indicated in Table 5.1, respectively). Based on this Figure, similar UV profiles were obtained for the runs with pH 7.4 and 8.0: first, a flow-through peak with a maximum around the 5 mL mark contained mostly protein and DNA as indicated by the vertical bars. Next, shallow peaks that extended up to approximately the 18 mL mark were observed; fractions corresponding to these peaks contained a small amount of DNA (green dotted bars) and phenol red (a component of the culture media) based on a visual inspection. The pool of fractions obtained between the 0 and 15 mL marks (Fractions #1 to #4) will hereby be referred to as 'flow-through' fractions (Table 5.1). At the 15 mL mark, the step elution was introduced by switching to the buffer without AS, and the response to this step happened around the 19 mL mark when the conductivity started to drop causing the virus to elute. The pool of fractions obtained between the 15 and 30 mL marks will hereby be referred to as 'elution' fractions and the total amount of virus recovered in these fractions was higher for the run using pH 7.4, where a total of 9.7×10^{8} $TCID_{50}$ was obtained, compared with 4.4×10^{8} $TCID_{50}$ with for run using pH 8.0. A small amount of DNA (15.1 ng and 16.5 ng, respectively) co-eluted with the virus, and protein amounts were below the detection limit of 10 µg/mL in both cases (Table 5.1). The reproducibility of the chromatograms shown in Figure 5.2 was confirmed by comparison with the chromatograms of their respective duplicates, runs #1 and #3 (results not shown). Although some variation in terms of the amounts of virus eluted in each fraction was observed, the total amount of virus recovered during the elution for the duplicate run using pH 7.4 (1.3×10^{9} $TCID_{50}$/mL) was still significantly higher than for the duplicate run using pH 8.0 (3.2×10^{8} $TCID_{50}$/mL). This

suggests that VSV was more stable during HIMC using pH 7.4 for binding buffer with 1 M AS. This pH was used in the remaining runs with changing AS concentrations in the binding buffer.

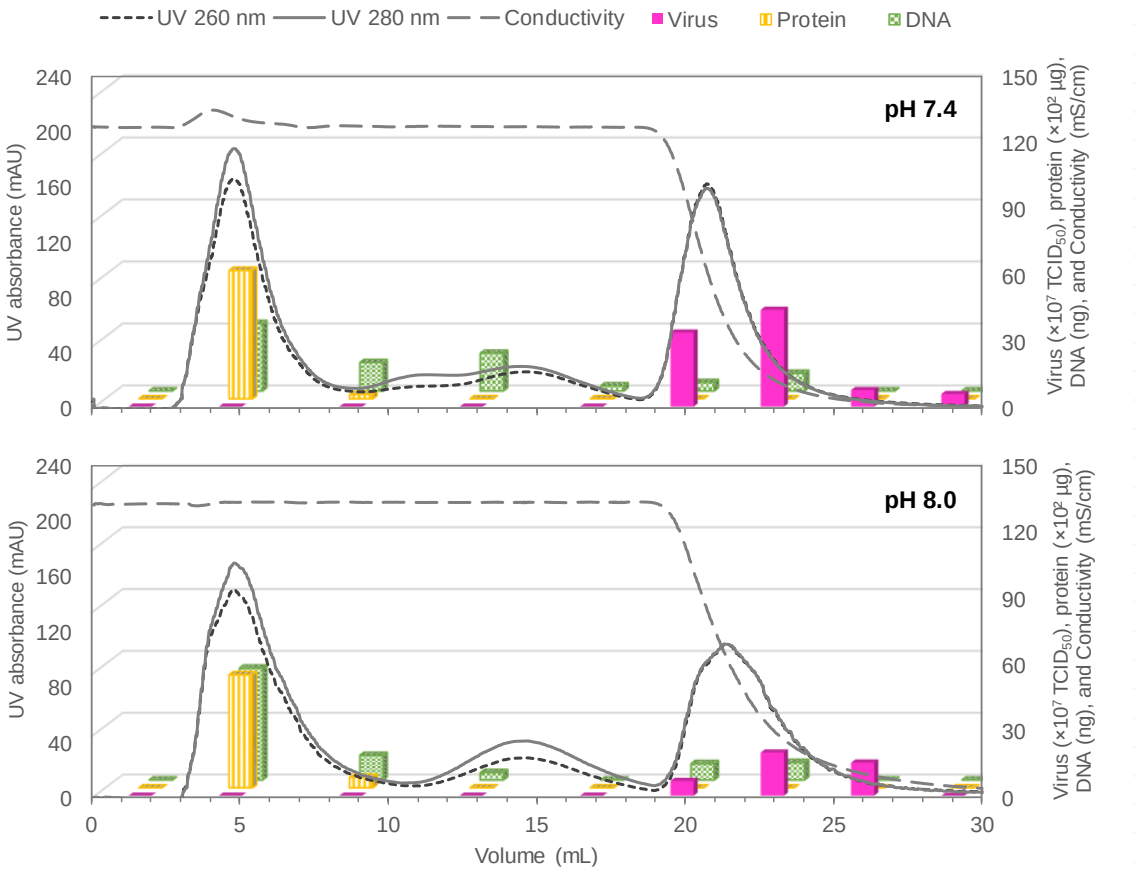

Figure 5.2. Results of chromatography Run #4 (top panel, using pH 7.4) and Run #2 (bottom panel, using pH 8.0). Solid lines and short-dashed lines correspond to the UV absorbance (mAU) at 280 nm and 260 nm, respectively; long-dashed lines correspond to the buffer conductivity (mS/cm); front solid pink bars correspond to the amount of virus ($\times 10^7$ $TCID_{50}$) in each fraction; middle yellow bars correspond to the amount of protein ($\times 10^2$ µg) in each fraction; and green dotted bars correspond to the amount of DNA (ng) in each fraction. The bars are aligned with the centre of each fraction.

Since the virus completely bound to the Sartobind Phenyl membrane when binding buffer with 1 M AS was used (i.e. no virus was detectable in the flow-through fractions),

the next step of the study focused on evaluating the effect of reducing the initial amount of AS, since lowering the AS concentrations contributes for better virus stability.[16] In this part of the study, binding buffers with four different initial AS concentrations (0.7, 0.8, 0.9, and 1.0 M) at a fixed pH of 7.4 were used in chromatography runs performed in duplicate. The UV profiles followed the trend observed earlier in the first part of the study (Figure 5.2). The total amounts of virus, protein, and DNA in the flow-through and elution fractions of each run are shown in Table 5.1. No virus was observed in the flow-through fractions, even when the lowest AS concentration was used initially (0.7 M), indicating a high degree of virus binding; varying amounts of protein and DNA were observed in the flow-through fractions as seen in Table 5.1, but no significant difference was observed across the four different conditions evaluated. For the elution fractions, no significant difference in terms of virus and DNA was observed across all runs (Table 5.1) and the average virus recovery across all runs was 47% ± 35% respective to the average amount of virus in the feed samples; the large standard deviation is associated with the known high errors of the $TCID_{50}$ assay.[33] The only difference was in terms of the total amount of protein in the elution fractions, which was below the detection limit of 10 µg/mL only for the runs using the highest and lowest AS concentrations (0.7 and 1.0 M) in the binding buffer. Runs using 0.8 and 0.9 M AS had considerable amounts of protein varying from 51.7 to 115.5 µg/mL. It is still unclear why better protein removal was achieved when 1.0 M and 0.7 M AS was used in the binding buffer, but it is likely related to the broad diversity of proteins present in the lysate, which all have distinct behaviour when in the presence of a kosmotropic salt such as AS. For a deeper understanding, finer protein characterization methods would be

needed to identify which specific proteins co-elute with the virus, however, this will not be addressed in this study.

Table 5.1. Total amount of virus, protein and DNA in the flow-through and elution fractions of HIMC runs investigating the effects of buffer pH and AS concentration in the binding buffer. Virus amounts and their standard deviations were calculated using the Spearman Karber method, protein and DNA averages and standard deviations were calculated based on duplicate measurements of each sample. BDL: below the detection limit.

Run #	Buffer pH	[AS] in binding buffer (M)	Amount in the flow-through (Fractions #1 – #4)			Amounts in the elution (Fractions #5 – #9)		
			Virus ($TCID_{50}$)	Protein (µg)	DNA (ng)	Virus ($TCID_{50}$)	Protein (µg)	DNA (ng)
1	8.0	1.0	BDL	5329 ± 94	56.3 ± 6.2	$3.2\times10^{8} \pm 5.9\times10^{7}$	BDL	9.3 ± 0.4
2	8.0	1.0	BDL	5997 ± 170	69.9 ± 7.3	$4.4\times10^{8} \pm 7.5\times10^{7}$	BDL	16.5 ± 0.8
3	7.4	1.0	BDL	5584 ± 6	19.9 ± 7.1	$1.3\times10^{9} \pm 2.2\times10^{8}$	BDL	3.9 ± 0.6
4	7.4	1.0	BDL	6424±3320	64.6 ± 7.7	$9.7\times10^{8} \pm 2.2\times10^{8}$	BDL	15.1±1.4
5	7.4	0.9	BDL	4892 ± 161	92.6 ± 7.6	$1.2\times10^{9} \pm 2.1\times10^{8}$	75.7±0.0	16.0±0.6
6	7.4	0.9	BDL	4557 ± 25	63.0 ± 8.6	$1.6\times10^{9} \pm 3.0\times10^{8}$	115.5±3.1	23.4±1.4
7	7.4	0.8	BDL	3735 ± 149	88.8 ± 18.7	$1.1\times10^{9} \pm 2.0\times10^{8}$	51.7 ± 1.5	5.0 ± 0.3
8	7.4	0.8	BDL	4618 ± 472	50.0 ± 3.4	$1.1\times10^{9} \pm 1.9\times10^{8}$	96.1 ± 1.0	BDL
9	7.4	0.7	BDL	5179 ± 252	97.7 ± 6.0	$1.1\times10^{9} \pm 2.0\times10^{8}$	BDL	3.6 ± 0.4
10	7.4	0.7	BDL	4361 ± 1	81.2 ± 3.9	$7.7\times10^{8} \pm 1.7\times10^{8}$	BDL	9.6 ± 0.9

5.4.2. Scale-up of hydrophobic interaction membrane chromatography runs for VSV purification

This last part of the study focused on scaling up the HIMC process to purify 300 mL of diluted VSV lysate with the 3 mL Sartobind Phenyl Nano device. Duplicate runs #11 and #12 were conducted using a buffer pH of 7.4 and a 1 M AS concentration in the binding buffer. These conditions were selected because they yielded the best results in the

low-volume runs discussed in the previous section. The feed material for these runs was produced in two batches using hyperflasks and had the composition indicated in Table 5.2.

Since the duplicate runs had comparable results, Figure 5.3 shows the results for only one of the runs. Figure 5.3-A shows the chromatogram where an increase in the UV absorbance is observed immediately after the start of the run and it extends throughout the whole sample loading phase (i.e. 0 to 300 mL marks), corresponding to the flow-through of protein and DNA. At the 300 mL mark, the wash step with binding buffer started and a drop in the UV signal is observed until it returned to baseline. A step elution was introduced at the 360 mL mark by applying buffer without any AS. The response seen by the drop in conductivity happened at approximately the 364 mL mark, which is followed by the virus elution peak. Figure 5.3-B focuses on the virus elution peak and provides the compositions of the fractions in terms of virus, protein, and DNA and Table 5.2 shows the detailed composition of the different fractions collected during the run.

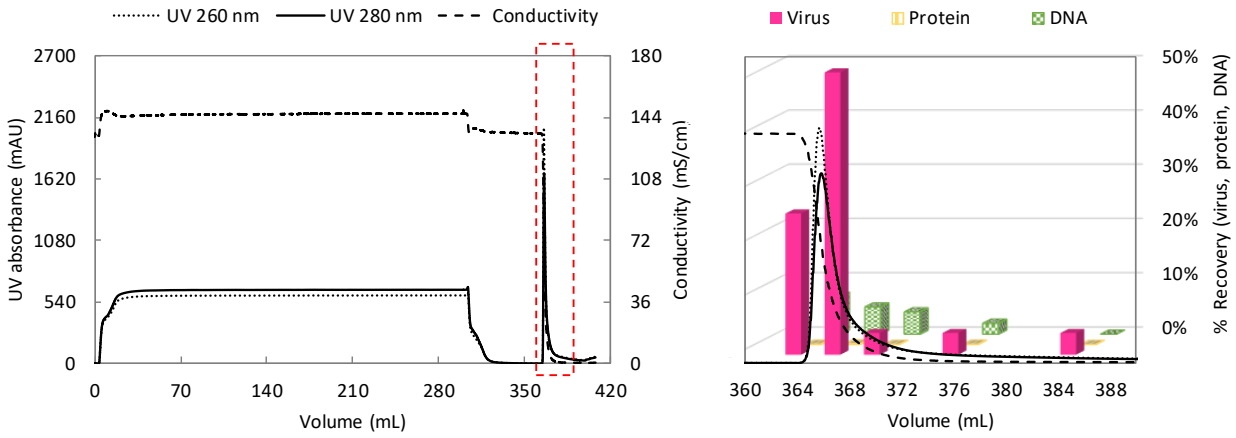

Figure 5.3. Results of HIMC for Run #11. Solid lines and short-dashed lines correspond to the UV absorbance (mAU) at 280 nm and 260 nm, respectively; long-dashed lines correspond to the buffer conductivity (mS/cm); front solid pink bars correspond to virus recovery respective to the amount in the feed; middle yellow bars

correspond to residual protein; and green dotted bars correspond to residual DNA in each fraction. The bars are aligned with the centre of each fraction.

Most VSV eluted between the 362 and 368 mL marks (78 ± 5% of the total in the feed for run #11 and 54 ± 13% for run 12). This represents a 50-fold concentration factor for VSV since the virus present in 300 mL of lysate was concentrated down to a 6 mL fraction. Meanwhile, good removal of impurities was achieved, especially of host-cell protein, where only an average of 0.2% of the total amount in the feed co-eluted with the virus. The average residual amount of DNA was 10%, which could be a potential concern since FDA guidelines establish a limit of 10 ng/dose of host-cell DNA in gene therapy products.[37] It is however important to emphasize that the lysates were applied onto the HIMC devices directly after clarification and dilution in high-salt buffer. To tackle the residual DNA issue, an enzymatic DNA digestion could be added before the HIMC and these unit operations could be optimized in conjunction, as it has been proven to be an effective strategy for the purification of adenoviruses.[32] Alternatively, a polishing step could be implemented after the HIMC to further remove host-cell DNA.

Table 5.2. Total amount of virus, protein and DNA in the different fractions of HIMC scale-up runs where 300 mL of VSV lysate was purified using a 3 mL Sartobind Phenyl Nano device. Virus amounts and their standard deviations were calculated using the Spearman Karber method, protein and DNA averages and standard deviations were calculated based on duplicate measurements of each sample. BDL: below the detection limit.

Run #	**Fraction interval**	**Feed**	**0 to 362 mL**	**362 to 365 mL**	**365 to 368 mL**	**368 to 371 mL**	**371 to 380 mL**	**380 to 403 mL**
	Total volume (mL)	**300**	**362**	**3**	**3**	**3**	**9**	**23**
11	Total VSV ($TCID_{50}$)	2.8×10^{11} $\pm1.7\times10^{10}$	BDL	7.2×10^{10} $\pm2.9\times10^{9}$	1.4×10^{11} $\pm3.7\times10^{9}$	1.1×10^{10} $\pm2.4\times10^{9}$	9.6×10^{9} $\pm1.1\times10^{9}$	1.5×10^{10} $\pm2.9\times10^{9}$

	Total protein (mg)	2114±75	2075±81	1.2±0.02	2.6±0.1	0.6±0.01	1.3±1.1	0.3±0.1
	Total DNA (µg)	138±4	97±5	10±0.4	6.9±1.3	5.7±0.1	2.2±0.1	0.2±0.01
12	Total VSV ($TCID_{50}$)	6.1×10^{11} $\pm1.0\times10^{11}$	BDL	7.2×10^{10} $\pm1.4\times10^{10}$	2.6×10^{11} $\pm4.4\times10^{10}$	3.6×10^{10} $\pm7.0\times10^{9}$	1.6×10^{10} $\pm1.9\times10^{9}$	2.4×10^{10} $\pm4.2\times10^{9}$
	Total protein (mg)	2210±75	2154±41	1.5±0.05	3.3±0.4	0.6±0.01	0.5±0.02	0.2±0.1
	Total DNA (µg)	93±1	57±4	4.7±4.2	3.1±1.3	3.5±0.1	1.2±0.1	BDL

5.5. Conclusions

This study demonstrates the efficient purification of VSV directly from culture media lysates using the Sartobind Phenyl HIMC device at relatively low AS concentrations in the binding buffer (up to 1 M AS) compared with those previously reported for the purification of different types of viruses with different HIC matrices.[12,13,15,16] To our knowledge, this is the first report of the implementation of HIMC for the purification of VSV and one of the first ones to apply this technology for virus purification. In the first part of the study where 1 mL of VSV lysate was purified using a 3 mL Sartobind Phenyl HIMC device, buffer pH of 7.4 resulted in a virus yield approximately 3 times that obtained using pH 8.0 when binding buffer with 1.0 M AS was used, demonstrating the importance of buffer pH in the virus stability. Next, for a fixed pH of 7.4, AS concentrations of 0.7, 0.8, 0.9 and 1.0 M in the binding buffer were tested and resulted in a high degree of virus binding, with no virus detectable in the flow-through fractions. Across all runs, similar amounts of virus and residual DNA were obtained in the elution, and the lowest amounts

of residual protein (below 10 µg/mL) were obtained with the runs performed with 0.7 and 1.0 M AS in the binding buffer. Finally, scale-up runs where 300 mL of VSV lysates were purified using the 3 mL HIMC Sartobind Phenyl device, with very promising results. The virus was concentrated down to a 6 mL fraction, with up to 78% recovery and with very low residual amounts of protein impurity, below 1% the amount in the feed and 10% of the amount of DNA. This HIMC process can be easily integrated in VSV manufacturing processes for the capture, concentration, and purification all in one relatively simple step.

5.6. Acknowledgements

Funding was provided by the Ontario Research Fund-Research Excellence program and the Natural Sciences and Engineering Research Council of Canada. Additional funding was provided by BioCanRx, a Network of Centres of Excellence program, in the form of a Summer Studentship Award to A. Noelle Wilton. The authors thank Ms. Natasha Kazhdan, from the McMaster Immunology Research Centre (Department of Pathology and Molecular Medicine), for her assistance with culturing the VSV batches.

5.7. References

1. Racine, T., Kobinger, G. P. & Arts, E. J. Development of an HIV vaccine using a vesicular stomatitis virus vector expressing designer HIV-1 envelope glycoproteins to enhance humoral responses. AIDS Res. Ther. 14, 2–7 (2017).
2. Gélinas, J. F. et al. Production of rVSV-ZEBOV in serum-free suspension culture of HEK 293SF cells. Vaccine 37, 6624–6632 (2019).
3. Malherbe, D. C. et al. A single dose of replication-competent VSV-vectored vaccine expressing SARS-CoV-2 S1 protects against virus replication in a hamster model of severe COVID-19. npj Vaccines 6, 91 (2021).

4. Felt, S. A. & Grdzelishvili, V. Z. Recent advances in vesicular stomatitis virus-based oncolytic virotherapy: A 5-year update. J. Gen. Virol. 98, 2895–2911 (2017).

5. Kiesslich, S., Vila-Chã Losa, J. P., Gélinas, J. F. & Kamen, A. A. Serum-free production of rVSV-ZEBOV in Vero cells: Microcarrier bioreactor versus scale-XTM hydro fixed-bed. J. Biotechnol. 310, 32–39 (2020).

6. Shen, C. F. et al. Development of suspension adapted Vero cell culture process technology for production of viral vaccines. Vaccine 37, 6996–7002 (2019).

7. Elahi, S. M., Shen, C. F. & Gilbert, R. Optimization of production of vesicular stomatitis virus (VSV) in suspension serum-free culture medium at high cell density. J. Biotechnol. 289, 144–149 (2019).

8. Ausubel, L. J. et al. Current Good Manufacturing Practice Production of an Oncolytic Recombinant Vesicular Stomatitis Viral Vector for Cancer Treatment. Hum. Gene Ther. 22, 489–497 (2011).

9. Kang, Y., Cutler, M. W., Ouattara, A. A. & Syvertsen, K. E. Purification processes for isolating purified vesicular stomatitis virus from cell culture. (2011).

10. Federspiel, M. J., Wegman, T. R., Langfield, K. K., Walker, H. J. & Stephan, S. A. Rhabdoviridae virus preparations. 1–5 (2010).

11. Gupta, S. K. & Shukla, P. Sophisticated cloning, fermentation, and purification technologies for an enhanced therapeutic protein production: A review. Front. Pharmacol. 8, 1–17 (2017).

12. Wolff, M. W., Siewert, C., Hansen, S. P., Faber, R. & Reichl, U. Purification of cell culture-derived modified vaccinia ankara virus by pseudo-affinity membrane adsorbers and hydrophobic interaction chromatography. Biotechnol. Bioeng. 107, 312–320 (2010).

13. Hansen, S. P., Faber, R., Reichl, U., Wolff, M. & Gram, A. P. Purification of vaccinia viruses using hydrophobic interaction chromatography. (2011).

14. Li, H. et al. A hydrophobic interaction chromatography strategy for purification of inactivated foot-and-mouth disease virus. Protein Expr. Purif. 113, 23–29 (2015).

15. Vincent, D. et al. The development of a monolith-based purification process for Orthopoxvirus vaccinia virus Lister strain. J. Chromatogr. A 1524, 87–100 (2017).

16. Weigel, T., Soliman, R., Wolff, M. W. & Reichl, U. Hydrophobic-interaction chromatography for purification of influenza A and B virus. J. Chromatogr. B Anal. Technol. Biomed. Life Sci. 1117, 103–117 (2019).

17. Fraud, N., Faber, R., Kiss, C. & Demmer, W. Hydrophobic-Interaction Membrane Chromatography for Large-Scale Purification of Biopharmaceuticals. Bioprocess Int. 2001, 30–35 (2009).

18. Muthukumar, S., Muralikrishnan, T., Mendhe, R. & Rathore, A. S. Economic benefits of membrane chromatography versus packed bed column purification of therapeutic proteins expressed in microbial and mammalian hosts. J. Chem. Technol. Biotechnol. 92, 59–68 (2017).

19. Ebert, S. & Fischer-Frühholz, S. Efficient aggregate removal from impure pharmaceutical active antibodies. Bioprocess Int. 9, 36–42 (2011).

20. Kuczewski, M., Schirmer, E., Lain, B. & Zarbis-Papastoitsis, G. A single-use purification process for the production of a monoclonal antibody produced in a PER.C6 human cell line. Biotechnol. J. 6, 56–65 (2011).

21. Kumar, V. & Rathore, A. S. Two-stage chromatographic separation of aggregates for monoclonal antibody therapeutics. J. Chromatogr. A 1368, 155–162 (2014).

22. Mayani, M., Narahari, C., Ehamparanathan, V., Kaligotla, H. & Martin, S. Application of HIC membrane chromatography ina a disposable 2,000 L clinical facility. 16, (2018).

23. Kuczewski, M., Fraud, N., Faber, R. & Zarbis-Papastoitsis, G. Development of a polishing step using a hydrophobic interaction membrane adsorber with a PER.C6®-derived recombinant antibody. Biotechnol. Bioeng. 105, 296–305 (2010).

24. Kosior, A., Antošová, M., Faber, R., Villain, L. & Polakovič, M. Single-component adsorption of proteins on a cellulose membrane with the phenyl ligand for hydrophobic interaction chromatography. J. Memb. Sci. 442, 216–224 (2013).

25. Ribeiro, D. A., Passos, D. F., Ferraz, H. C. & Castilho, L. R. Intermediate purification of CHO-derived recombinant human Factor IX using hydrophobic interaction membrane-based chromatography and its comparison to a sulfated resin. Electrophoresis 38, 2900–2908 (2017).

26. Raiado-Pereira, L., Prazeres, D. M. F. & Mateus, M. Impact of plasmid size on the purification of model plasmid DNA vaccines by phenyl membrane adsorbers. J. Chromatogr. A 1315, 145–151 (2013).

27. Raiado-Pereira, L., Vega, J. D. La, Prazeres, D. M. F. & Mateus, M. Development of a phenyl membrane chromatography-based process yielding pharmaceutical grade plasmid deoxyribonucleic acid for mammalian cells transfection. J. Chromatogr. A 1337, 67–74 (2014).

28. Limonta, M., Zumalacárregui, L., Vidic, U. & Lendero-Krajnc, N. Comparison of CIM C4-HLD monolithic column with Sartobind phenyl membrane column for pIDKE2 purification. Chinese J. Chromatogr. 35, 1028–1036 (2017).

29. McNally, D. J., Piras, B. A., Willis, C. M., Lockey, T. D. & Meagher, M. M. Development and Optimization of a Hydrophobic Interaction Chromatography-Based Method of AAV Harvest, Capture, and Recovery. Mol. Ther. - Methods Clin. Dev. 19, 275–284 (2020).

30. Valkama, A. J. et al. Development of Large-Scale Downstream Processing for Lentiviral Vectors. Mol. Ther. - Methods Clin. Dev. 17, 717–730 (2020).

31. Lothert, K., Pagallies, F., Feger, T., Amann, R. & Wolff, M. W. Selection of chromatographic methods for the purification of cell culture-derived Orf virus for its application as a vaccine or viral vector. J. Biotechnol. 323, 62–72 (2020).

32. Kawka, K. et al. Integrated development of enzymatic DNA digestion and membrane chromatography processes for the purification of therapeutic adenoviruses. Sep. Purif. Technol. 254, 117503 (2021).

33. Roldão, A., Oliveira, R., Carrondo, M. J. T. & Alves, P. M. Error assessment in recombinant baculovirus titration: Evaluation of different methods. J. Virol. Methods 159, 69–80 (2009).

34. Finney, D. J. Statistical Method in Biological Assay. (Charles Griffin & Company Limited, 1952).

35. Baumann, P., Baumgartner, K. & Hubbuch, J. Influence of binding pH and protein solubility on the dynamic binding capacity in hydrophobic interaction chromatography. J. Chromatogr. A 1396, 77–85 (2015).

36. Shoaebargh, S. et al. Sterile filtration of oncolytic viruses: An analysis of effects of membrane morphology on fouling and product recovery. J. Memb. Sci. 548, 239–246 (2018).

37. FDA & CBER. Chemistry, Manufacturing, and Control (CMC) Information for Human Gene Therapy Investigational New Drug Applications (INDs) - Guidance for Industry. (2020).

Chapter 6

Economic analysis of adenovirus manufacturing processes for gene therapy applications

6. Economic analysis of adenovirus manufacturing processes for gene therapy clinical applications

Karina Kawka, Shayna Earle, Ian Gough, Nicholas Graham, Yuki Abe, Maria Fe C. Medina, David R. Latulippe

Prepared for Journal submission

6.1. Abstract

Advanced manufacturing processes need to be developed to keep up with an increasing demand for novel virus-based therapeutics, so these novel therapeutics can be produced in cost-effective ways. Virus manufacturing processes rely on multiple co-dependent upstream and downstream unit operations that need to be carefully designed to minimize product losses and maximize purity. Modelling and simulation are powerful tools to understand, evaluate, and optimize complex manufacturing processes in general. It can also serve as a decisional tool in the selection of operating parameters. However, the application of these tools in the field of biomanufacturing is still considered to be in its infancy. In the present study, a model of a complete adenovirus production process was developed using BioSolve Process in the context of gene therapy applications for late-stage clinical trials or early commercialization (i.e. targeting the production of 2000 doses per year). The analysis of the model permitted the identification of capital costs and quality control testing as the major cost drivers for a base scenario, significantly contributing to the cost-of-goods (COG). The model was also used to investigate the feasibility of using

membrane adsorbers (MAs) to replace conventional resins in chromatography and polishing steps of virus purification. MAs were found to offer savings of more than 20% in the COG/dose. This is one of the first studies to assess the financial benefit of using MAs in virus manufacturing, adding to the already well-known technical advantages of this technology. Finally, sensitivity analyses were applied to identify key process parameters for both the scenarios using MAs or resins and the impact of replacing DNA digestion enzymes (i.e. substituting Benzonase by Denarase, a cheaper but equally effective alternative), was also addressed. Considering practical limitations in a comprehensive analysis of the economic aspects of virus manufacturing will help address critically outstanding questions in the field and will guide a more rational selection of process conditions. Such an approach will enable the development of cost-effective ways to produce therapeutic viruses at various scales of manufacturing, ultimately benefiting patients to have fast and affordable access to new treatment options

6.2. Introduction

In the past few years, the world has seen considerable advances in the field of gene and cell therapy, with a number of new ground-breaking biotherapeutics being approved for the treatment of cancer and genetic diseases.[1] Viruses are used as vectors in most clinical trials for these new therapies, being applied directly in vivo (i.e., administered directly into the patient) or ex vivo settings (i.e., the therapeutic virus is used to transform the patients' cells in the lab before being infused back into the patient, as in CAR-T cell therapies).[1,2] Adenoviruses were the first type of vector to be applied in vivo,[3] and they are currently one of the main types of viruses used in gene therapy clinical trials, along with adeno-associated

viruses (AAV) and lentiviruses.[1] Recent efforts devoted to increasing the efficacy, safety, and development of new adenoviral vectors[1,4] suggests that they are likely to retain their position as one of the most important tools for gene therapy in the long term.

Unfortunately, approved gene and cell therapy products are highly expensive – sometimes costing millions of dollars per treatment – which is a significant barrier currently preventing patients from accessing these promising new drugs.[5] These high prices are due to a range of factors, including the high costs associated with development, manufacturing, and analytical testing.[6,7] With respect to manufacturing in particular, it will be critical to develop novel advanced processes to keep up with the rapidly-growing list of novel virus-based therapeutics.[7]

Process and economic modelling is seen by experts as one of the most effective means of improving manufacturing processes for novel biotherapeutics.[8] Modelling and simulation can also provide a deeper understanding of processes and help to identify critical parameters, thus making them powerful tools in the implementation of quality-by-design (QbD) initiatives for process development.[9] However, the modelling of gene and cell therapy manufacturing processes is still considered to be in its infancy.[10] At present, the literature contains only a handful of reports focusing process modeling to improve economic aspects of AAV and lentivirus manufacturing processes.[11-13] Thus, as long as key product differences are accounted for, this field could benefit from studies examining closely-related areas, such as cell therapy, vaccines, and other more traditional biotherapeutics, such as monoclonal antibodies (MAb). For example, adenoviruses can be used either as vectors for vaccines – with some of the vaccines against COVID-19 being

currently based on adenoviruses (AstraZeneca, Janssen, and Sputnik)[14] – or for gene therapy applications. However, there are key differences between vaccines and gene therapy that will significantly impact typical process scales. For instance, in gene therapy phase III clinical trials, the number of patients enrolled can vary significantly from tens to hundreds of patients, with high dosages in the order of 10^{11} to 10^{13} viral particles (PT) per dose.[15-17] On the other hand, for vaccines, dosages are typically lower, but the number of patients is dramatically higher. Ferreira et al.[18] recently used SuperPro Designer (Intelligen) to model adenoviral COVID-19 vaccine production, with a cost analysis based on 400 to 800 million doses per year and 10^{10} PT per dose. Their findings highlighted significant differences in the estimated cost-of-goods (COG) per dose, which is reported to be in the range of approximately 0.20 USD for vectored vaccines,[18] but over thousands of dollars per dose for gene therapy vectors (i.e., previous reports estimate approximately 12,000 USD/dose for AAV vectors[11] and approximately 1,500 USD/dose for lentiviral vector production for cell therapy applications).[12]

In the literature, modelling and cost analyses of biomanufacturing processes are typically classified into two categories. The first category focuses on developing new modelling frameworks and applying them to specific manufacturing cases, while the second focuses on modelling and simulating processes using commercially available software such as BioSolve Process (Biopharm Services) or SuperPro Designer (Intelligen). The remainder of this section will provide a brief overview of the main studies related to these two categories.

With respect to the development of modelling frameworks, Comisel et al.[12] developed a novel decisional tool comprising a model that had been integrated with an optimization algorithm to minimize COG in lentivirus production. Their findings showed that their model was able to reduce costs by up to 90% when the process switched from using cell cultures in multi-trays to suspension or fixed-bed bioreactors at large processing scales. In a recent follow-up study,[13] Comisel et al. further refined their decisional tool by including development costs and a project valuation model. They used this new framework to determine the best time to implement stable producer cell lines during the development of lentivirus- and AAV-based therapeutics. With respect to upstream manufacturing, Farid et al.[19] developed a tool that used hierarchical modelling to determine the COG of cell-culture-based products, while Lim et al.[20] described a tool for MAb process modelling and cost analysis under uncertain conditions and applied it to make decisions regarding pooling strategies in perfusion cell cultures. Conversely, Stacey et al.[21] proposed a framework for cell-culture-based processes based on an ordinary differential equation modelling paradigm. In the field of cell therapy, Abou-El-Enein et al.[22] proposed a new technique to estimate manufacturing costs in Good Manufacturing Practice (GMP) areas, while a number of other studies have proposed different decisional tools to address process cost-effectiveness.[23-27]

With regards to the use of commercially available software, BioSolve Process (Biopharm Services) has been applied for modelling and economic analysis in the fields of monoclonal antibodies,[28,29] cell therapies,[30,31] AAV vectors,[11] and other biomolecules. For instance, Cameau et al.[11] used BioSolve Process to create and analyze models for

determining the most economic cell culturing option for the production of AAV for gene therapy applications. Their analysis considered and compared numerous different scenarios, with findings demonstrating significant cost savings from using fixed-bed bioreactors instead of scaling-out the process by using multi-trays. In a different study, Lopes et al.[31] used BioSolve Process to model a CAR-T cell therapy process wherein T cells are harvested from the patient and then passed through all expansion and modification stages to create a final cryopreserved product. Their findings identified the cost associated with the lentiviral vector used to introduce the CAR genetic information into the T cells as one of the major cost-drivers, reinforcing the importance of minimizing virus manufacturing costs.

In the present study, BioSolve Process was applied to model a complete process for manufacturing adenoviral vectors for gene therapy applications, specifically within the context of dose production for late-stage clinical trials or small-scale commercial applications (i.e., targeting a production rate of 2000 doses/year). The models were used to compare base-scenarios using either membrane adsorbers (MA) or conventional resins in the chromatography steps of the purification processes. These comparisons are of particular interest because MAs possess well-known technical advantages for purifying large molecules (e.g., viruses), including their large pore sizes, which provide accessible binding sites and enable convective mass transfer and the use of high flow rates.[32] However, no previous studies in the literature have examined the economical aspects of using MAs or resins for virus purification. The analysis of the model also included a sensitivity analysis in order to identify critical process parameters as areas of opportunity to minimize COG.

6.3. Model construction and analysis

The adenovirus production models used in this research were created using BioSolve Process 8.1.5.3 (Biopharm Services Ltd.). The order of the unit operations considered in the model is shown in Figure 6.1. The target throughput for the base scenarios was assumed to be 2,000 doses/year, and the model also accounted for two different dosages typically used in adenovirus-based gene therapy clinical trials: 1×10^{12} PT/dose and 1×10^{13} PT/dose.[33-36] This model considers only the production of the drug substance, not the drug product; furthermore, it also does not consider the expenses associated with drug development, sterile fill, and finish steps. The general input parameters of the models are shown in Table 6.1. The unit operations with key input parameters for each process step are summarized in Table 6.2.

Table 6.1. General input parameters for the base scenarios created on BioSolve.

Parameter	Value
Dose size	1×10^{12} PT/dose or 1×10^{13} PT/dose [33-36]
Target throughput (doses produced per year)	2000 doses/year
Plant capacity utilization	80%
Bioreactor type	Single-use stirred tanks
Number of bioreactors available in the facility	1
Maximum size for bioreactor bag	2000 L
Solution preparation	Single-use tanks
Campaign length	12 months

In the model, the process begins with a seed train comprised of 4 cell-growth steps in shaker flasks, followed by a 2-phase fed-batch cell growth in a single-use stirred tank bioreactor. A suspension of human embryonic kidney 293 (HEK-293) cells, which are extensively used for adenovirus production,[37] was selected as the platform for the creation of the model, while HyClone CDM4HEK293 serum-free media (Cytiva) was selected for

the seed and production steps. Pricing for all components was retrieved from the supplier's website. Growth times were calculated based on kinetic equations of cell growth,[38] using the doubling times reported in the literature for suspension HEK-293 cells (Table 6.2). The fed-batch production step began by using 20% of the bioreactor volume, and then filling it with full capacity with media once a cell density of 2×10^6 cells/mL had been achieved.[39] Once a cell density of 1×10^6 cells/mL had been achieved,[33] a media-exchange step was performed wherein 90% of the culture media was removed via a microfilter. This step was immediately followed by adding fresh culture media and infecting the cells with an adenovirus seed culture using a multiplicity of infection (MOI) of 10.[33] The virus propagation procedure was carried out for 48 h (Chapter 4).[40] A virus titer of 1×10^{13} PT/L was assumed to have been achieved in the bioreactor.[37] The cost of the adenovirus seed stock was estimated to be 5,000 USD/10^{12} PT; since this is a very specific raw material, costs will vary widely depending on the facility and the initial method of production. Sensitivity analyses were later conducted to address the impact of this material cost in the total COG/dose, and to determine how critical this is for the accuracy of the study. These analyses are discussed later in this paper.

Next, the cells containing adenovirus were harvested using a microfiltration step similar to the one used in the media exchange portion of the fed-batch culture step. A 10-fold cell concentration factor was assumed during this harvesting step.[41] Although prior findings have shown that microfiltration is able to provide very high cell-recovery yields (~100%),[41,42] a safety factor was implemented; thus, a recovery rate of only 90% was assumed. In the next step, which combined cell disruption and DNA digestion, the

procedure described by Moleirinho et al. was adopted for the base scenario, wherein the cells were incubated for 4 h in the presence of 0.5% polysorbate 20 and 100 U/mL of Benzonase.[43] In accordance Chapter 4, the recovery of adenovirus during this step was assumed to be 60%.[40] In subsequent analyses Denarase (a cheaper alternative to Benzonase) was used as a substitute for Benzonase to determine how this change impacted the COG; the results of this analysis are presented in Section 6.4.5. Next, a clarification step was added to the model, whereby cell debris was removed using microfilters. The recovery rate in this step was assumed to be 90%.[44,45]

The host-cell protein and DNA was removed via a chromatography step operated in bind-and-elute (B&E) mode and using anion-exchange (AEX) matrices. In this step, the virus binds to the chromatography matrix, and is then eluted by increasing the salt concentration. To further remove host-cell impurities from the solution (i.e., to polish it), another chromatography step was implemented in flow-through (FT) mode, wherein the product flows through the chromatography matrix while the impurities are retained. As discussed above, either MAs or resins were used to create the base-scenarios, with subsequent analysis being conducted to compare the two technologies. The final two steps of the modelled process consisted of an ultrafiltration/diafiltration (UF/DF) step to exchange the product into formulation buffer (recovery was assumed to be 90%),[46] and a sterile filtration step, which has been reported to provide very high yields of adenovirus (~100%).[43,46] Nonetheless, a safety factor was implemented, and the models assumed a recovery rate of 90%.

Two base-scenarios were created in which all unit operations parameters were the same. The exception to this was the two chromatography steps, where:

- Base-scenario 1 (MA scenario) used AEX Sartobind Q MA (Sartorius) for the chromatography B&E step and Sartobind salt tolerant (STIC) MA (Sartorius) for the chromatography polishing FT step.
- Base-scenario 2 (resin scenario) used AEX resins for the chromatography B&E step and size-exclusion chromatography (SEC) resins for the chromatography polishing FT step.

More details about both base scenarios are provided in Table 6.2.

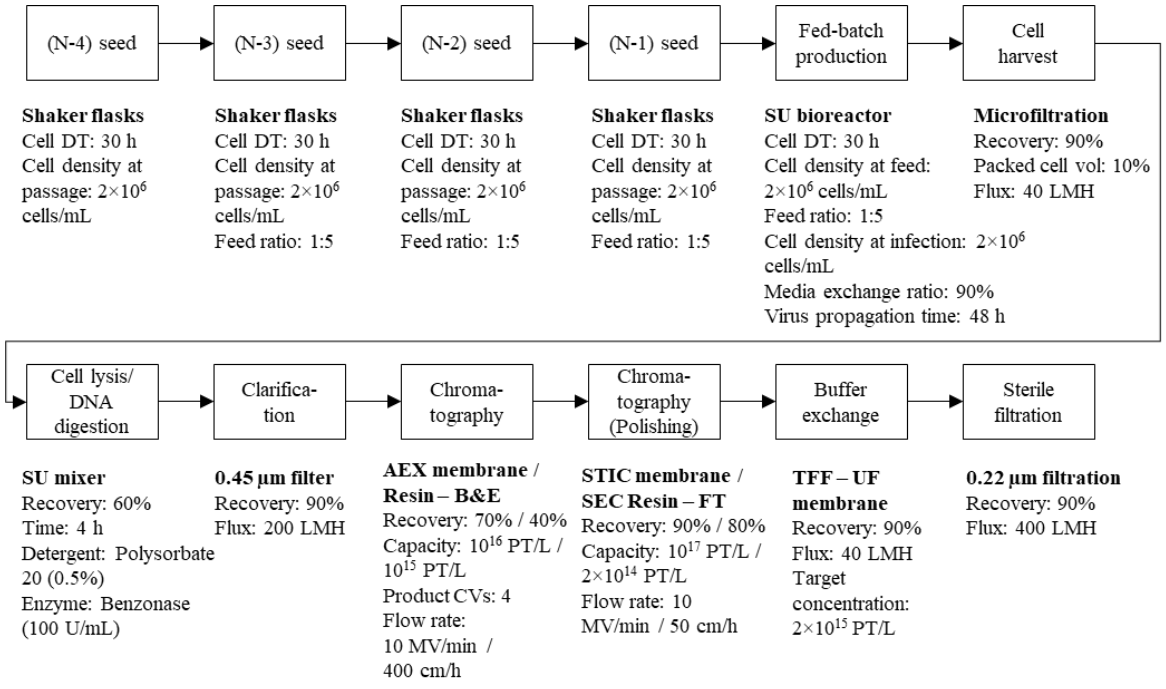

Figure 6.1. Process sequence and unit operation details used in the model. The MA base scenario used membranes in the two chromatography steps, while the resin base scenario used resins in the two chromatography steps.

Table 6.2. Model unit operation input parameters and quality control tests.

Step	Unit operation	Parameters	References	Quality control tests[47]
1-4	Seed culture	Cell doubling time: 30 h Feed ratio: 5 Cell density at passage: 2×10^6 cells/mL	38,39,48 - 39	Viable cell count
5	Fed-batch production culture	Cell doubling time (phase I and II): 30 h Vessel volume used in Phase I: 20% Cell density at feed: 2×10^6 cells/mL Cell density at infection: 1×10^6 cells/mL MOI: 10 Virus propagation time after infection: 48 h Media exchange, filter flux: 40 L/m²/h Media exchange, duration: 6 h Media exchange, cell concentration factor: 10× Virus yield: 1×10^{13} PT/L	38,39,48 - 39 33 33 40 41 - 41 37	Viable cell count Mycoplasma
6	Cell harvest	Cell recovery: 90% Filter flux: 40 L/m²/h Duration: 6 h Cell concentration factor: 10×	41,42 41 - 41	
7	Cell disruption and DNA digestion	Virus recovery: 60% ** Detergent concentration: 0.5% Benzonase concentration: 100 U/mL Time: 4 h	40 43 40,43 40,43	Total and infectious virus titer Residual DNA
8	Clarification	Virus recovery: 90% Filter flux: 200 L/m²/h Duration: 2 h Filter capacity: 400 L/m²	44,45 49,50 - 50	Total and infectious virus titer
9	Chroma-tography (B&E)	*MA Model* MA type: Sartobind Q Virus recovery: 70% Membrane capacity: 10^{16} VP/L Maximum number of uses: 4 Flow rate: 10 MV/min Product elution volume: 4 MVs *Resin Model* Resin type: AEX resin Virus recovery: 40% Resin capacity: 10^{15} VP/L Maximum number of uses: 50 Flow rate: 400 cm/h Product elution volume: 4 CVs	- 40 46 - - - - 51 51 - 51 -	Total and infectious virus titer pH Purity
10	Chroma-tography (FT polishing)	*MA Model* MA type: Sartobind STIC Virus recovery: 90% Membrane capacity: 10^{17} VP/L * Maximum number of uses: 1 Flow rate: 10 MV/min *Resin Model* Resin type: size-exclusion (SEC) Virus recovery: 80%	- 52 - 52 - - 43,53	Total and infectious virus titer pH Purity

		Resin capacity: 1.6×10^{14} VP/L **	[43]	
		Maximum number of uses: 50	-	
		Flow rate: 50 cm/h	[54]	
11	Buffer exchange	Virus recovery: 90%	[46]	Total and infectious virus titer
		Filter flux: 40 L/m²/h	[55]	pH
		Duration: 1 h	-	Purity
		Target final virus concentration: 2×10^{15} VP/L	-	
12	Sterile filtration	Virus recovery: 90%	[43,46]	Total and infectious virus titer pH Purity Bioburden Endotoxins Residual HCP UV spectrometry Conductivity
		Flux: 400 L/m²/h	-	
		Duration: 0.5 h	-	
		Filter capacity: 400 L/m²	-	

* Estimated based on Sartobind STIC capacity for DNA binding (10 mg/mL), considering residual DNA amounts of 1 µg/mL in the feed. ** Capacity estimated based on the results reported in the article.

All equipment, consumables, and amounts of materials were sized by BioSolve to attain the specified target throughput. To successfully run the model, the BioSolve library of equipment and consumable sizes and prices was supplemented with information regarding MAs and filters that were not originally present in the database. This was achieved via an extensive data survey to gather the technical specifications and prices of commercially available consumables. The results of the MA survey are provided in Table E1 of Appendix E, which displays details relating to all the main commercially available MA materials. As discussed above, only the costs associated with Sartobind Q and Sartobind STIC MA were considered in the scenarios. A similar survey-based approach was used to gather list prices for microfilters based on Millipore Optiseal devices and their respective specifications and prices listed on the supplier's website.

Analysis was performed by using BioSolve's advanced scenarios feature to run hundreds of scenarios evaluating the effect of different parameters (Table 6.3). These

analyses aimed to identify cost-drivers, critical process parameters, and explore areas of opportunity to reduce production costs.

- The COG/dose was estimated for the base scenarios, which assumed dosages of 1×10^{12} or 1×10^{13} PT/dose.
- The COG breakdown was determined for the different scenarios at different dosages to identify key cost drivers and how each unit operation contributed to the total COG.
- The effect of processing scale on the COG was also determined for the different scenarios to identify the trends that emerged in the COG as scale increased.
- Sensitivity analyses were performed by changing the key process parameters listed in Table 6.3 and quantifying their impact on the COG to identify which were most critical.
- Finally, a case study was conducted to examine whether and to what extent substituting Benzonase with a cheaper alternative (Denarase) could reduce costs.

Table 6.3. Parameters used for sensitivity analysis of MA and resin scenarios to produce 2,000 doses/year for dose sizes of 1×10^{12} PT/dose or 1×10^{13} PT/dose.

Parameter	Worst case	Base-scenario	Best case
Titer in bioreactor (PT/L)	9.0×10^{12} PT/L	1.0×10^{13} PT/L	1.1×10^{12} PT/L
Capacity utilization of the plant	72%	80%	88%
Virus yield in the cell disruption/DNA digestion step	54%	60%	66%
Virus yield in the chromatography B&E step	63% (MA model) 36% (Resin model)	70% (MA model) 40% (Resin model)	77% (MA model) 44% (Resin model)
QC cost (USD/batch)	52,293	47,539	42,785

Benzonase cost (USD/kU)	4.66	3.73	2.80
Culture media cost (USD/kg)	2,834	2,267	1,700
Virus seed stock cost (USD/10^{12} PT)	6,250	5,000	3,750

6.4. Results and Discussion

6.4.1. Estimated COG for MA and resin base scenarios assuming dosages of 1×10^{12} and 1×10^{13} PT/dose

BioSolve was used to model two adenovirus production base scenarios: one that employed MAs for virus purification in the chromatography B&E, and FT polishing steps (MA scenario), and one that used conventional resins (resin scenario). All other unit operations were the same for both scenarios; details relating to the input parameters are provided in Figure 6.1 and Tables 6.1 and 6.2. The estimated COG/dose for the MA and resin base scenarios – assuming dose sizes of 1×10^{12} PT/dose and 1×10^{13} PT/dose, respectively – are shown in Table 6.4. As the results show, the MA scenario always provided a lower COG than the resin scenario. For example, the use of resins resulted in a COG that was 13% higher compared to the MA scenario at 1×10^{12} PT/dose; more significantly, the COG was 30% higher for the resin scenario when 1×10^{13} PT/dose dosage was assumed. These differences are mainly due to the lower virus recovery rates observed in the resin base case for both the B&E chromatography (i.e., 40% with resin and 70% with MA) and polishing (i.e., 80% with resin and 90% with MA) steps, respectively. This resulted in overall recovery rates of 13% and 25% for the full downstream processes of the resin and MA base cases, respectively. In this situation, the higher COG observed in the resin base case was directly related to the larger-sized equipment and higher amounts of

consumables and materials required to produce sufficient quantities of virus in the steps preceding the chromatography in order to achieve the target throughput. For instance, the volume of culture in the bioreactor was significantly larger (45 L) in the resin scenario compared to the MA scenario (23 L) when a dosage of 1×10^{12} PT/dose was assumed; similarly, the resin scenario required 442 L of volume culture, compared to 225 L for the MA scenario, when a dosage of 1×10^{13} PT/dose was assumed. Although the technical advantages of using MAs instead of resins for the purification of large biomolecules such as viruses has been well-described in the literature, the present study is among the first to demonstrate that there are also financial benefits to using MAs.

Table 6.4. COG per dose estimated to produce 2,000 or 20,000 doses/year using the MA or resin models for dose sizes of 1×10^{12} PT/dose or 1×10^{13} PT/dose.

Target Throughput	**BioSolve Scenario**	**COG/dose for a dose size of:**	
		1×10^{12} PT/dose	**1×10^{13} PT/dose**
2,000 doses/year	MA	3,267 USD/dose	5,039 USD/dose
	Resin	3,694 USD/dose	6,581 USD/dose
20,000 doses/year	MA	504 USD/dose	1,712 USD/dose
	Resin	658 USD/dose	3,599 USD/dose

6.4.2. COG breakdown for MA base scenarios assuming dosages of 1×10^{12} and 1×10^{13} PT/dose

BioSolve Process accounts for 5 main categories when calculating COG: capital charges, materials (including costs relating to media, buffers, water, cleaning, raw materials, and quality control tests), consumables (including costs relating to resins or MAs, bags, filters, etc.), labour (including process, quality, and indirect labour), and other costs (including costs associated with insurance, waste management, maintenance, and utilities). Figure 6.2 shows the COG breakdown for these 5 categories in the overall MA scenarios,

assuming dosages of 1×10^{12} and 1×10^{13} PT/dose (left and right panels, respectively) and a production target of 2,000 doses per year. As can be seen for the 1×10^{12} PT/dose scenario, capital costs and quality control tests contribute to most of the COG (34% and 26%, respectively). In contrast, capital costs and quality control testing only account for 20% and 11% of the COG, respectively, in the scenario using the higher dosage of 1×10^{13} PT/dose. These values are presented in detail in Tables E2 and E3 in the Appendix E. The cost associated with quality control testing remained constant (47,540 USD/batch) independent of the dosage size, as it was dependent on the tests that needed to be run during different stages of the process. For reference, the simulations resulted in the production of 36 batches per year in both dosage cases. The costs of the quality control tests were reasonably close to the range of 15,000 USD to 40,000 USD per batch reported in the literature for the production of AAV and lentivirus, respectively.[11,12] In this study, however, we discretized the different QC tests performed at different unit operations (Table 6.2) according to recommendations outlined in the literature.[47] These results can be found in Tables E2-E5 in Appendix E.

Other parameters besides capital and QC tests became more important in the higher 1×10^{13} PT/dose scenario, including the costs associated with culture media and other raw materials due to the larger production volumes. In particular, the raw materials costs for both scenarios were strongly driven by the cost of Benzonase, which is the enzyme that is used to digest DNA in the cell disruption/DNA digestion step. In the 1×10^{12} PT/dose scenario, Benzonase accounted for 2,574 USD of the 3,732 USD in direct raw materials costs, while in the 1×10^{13} PT/dose scenario it accounted for 25,178 USD of the 36,505 USD

in direct raw materials costs. Since the Benzonase's significant impact on virus manufacturing costs is well-known in the field,[37] this topic will be explored in further detail in subsequent sections of this paper.

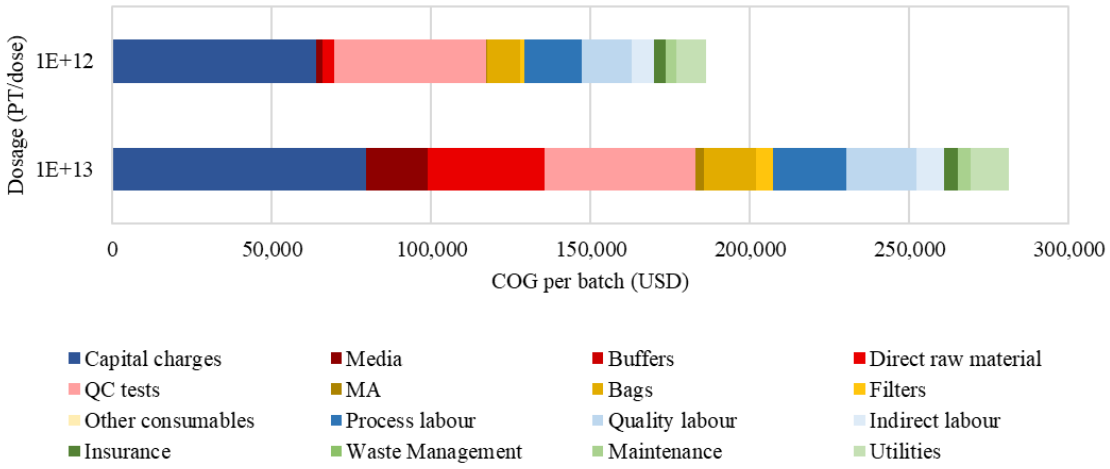

Figure 6.2. Overall COG breakdown for the MA scenario targeting the production of 2,000 doses/year and dosages of 1×10^{12} PT/dose (left) and 1×10^{13} PT/dose (right).

Figure 6.3 shows a breakdown of the per-batch COG for each unit operation in the MA scenario based on the 5 analyzed cost categories at assumed dosages of 1×10^{12} and 1×10^{13} PT/dose (top and bottom panels, respectively) and a production target of 2,000 doses per year. For both dosages, the fed-batch culture accounted for the greatest individual contribution to the COG; however, the combined downstream unit operations (i.e., from cell harvest to sterile filtration) comprised approximately 60% of the COG. This result is consistent with prior findings identifying downstream processing as the greatest contributor to viral vector production costs,[56] thus further affirming the need for more efficient large-scale virus-purification methods. A simple comparison of the COG breakdown for the two

dosages reveals that material costs related to the fed-batch culture and cell disruption/DNA digestion steps contribute significantly more to the overall COG at higher dosages; as noted above, this increase is the product of the need for more culture media and Benzonase in the 1×10^{13} PT/dose scenario. The COG breakdown for the resin scenario is illustrated in the Appendix E (Figure E1). Overall, the distribution of costs closely followed the trends observed for the MA scenario, but the cost associated with materials (i.e., culture media and Benzonase) was even more pronounced in the higher-dose condition. This increase is associated with the larger processing volumes required prior to the chromatography unit operations in the resin scenario, as discussed in Section 6.4.1.

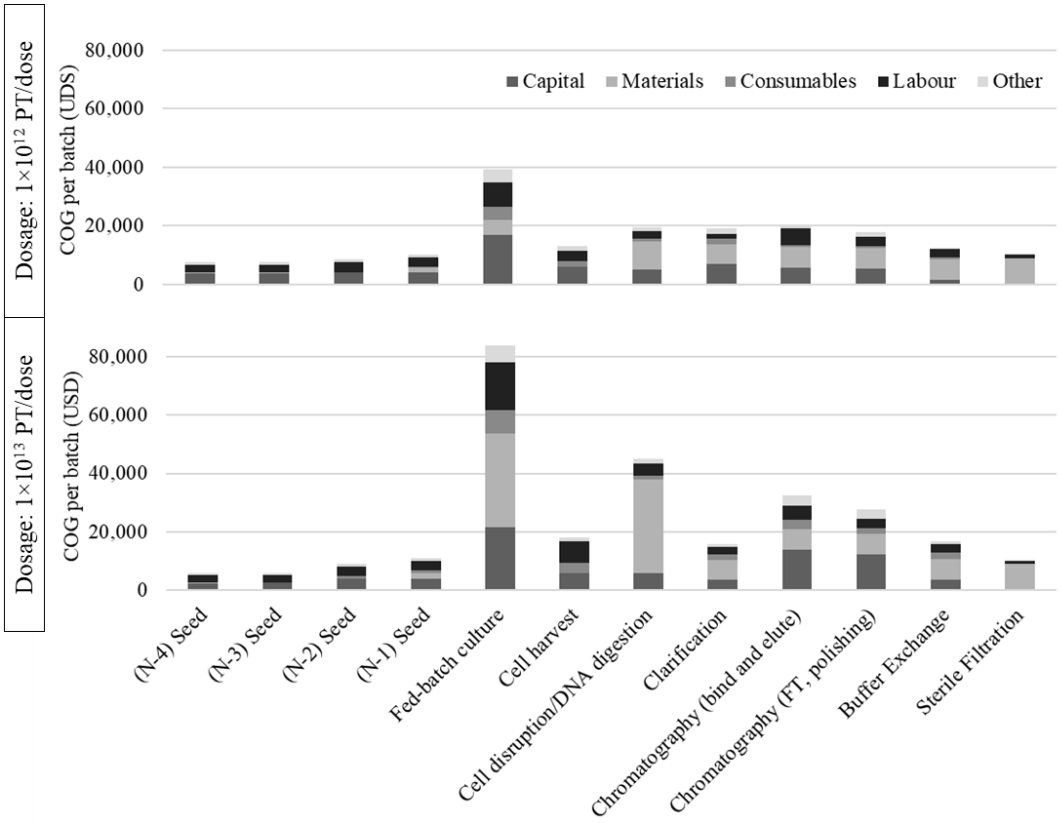

Figure 6.3. COG per-batch breakdown for MA scenario assuming a dose size of 1×10^{12} PT/dose (top panel) and 1×10^{13} PT/dose (bottom panel) and a production target of 2,000 doses/year. The per-batch COG is

presented for all the unit operations (listed at bottom) based on the five major different cost types (i.e., capital, materials, consumables, labour, and other) indicated by the different colours, respectively.

6.4.3. Effect of target throughput on COG for MA and resin scenarios assuming dosages of 1×10^{12} and 1×10^{13} PT/dose

Figure 6.4 shows the trends in COG per dose as target throughput is increased from 500 to 5,000 doses/year. All four simulations showed the same approximate exponential decay in COG/dose as a function of scale; for the MA scenario with a dosage of 1×10^{12} PT/dose, the COG was estimated to drop from 15,733 USD/dose to 2,817 USD/dose when the target throughput was increased from 500 to 5,000 doses. As discussed earlier, the costs of the resin scenario were higher than those of the MA scenario at all tested dosages, but this disparity was particularly pronounced for the 1×10^{13} PT/dose scenario. The raw data obtained from the simulations is provided in Table E6 in Appendix E.

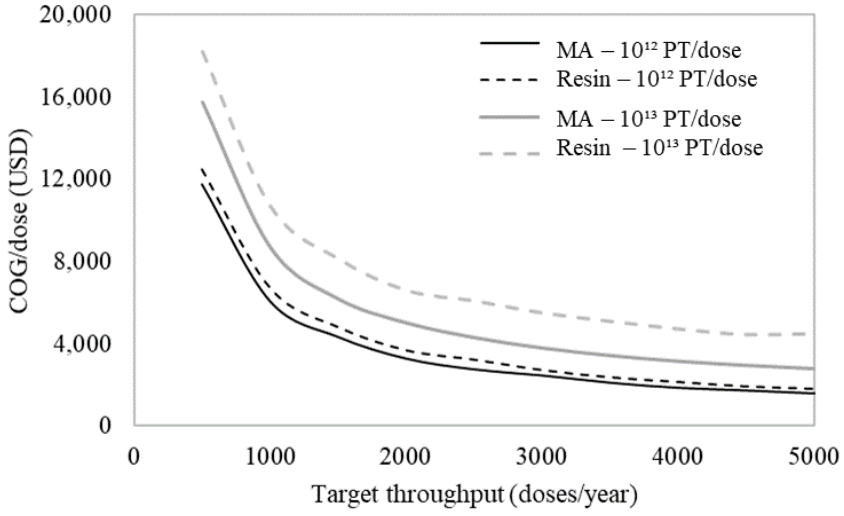

Figure 6.4. COG/dose as a function of target throughput (doses produced per year) for MA (solid lines) and resin (dashed lines) scenarios assuming a dosage of 1×10^{12} PT/dose (black lines) and 1×10^{13} PT/dose (gray lines).

6.4.4. Sensitivity analysis for the MA and Resin models to produce 2,000 doses/year for dosages of 1×10^{12} or 1×10^{13} PT/dose

A sensitivity analysis was conducted by varying the key process parameters listed in Table 6.3 and evaluating how these changes impacted the COG of the MA and resin scenarios, assuming dosages of 1×10^{12} or 1×10^{13} PT/dose. For this analysis, all parameters were varied by 10%, except for the costs of materials (Benzonase, culture media, and virus seed stock), which were varied by 25% (a commonly used variation for material costs in the literature).[57] In the simulations, each parameter was varied individually, with the others being maintained at the baselines indicated in Table 6.3. Figure 6.5 shows tornado plots created using the results of the analysis, while the raw data that was used to generate the graphs is presented in Tables E7 and E8 in Appendix E. For reference, the per-dose COGs for each of the 4 base-scenarios are given in Table 6.4: 3,267 USD/dose for the MA scenario assuming 1×10^{12} PT/dose; 5,039 USD/dose for the MA scenario assuming 1×10^{13} PT/dose; 3,694 USD/dose for the resin scenario assuming 1×10^{12} PT/dose; and 6,581 USD/dose for the resin scenario assuming 1×10^{13} PT/dose.

As can be seen in Figure 6.5, the evaluated parameters generally had very distinct effects for each base case when the lower dosage of 1×10^{12} PT/dose was assumed (comparing top and bottom left panels). However, at the higher dosage of 1×10^{13} PT/dose, the same parameters had similar effects on the COG of the MA and resin scenarios (comparing top and bottom right panels). The different profiles in the tornado plots across the scenarios also illustrate how the impact of the parameters is highly dependent on the

particularities of each process; therefore, caution should be taken, and conclusions should not be extrapolated across different scenarios and conditions.

Still looking at Figure 6.5, a 10% decrease in the titer obtained in the bioreactor caused a 9% increase in the COG for the MA scenario assuming a dosage of 1×10^{12} PT/dose; however, increasing the titer by 10%, only reduced the COG by 3%. Similarly, increasing the yield of the chromatography B&E step reduced the COG by 1%, while decreasing the yield increased it by 8%. The plant's capacity utilization had a significant effect in all 4 scenarios, which presented an interesting trend: under the conditions considered in this part of the study, increasing the capacity utilization – which would be beneficial from the perspective of harnessing a space's maximum capacity – caused the COG to increase. This result indicates the model's potential usefulness for finding the optimum capacity utilization for minimizing costs for a given plant.

With respect to raw materials (i.e., Benzonase, culture media, and virus feed stock), varying the costs of each material by 25% had a practically negligible impact in the lower dosage case (i.e., 1×10^{12} PT/dose), but a slightly greater impact in the higher dosage case (i.e., 1×10^{13} PT/dose). Of the materials tested, the variations to Benzonase had the greatest impact, resulting in a change of ±2% in the MA scenario and ±3% in the resin scenario, assuming 1×10^{13} PT/dose. Another important parameter to consider is the cost of the virus seed stock, which was only roughly estimated and input in the BioSolve library of costs (see Section 6.3) with questionable accuracy. Altering this parameter by 25% resulted in a change of ±1% in the MA scenario and ±2% in the resin scenario, assuming

1×10^{13} PT/dose. The sensitivity analysis results indicated that the virus seed stock is not a critical parameter for the COG, thus the initial cost assumption was maintained.

Finally, the sensitivity analysis for the resin scenario assuming 1×10^{12} PT/dose yielded very interesting results. Specifically, increases in COG were observed for both the best- and worst-case scenarios for titer in the bioreactor and virus yields in the DNA digestion and chromatography B&E steps. Further investigation of the simulation outputs revealed that this behaviour was attributable to the filters being used in the buffer exchange (part of the fed-batch culture step) and cell harvesting steps. BioSolve 0.35 m² filters were used for these steps in the base scenario, while BioSolve 0.19 m² filters were used for the best-case scenarios for titer and yield in the DNA digestion and chromatography B&E steps due to the smaller bioreactor volumes; for the worst-case scenario, the same 0.35 m² filters from the base-scenario were used. The consumables for the 0.19 and 0.35 m² filters cost 185 USD and 368 USD, respectively. However, since the flow rate obtained with the 0.19 m² filter was significantly lower than the rate obtained for the 0.35 m² filter (assuming a constant flux for the two filters), the associated labour costs were higher compared to the base-case; while the base-scenario had a total labour cost of 3609 USD/batch, the best-case scenario had a labour cost of approximately 5200 USD/batch. This increase in labour costs was due to the smaller filter's slower operation time and was the key contributor to the increased COG in the best-case scenario (bottom left panel, Figure 6.5). The results of this investigation once again demonstrate the power of such simulation tools to guide process-development decisions. In a real application, it may be preferable to use a larger filter at

reduced capacity rather than a smaller filter at full capacity, as the use of a smaller filter would require more time, thus incurring higher labour costs.

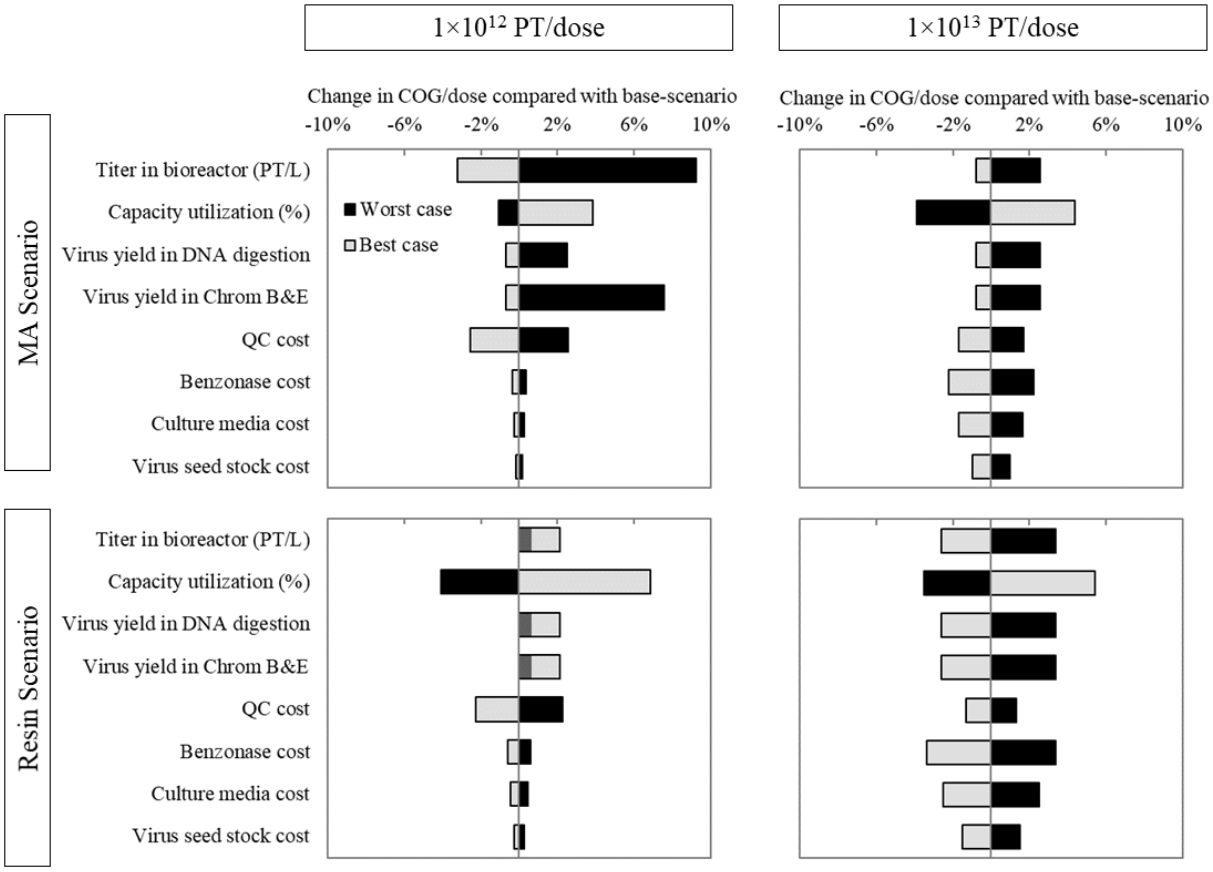

Figure 6.5. Tornado plots showing the sensitivity analysis results for the MA scenario assuming 1×10^{12} PT/dose (top left panel); the MA scenario assuming 1×10^{13} PT/dose (top right panel); the resin scenario assuming 1×10^{12} PT/dose (bottom left panel); and the resin scenario assuming 1×10^{13} PT/dose (bottom right panel). All scenarios use a production target of 2,000 doses/year. The black bars indicate the percent change in COG in the worst-case scenario in relation to the base scenario, and the light gray bars indicate the percent change in COG in the best-case scenario in relation to the base scenario, as shown in Table 6.3.

6.4.5 Quantifying savings from using Denarase as an alternative to Benzonase for DNA digestion in MA and resin scenarios targeting the production of 2,000 doses/year assuming a dosage of 1×10^{13} PT/dose

Experimental results in Chapter 4 demonstrate that Denarase slightly outperforms Benzonase in the DNA digestion step during adenovirus downstream processes.[40] Given that Denarase is a cheaper alternative to Benzonase (1.34 USD/kU compared to approximately 3.73 USD/kU, respectively; prices based on suppliers' listed cost for a 5 MU vial), the developed BioSolve model of adenovirus production was employed to assess how the use of Denarase impacts the total COG/dose. In addition to investigating how switching enzymes influences COG/dose, further tests were conducted to examine the effect of using lower concentrations of enzyme (10 U/mL). These tests were performed based on findings detailed in our previous publication, which showed that the use of 10 U/mL of Benzonase or Denarase yielded similar performance in reducing DNA amounts at longer digestion times (i.e., 4 hours).[40] It is also worth noting that these experimental conditions differed from those used for the base-scenarios, where the DNA-digestion and cell-disruption steps were combined.[43] However, there is still value in using simulations to explore whether and to what extent using less enzyme impacts the COG, as such information can guide process development decisions with respect to the use of lower enzyme concentrations.

Table 6.5 shows the COG estimated for the MA and resin models when Benzonase or Denarase were applied in the cell-disruption/DNA-digestion steps at concentrations of 10 U/mL and 100 U/mL, assuming a dosage of 1×10^{13} PT/dose and a production target of 2,000 doses/year. As can be seen, switching from the use of 100 U/mL of Benzonase to

100 U/mL of Denarase can reduce the COG/dose by 6%; if it is feasibility to use 10 U/mL of Denarase instead, the savings can reach approximately 9%.

Table 6.5. COG for the MA and resin scenarios, assuming a dosage of 1×10^{13} PT/dose and a production target of 2,000 doses/year.

Scenario	Enzyme concentration (U/mL)	COG/dose (USD)	
		Benzonase	Denarase
MA	10	4,633	4,604
	100	5,039	4,750
Resin	10	5,781	5,724
	100	6,581	6,011

6.5. Conclusions

In this study, BioSolve Process was used to develop a detailed model of adenovirus production for gene therapy applications, with strong literature support for the assumptions regarding each unit operation. Analyses of the model using BioSolve's advanced scenarios feature enabled the identification of key cost-drivers and critical process parameters. This study is among the first to provide evidence of the financial benefits of using MAs in place of conventional resin-based matrices in the chromatographic steps required to remove host-cell protein and DNA. For example, the COGs of the base-case scenario were estimated to be 5,039 and 6,581 USD/dose with the use of MAs and resins, respectively, assuming an adenovirus dosage of 10^{13} PT/dose and a production target of 2,000 doses/year. At this processing scale, capital and QC costs were the key cost drivers. Among the materials used for production, culture media and Benzonase were the largest drivers of the COG. Overall, downstream unit operations were found to account for approximately 60% of the COG, which is in agreement with prior reports in the literature.[56] Furthermore, sensitivity analysis was demonstrated to be a powerful tool for guiding

process development decisions. For instance, sensitivity analysis was used to identify a trade-off between using a smaller filter for a longer time period or a larger filter for a shorter time period during the buffer-exchange and cell-harvesting steps in a scenario wherein resins were used for the chromatography step, and a production target of 2,000 doses per year and a dosage of 10^{12} PT/dose were assumed. The developed model can also be used to guide the selection of the most economic option. Finally, the replacing Benzonase with the cheaper enzyme, Denarase, resulted in significant cost-savings, reducing the COG/dose by up to 9%. In sum, this study demonstrates that COG/dose can be significantly reduced by implementing small changes such as replacing Benzonase with a more inexpensive option (i.e., Denarase) and using MAs instead of resins, thus contributing to the development of cost-effective virus manufacturing processes and, by extension, increasing patient access to new ground-breaking drugs.

6.6. Acknowledgements

Funding was provided by the Ontario Research Fund-Research Excellence program and the Natural Sciences and Engineering Research Council of Canada. Additional funding was provided by BioCanRx, a Network of Centres of Excellence program, in the form of a Summer Studentship Award to Shayna Earle. The authors thank Dr Jennifer Quizi, BioCanRx Director of Biotherapeutics Operations, for her valuable feedback and ideas during the construction and analysis of the virus manufacturing models.

6.7. References

1. Bulcha, J. T., Wang, Y., Ma, H., Tai, P. W. L. & Gao, G. Viral vector platforms within the gene therapy landscape. Signal Transduct. Target. Ther. 6, (2021).

2. Ginn, S. L., Amaya, A. K., Alexander, I. E., Edelstein, M. & Abedi, M. R. Gene therapy clinical trials worldwide to 2017 - an update. J. Gene Med. e3015 (2018). doi:10.1002/jgm.3015

3. Crystal, R. G. Adenovirus: The first effective in vivo gene delivery vector. Hum. Gene Ther. 25, 3–11 (2014).

4. Ballmann, M. Z. et al. Human AdV-20-42-42, a promising novel adenoviral vector for gene therapy and vaccine product development. J. Virol. (2021). doi:10.1128/jvi.00387-21

5. Tang, R. & Xu, Z. Gene therapy: a double-edged sword with great powers. Mol. Cell. Biochem. 474, 73–81 (2020).

6. Gene therapy's next installment. Nat. Biotechnol. 37, 697–697 (2019).

7. Moleirinho, M. G., Silva, R. J. S., Alves, P. M., Carrondo, M. J. T. & Peixoto, C. Current challenges in biotherapeutic particles manufacturing. Expert Opin. Biol. Ther. 20, 451–465 (2020).

8. Erickson, J. et al. End-to-end collaboration to transform biopharmaceutical development and manufacturing. Biotechnol. Bioeng. 118, 3302–3312 (2021).

9. Patel, H., Parmar, S. & Patel, B. A comprehensive review on quality by design (QbD) in pharmaceuticals. Int. J. Pharm. Sci. Rev. Res. 21, 223–236 (2013).

10. Sarkis, M., Bernardi, A., Shah, N. & Papathanasiou, M. M. Decision support tools for next-generation vaccines and advanced therapy medicinal products: present and future. Curr. Opin. Chem. Eng. 32, 100689 (2021).

11. Cameau, E., Pedregal, A. & Glover, C. Cost modelling comparison of adherent multi-trays with suspension and fixed-bed bioreactors for the manufacturing of gene therapy products. Cell Gene Ther. Insights 5, 1663–1674 (2019).

12. Comisel, R. M., Kara, B., Fiesser, F. H. & Farid, S. S. Lentiviral vector bioprocess economics for cell and gene therapy commercialization. Biochem. Eng. J. 167, 107868 (2021).

13. Comisel, R. M., Kara, B., Fiesser, F. H. & Farid, S. S. Gene therapy process change evaluation framework: transient transfection and stable producer cell line comparison. Biochem. Eng. J. Pre-proof, 108202 (2021).

14. Kamen, A. A. Vectored-Vaccine Platforms Enabled Rapid Development of Safe and Effective Vaccines in Response to COVID-19 Pandemic Situation. Vaccines 9, (2021).

15. Russell, S. et al. Efficacy and safety of voretigene neparvovec (AAV2-hRPE65v2) in patients with RPE65 -mediated inherited retinal dystrophy: a randomised, controlled, open-label, phase 3 trial. Lancet 390, 849–860 (2017).

16. Penny, W. F., Henry, T. D., Watkins, M. W., Patel, A. N. & Hammond, H. K. Design of a Phase 3 trial of intracoronary administration of human adenovirus 5 encoding human adenylyl cyclase type 6 (RT-100) gene transfer in patients with heart failure with reduced left ventricular ejection fraction: The FLOURISH Clinical Trial. Am. Heart J. 201, 111–116 (2018).

17. Boorjian, S. A. et al. Intravesical nadofaragene firadenovec gene therapy for BCG-unresponsive non-muscle-invasive bladder cancer: a single-arm, open-label, repeat-dose clinical trial. Lancet Oncol. 22, 107–117 (2021).

18. Ferreira, R. G., Gordon, N. F., Stock, R. & Petrides, D. Adenoviral Vector COVID-19 Vaccines: Process and Cost Analysis. Processes 9, 1430 (2021).

19. Farid, S. S., Novais, J. L., Karri, S., Washbrook, J. & Titchener-Hooker, N. J. A tool for modeling strategic decisions in cell culture manufacturing. Biotechnol. Prog. 16, 829–836 (2000).

20. Lim, C. A. et al. Application of a decision-support tool to assess pooling strategies in perfusion culture processes under uncertainty. Biotechnol. Prog. 21, 1231–1242 (2005).

21. Stacey, A. J., Cheeseman, E. A., Glen, K. E., Moore, R. L. L. & Thomas, R. J. Experimentally integrated dynamic modelling for intuitive optimisation of cell based processes and manufacture. Biochem. Eng. J. 132, 130–138 (2018).

22. Abou-El-Enein, M. et al. Good Manufacturing Practices (GMP) manufacturing of advanced therapy medicinal products: A novel tailored model for optimizing performance and estimating costs. Cytotherapy 15, 362–383 (2013).

23. Simaria, A. S. et al. Allogeneic cell therapy bioprocess economics and optimization: Single-use cell expansion technologies. Biotechnol. Bioeng. 111, 69–83 (2014).

24. Hassan, H. et al. Allogeneic cell therapy bioprocess economics and optimization: Downstream processing decisions. Regen. Med. 10, 1045 (2015).

25. Jenkins, M. J. & Farid, S. S. Cost-effective bioprocess design for the manufacture of allogeneic CAR-T cell therapies using a decisional tool with multi-attribute decision-making analysis. Biochem. Eng. J. 137, 192–204 (2018).

26. Pereira Chilima, T. D., Moncaubeig, F. & Farid, S. S. Impact of allogeneic stem cell manufacturing decisions on cost of goods, process robustness and reimbursement. Biochem. Eng. J. 137, 132–151 (2018).

27. Glen, K. E., Cheeseman, E. A., Stacey, A. J. & Thomas, R. J. A mechanistic model of erythroblast growth inhibition providing a framework for optimisation of cell therapy manufacturing. Biochem. Eng. J. 133, 28–38 (2018).

28. Pollard, D., Brower, M., Abe, Y., Lopes, A. G. & Sinclair, A. Standardized Economic Cost Modeling for Next-Generation MAb Production. Bioprocess Int. 14, 14–23 (2016).

29. Pleitt, K., Somasundaram, B., Johnson, B., Shave, E. & Lua, L. H. L. Evaluation of process simulation as a decisional tool for biopharmaceutical contract development and manufacturing organizations. Biochem. Eng. J. 150, 107252 (2019).

30. Torres-Acosta, M. A., Harrison, R. P., Csaszar, E., Rito-Palomares, M. & Brunck, M. E. G. Ex vivo manufactured neutrophils for treatment of neutropenia-A process economic evaluation. Front. Med. 6, 1–12 (2019).

31. Lopes, A. G., Noel, R. & Sinclair, A. Cost analysis of vein-to-vein CAR T-cell therapy: automated manufacturing and supply chain. Cell Gene Ther. Insights 6, 487–510 (2020).

32. Orr, V., Zhong, L., Moo-Young, M. & Chou, C. P. Recent advances in bioprocessing application of membrane chromatography. Biotechnol. Adv. 31, 450–465 (2013).

33. Altaras, N. E. et al. Production and formulation of adenovirus vectors. in Advances in Biochemical Engineering/Biotechnology 99, 193–260 (2005).

34. Chang, J. et al. A Phase I study of KH901, a conditionally replicating granulocyte-macrophage colony-stimulating factor: Armed oncolytic adenovirus for the treatment of head and neck cancers. Cancer Biol. Ther. 8, 676–682 (2009).

35. Freytag, S. O. et al. Prospective Randomized Phase 2 Trial of Intensity Modulated Radiation Therapy With or Without Oncolytic Adenovirus-Mediated Cytotoxic Gene Therapy in Intermediate-Risk Prostate Cancer. Int. J. Radiat. Oncol. Biol. Phys. 89, 268–276 (2014).

36. Rosenthal, E. L. et al. Phase I dose-escalating trial of Escherichia coli purine nucleoside phosphorylase and fludarabine gene therapy for advanced solid tumors. Ann. Oncol. 26, 1481–1487 (2015).

37. Vellinga, J. et al. Challenges in Manufacturing Adenoviral Vectors for Global Vaccine Product Deployment. Hum. Gene Ther. (2014). doi:10.1089/hum.2014.007

38. Lorenzo, E. et al. Plasticity of the HEK-293 cells, related to the culture media, as platform to produce a subunit vaccine against classical swine fever virus. AMB Express 9, 139 (2019).

39. Gardner, T. A. et al. Serum-free recombinant production of adenovirus using a hollow fiber capillary system. Biotechniques 30, 422–427 (2001).

40. Kawka, K. et al. Integrated development of enzymatic DNA digestion and membrane chromatography processes for the purification of therapeutic adenoviruses. Sep. Purif. Technol. 254, 117503 (2021).

41. Maiorella, B., Dorin, G., Carion, A. & Harano, D. Crossflow microfiltration of animal cells. Biotechnol. Bioeng. 37, 121–126 (1991).

42. Howell, J. A., Lojkine, M. & Pritchard, M. Cell Harvesting Using Cross Flow Microfiltration. in Chromatographic and Membrane Processes in Biotechnology 237–252 (Kluwer Academic Publishers, 1991). doi:10.1007/978-94-011-3470-5_12

43. Moleirinho, M. G. et al. Clinical-Grade Oncolytic Adenovirus Purification Using Polysorbate 20 as an Alternative for Cell Lysis. Curr. Gene Ther. 18, 366–374 (2018).

44. Fernandes, P. et al. Bioprocess development for canine adenovirus type 2 vectors. Gene Ther. 20, 353–360 (2013).

45. Cherradi, Y. et al. Filter-based clarification of viral vaccines and vectors. Bioprocess Int. 16, 48–53 (2018).

46. Peixoto, C., Ferreira, T. B., Sousa, M. F. Q., Carrondo, M. J. T. & Alves, P. M. Towards purification of adenoviral vectors based on membrane technology. Biotechnol. Prog. 24, 1290–1296 (2008).

47. Wright, J. F. Quality Control Testing, Characterization and Critical Quality Attributes of Adeno-Associated Virus Vectors Used for Human Gene Therapy. Biotechnol. J. 16, 1–5 (2021).

48. Muller, N., Girard, P., Hacker, D. L., Jordan, M. & Wurm, F. M. Orbital shaker technology for the cultivation of mammalian cells in suspension. Biotechnol. Bioeng. 89, 400–406 (2005).

49. Roush, D. J. & Lu, Y. Advances in primary recovery: Centrifugation and membrane technology. Biotechnol. Prog. 24, 488–495 (2008).

50. Carvalho, S. B. et al. Efficient filtration strategies for the clarification of influenza virus-like particles derived from insect cells. Sep. Purif. Technol. 218, 81–88 (2019).

51. Lucero, A. T. et al. Purification of adenoviral vector serotype 5 for gene therapy against alcoholism using anion exchange chromatography. J. Chem. Technol. Biotechnol. 92, 2445–2452 (2017).

52. Nestola, P. et al. Rational development of two flowthrough purification strategies for adenovirus type 5 and retro virus-like particles. J. Chromatogr. A 1426, 91–101 (2015).

53. Nestola, P. et al. Adenovirus purification by two-column, size-exclusion, simulated countercurrent chromatography. J. Chromatogr. A 1347, 111–121 (2014).

54. Healthcare, G. Scalable process for adenovirus production. Cytiva (2018).

55. Kalbfuss, B. et al. Harvesting and concentration of human influenza A virus produced in serum-free mammalian cell culture for the production of vaccines. Biotechnol. Bioeng. 97, 73–85 (2007).

56. Wolf, M. W. & Reichl, U. Downstream processing of cell culture-derived virus particles. Expert Rev. Vaccines 10, 1451–1475 (2011).

57. Torres-Acosta, M. A., Aguilar-Yañez, J. M., Rito-Palomares, M. & Titchener-Hooker, N. J. Economic analysis of royalactin production under uncertainty: Evaluating the effect of parameter optimization. Biotechnol. Prog. 31, 744–749 (2015).

Chapter 7

Conclusions and recommendations for future work

7. Conclusions and recommendations for future work

7.1. Conclusions

The rise of viruses as novel biotherapeutics brings great promise for patients as effective and potentially curative treatments. Although several gene therapies, oncolytic viruses, and cell therapies have already been approved worldwide using viruses as a key part of the treatment as discussed in Chapter 1, manufacturing these drugs is still a challenge that contributes to their high prices.[1] A good part of this problem is associated with the downstream portion of the process, currently considered the bottleneck of virus manufacturing.[2] This thesis tackles a series of challenges associated with viral vector downstream processes by focusing on (but not staying limited to) the development of scalable membrane chromatography (MC) technologies for the removal of host-cell protein and DNA. As it was evidently presented in Chapter 4 based on experimental results, the performance of preceding unit operations can have a significant impact on the performance of the separation in the MC step. Therefore, process development will benefit from integrated approaches that consider multiple steps of the process at once. This mentality constitutes the essence of this thesis, which addresses: different MC device design and membrane options and their impact on adenovirus purification (Chapters 2 and 3, respectively); the optimization of MC processes in conjunction with additional preceding unit operations (Chapter 4); the first report of the development of a hydrophobic interaction MC process for the purification of a rhabdovirus (Chapter 5); and the implementation of BioSolve Process as a tool to model virus manufacturing processes to investigate the effect

of different process parameters, including the use of MC or conventional resin-based chromatography, in the cost-of-goods (COG) of virus production (Chapter 6). Synergistically, these contributions advance membrane technologies along with virus manufacturing processes in benefit of the development of novel biotherapeutics.

Membrane chromatography presents ideal characteristics for the purification of viruses, presenting large pore sizes, convective mass transfer, and accessible binding sites, besides being a scalable technology well suited for single-use applications in the biopharmaceutical industry.[3] However, conventional MC devices are often criticized for their low separation resolution compared with resins or monoliths.[4] This is associated with the poor flow distribution inside the devices, caused by ineffective physical designs and large dead volumes,[4] and not the membrane itself. In Chapter 2, the laterally-fed membrane chromatography (LFMC) device was introduced as an improved alternative to conventional MC devices for the purification of therapeutic adenoviruses. The LFMC is a carefully designed device with minimal dead volume and a simple flow path that maximizes resolution while minimizing sample dilution. Through a comparison using the Sartobind Q membrane either in an LFMC or in a conventional radial flow-based MC device, both containing 1 mL of membrane, the LFMC was found to cause 50% less sample dilution while providing better separation of host-cell protein and DNA when a gradient elution strategy was applied. In addition to previous reports on the performance of the LFMC for protein separation, this study confirmed the superiority of the new technology over conventional devices at 1 mL scale also for the purification of viruses.

Motivated by the dramatic dependence of membrane performance on device design as discussed above, the goal of Chapter 3 was to directly compare the two most popularly used MC membranes for virus purification: Sartobind Q and Mustang Q. To our knowledge, these membranes have not yet been compared using the same device format. They are based on regenerated cellulose and polyethersulfone (PES), respectively, and are both anion-exchange (AEX) membranes functionalized with quaternary ammonium ligands. The membranes also differ in terms of pore sizes, with Sartobind having larger, greater than 3 μm pores and Mustang having smaller, approximately 0.8 μm pores. Using LFMC devices containing 1 mL of each membrane, characterization and adenovirus purification experiments were conducted. The major difference identified was the fact that both virus and DNA impurities eluted later from Mustang Q when the same gradient elution was applied. This translated in lower resolution, and at the end, the virus purified with Sartobind Q had virtually half of the amount of DNA impurity compared with the virus purified with Mustang Q. Conducting such fine characterizations of different membranes in the development of MC processes are essential to guide the selection of the most favourable option.

Initial attempts to improve DNA removal in the LFMC process described in Chapter 2 focused on optimizing the MC step alone, but did not significantly improve the purity. The target established by the FDA for host-cell DNA impurity in gene therapy products is less than 10 ng/dose with fragments shorter than 10 base pairs (bp).[5] In the process, it was observed that Benzonase, the enzyme used in the DNA digestion step that preceded the MC, was not achieving the performance claimed by its manufacturer of

'completely digesting DNA to single base pairs' when used as indicated (1 U/mL for 30 min at 37°C in this case). A new approach was then designed where the DNA digestion and the clarification unit operations that precede the MC were optimized in conjunction as presented in Chapter 4. An intensive set of experiments was conducted involving the evaluation of new enzymes as an alternative to Benzonase (i.e. Denarase), design-of-experiments (DOE) evaluating the effect of digestion conditions and enzyme type, high-throughput screening of MC conditions using 96-well plates containing the membrane adsorber, and LFMC using 1 mL devices containing Sartobind Q. The optimal condition was found to be that where the order of unit operations was inverted, with clarification now preceding DNA digestion, and with new digestion conditions using 10 U/mL of Denarase, for 4 h at 37 °C, the removal of DNA was improved 80-fold, while the amount of virus processed was scaled-up 10-fold. In the end, the product had less than 80 ng/dose of DNA, which could be removed in a subsequent polishing step more easily than the 6500 ng/dose that was remaining before the optimization.

Rhabdoviruses including vesicular stomatitis virus (VSV) are promising candidates as oncolytic viruses are currently the focus of multiple studies in the development of new cancer immunotherapies.[6] Chapter 5 describes the development of an MC process for the purification of VSV. It was interesting that initial attempts to implement the same process developed in Chapter 2 for the purification of adenoviruses using an AEX membrane, was highly unsuccessful for VSV, resulting in recoveries lower than 7%. Additional tests evaluated a pseudo-affinity membrane, Sartobind sulfated cellulose (SC), to which certain enveloped viruses can bind.[7-9] However, VSV did not present any sort of

affinity for this membrane under the conditions employed. Finally, Sartobind Phenyl, the first hydrophobic interaction membrane chromatography (HIMC) material commercially available was tested and presented promising results. In this process, the virus bound to the membrane under high ammonium sulfate (AS) concentrations while most of the protein and DNA from the host-cells was removed in the flow-through fractions; later the virus was eluted by applying buffer free of AS. Buffer pH was found to have a significant effect on virus stability, with pH 7.4 being the most appropriate. Sartobind Phenyl was also successful in removing phenol red, a pH indicator that was present in the culture media used to produce VSV. After a series of adjustments, the process was scaled up to purify to 300 mL of diluted virus lysate using a 3 mL Sartobind Phenyl Nano device and resulted in up to 80% virus recovery, with the removal of more than 99% of proteins and 84% of DNA. To our knowledge, this is the first report of the implementation of HIMC for VSV purification and one of the firsts for virus purification in general. HIMC materials, therefore, bring a new promising alternative for the purification of different types of viruses. Future work in this area should focus on further reducing the residual DNA impurities after HIMC. To do so, a DNA digestion step can be added before the chromatography and both processes optimized following a similar integrated approach as that presented in Chapter 4.

The collection of data presented in Chapters 2 to 4 along with an extensive literature search on the details of each unit operation of virus production was used in the creation of a model of an adenovirus manufacturing process for gene therapy clinical applications using BioSolve as described in detail in Chapter 6. Once such a model is

established, there are endless possibilities for analysis through the simulation of multiple scenarios. The model was therefore used to investigate the economic feasibility of the use of MC technologies as opposed to conventional resins in the chromatography and polishing steps of the process. For a scenario targeting the production of 2,000 doses/year, with a dosage of 10^{13} virus particles (PT)/dose, the COG was estimated at 5,039 USD/dose for when MC was used, and 6,581 USD/dose for when resins were used. This difference of more than 30% for this scenario is one of the first reports in the literature with a quantitative measure of the financial benefit associated with using MC. For the MC scenario, the major cost drivers were identified to be capital, quality control, and material costs. Downstream unit operations accounted for approximately 60% of the COG, confirming previous reports on the costly characteristics of downstream processes.[10] To investigate the economical aspects of switching DNA digestion enzymes as a sequence to the work presented in Chapter 4, the model was used to quantify the COG when either Benzonase or Denarase were used. Assuming the enzymes have similar performances and that the same optimized condition discussed in Chapter 4 was implemented (10 U/mL, 4 h digestion), the COG was found to reduce by only less than 1% with adopting Denarase instead of Benzonase. However, for a scenario where more enzyme was needed (100 U/mL, 4 h digestion), the savings associated with using Denarase increased to 6%. Within the assumptions taken throughout model construction, the analyses presented in Chapter 6 are a brief demonstration of the power of modelling and simulation tools as a guide for process characterization and development decisions. It can serve as a guide for future gene therapy manufacturing modelling studies, besides being a source of information on unit operations.

7.2. Recommendations for future work

7.2.1. Development of novel membrane adsorber materials and ligands for virus purification

All the MC processes described in Chapters 2 to 5 used commercially available membrane adsorbers with different chemistries and that are typically used in bioprocesses in general.[11] These membranes are based on non-specific electrostatic or hydrophobic interactions between the virus, impurities, and the matrix. The separation is therefore based on subtle differences in the strength of the interactions, which makes it virtually impossible to completely isolate one compound from its impurities while achieving satisfactory recoveries. The field would greatly benefit from the creation of new membrane adsorbers especially designed for virus purification, with enhanced mechanical properties and high binding capacity, as well as selective ligands capable of isolating viruses through affinity or pseudo-affinity interactions. Given the diversity of virus types, shapes, and compositions, it is a stretch to expect that a generic ligand would work for almost all types of viruses, equivalently to how protein A chromatography works for the affinity-based separation of monoclonal antibodies. However, there already exists successful examples of such ligands specific for certain types of viruses as shown in Table 7.1.[12] Most of these technologies use complex molecules and still suffer from poor ligand stability, high cost, and the need for harsh operating conditions.[13] From Table 7.1, Heparin affinity and pseudo-affinity by sulfated cellulose are currently the most successful examples applied in virus purification.

Table 7.1. Affinity chromatography mechanisms used for virus purification. Adapted from elsewhere.[12]

Type of affinity	Mechanism	Main virus targets
Pseudo-affinity	Sulfate groups in sulfated cellulose resemble heparin, to which certain virus envelopes have affinity for	Influenza,[7] vaccina,[8] Orf virus[9]
Heparin affinity	In AAV, a cluster of amino acids responsible for virus-cell attachment binds to heparin.[14,15]	Herpes simplex, hepatitis B and C, AAV, retrovirus, lentivirus, vaccinia, foot-and-mouth disease, baculovirus.[13]
Immunoaffinity	Antibody-antigen interactions.[13]	Hepatitis, poliovirus, AVV (serotypes 1, 2, 3, 5), measles.[13]
Lectin affinity	Oligosaccharides present on glycoproteins from the viral envelope interact with specific types of lectins.[16]	Influenza A, baculovirus, herpes simplex.[13]
Metal affinity	Electron donor groups on the surface of the virus (i.e. tagged with histidine) interact with metal ions.[13]	Recombinant baculovirus, AAV, foot-and-mouth disease, retrovirus, influenza, lentivirus.[13]
Dye ligands	Procion blue-HB and Cibacron blue 3GA dyes were found to bind to hepatitis B viruses.[17]	Hepatitis B.[17]
Mucin affinity	AAV-5 binds to mucin on the surface of cells.[18]	AAV-5.[18]
Avidin affinity	Biotin expressed on the surface of modified AAV capsids interact with avidin columns.[19]	Modified AAV (serotypes 1, 2, 3, 4, 5).[19]
Peptide affinity	Using phage-display, AAV-8 was found to bind to the peptide sequence GYVSRHP.[20]	AAV-8,[20] norovirus, porcine parvovirus, rotavirus, poliovirus.[13]
DNA aptamer affinity	A 64-base DNA aptamer binds whole vaccinia viruses.[21]	Vaccinia.[21]

Pseudo-affinity interaction in sulfated cellulose membrane adsorbers is particularly interesting and are already commercially available; viruses that are known to bind to sulfated cellulose include influenza, vaccinia, and Orf viruses;[7-9] all enveloped. The nature of the interaction is highly virus-specific since VSV (also an enveloped virus), did not present pseudo-affinity for this membrane as discussed in Chapter 5. Sulfated cellulose is a simple and stable ligand that acts by resembling the highly-sulfated heparin present on the surface of cells, and to which certain virus envelopes have affinity for,[22] and is considered to be a type of multimodal ligand as it has a combination of complex interactions with viruses.[23] Its success raises the possibility of the identification of new types of multimodal ligands that can be ideally suited for each type of virus. Combined with the

ideal characteristics of MC base-materials, these ligands can provide powerful new virus purification in the future.

Apart from sulfated cellulose membranes, presently most multimodal membrane adsorbers available or under development have salt-tolerant characteristics, as in the case of Sartobind STIC (salt-tolerant interaction chromatography) from Sartorius, Purexa MQ from Purilogics, and Natrix HD-Sb from Millipore. They all have ligands that combine ion-exchange and hydrophobic interactions and can bind certain products at high salt concentrations. Fine adjustment of binding and elution conditions has the potential to yield high-purity products.

With respect to new membrane base materials, these must have large enough pores to allow virus to permeate and easily access binding sites. Well-established base materials such as Sartobind's reinforced cellulose, Mustang's polyethersulfone, and Natrix's polyacrylamide hydrogel base materials currently offer adequate characteristics for the purification of biomolecules. More recently developed base materials that have the potential to gain more space in the field in the next few years include the Fibro™ chromatography electrospun materials from Cytiva, which offer a uniform matrix of fibres well suited for biomolecule purification, and Terapore's block copolymer membranes with extremely uniform and tunable pore sizes that can potentially be customized specifically for the purification of large biomolecules such as viruses.

With the help of high-throughput screening platforms as discussed in the next section, research groups focused on membrane development for virus purification could act

as future ‘contract membrane development organizations (CMDOs)’ and offer personalized membrane solutions for clients developing new virus-based therapeutics, similarly to how contract development and manufacturing organizations (CDMOs) currently offer process development services.

7.2.2. High-throughput screening platforms

One of the main takeaways of this thesis is that integration is key during viral vector manufacturing process development. It is insufficient to optimize one unit operation individually when it is surrounded by other directly related operations and upstream conditions. True optimum conditions can more easily be achieved if a good and holistic understanding of the process is in place. However, this comes at the cost of laborious and highly experimental assessments of combinations of different process conditions. New frameworks for modelling and simulation are effective options for scenario analysis and decisional tools (Chapter 6), but still, high-quality experimental data needs to be acquired before it is fed into models. More importantly for the field of virus chromatography, where each vector has particularities that are hard to predict if not through experimental testing.

It is labour-intensive to test membrane materials if they are developed as described in Section 7.2.1 or to even screen for MC conditions with a single membrane as was discussed in Chapter 4. This is due to the very large number of experiments required as part of DOEs and other optimization approaches, and the even larger number of samples generated. Future analytical tools will need to be faster and more accurate for virus detection as will be addressed in Section 7.3.3. High-throughput approaches offer a solution to these challenges and can accelerate downstream process development, besides playing

an essential role in the implementation of Quality by Design (QbD) principles.[24] Scale-down model systems and miniaturized versions of modules used in the different unit operations can allow the execution of multiple experiments at a time, save reagents and materials, and can potentially be integrated with automated systems.[24] The development of high-throughput MC testing modules, in conjunction with compatible and accurate analytical tools can be a powerful way to enable the development of novel membranes and processes in general.

7.2.3. Advanced analytical tools for the characterization of product and impurities

7.2.3.1. Virus analytical tools

The development of new analytical methods for the characterization of viruses and impurities is a much-needed advancement for the field of viral vector manufacturing. Techniques currently in place often suffer from high variability and error, which for virus infectivity assays can be as high as ±30%.[25] In some cases, virus analysis can be prone to the subjective interpretation of the individual conducting the analysis as discussed in detail in Appendix D for the fifty percent tissue culture infective dose ($TCID_{50}$) assay. To speed up process development, faster, cheaper, and less variable analytical methods need to be developed. These techniques will enable quick testing of the samples generated in high-throughput experiments discussed in the previous section and will enable the creation of online process monitoring and control tools.

7.2.3.2. Accurate detection of host-cell DNA concentration and fragment sizes using qPCR methods

The main goal of Chapter 4 was to improve the removal of host-cell DNA in adenovirus purification processes as a means to attend the FDA's requirements for gene therapy products, which should have less than 10 ng/dose of DNA with fragments sizes shorter than 200 bp,[5] to guarantee the absence of functional genes. Picogreen, a fluorescence-based assay, was used to determine the total DNA amount in samples and it is indeed a versatile analytical method largely used in the literature, being able to detect fragments as short as 4 bp.[26] This technique, however, does not provide information regarding DNA fragment size. In Chapter 4, agarose gel-electrophoresis was applied to determine the fragment sizes before and after DNA digestion. Although the technique was enough to provide a high-level profile of the fragments in the sample, it is limited by the amount of DNA that can be visualized on the gel and does not provide quantitative information on how much of each fragment size is in the sample.

Quantitative polymerase chain reaction (qPCR) is an extremely sensitive method commonly employed in the biopharmaceutical industry to detect total residual DNA without profiling fragment size.[27] Aiming to harness the potential of qPCR, André et al.[27] proposed a technique for quantification and size evaluation of residual host-cell DNA in vaccines that can be used for a more comprehensive and accurate characterization of DNA impurities in virus-based products. For the detection of DNA from human cell lines, the method is based on the use of sets of primers that target a conserved ribosomal 18S RNA gene that repeats multiple times in the genome.

We have conducted preliminary experiments applying the technique described by André et al.[27] to analyse adenovirus lysates digested under different conditions and obtained

promising initial results that confirm the feasibility of the assay. Details on standard operating procedure used in these tests are provided in Appendix F. The primers were designed by the authors to target regions of the human genome that generate amplicons shorter and larger than 200 bp; more specifically, 123 bp and 254 bp amplicons as detailed below:

- Forward primer used for 123 bp amplicon: 5'-GCAATTAT TCCCCATGAACG-3'.
- Forward primer used for the 254 bp amplicon: 5'-AACAGGTCT GTGATGCCCTT-3'.
- The same reverse primer was used for both amplicons: 5'-GGCCTCACT AAACCATCCAA-3'.

First, calibration curves were created correlating the cycle threshold (Ct) with the logarithm of the DNA amount of a serially-diluted sample of human genomic DNA standard. The amplification data for different dilutions of the standard human genomic DNA using the primers for the 254 bp and 123 bp amplicons are shown in Figure 7.1 panels A and B. The calibration curves for the two amplicons are shown in Figure 7.1 and overall presented good linearity and agreed with what has been previously reported.[27]

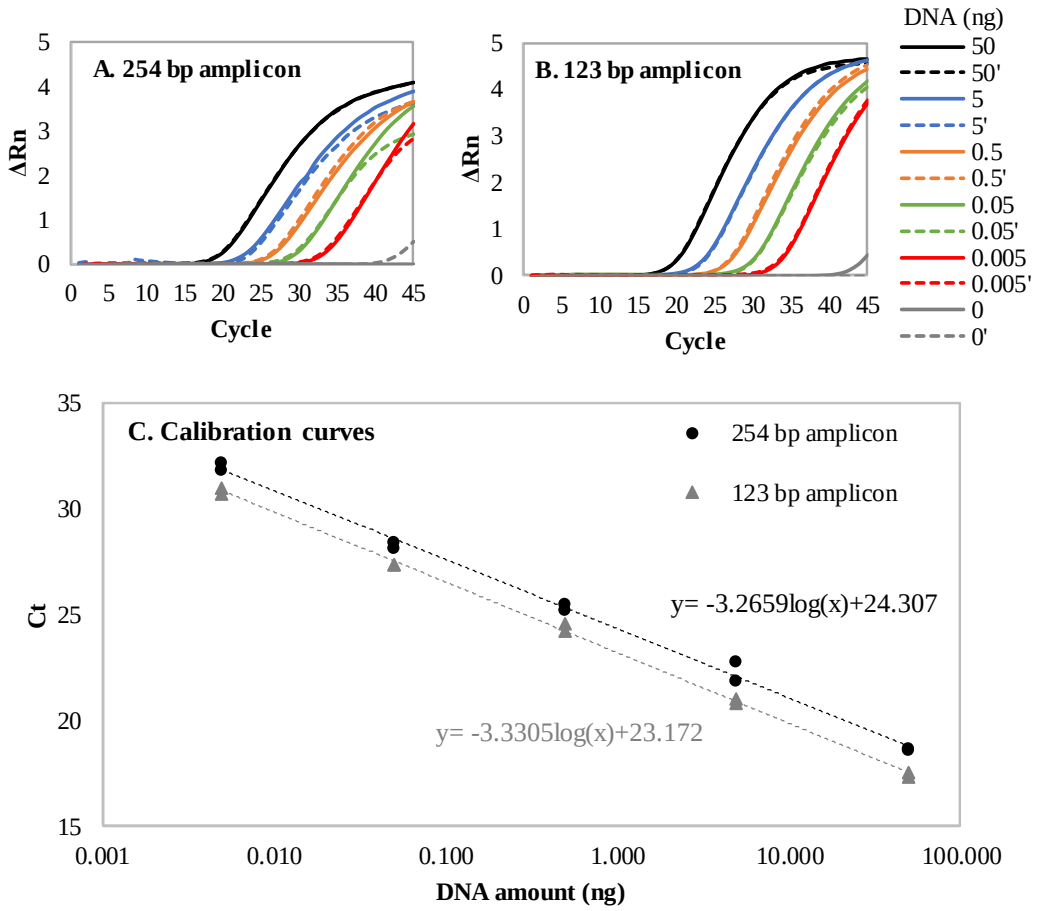

Figure 7.1. qPCR amplification data using for standard human genomic DNA targeting regions that generate 254 bp amplicons (panel A) and 123 bp amplicons (panel B), displaying the fluorescence normalized reporter value (ΔRn) as a function of cycle number. C: qPCR assay calibration curves with standard human genomic DNA, for the 123 bp (grey triangles) and 254 bp (black circles) amplicons. Dashed lines represent the respective linear regression for each of the calibration curves.

Adenovirus lysates digested with Benzonase and control lysates incubated without any enzyme were cleaned using the DNA clean and concentration kit from Zymo and assayed through qPCR assay using primers for either the 123 bp or 254 bp amplicons in separate reactions. The conditions of the DNA digestion, as well as the results of the amounts of amplicons calculated based on the calibration curves, are shown in Table 7.2.

There was a reduction in the concentration of DNA relative to both amplicons after digestion for both 4 and 24 h. The amounts of 254 bp amplicons were consistently always lower than the amounts of 123 bp amplicons, especially on the digested samples, which agrees with the fact that all 254 bp fragments were detected by both the 123 bp assay and the 254 bp assay, while shorter fragments, between these two sizes, only picked up by the 123 bp assay. A significant reduction in the amounts of both amplicons was also seen for the digested lysates with increasing digestion time. In fact, the sample digested for 24 h, had below the detection limit (BDL) amounts of the 254 bp amplicon. The method still needs to be validated, but if these results are confirmed, there is a good chance the sample digested for 24 h would pass the requirement of having less than 200 bp fragments.

Table 7.2. DNA amounts based on the qPCR assay for the determination of fragment size. Lysates were digested for 4 h and 24 h either in the absence of enzyme (Controls) or with 10 U/mL of Benzonase. DNA amounts for each amplicon were calculated based on calibration curves generated using standard human genomic DNA.

Digestion time	**Control (no enzyme)**		**Digested lysate (10 U/mL Benzonase)**	
	123 bp amplicon	**254 bp amplicon**	**123 bp amplicon**	**254 bp amplicon**
4 h	47 ± 3 ng/mL	37 ± 1 ng/mL	22 ± 3 ng/mL	10 ± 2 ng/mL
24 h	39 ± 6 ng/mL	38 ± 6 ng/mL	9 ± 1 ng/mL	BDL (<5 ng/mL)

Although the method does not provide the full profile of DNA fragment sizes present in the sample, it gives a much better indication regarding fragments around the 200 bp requested by the FDA's guidelines than more rudimentary methods such as agarose gel electrophoresis used in Chapter 4. Additional targets for different sizes of amplicons and the targeting of additional highly repeating regions of the genome can further refine the DNA profiling provided by this technique. This technique is compatible with high-

throughput analysis platforms, can be automated, and upon validation, can be a powerful resource in the development of virus purification processes.

7.3. References

1. Gene therapy's next instalment. Nat. Biotechnol. 37, 697–697 (2019).
2. Terova, O., Soltys, S., Hermans, P., De Rooij, J. & Detmers, F. Overcoming Downstream Purification Challenges for Viral Vector Manufacturing: Enabling Advancement of Gene Therapies in the Clinic. Cell Gene Ther. Insights 4, 101–111 (2018).
3. Orr, V., Zhong, L., Moo-Young, M. & Chou, C. P. Recent advances in bioprocessing application of membrane chromatography. Biotechnol. Adv. 31, 450–465 (2013).
4. Gagnon, P. The emerging generation of chromatography tools for virus purification. BioProcess Int 24–30 (2008).
5. FDA & CBER. Chemistry, Manufacturing, and Control (CMC) Information for Human Gene Therapy Investigational New Drug Applications (INDs) - Guidance for Industry. (2020).
6. Felt, S. A. & Grdzelishvili, V. Z. Recent advances in vesicular stomatitis virus-based oncolytic virotherapy: A 5-year update. J. Gen. Virol. 98, 2895–2911 (2017).
7. Weigel, T. et al. A membrane-based purification process for cell culture-derived influenza A virus. J. Biotechnol. 220, 12–20 (2016).
8. Wolff, M. W., Siewert, C., Hansen, S. P., Faber, R. & Reichl, U. Purification of cell culture-derived modified vaccinia ankara virus by pseudo-affinity membrane adsorbers and hydrophobic interaction chromatography. Biotechnol. Bioeng. 107, 312–320 (2010).
9. Lothert, K., Pagallies, F., Feger, T., Amann, R. & Wolff, M. W. Selection of chromatographic methods for the purification of cell culture-derived Orf virus for its application as a vaccine or viral vector. J. Biotechnol. 323, 62–72 (2020).
10. Wolf, M. W. & Reichl, U. Downstream processing of cell culture-derived virus particles. Expert Rev. Vaccines 10, 1451–1475 (2011).
11. Zydney, A. L. New developments in membranes for bioprocessing – A review. J. Memb. Sci. 620, 118804 (2021).
12. Kawka, K. Rational development of novel multimodal chromatography membranes for virus purification. (PhD Comprehensive Examination Report, Department of Chemical Engineering, McMaster University, 2020).

13. Zhao, M. et al. Affinity chromatography for vaccines manufacturing: Finally ready for prime time? Vaccine 37, 5491–5503 (2019).

14. Kern, A. et al. Identification of a Heparin-Binding Motif on Adeno-Associated Virus Type 2 Capsids. J. Virol. 77, 11072–11081 (2003).

15. Zhang, F. et al. Characterization of interactions between heparin/glycosaminoglycan and adeno-associated virus. Biochemistry 52, 1–7 (2013).

16. Opitz, L., Salaklang, J., Büttner, H., Reichl, U. & Wolff, M. W. Lectin-affinity chromatography for downstream processing of MDCK cell culture derived human influenza A viruses. Vaccine 25, 939–947 (2007).

17. Brown, R. A. & Combridge, B. S. Binding of hepatitis virus particles to immobilised Procion Blue-HB and Cibacron Blue 3GA. J. Virol. Methods 14, 267–274 (1986).

18. Auricchio, A., O'Connor, E., Hildinger, M. & Wilson, J. M. A single-step affinity column for purification of serotype-5 based adeno-associated viral vectors. Mol. Ther. 4, 372–374 (2001).

19. Arnold, G. S., Sasser, A. K., Stachler, M. D. & Bartlett, J. S. Metabolic Biotinylation Provides a Unique Platform for the Purification and Targeting of Multiple AAV Vector Serotypes. Mol. Ther. 14, 97–106 (2006).

20. Pulicherla, N. & Asokan, A. Peptide affinity reagents for AAV capsid recognition and purification. Gene Ther. 18, 1020–1024 (2011).

21. Nitsche, A. et al. One-step selection of Vaccinia virus-binding DNA aptamers by MonoLEX. BMC Biotechnol. 7, 1–12 (2007).

22. Opitz, L., Lehmann, S., Reichl, U. & Wolff, M. W. Sulfated membrane adsorbers for economic pseudo-affinity capture of influenza virus particles. Biotechnol. Bioeng. 103, 1144–1154 (2009).

23. Freed, A. S., Garde, S. & Cramer, S. M. Molecular simulations of multimodal ligand-protein binding: Elucidation of binding sites and correlation with experiments. J. Phys. Chem. B 115, 13320–13327 (2011).

24. Łącki, K. M. High throughput process development in biomanufacturing. Curr. Opin. Chem. Eng. 6, 25–32 (2014).

25. Comisel, R. M., Kara, B., Fiesser, F. H. & Farid, S. S. Lentiviral vector bioprocess economics for cell and gene therapy commercialization. Biochem. Eng. J. 167, 107868 (2021).

26. Dragan, A. I. et al. Characterization of PicoGreen interaction with dsDNA and the origin of its fluorescence enhancement upon binding. Biophys. J. 99, 3010–3019 (2010).

27. André, M., Reghin, S., Boussard, E., Lempereur, L. & Maisonneuve, S. Universal real-time PCR assay for quantitation and size evaluation of residual cell DNA in human viral vaccines. Biologicals 44, 139–149 (2016).

Appendix A: Optimization and scale-up of laterally-fed membrane chromatography (LFMC) for adenovirus purification using the Sartobind Q membrane

A1. Optimization of membrane loading conditions for adenovirus purification using 1 mL LFMC devices

A series of tests were conduced aiming to further optimize the chromatography conditions applied in Chapter 2 and to also to attempt to increase the volume of lysate purified by a 1 mL Sartobind Q LFMC device. The same method described in Chapter 2 was applied to generate the lysates, where a DNA digestion step with 1 U/mL of Benzonase for 30 minutes was performed prior to the chromatography. Also, similar chromatography conditions to the ones applied in Chapter 2 with stepwise elution were used in this part of the study, where buffer A (10 mM HEPES, 4% sucrose, pH 7.4) and buffer B (10 mM HEPES, 4% sucrose, 2 M NaCl, pH 7.4) were mixed to yield different NaCl salt concentration. All analysis of virus, protein, and DNA were done using hexon staining, BCA, and Picogreen assays, respectively, as described in Chapter 2. The key differences from Chapter 2 were in terms of loading a larger volume of virus lysate onto the membrane: lysate from 50 mL of culture (which was reduced to 1 mL of lysate after the pre-chromatography sample processing steps) as opposed to only 5 mL of culture (which reduced to 0.1 mL of lysate) in Chapter 2; and using different salt concentrations at the loading step: 0.30, 0.36, and 0.40 M NaCl, as opposed to using only 0.40 M as described in Chapter 2. After loading the virus onto the membrane, the same 2-step elution procedure

described in Chapter 2 was used, where 0.60 M NaCl was applied for virus elution, and 1 M NaCl was applied for DNA impurity elution.

Figure A1 below shows the results for three runs using different salt concentrations in the loading buffer as indicated for 0.40, 0.36, 0.30 M NaCl, respectively. Table A1 shows the amount of virus, protein, and DNA in each of the chromatography fraction. As it can be seen, significant amount of virus was present in the flow-through of the run starting with the highest salt concentration, 0.40 M, indicating most virus (approximately 53%) was not able to bind to the membrane due to high ionic strength. This differs from Chapter 2, where very low amounts of virus were observed in the flow-through for the same loading condition, however, the larger volume of lysate loaded in this part of the study (1 mL) has overwhelmed the membrane in a way that significant amounts of virus were lost in the flow-through. Virus was able to appropriately bind to the membrane under binding buffer conditions of 0.36 M, with only 0.2% virus observed in the flow-through, and 0.30 M, where no virus was detected in the flow-through. Considering the two fractions containing most of the eluted virus (i.e. fractions between the 9 and 14 mL marks), only 9% virus recovery was obtained with for the run starting with 0.4 M NaCl in the loading buffer. The low recovery is associated with low binding due to exceedingly high ionic strength. The eluted virus recovery was 81% and 68%, respectively, for the runs starting with binding buffer containing 0.36 and 0.30 M NaCl. Considering these two runs that resulted in satisfactory virus recoveries, the level of protein impurity was lower for the run starting with 0.36 M NaCl in the binding buffer, where 3% of the initial amount of protein was observed, versus 6% for the run starting at 0.30 M NaCl. This observation agrees with

the theory where more protein was allowed to bind to the membrane at lower salt concentrations in the loading phase, and later co-eluted with the virus. Finally, similar and significant amounts of DNA impurity co-eluted with the virus in these two fractions, approximately 55% of the initial amount of DNA. Therefore, given the slightly higher virus recovery and the greater purity in terms of residual proteins, a loading condition of 0.36 M NaCl was chosen for the remaining experiments discussed below and in Chapters 3 and 4.

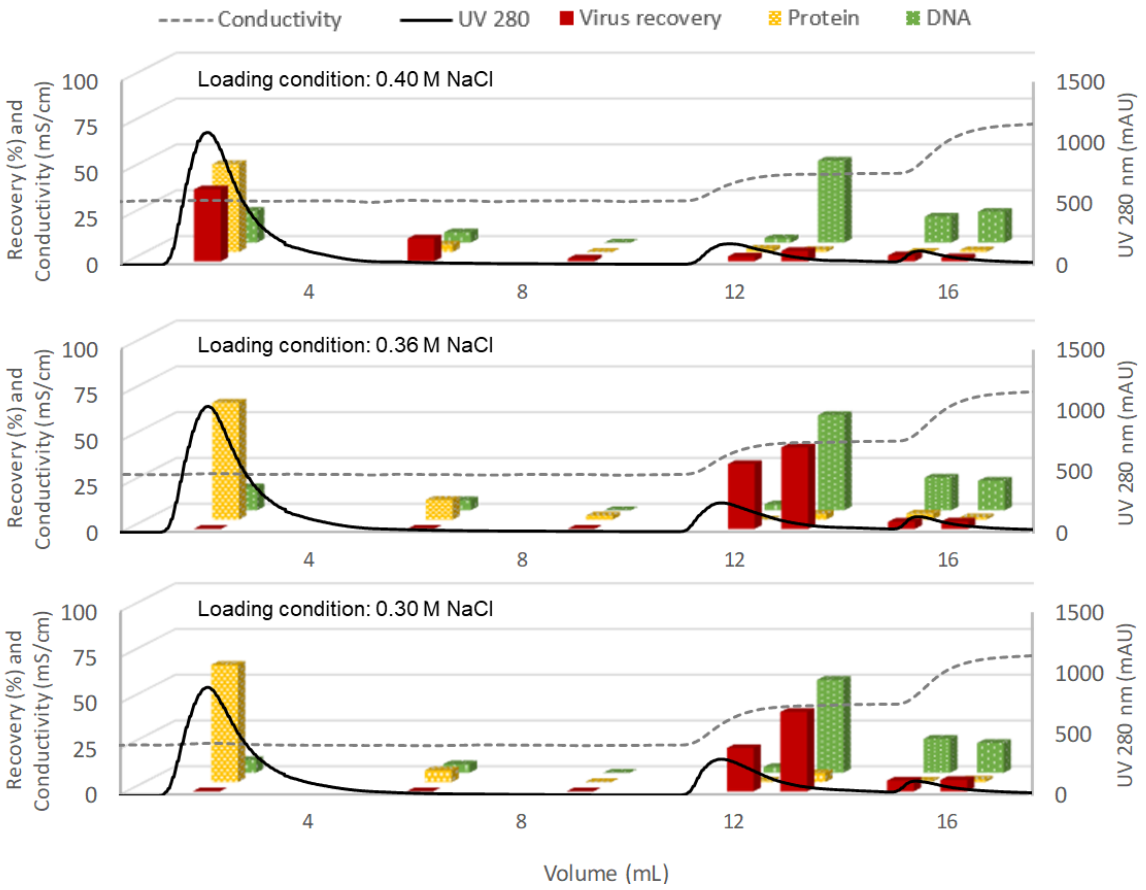

Figure A1. Chromatograms for adenovirus purification via stepwise elution strategy with a 1 mL LFMC device for membrane loading buffer containing 0.40 M NaCl (top panel), 0.36 M NaCl (middle panel), and 0.30 M NaCl (bottom panel). The dashed line indicates the conductivity, and the solid line indicates the UV absorbance at 280 nm (refer to the secondary axis). The 3D bar charts display the amount of adenovirus (front red bars), total protein (middle yellow bars), and total DNA (back green bars) within each fraction as a percentage of the amount in the 1 mL injected feed sample.

Table A1. Percent amount of virus, protein and DNA with respect to the amount in the feed in the different fractions of LFMC runs using different NaCl concentrations in the loading buffer. BDL: below the detection limit.

[NaCl] in load buffer ↓	Fraction interval →	0-3 mL	3-6 mL	6-9 mL	9-12 mL	12-14 mL	14-16 mL	16-17 mL
0.40 M	Virus (%)	39	12	2	3	6	3	2
	Protein (%)	48	4	BDL	2	1	BDL	1
	DNA (%)	17	6	BDL	2	45	14	17
0.36 M	Virus (%)	BDL	0.1	0.1	36	45	4	4
	Protein (%)	64	11	2	BDL	3	3	1
	DNA (%)	13	5	BDL	3	52	18	16
0.30 M	Virus (%)	BDL	BDL	BDL	24	43	6	6
	Protein (%)	64	6	BDL	1	5	1	1
	DNA (%)	7	5	BDL	3	51	19	16

A2. Scale-up of adenovirus purification using 1 mL LFMC devices

As a continuation to the work described in Section A1, this part of the study focused on increasing the amount of adenovirus lysate purified using the 1 mL LFMC device. The methods applied were the same, with loading buffer containing 0.36 M NaCl, but for the virus elution step, 0.56 M NaCl (as opposed to 0.6 M) was implemented, in an attempt to reduce the residual amount of DNA co-eluting with the virus. Figure A2 below shows the results of runs using lysates from 50 mL, 100 mL, and 200 mL of culture respectively. For all cases, the lysate obtained according to the procedure described above and in Chapter 2 was diluted in loading buffer to a final volume of approximately 5 mL and injected onto the membrane using a 5 mL sample loop. Additionally, the run with lysate from 200 mL of culture was arbitrarily ran for a shorter volume interval (20 mL) and lesser fractions were collected compared with the other two runs (27 mL). Despite this difference between the runs, the results of the 200 mL run are still useful to reach important conclusions as discussed below.

From the results shown in Figure A2 and Table A2, it was clear that 50 mL and 100 mL of culture could be successfully purified with a 1 mL LFMC device, with very low losses of unbound virus in the flow-through. However, 11% of the initial amount of virus was observed in the flow-through for the run using lysates from 200 mL of culture, indicating the capacity of the membrane was reached for these loading conditions. For the run with 50 mL of culture, a 63% virus recovery was obtained in the two main virus elution fractions (between the 16 and 20 mL marks), with 2% of the initial amount of protein and 21% of the initial amount of the DNA. A higher virus recovery of 89% was observed in the run with 100 mL of culture, with 2% of the initial amount of protein, and 29% of the initial amount of DNA. Although significant, this amount of residual DNA represents an improvement compared with the results shown in Section A1, where approximately 55% of the initial amount of DNA co-eluted with the virus. The improvement is associated with the use of 0.56 M NaCl in the virus elution buffer as opposed to the 0.60 M discussed in Chapter 2 and Section A1. The observation of significant amounts of DNA even after this adjustment in elution conditions has largely motivated the study described in Chapter 4, where the DNA digestion was optimized along with the membrane chromatography step in order to further improve DNA removal.

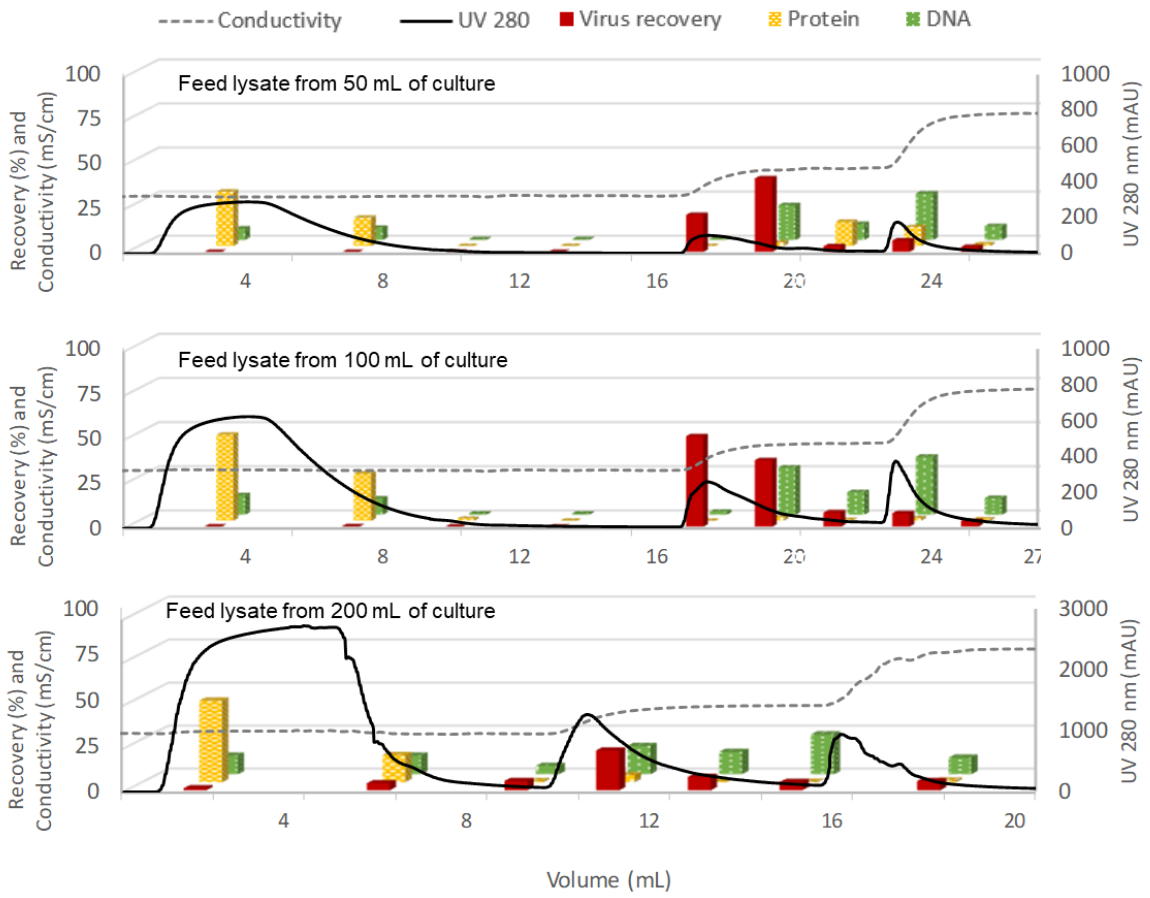

Figure A2. Chromatograms for adenovirus purification via stepwise elution strategy with a 1 mL LFMC device using feed lysates prepared from 50 mL of cell culture (top panel), 100 mL of culture (middle panel), and 200 mL of culture (bottom panel). The dashed line indicates the conductivity, and the solid line indicates the UV absorbance at 280 nm (refer to the secondary axis). The 3D bar charts display the amount of adenovirus (front red bars), total protein (middle yellow bars), and total DNA (back green bars) within each fraction as a percentage of the amount in the feed sample.

Table A2. Percent amount of virus, protein and DNA with respect to the amount in the feed in the different fractions of LFMC runs using different amounts of feed lysate. BDL: below the detection limit.

Run with lysate from 50 mL of culture	**Fraction interval →**	**0-4 mL**	**4-8 mL**	**8-12 mL**	**12-16 mL**	**16-18 mL**	**18-20 mL**	**20-22 mL**	**22-24 mL**	**24-27 mL**
	Virus (%)	BDL	BDL	BDL	BDL	21	42	3	7	3
	Protein (%)	31	16	BDL	BDL	BDL	2	14	11	1
	DNA (%)	6	7	BDL	BDL	1	20	9	26	8
Run with lysate from 100 mL of culture	**Fraction interval →**	**0-4 mL**	**4-8 mL**	**8-12 mL**	**12-16 mL**	**16-18 mL**	**18-20 mL**	**20-22 mL**	**22-24 mL**	**24-27 mL**
	Virus (%)	0.1	0.2	0.1	BDL	51	38	8	8	3
	Protein (%)	49	27	1	BDL	BDL	2	BDL	1	1
	DNA (%)	11	9	1	1	2	27	13	33	9

Run with lysate from 200 mL of culture	Fraction interval →	0-4 mL	4-8 mL	8-10 mL	10-12 mL	12-14 mL	14-16 mL	16-20 mL	-	-
	Virus (%)	1	4	5	23	8	5	5	-	-
	Protein (%)	47	16	1	4	BDL	BDL	1	-	-
	DNA (%)	11	11	5	16	13	23	10	-	-

A3. Scale-up of adenovirus purification using 10 mL LFMC devices

To further scale up the amount of virus purified as described in Section A2, a 10 mL LFMC device was fabricated and tested for the purification of adenovirus lysates from 200, 400, and 800 mL of culture. Figure A3 below shows a 1 mL LFMC and a 10 mL LFMC side by size. The 10 mL device design followed the same pattern described for the 1 mL device in Chapter 2, but it was scaled in a such a way that it contains a stack of 20 layers of Sartobind Q, each measuring 8 cm by 2.3 cm. The same procedure described in Section A2 was applied for the experiments with the 10 mL, but the lysate was injected using the sample pump of the BioRad NGC system and experiments were ran at 15 mL/min.

Figure A3. LFMC devices containing 1 mL (left) and 10 mL (right) of the Sartobind Q membrane.

Figure A4 and Table A3 below show the results for the runs with the 10 mL LFMC device. For all three runs, no virus was detected in the flow-through fractions, and the virus recovery in the 4 main fractions containing the eluted virus as indicated by the red bars in the Figure were 48%, 67%, and 54%, for the runs with lysates from 200, 400, and 800 mL of culture, respectively. These results are in good agreement with the obtained above with the 1 mL LFMC device, where up to 100 mL of culture was successfully purified. Similar removals of protein and DNA were observed across all runs, where an average of 15% of both species co-eluted with the virus. The results presented in this Appendix demonstrate the successful scalability of the LFMC technology from 1 mL to 10 mL devices for the purification of adenovirus lysates from up to 800 mL of culture. Larger volumes could have potentially been purified with the 10 mL device since the binding capacity was not reached (i.e. no virus was observed in the flow-through) when the largest volume was purified.

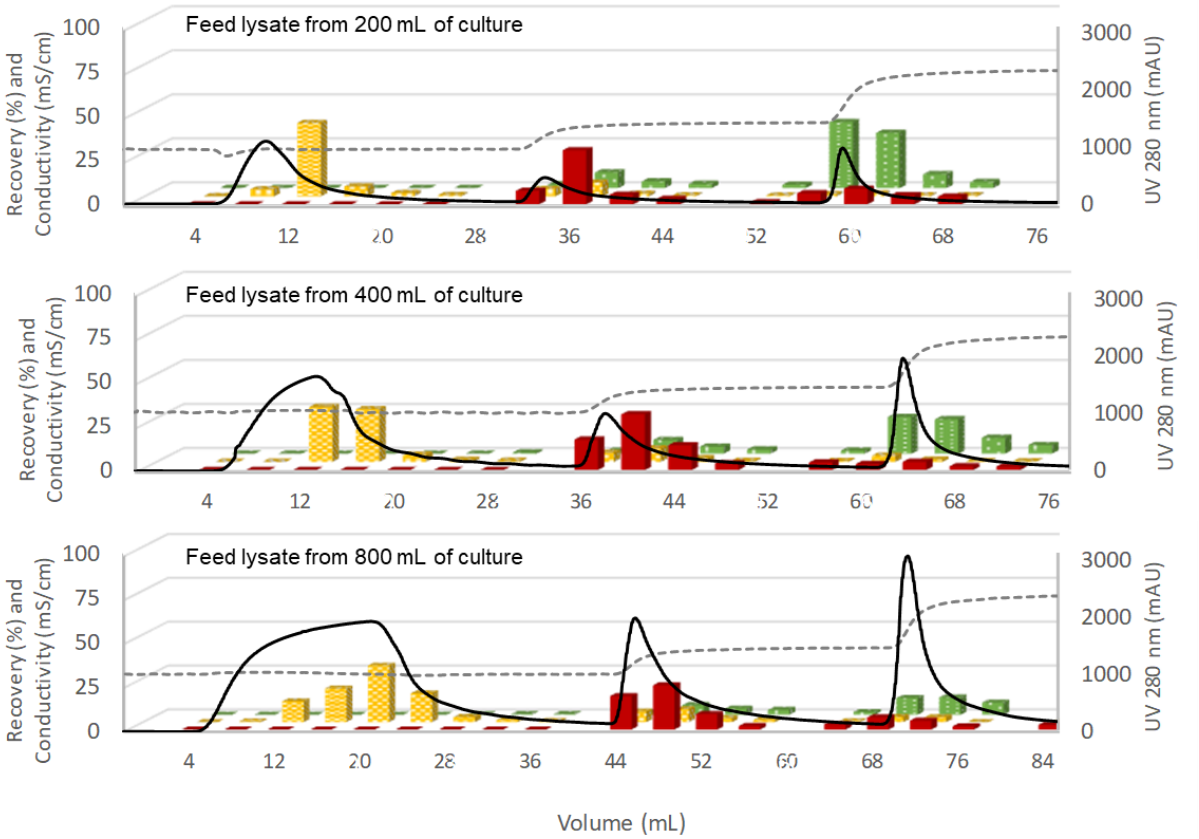

Figure A4. Chromatograms for adenovirus purification via stepwise elution strategy with a 10 mL LFMC device using feed lysates prepared from 200 mL of cell culture (top panel), 400 mL of culture (middle panel), and 800 mL of culture (bottom panel). The dashed line indicates the conductivity, and the solid line indicates the UV absorbance at 280 nm (refer to the secondary axis). The 3D bar charts display the amount of adenovirus (front red bars), total protein (middle yellow bars), and total DNA (back green bars) within each fraction as a percentage of the amount in the feed sample.

Table A3. Percent amount of virus, protein and DNA with respect to the amount in the feed in the different fractions of 10 mL LFMC runs using different amounts of feed lysate. BDL: below the detection limit.

Run with lysate from 200 mL of culture	**Fraction interval →**	**0-4 mL**	**4-9 mL**	**9-14 mL**	**14-19 mL**	**19-24 mL**	**24-29 mL**	**30-35 mL**	**35-39 mL**	**39-44 mL**	**44-50 mL**	**50-55 mL**	**55-59 mL**	**59-64 mL**	**64-68 mL**	**68-76 mL**	-	-	-
	Virus (%)	BDL	BDL	BDL	BDL	BDL	BDL	8	31	6	3	1	6	9	5	4	-	-	-
	Protein (%)	BDL	4	42	6	2	1	4	8	1	1	BDL	1	2	1	1	-	-	-
	DNA (%)	BDL	BDL	BDL	BDL	BDL	BDL	2	9	4	2	2	37	31	8	3	-	-	-
Run with lysate from 400 mL of culture	**Fraction interval →**	**0-4 mL**	**4-9 mL**	**9-14 mL**	**14-19 mL**	**19-24 mL**	**24-29 mL**	**30-35 mL**	**35-39 mL**	**39-44 mL**	**44-50 mL**	**50-55 mL**	**55-59 mL**	**59-64 mL**	**64-68 mL**	**68-72 mL**	**72-76 mL**	-	-
	Virus (%)	BDL	BDL	BDL	BDL	BDL	BDL	BDL	17	32	14	4	4	3	5	2	2	-	-
	Protein (%)	BDL	BDL	31	30	4	1	1	5	8	2	1	1	4	1	0	0	-	-
	DNA (%)	BDL	BDL	BDL	BDL	BDL	BDL	1	2	8	4	2	2	21	20	9	5	-	-
Run with lysate from 800 mL of culture	**Fraction interval →**	**0-4 mL**	**4-9 mL**	**9-14 mL**	**14-19 mL**	**19-24 mL**	**24-28 mL**	**28-32 mL**	**32-36 mL**	**36-40 mL**	**40-45 mL**	**45-50 mL**	**50-55 mL**	**55-60 mL**	**60-65 mL**	**65-70 mL**	**70-75 mL**	**75-80 mL**	**80-84 mL**
	Virus (%)	BDL	BDL	BDL	BDL	BDL	BDL	BDL	BDL	BDL	19	25	9	2	3	7	5	2	3
	Protein (%)	BDL	BDL	12	19	32	16	3	1	1	6	7	2	1	BDL	3	3	BDL	BDL
	DNA (%)	BDL	BDL	BDL	BDL	BDL	BDL	BDL	BDL	BDL	1	5	3	3	1	10	10	7	4

Appendix B: Supplemental information for Chapter 4

Integrated development of enzymatic DNA digestion and membrane chromatography processes for the purification of therapeutic adenoviruses

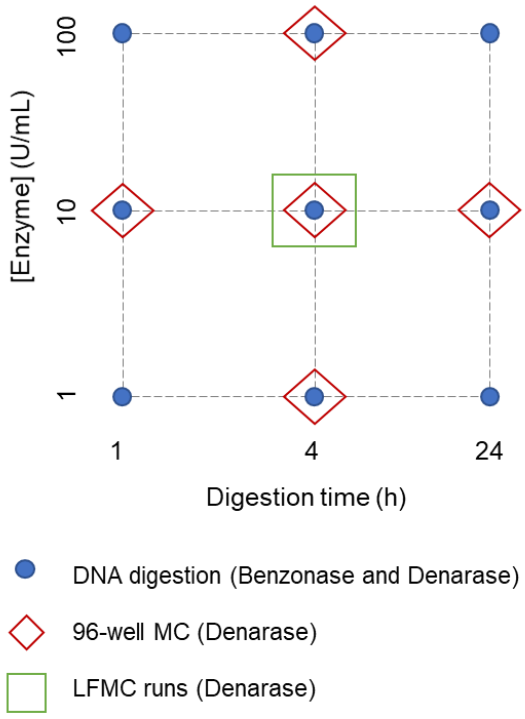

Figure B1. DOE conditions for DNA digestion time and enzyme concentration for the different studies described. All DNA digestion experiments were conducted at 37°C. Circles: all DNA digestion conditions tested with Benzonase and Denarase. Diamonds: DNA digestion conditions with Denarase used before MC in a 96-well format. Square: DNA digestion conditions with Denarase used before LFMC runs.

Table B1. Results of the 3^2 full factorial DOE using Benzonase and Denarase.

Run	Enzyme (U/mL)	Time (h)	Benzonase		Denarase	
			DNA (ng/mL)	Virus (IFU/mL)	DNA (ng/mL)	Virus (IFU/mL)
1	1	1	44979.5	4.73E+10	15537.3	2.39E+10
2	1	4	2972.6	2.49E+10	1951.1	1.65E+10
3	1	24	799.2	4.00E+08	189.0	2.11E+08
4	10	1	4380.9	4.15E+10	1678.8	2.07E+10
5	10	4	1480.0	1.65E+10	879.3	1.09E+10

6	10	24	923.8	1.11E+09	243.9	7.20E+07
7	100	1	1814.2	3.29E+10	820.4	1.51E+10
8	100	4	1010.0	6.80E+09	533.2	3.59E+09
9	100	24	465.2	3.47E+07	143.5	6.53E+07
10	1	1	40559.3	4.20E+10	17132.8	2.48E+10
11	1	4	3120.6	2.29E+10	1706.3	1.61E+10
12	1	24	695.5	3.29E+08	214.1	1.37E+08
13	10	1	5860.7	4.11E+10	1853.9	1.73E+10
14	10	4	1396.1	1.91E+10	979.1	1.12E+10
15	10	24	559.8	1.23E+08	261.9	1.41E+08
16	100	1	1677.7	3.44E+10	836.2	1.17E+10
17	100	4	1113.8	8.67E+09	516.2	5.20E+09
18	100	24	451.3	5.47E+07	176.8	7.60E+07

DOE analysis using R

Linear regression models were generated based on the DOE results using RStudio (version 1.3.959). To fit a linear model, different data transformations were applied to all variables. Enzyme concentration and digestion time were transformed to bring the DOE conditions within the range of -1 and +1, as shown by Equations B1 and B2, respectively. DNA and virus concentration were both log-transformed as shown by Equations B3 and B4.

$$E = \frac{\log(Enzyme\ concentration) - Center\ Point}{0.5(Range)} \quad \text{Equation B1}$$

$$D = \frac{\sqrt{Time} - Center\ Point}{0.5(Range)} \quad \text{Equation B2}$$

$$y_1 = \log(DNA\ concentration) \quad \text{Equation B3}$$

$$y_2 = \log(Virus\ concentration) \quad \text{Equation B4}$$

The R code provided below was used to generate linear models for y1 and y2 as functions of E and D for both Denarase and Benzonase. The model coefficients, ANOVA, R^2, and other statistical measurements for each of the 4 obtained models are shown in Table B2. As can be seen in Table B2, both the transformed parameters of the DOE (E and D) and the interaction between them had a statistically significant effect (P-value < 0.05) on the transformed Log (DNA concentration) variable for both enzymes. The R^2 of the models for Log (DNA concentration) were 0.932 and 0.849 for Denarase and Benzonase, respectively. Both transformed parameters (E and D) had a statistically significant effect (P-value < 0.05) on Log (Virus concentration). The R^2 values for Log (Virus concentration) were 0.976 and 0.955 for Denarase and Benzonase, respectively.

R code used in the DOE statistical analysis

```
# combinations of Enzyme Concentration (U/mL units) and Digestion time (h) used in the DOE
Enzyme = c(1, 1, 1, 10, 10, 10, 100, 100, 100, 1, 1, 1, 10, 10, 10, 100, 100, 100)
Time = c(1, 4, 24, 1, 4, 24, 1, 4, 24, 1, 4, 24, 1, 4, 24, 1, 4, 24)
# Map to coded variables: subtract the center point and divide by 0.5*(range)
E = (log10(Enzyme) - 1) / (0.5 * (2-0))
D_raw = sqrt(Time)
D = (D_raw - mean(range(D_raw))) / (0.5*(diff(range(D_raw))))
# Raw data obtained experimentally - the concentrations of DNA and virus after the digestion using their respective enzyme type, concentration, and time conditions
DNA_Denarase = c(15537.3, 1951.1, 189, 1678.8, 879.3, 243.9, 820.4, 533.2, 143.5, 17132.8, 1706.3, 214.1, 1853.9, 979.1, 261.9, 836.2, 516.2, 176.8)
Virus_Denarase = c(2.39E+10, 1.65E+10, 2.11E+08, 2.07E+10, 1.09E+10, 7.20E+07, 1.51E+10, 3.59E+09, 6.53E+07, 2.48E+10,1.61E+10, 1.37E+08, 1.73E+10,1.12E+10, 1.41E+08, 1.17E+10, 5.20E+09, 7.60E+07)
DNA_Benzonase = c(44979.5, 2972.6, 799.2, 4380.9, 1480.0, 923.8, 1814.2, 1010.0, 465.2, 40559.3, 3120.6, 695.5, 5860.7, 1396.1, 559.8, 1677.7, 1113.8, 451.3)
```

```
Virus_Benzonase = c(4.73E+10, 2.49E+10, 4.00E+08, 4.15E+10, 1.65E+10, 1.11E+09, 3.29E+10, 6.80E+09, 3.47E+07, 4.20E+10, 2.29E+10, 3.29E+08, 4.11E+10, 1.91E+10, 1.23E+08, 3.44E+10, 8.67E+09, 5.47E+07)

# Log transforms on the outputs

y1_Denarase = log10(DNA_Denarase)

y2_Denarase = log10(Virus_Denarase)

y1_Benzonase = log10(DNA_Benzonase)

y2_Benzonase = log10(Virus_Benzonase)

# Least-squares modelling with coded variables

lm_DNA_Denarase = lm(y1_Denarase ~ D*E)

lm_Virus_Denarase = lm(y2_Denarase ~ D*E)

lm_DNA_Benzonase = lm(y1_Benzonase ~ D*E)

lm_Virus_Benzonase = lm(y2_Benzonase ~ D*E)

summary(lm_DNA_Denarase)

plot(lm_DNA_Denarase)

residuals(lm_DNA_Denarase)

summary(lm_Virus_Denarase)

plot(lm_Virus_Denarase)

residuals(lm_Virus_Denarase)

summary(lm_DNA_Benzonase)

plot(lm_DNA_Benzonase)

residuals(lm_DNA_Benzonase)

summary(lm_Virus_Benzonase)

plot(lm_Virus_Benzonase)

residuals (lm_Virus_Benzonase)
```

Table B2. Results of the linear models for Log (DNA concentration) and Log (Virus concentration) as functions of the transformed parameters enzyme concentration (E, calculated using Equation B1) and digestion time (D, calculated using Equation B2) for Denarase and Benzonase using R (RStudio).

	Log (DNA concentration)	Log (Virus concentration)
Denarase	Call: lm(formula = y1_Denarase ~ D * E) Residuals: Min 1Q Median 3Q Max -0.270580 -0.107110 0.008082 0.088204 0.312751 Coefficients: Estimate Std. Error t value Pr(>|t|) (Intercept) 2.82544 0.04158 67.958 < 2e-16 *** D -0.55112 0.04814 -11.447 1.71e-08 *** E -0.27989 0.05092 -5.497 7.87e-05 *** D:E 0.26463 0.05897 4.488 0.000511 *** --- Signif. codes: 0 ‘***’ 0.001 ‘**’ 0.01 ‘*’ 0.05 ‘.’ 0.1 ‘ ’ 1 Residual standard error: 0.1732 on 14 degrees of freedom Multiple R-squared: 0.9323, Adjusted R-squared: 0.9178 F-statistic: 64.28 on 3 and 14 DF, p-value: 1.983e-08	Call: lm(formula = y2_Denarase ~ D * E) Residuals: Min 1Q Median 3Q Max -0.21339 -0.14178 -0.02557 0.11176 0.25519 Coefficients: Estimate Std. Error t value Pr(>|t|) (Intercept) 9.229601 0.042308 218.151 < 2e-16 *** D -1.158876 0.048993 -23.654 1.09e-12 *** E -0.205087 0.051817 -3.958 0.00143 ** D:E -0.008657 0.060004 -0.144 0.88734 --- Signif. codes: 0 ‘***’ 0.001 ‘**’ 0.01 ‘*’ 0.05 ‘.’ 0.1 ‘ ’ 1 Residual standard error: 0.1763 on 14 degrees of freedom Multiple R-squared: 0.9763, Adjusted R-squared: 0.9712 F-statistic: 191.9 on 3 and 14 DF, p-value: 1.324e-11
Benzonase	Call: lm(formula = y1_Benzonase ~ D * E) Residuals: Min 1Q Median 3Q Max -0.39749 -0.04475 0.01586 0.10154 0.41133 Coefficients: Estimate Std. Error t value Pr(>|t|) (Intercept) 3.21536 0.05974 53.825 < 2e-16 *** D -0.47630 0.06918 -6.885 7.5e-06 *** E -0.30296 0.07316 -4.141 0.000999 *** D:E 0.24706 0.08472 2.916 0.011277 * --- Signif. codes: 0 ‘***’ 0.001 ‘**’ 0.01 ‘*’ 0.05 ‘.’ 0.1 ‘ ’ 1 Residual standard error: 0.2489 on 14 degrees of freedom Multiple R-squared: 0.849, Adjusted R-squared: 0.8166 F-statistic: 26.24 on 3 and 14 DF, p-value: 5.243e-06	Call: lm(formula = y2_Benzonase ~ D * E) Residuals: Min 1Q Median 3Q Max -0.26936 -0.14033 -0.06009 0.09357 0.76226 Coefficients: Estimate Std. Error t value Pr(>|t|) (Intercept) 9.48019 0.06187 153.225 < 2e-16 *** D -1.19712 0.07165 -16.709 1.21e-10 *** E -0.28628 0.07578 -3.778 0.00204 ** D:E -0.18710 0.08775 -2.132 0.05118 . --- Signif. codes: 0 ‘***’ 0.001 ‘**’ 0.01 ‘*’ 0.05 ‘.’ 0.1 ‘ ’ 1 Residual standard error: 0.2578 on 14 degrees of freedom Multiple R-squared: 0.9548, Adjusted R-squared: 0.9451 F-statistic: 98.52 on 3 and 14 DF, p-value: 1.192e-09

Composition of samples obtained during membrane chromatography (MC) runs using a 96-well filter plate format

Table B3 displays the composition of each fraction from the MC runs using the 96-well filter plate: the feed sample (Initial), flow-through (FT), first elution (E1), and second elution (E2). All listed values are averages and standard deviations of duplicate measurements for each sample. Experiments were run in duplicate for each DNA digestion condition. The recovery in E1 is reported as the percentage of total infectious particles observed in fraction E1 with respect to the total initial amount of virus in the initial feed. The detection limits for DNA and protein concentrations were 2 ng/mL and 5 µg/mL, respectively. Samples with concentrations 'below detection limit' (BDL) are indicated.

Table B3. Virus, DNA, and protein concentrations in the fractions obtained during MC using a 96-well format. Results are shown for each set of duplicate MC runs under each DNA digestion condition.

Fraction →		Initial	FT	E1	E2	% Recovery in E1
Volume (µL) →		38	438	400	400	
Digestion conditions ↓		Virus concentration (IFU/mL)				
[Denarase] (U/mL)	Time (h)					
1	4	7.3E+09 ± 3.5E+08	1.6E+06 ± 1.1E+05	3.5E+08 ± 7.1E+07	2.0E+07 ± 7.1E+05	50% ± 11%
		9.8E+09 ± 1.1E+09	1.4E+06 ± 1.8E+05	3.9E+08 ± 7.1E+06	2.6E+07 ± 2.1E+06	42% ± 5%
10	1	1.4E+10 ± 2.5E+09	2.2E+06 ± 4.2E+05	7.7E+08 ± 4.2E+07	3.5E+07 ± 2.1E+06	59% ± 11%
		1.6E+10 ± 3.2E+09	2.4E+06 ± 6.4E+05	8.8E+08 ± 1.3E+08	4.3E+07 ± 3.5E+05	57% ± 14%
10	4	9.3E+09 ± 1.8E+09	1.1E+06 ± 3.2E+05	6.5E+08 ± 2.5E+07	3.6E+07 ± 8.5E+06	74% ± 14%
		9.0E+09 ± 7.1E+08	6.5E+05 ± 7.1E+04	6.8E+08 ± 5.7E+07	3.2E+07 ± 4.6E+06	79% ± 9%
10	24	6.5E+07 ± 1.4E+07	4.0E+04 ± 1.4E+04	9.3E+05 ± 8.1E+05	9.8E+04 ± 1.1E+04	15% ± 14%
		7.8E+07 ± 4.6E+07	8.0E+03 ± 1.4E+03	1.0E+06 ± 1.4E+05	2.0E+05 ± 2.1E+04	14% ± 8%
100	4	3.2E+09 ± 8.5E+08	3.2E+05 ± 1.4E+04	1.4E+08 ± 2.3E+07	1.6E+07 ± 5.3E+06	47% ± 15%
		3.3E+09 ± 3.5E+07	3.5E+05 ± 3.5E+03	2.2E+08 ± 3.5E+06	1.8E+07 ± 5.3E+06	72% ± 1%
0	0	1.7E+10 ± 7.1E+08	4.6E+06 ± 6.4E+05	1.1E+09 ± 3.2E+08	3.2E+07 ± 3.9E+06	71% ± 21%
		1.8E+10 ± 9.2E+09	4.4E+06 ± 4.6E+05	9.4E+08 ± 5.7E+07	1.9E+07 ± 8.1E+06	57% ± 30%
Fraction →		Initial	FT	E1	E2	% Recovery in E1
Volume (µL) →		38	438	400	400	
Digestion conditions ↓		DNA concentration (ng/mL)				
[Denarase] (U/mL)	Time (h)					
1	4	611.7 ± 46.5	BDL	8.0 ± 0.2	11.5 ± 0.6	14% ± 1%
		330.4 ± 66.1	BDL	BDL	6.7 ± 0.1	BDL <6%
10	1	531.0 ± 141.7	4.7 ± 0.05	14.3 ± 0.4	10.5 ± 0.7	28% ± 8%
		534.6 ± 142.4	5.0 ± 0.3	15.8 ± 0.4	12.3 ± 0.8	31% ± 8%
10	4	316.4 ± 32.0	2.2 ± 0.2	8.9 ± 0.3	BDL	30% ± 3%
		337.7 ± 37.4	1.9 ± 0.1	10.1 ± 0.6	BDL	31% ± 4%
10	24	114.0 ± 15.5	BDL	BDL	BDL	BDL <6%
		114.9 ± 27.1	BDL	BDL	BDL	BDL <6%
100	4	212.3 ± 50.3	3.7 ± 0.4	6.8 ± 0.3	BDL	34% ± 8%
		242.3 ± 59.4	4.3 ± 0.6	6.6 ± 0.5	BDL	29% ± 7%
0	0	16376.8 ± 1590.4	5.6 ± 0.7	139.6 ± 2.5	129.7 ± 3.0	9% ± 1%
		14475.7 ± 399.4	6.0 ± 0.7	142.6 ± 2.4	136.4 ± 4.4	10% ± 0%
Fraction →		Initial	FT	E1	E2	% Recovery in E1
Volume (µL) →		38	438	400	400	
Digestion conditions ↓		Protein concentration (µg/mL)				
[Denarase] (U/mL)	Time (h)					
1	4	3523.6 ± 399.5	167.4 ± 50.3	15.2 ± 1.8	7.4 ± 0.4	5% ± 1%
		1951.0 ± 315.1	117.5 ± 14.1	5.6 ± 0.04	BDL	3% ± 0.5%
10	1	3307.9 ± 525.5	176.9 ± 57.3	17.7 ± 0.1	7.1 ± 0.1	6% ± 1%
		2618.3 ± 707.8	197.2 ± 4.9	10.7 ± 0.7	BDL	4% ± 1%
10	4	2969.7 ± 345.6	195.8 ± 12.4	10.2 ± 0.8	BDL	4% ± 0.5%
		3051.5 ± 590.5	198.1 ± 3.3	9.6 ± 0.6	BDL	3% ± 1%
10	24	2615.9 ± 557.0	155.8 ± 62.3	7.1 ± 0.1	6.6 ± 0.04	3% ± 1%
		2449.1 ± 362.8	137.7 ± 43.8	4.2 ± 0.5	BDL	2% ± 0.4%
100	4	3373.6 ± 282.8	197.8 ± 76.4	13.3 ± 0.4	7.0 ± 0.2	4% ± 0.4%
		3301.3 ± 638.0	187.3 ± 91.0	7.4 ± 0.5	BDL	2% ± 0.5%
0	0	3683.8 ± 80.9	207.7 ± 52.9	17.7 ± 4.0	6.4 ± 1.9	5% ± 1%
		3227.8 ± 1058.7	178.2 ± 90.1	18.5 ± 0.4	BDL	6% ± 2%

Appendix C: Supplemental information for Chapter 5

Purification of vesicular stomatitis virus (VSV) using hydrophobic interaction membrane chromatography

C1. VSV purification using Sartobind Q anion-exchange membrane chromatography

Anion-exchange (AEX) membrane chromatography (MC) using the Sartobind Q membrane in 1 mL LFMC devices was attempted to purify VSV lysates prepared according to Chapter 5. A similar MC procedure as that applied for adenovirus purification in Chapter 2 was applied. Briefly, the membrane was equilibrated with buffer A (10 mM HEPES, 4% sucrose, pH 7.4) and 1 mL of VSV lysate was injected. A wash step was performed with buffer A and a gradient elution strategy was applied by increasing the NaCl concentration in the buffer from zero to 1 M over 5 membrane volumes. The results for this run are shown in Figure C1 below, where a first flow-through peak can be observed and consisted of mostly protein and DNA; no virus was detected in those fractions suggesting VSV successfully bound to the membrane. The second peak observed corresponds to the elution peak, where unfortunately, very low virus recoveries were observed based on the $TCID_{50}$ assay results. Significant amounts of protein and DNA were observed between the 6 and 8 mL marks (31% and 13%, respectively, relative to the total amounts in the feed). The overall VSV recovery after the gradient elution was applied (between the 6 and 11 mL marks) was only 8.8% in this run. Repeat experiments confirmed low VSV recoveries with Sartobind Q. Further investigation would be necessary to accurately explain the reasons for

low recoveries, which could be either associated with losses in virus stability and infectivity during the process, or irreversible binding to the Sartobind Q membrane.

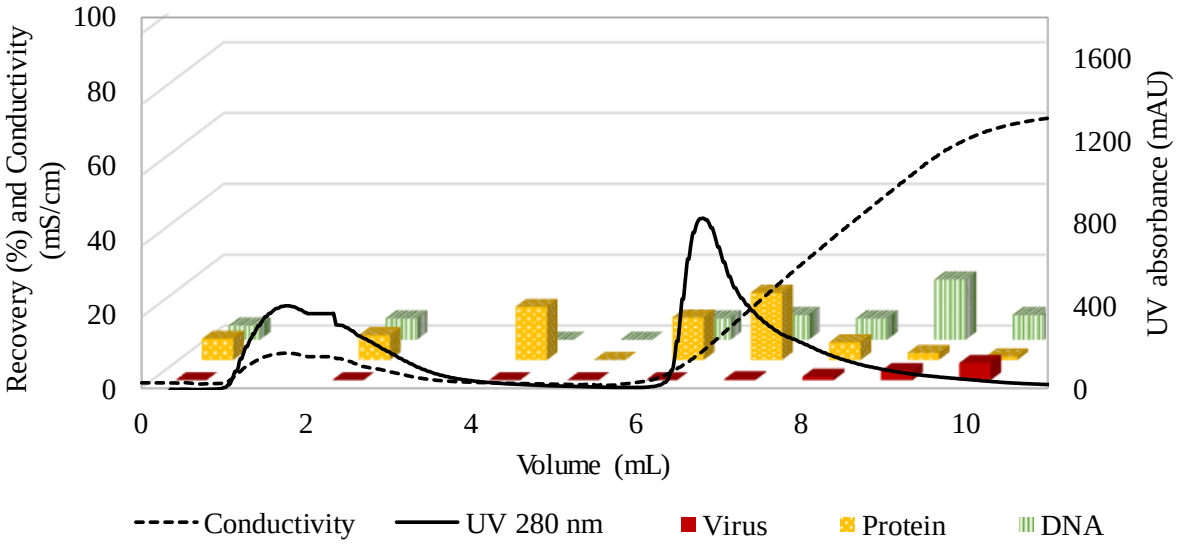

Figure C1. Chromatogram for VSV purification via gradient elution with a 1 mL Sartobind Q LFMC device. The dashed line indicates the conductivity, and the solid line indicates the UV absorbance at 280 nm (refer to the secondary axis). The 3D bar charts display the amount of VSV (front red bars), total protein (middle yellow bars), and total DNA (back green bars) within each fraction as a percentage of the amount in the 1 mL injected feed sample.

C2. VSV purification Sartobind Sulfated Cellulose (SC) pseudo-affinity membrane chromatography

The second attempt to purify VSV was using the Sartobind SC membrane, to which certain viruses such as vaccinia and influenza are able to bind via pseudo-affinity interactions are discussed in Chapter 5. However, as it can be seen in Figure C2 below, both trials were unsuccessful since VSV was completely eluted in the flow-through fractions and therefore was not able to bind to this membrane. For reference, in Figure C2 panel A, the same buffer conditions as those described in Section C1 were applied; and in

panel B a citric-acid based buffer was used according to previous literature reports for influenza purification using the Sartobind SC membrane.[1]

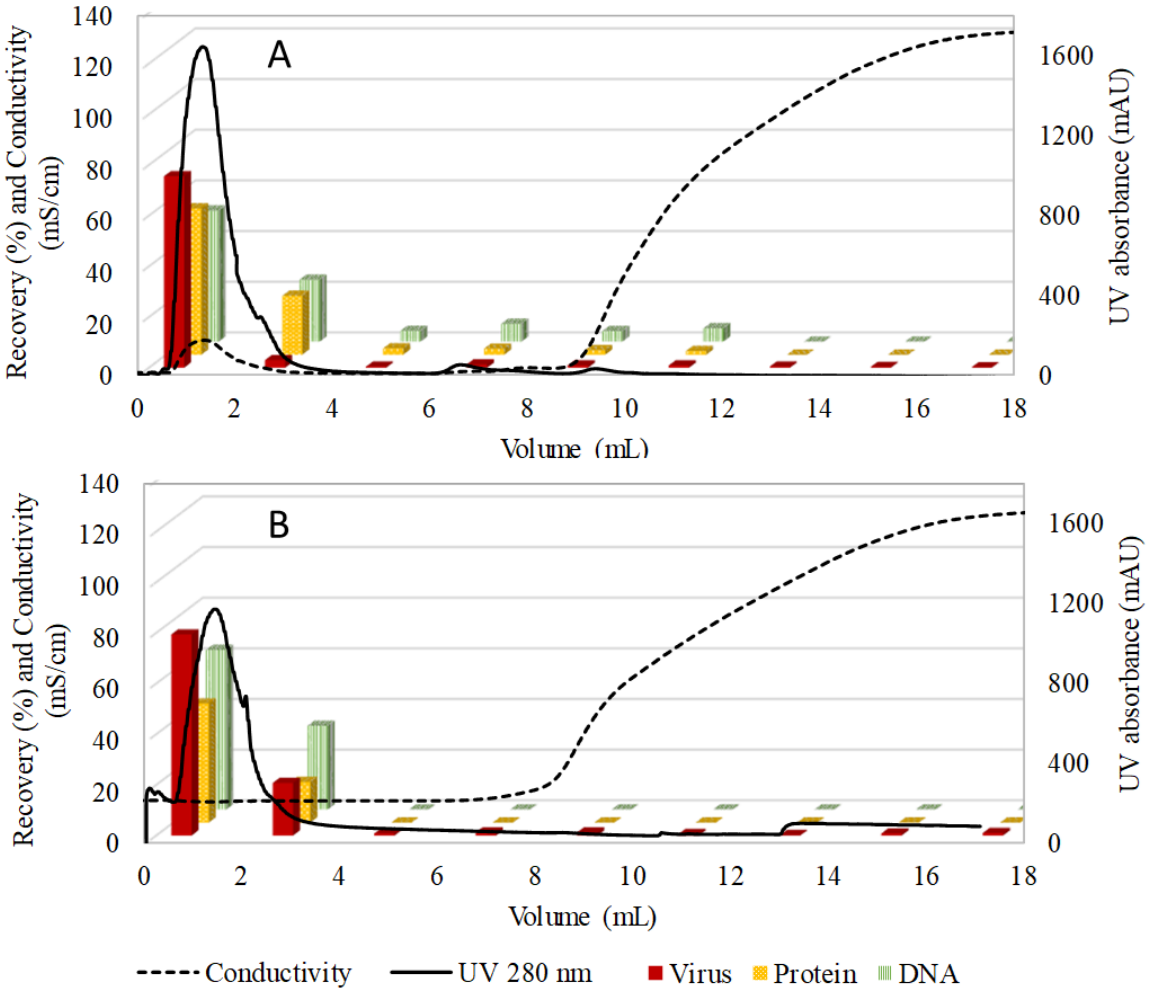

Figure C2. Chromatograms for VSV purification via gradient elution with a 1 mL Sartobind Sulfated Cellulose LFMC device. A: using HEPES-based buffers and B: using citric acid-based buffers. The dashed line indicates the conductivity, and the solid line indicates the UV absorbance at 280 nm (refer to the secondary axis). The 3D bar charts display the amount of VSV (front red bars), total protein (middle yellow bars), and total DNA (back green bars) within each fraction as a percentage of the amount in the 1 mL injected feed sample.

1. S. Hansen, R. Faber, U. Reichl, M. Wolff, A. Gram, Purification of vaccinia viruses using hydrophobic interaction chromatography, US 91903201 B2, 2015.

Appendix D: A critical evaluation of the fifty percent tissue culture infective dose ($TCID_{50}$) assay for the titration of vesicular stomatitis virus (VSV)

Karina Kawka, Evan Wright, A. Noelle Wilton, Maria Fe C. Medina, David R. Latulippe

Prepared for Journal submission

D1. Abstract

Virus infectivity assays are essential during the development of manufacturing processes of virus-based therapeutics to ensure product stability through the process. The fifty percent tissue culture infective dose ($TCID_{50}$) assay is one of the most widely used techniques for infectious titer determination, however, the final titer estimate can be highly affected by assumptions taken by the individual analysing the data. This is particularly important in the case of 'skipped wells' during virus titration using well plates that consists of a negative response to infection between two positive responses. The relevance of skipped wells was demonstrated through an analysis of historical $TCID_{50}$ raw data, where skipped wells occurred in 15% of the over 1000 situations analysed. In the context of virus manufacturing, the recovery of a VSV chromatography run was estimated at 36% or 87% depending on the assumptions taken during $TCID_{50}$ data interpretation. Plaque assay was found to offer a more accurate and less prone to interpretation alternative under the conditions used in this study. Given the critical effect of interpretation, this study reinforces the need for objective and consistent strategies for $TCID_{50}$ data analysis.

D2. Introduction

Analytical tools play a key role in the development of virus manufacturing processes. Virus detection typically relies on measuring infectivity, total nucleic acid or protein, or total viral particles through different methods.[1] In the context of manufacturing, viruses can be exposed to relatively harsh conditions, so it is important to monitor virus infectivity throughout the process to ensure its stability and to determine the yields of the various unit operations. The most commonly used methods for measuring virus infectivity are the fifty percent tissue culture infective dose ($TCID_{50}$), plaque assays, and immunofluorescence foci assays.[1] The $TCID_{50}$ method is often preferred when a large number of samples is to be analysed,[2] and it is a more economical method compared with other assays.[3]

Although $TCID_{50}$ can be performed in live animals,[1] this study will focus on the version of the assay using cell culture. $TCID_{50}$ can be used to detect any virus that causes a cytopathic effect over 5 to 20 days.[1] The assay consists of infecting cells typically grown in well plates with samples of virus serially diluted to the end-point.[4] The $TCID_{50}$ titer calculated represents the dilution needed to infect 50% of cell culture wells.[4] Different strategies exist to determine if a culture of cells was infected and it can be based on the observation of cytopathic effect directly,[3] the use of dyes to stain intact cells,[5,6] or the observation of fluorescence in the case the virus carries a gene for green fluorescent protein (GFP),[7] for example. The latter option results in easier and faster detection as plates can be scanned and the presence of any green fluorescence foci indicate infection.[3] Figure D1 shows a typical 96-well plate obtained from an assay to determine the titer of vesicular

stomatitis virus (VSV) expressing green fluorescent protein (GFP) in Vero cell culture. The serial dilution starts at the first row and goes down the plate using a fixed fold-dilution between each row. The plate was used to analyse two samples, with 6 replicates each as indicated. Black and light grey wells correspond to infected and uninfected cells, respectively.

The Spearman-Karber method is widely used to calculate the endpoint dilution that causes the infection of 50% of the wells,[8] as its accuracy is considered superior to that of other methods such as the Reed-Muench and Dragstedt-Behrens methods.[9] The equations shown in the materials and methods section were based on Finney[10] and can be used to estimate the $TCID_{50}$ titer according to the Spearman-Karber method. The key parameter in the calculation is the number of negative responses 'r' that needs to be input in Equation D1. However, determining the negative responses is subject to interpretation, resulting in high variability in the results, depending on the assumptions made by the individual.[11]

A common occurrence in $TCID_{50}$ assays using cell culture in well plates are the 'skipped wells' observed in Figure D1. In the literature, this event has been observed in multiple studies focused on different viruses.[4–7,12,13] Apart from Karakus et al.[5] which briefly acknowledged skipped wells as caused by 'stochastic events', to our knowledge, the reasons for them or their impact on the calculated titers have not yet been addressed in detail in the literature. The objective of this study is to determine the frequency at which skipped wells occur in the titration of VSV expressing GFP and how different approaches for interpreting the results can impact the calculated yields in chromatography experiments

for VSV purification. Finally, the variability of the $TCID_{50}$ and a plaque assay for VSV titration is compared.

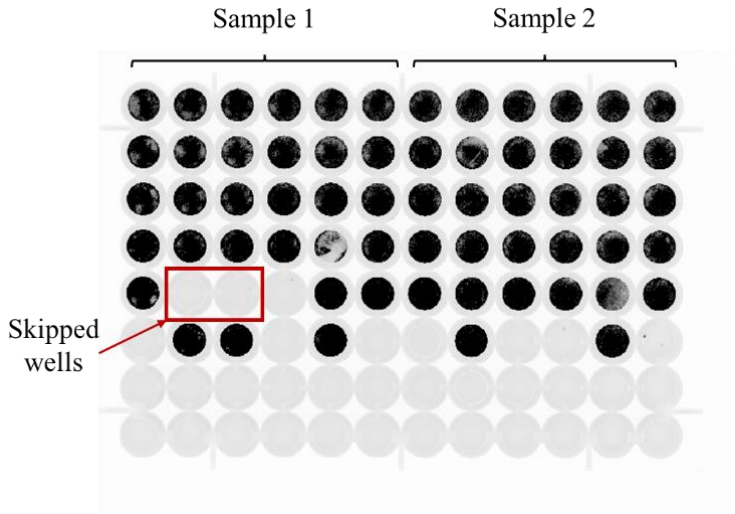

Figure D1. A typical well plate used in the titration of VSV expression GFP through the $TCID_{50}$ assay. Each row corresponds to repeats of a given serial dilution. The first 6 columns are repeats of sample 1 and the last 6 rows are repeats of sample 2. Black wells correspond to infected cells (i.e. presenting green fluorescence) and light grey wells correspond to uninfected cells. Skipped wells are indicated, where there is a negative response between two positive responses.

D3. Materials and methods

VSV cultures were prepared as described in Chapter 5. The method for the $TCID_{50}$ assay was adapted from Roldão et al.[3] and the titer was calculated using the Spearman-Karber method.[10] Briefly, 100 µL of Vero cell suspensions in supplemented Dulbecco's minimal essential medium (DMEM) containing 2×10^5 cells/mL were seeded in each well of a clear flat-bottom 96-well plate (Corning) and incubated for 24 hours. On the next day, an aliquot of the virus stock was thawed and pre-diluted 10^4 fold in DMEM supplemented with 10% fetal bovine serum (FBS, Gibco) and 1% L-glutamine (BioShop). A new 96-well

plate was filled with 120 µL/well of supplemented DMEM for the virus serial dilutions, and 30 µL of the pre-diluted stock was added to 6 wells of the first row of wells. After mixing by pipetting multiple times using a multichannel pipette, 30 µL from the first row of wells were transferred to the second row and the process was repeated until reaching the last row. Finally, the serial dilutions were used to infect the cells grown in the 96-well plates, prepared one day earlier. For that, the old media was removed and 100 µL of the serial dilutions were added to each well. The plate with the cells was incubated at 37°C and 5% CO2 for 48 hours before being scanned for fluorescence using an Amersham™ Typhoon scanner (GE) with an emission wavelength of 523 nm and a photomultiplier tube potential of 600 V.

VSV titer was calculated according to the Spearman-Karber method.[10] Equation D1 corresponds to the general equation used to obtain the titer, where M is the mean 50% infectious dose, x_k is the dose of the highest dilution (8 in this study since a 96-well plate has 8 rows), r is the total number of negative responses (i.e. number of wells negative for GFP expression), d is the spacing between the dilutions (1 in this study) and n is the number of wells per dilution (6 in this study). The virus titer was obtained using Equation D2, where F is the dilution factor between each row of the 96-well plate (5 in this study) and PF is the pre-dilution factor the sample was submitted in the microcentrifuge tube before being transferred to the 96-well plates. The variance (V) of M was calculated using Equation D3, where r_i is the number of negative responses in row 'i' of the 96-well plate. V was then transformed to units of $TCID_{50}$/mL using Equation D4. The standard deviation was finally calculated as the square root of the variance of the titer.

$$M = x_k + d\left(0.5 - \frac{1}{n}r\right) \quad \textit{(Equation D1)}$$

$$\text{Titer}\left(\frac{TCID_{50}}{mL}\right) = 10 \times F^M \times PF \quad \textit{(Equation D2)}$$

$$V(M) = \frac{d^2}{n^2\,(n-1)} \sum_{i=1}^{i} r_i\,(n - r_i) \quad \textit{(Equation D3)}$$

$$V(Titer) = V(M)\left(\frac{10\log(F) \times F^M}{PF}\right)^2 \quad \textit{(Equation D4)}$$

A plaque assay method for VSV titration adapted from Karakus et al.[5] was used to compare with the $TCID_{50}$ method. Vero cells were seeded in 6-well plates (Corning) by adding 2 mL of a suspension containing 2×10^5 cells/mL in supplemented DMEM. On the next day, the old media was removed, and the cells were infected with 100 µL serially-diluted virus in supplemented DMEM. A 1% agarose solution was mixed with 2× supplemented DMEM, both at 44 °C and 2 mL of the mixture was used to overlay the infected cells. After solidification, the plates were incubated for 24 hours to allow for the formation of plaques. Next, a 1 mL aliquot of 3.7% formaldehyde solution was added to each well to fix the cells and incubated for 20 min at room temperature. The solution was removed along with the agarose layer and the cells were stained with 1 mL of a 0.2% crystal violet in a 20% ethanol solution for 10 minutes. Finally, the wells were washed with tap water and allowed to dry before counting the plaques. The number of plaques forming units (PFU) per mL was calculated based on the dilution factor and the volume used to infect each well.

D4. Results and Discussion

D4.1. Frequency of occurrence of skipped wells during titration of VSV using $TCID_{50}$

In this study, the term 'skipped well' refers to a well in a 96-well plate for virus titration via $TCID_{50}$ assay that is uninfected, but it is between two infected wells as discussed in the introduction. This is a common occurrence in the literature, as seen in different works focused on different types of viruses.[4–7,12,13] To determine the frequency at which skipped wells happen, we have done an in-depth analysis of historical $TCID_{50}$ raw data in our lab by looking at images of 96-well plates used for VSV titration via the $TCID_{50}$ assay over the span of approximately 2 years. Based on the observation of 1171 columns of 96-well plates, 171 columns had at least 1 skipped well. There were also cases where 2, 3, or 4 wells were skipped before an infected well. Figure D2 shows the breakdown of 96-well plate columns that had different numbers of skips. In this dataset, it can be concluded that skipped wells happened in 15% of the cases.

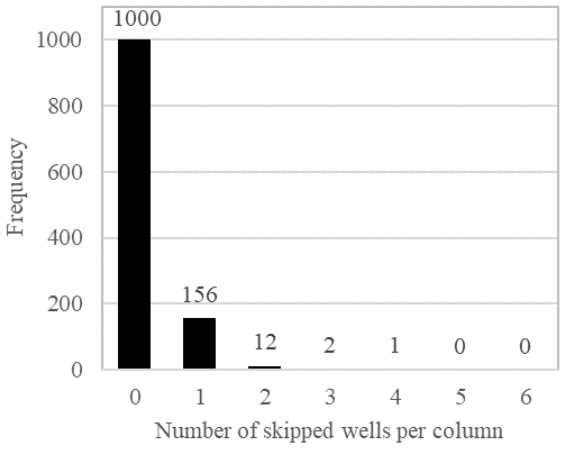

Figure D2. Frequency of skipped wells in historical raw data from an analysis of images of 96-well plates for VSV titration via the $TCID_{50}$ assay.

D4.2. Effect of skipped wells on the calculated recovery of VSV chromatography runs

In the literature, skipped wells are typically treated as they are. In other words, when counting the negative responses to input in the equations, the skipped-well is treated as negative, and the following positive well is normally treated as positive. However, given the complexity of biological systems, this assumption is open to interpretation since the reasons for a skipped well can be multiple. We propose three different approaches below with different ways to treat skipped wells when determining the number of negative responses in Equation D1.

- Approach 1: Skipped, negative wells are simply treated as negative as they appear in the image.
- Approach 2: Skipped, negative wells before a positive well are false negatives and therefore are treated as positive. This assumption considers that, although there were infectious particles present in the culture of the skipped well, local conditions such as local low cell density or contamination, prevented cell infection.
- Approach 3: Positive wells after a negative well are false-positive, and therefore treated as negative. This assumption considers that the infectious particles in that positive well are originally from contamination during the procedure.

To investigate the impact of using these different approaches on the final recovery of a chromatography run, we randomly selected run 5 from Chapter 5 as a case study. In Chapter 5, all titers were estimated according to approach 1. Table D1 shows the estimated titers for the feed and elution samples from run 5. For the feed sample, which used one set

of 6 columns from a 96-well plate, there were occurrences of a skipped well in two of the six columns. For the elution samples, which corresponded to 4 chromatography fractions that were assayed using 4 sets of 6 columns from a 96-well plate, there was a total of 3 occurrences of a skipped well. As it can be seen, both the feed and elution titers vary significantly depending on the approach used to treat the different skipped wells observed in the samples. This reflected on the overall recovery or yield of the chromatography run, which was found to be extremely sensitive to the approach used, varying from as low as 36% when approach 2 was used, to 87% when approach 3 was used.

Table D1. Calculated titers in the feed and elution samples from run 5 (Chapter 5), according to the 3 different approaches for treating the skipped wells in the titration of VSV via the $TCID_{50}$ assay.

Approach	**VSV particles in the feed ($TCID_{50}$)**	**VSV particles in the elution ($TCID_{50}$)**	**VSV recovered in the elution fractions**
1	2.04×10^{9}	1.12×10^{9}	55%
2	3.49×10^{9}	1.26×10^{9}	36%
3	1.19×10^{9}	1.04×10^{9}	87%

D4.3. Variability of the $TCID_{50}$ and plaque assays for VSV titration

This part of the study addressed the variability of the $TCID_{50}$ and plaque assays by analysing the same sample multiple times with each assay. A sample of VSV had its titer determined via the $TCID_{50}$ assay by three different operators, a total of 10 repeats each (therefore a total of 30 independent replicates), at the same time and under the same procedure conditions. In parallel, the same sample was also analysed using plaque assay in 6 independent replicates. Figure D3 contains the Box and Whisker plots for the 30 $TCID_{50}$ replicates using each of the 3 approaches for treating skipped wells as discussed in the previous section, and the 6 plaque assay replicates. Overall, the $TCID_{50}$ assay presented

greater variability compared with the plaque assay; it also resulted in higher absolute titer averages, in good agreement with literature reports for other viruses.[2] As expected, the average titer was different for each of the approaches used to deal with skipped wells, where it was found to be 5.07×10^9 $TCID_{50}$/mL for approach 1, 6.32×10^9 $TCID_{50}$/mL for approach 2, and 4.24×10^9 $TCID_{50}$/mL for approach 3. With the plaque assay, the average titer was 2.23×10^9 plaque-forming units (PFU)/mL. This indicates that the plaque assay could be preferred as a less variable, and less prone to interpretation alternative to the $TCID_{50}$ assay for the titration of samples that require more accurate estimates.

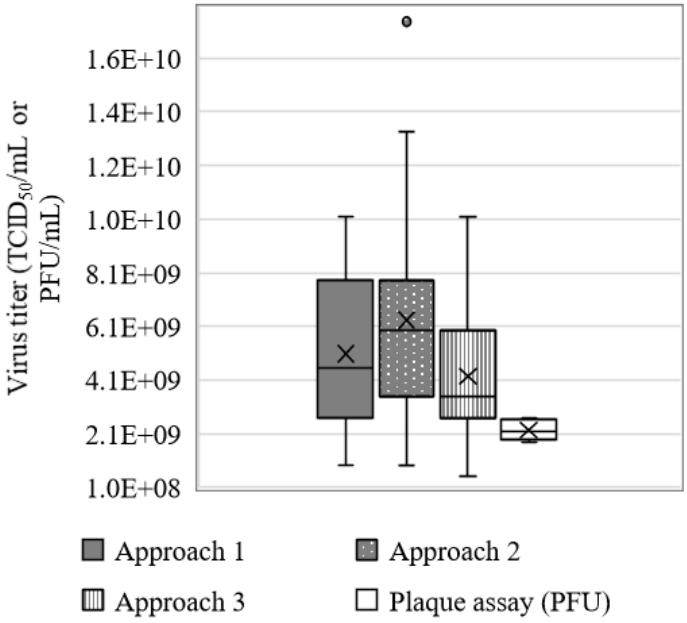

Figure D3. VSV titer estimated by $TCID_{50}$ (30 independent replicates, using three different approaches for interpreting skipped wells), and by plaque assay (6 independent replicates).

D5. Conclusions

Skipped wells are a common occurrence in $TCID_{50}$ assays for virus titration using cell culture in well plates. Although often reported in the literature, the impact of the technician's assumptions on interpreting skipped wells has not been addressed in detail. In this study, it was found that skipped wells happened in 15% of the cases of assays for the titration of VSV expressing GFP. Three approaches were proposed for interpreting skipped wells and consisted of 1: treating negative and positive wells as they appear; 2: treating a skipped negative well as a false-negative, therefore considering it as positive; and 3: treating a positive well after a skipped well as being a false-positive and therefore considering it as negative. When the three approaches were used in the analysis of $TCID_{50}$ results of a chromatography run for VSV purification, the yield of the process varied significantly from only 36% (approach 2) to 87% (approach 3), indicating the critical effect of interpretation in $TCID_{50}$ raw data analysis, and the importance of establishing an objective and consistent strategy. Finally, the plaque assay was shown to have less variability, and can be a good alternative less prone to interpretation for when more accurate estimates of VSV titer are necessary.

D6. Acknowledgements

Funding was provided by the Ontario Research Fund-Research Excellence program and the Natural Sciences and Engineering Research Council of Canada. Additional funding was provided by BioCanRx, a Network of Centres of Excellence

program, in the form of a Summer Studentship Award to A. Noelle Wilton. The authors thank Dr Jake Nease for his contribution on the analysis of the $TCID_{50}$ data.

D7. References

1. Pankaj, K. Virus Identification and Quantification. Mater Methods 3, (2013).
2. Smither, S. J. et al. Comparison of the plaque assay and 50% tissue culture infectious dose assay as methods for measuring filovirus infectivity. J. Virol. Methods 193, 565–571 (2013).
3. Roldão, A., Oliveira, R., Carrondo, M. J. T. & Alves, P. M. Error assessment in recombinant baculovirus titration: Evaluation of different methods. J. Virol. Methods 159, 69–80 (2009).
4. Darling, A. J., Boose, J. A. & Spaltro, J. Virus assay methods: Accuracy and validation. Biologicals 26, 105–110 (1998).
5. Karakus, U., Crameri, M., Lanz, C. & Yanguez, E. Propagation and titration of influenza viruses. in Trends in microbiology 26, 809–810 (2018).
6. Loeffen, W. et al. Development of a virus neutralisation test to detect antibodies against Schmallenberg virus and serological results in suspect and infected herds. Acta Vet. Scand. 54, 44 (2012).
7. Biacchesi, S. et al. Rapid human metapneumovirus microneutralization assay based on green fluorescent protein expression. J. Virol. Methods 128, 192–197 (2005).
8. Wulff, N. H., Tzatzaris, M. & Young, P. J. Monte Carlo simulation of the Spearman-Kaerber $TCID_{50}$. J. Clin. Bioinforma. 2, 5 (2012).
9. Miller, R. G. Nonparametric estimators of the mean tolerance in bioassay. Biometrika 60, 535–542 (1973).
10. Finney, D. J. Statistical Method in Biological Assay. (Charles Griffin & Company Limited, 1952).
11. Gustafsson, R. K. L., Engdahl, E. E. & Fogdell-Hahn, A. Development and validation of a Q-PCR based $TCID_{50}$ method for human herpesvirus 6. Virol. J. 9, 1 (2012).
12. Von Nordheim, M., Boinay, M., Leisi, R., Kempf, C. & Ros, C. Cutthroat trout virus—towards a virus model to support hepatitis e research. Viruses 8, 1–12 (2016).
13. Aoki-Utsubo, C., Chen, M. & Hotta, H. Virucidal and Neutralizing Activity Tests for Antiviral Substances and Antibodies. Bio-Protocol 8, 1–12 (2018).

Appendix E: Supplemental Information for Chapter 6

Economic analysis of adenovirus manufacturing processes for gene therapy clinical applications

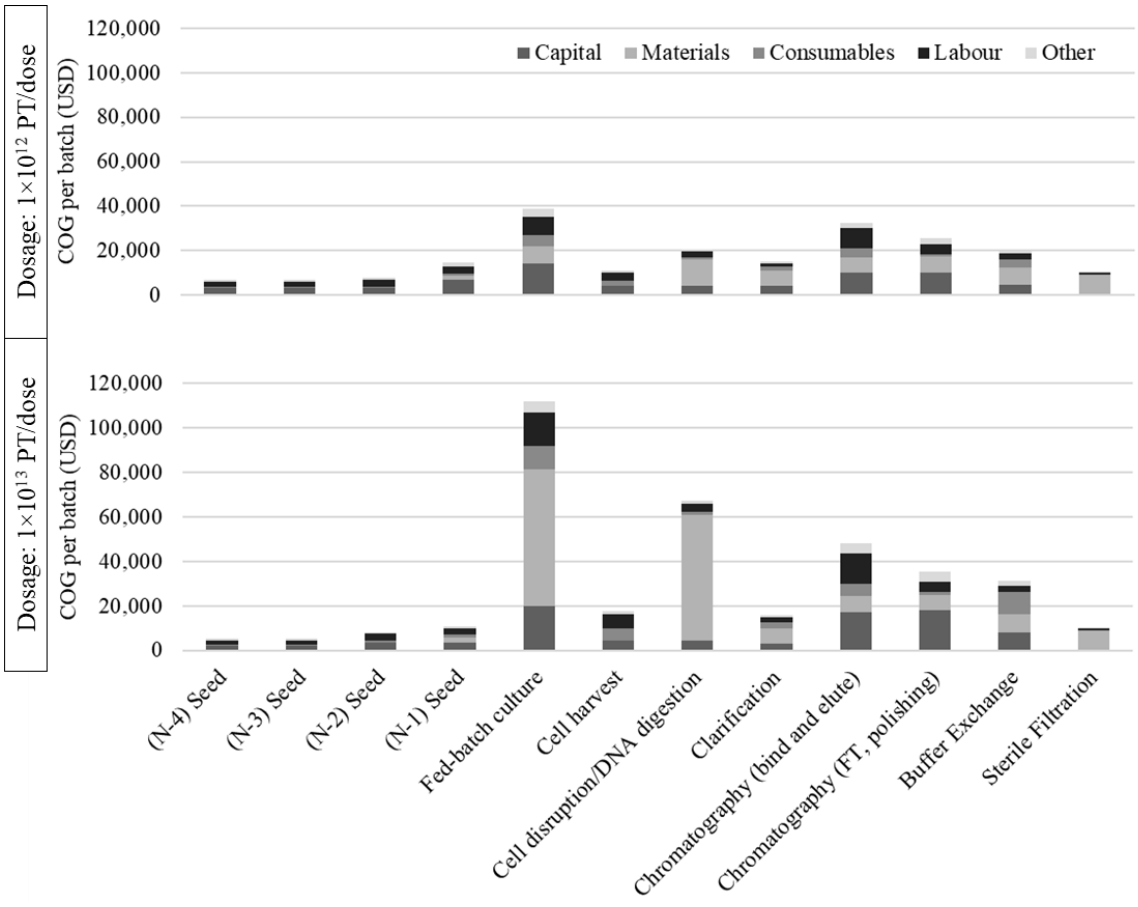

Figure E1. COG per batch breakdown for MA scenario assuming a dosage of 1×10^{12} PT/dose (top panel) and 1×10^{13} PT/dose (bottom panel) targeting the production of 2000 doses/year. The COG per batch is presented for all the unit operations indicated at the bottom for the different types of costs (capital, materials, consumables, labour, and other), indicated by the different colors.

Table E1. Technical specifications and costs of commercially available membrane chromatography devices

	Model	Type	Membrane Adsorber	Applications	Binding Capacities	Other Performance Metrics	Operating Time	Volume (mL) / Weight (g) / Price	Usage	CIP	Geometry‡
Pall	Mustang Q	AEX (Strong)	PES membrane 0.8 µm pores Quaternary and primary amine ligands	DNAs, viruses, HCP (-)	DNA: 30 mg/mL BSA: 70 mg/mL BSA: 56 mg/mL		10 CV/min	10, 60, 260, 520, 780 mL	Single-Use	1 M NaOH for one cycle (30 min)	Capsule: 16 pleated membrane layers
								5, 140, 5000 mL (187.2g, 768g, 10.3 kg)	Reusable (Q XT)		
	Mustang E	AEX (Weak)	PES membrane 0.2 µm pores Diethylamine ligands	Endotoxin removal from process streams	4×10^6 EU/mL Endotoxin			10, 40, 160, 320, 480 mL	Single-Use		Capsule: 3 pleated membrane layers
	Mustang S	CEX (Strong)	PES membrane 0.8 µm pores Sulfonic acid ligands	HCP (+)	Lysozyme: 47 mg/mL IgG: 60 mg/mL			10, 60, 260, 520, 780 mL	Single-Use		Capsule: 16 pleated membrane layers
Sartorius*	Sartobind Q†,††	AEX (Strong)	RC membrane > 3 µm pores Quaternary amine ligands	DNAs, viruses, HCP (-), Endotoxins	BSA: 29 mg/mL	DNA > 2 LRV Endotoxins > 2.8 LRV HCP: 1.9 LRV	4 mm Bed Height: 20 CV/min. 8 mm Bed Height: 5 CV/min	1 75 200 400 600 2,500 800* 10 400 760 1,300 1,900 16kg 4,900 296 1,162 3,497 6,604 8,557 25,653 6,054 *Cassette.	4 mm Bed Height: Flow Through	1 M NaOH for one cycle (30 min)	Capsule: Spiral-Wound or Cassette: Stacked Flat-Sheets
								3 150 400 800 1,200 5,000 1,600* 10 400 760 1,300 1,900 16kg 4,900 226 3,091 6,971 11,430 15,365 44,032 7,063 *Cassette.	8 mm Bed Height: Bind and Elute		
	Sartobind STIC PA†† (Salt Tolerant Interaction Chromatography)	AEX (Weak)	RC membrane > 3 µm pores Primary amine as ligand	DNAs, viruses, HCP (-)	BSA: 50 mg/mL in 150 mM NaCl BSA: 36 mg/mL in 200 mM NaCl DNA: 22 mg/mL	MMV Virus: > 4.96 LRV		1 75 200 400 600 2,500 800* 10 400 760 1,300 1,900 16kg 4,900 237 1,602 4,728 8,201 11,271 29,067 7,063 *Cassette.	4 mm Bed Height: Flow Through (Polishing) Single-Use	N/A	Capsule: Spiral-Wound or Cassette: Stacked Flat-Sheets
	Sartobind S	CEX (Strong)	RC membrane > 3 µm pores Sulfonic acid ligands	HCP (+)	Lysozyme: > 29 mg/mL			1 75 200 400 600 2,500 10 400 760 1,300 1,900 16kg 296 1,162 3,497 6,604 8,557 25,653	4 mm Bed Height: Flow Through	1 M NaOH for one cycle (30 min)	Capsule: Spiral-Wound or Cassette: Stacked Flat-Sheets
								3 150 400 800 1,200 5,000 1,600* 10 400 760 1,300 1,900 16kg 4,900 226 3,091 6,971 11,430 15,365 44,032 7,063 *Cassette.	8 mm Bed Height: Bind and Elute		

	Model	Type	Membrane Adsorber	Applications	Binding Capacities	Other Performance Metrics	Operating Time	Volume (mL) / Weight (g) / Price	Usage	CIP	Geometry‡
	Sartobind Phenyl	HIC	RC membrane > 3 µm pores Phenyl as ligands	Aggregates, HCP, viruses, endotoxins, lipids, leached ligands	IgG: 14.6 mg/mL (at 0.9 M $(NH_4)_2SO_4$)			3 | 150 | 400 | 800 | 1,200 | 5,000 | 1,600* 10 | 400 | 760 | 1,300 | 1,900 | 16kg | 4,900 247 | 2,981 | 6,971 | 11,430 | 15,365 | 44,032 | 9,656 *Cassette.	8 mm Bed Height: Bind and Elute	1 M NaOH for one hour.	Capsule: Spiral-Wound or Cassette: Stacked Flat-Sheets
Millipore Sigma**	Natrix HD Q	AEX (Strong)	Polyacrylamide hydrogel membrane 0.4 µm pores Quaternary amine ligands	DNAs, viruses, HCP (-)	BSA: > 200 mg/mL BSA: >300 mg/mL DNA: > 20 mg/mL	MMV & MLV Virus: approx. 5 LRV	5-25 CV/min	15 | 115 | 460 1090 | 2230 | 7930	Single-Use	30 mM NaOH, 1 M NaCl for 3 CV.	Capsule: Pleated Membrane with 0.5 mm Bed Height
Purilogics	Purexa D	AEX (Weak)	Diethylamine ligands	DNAs, viruses, HCP (-)	DNA: > 40 mg/mL			0.1 mL, 0.2 mL [18]			
Cytiva (Discontinued in April 2021)	ReadyToProcess Adsorber Q†††	AEX (Strong)	RC membrane > 3 µm pores Quaternary amine ligands	DNAs, viruses, HCP (-), Endotoxins	BSA: 29 mg/mL	DNA > 2 LRV Endotoxins > 2.8 LRV HCP: 1.9 LRV	4 mm Bed Height: 20 CV/min. 8 mm Bed Height: 5 CV/min	1 | 75 | 200 | 400 | 600 | 2,500 10 | 400 | 760 | 1,300 | 1,900 | 16kg 676 /4 251 /1 | 3,595 (/4) | 2,704 | 5,107 | 6,614 | 20,723* *USD 3 | 150 | 400 | 800 | 1,200 | 5,000 10 | 400 | 760 | 1,300 | 1,900 | 16kg 676 (/4) | 2,265 | 5,107 | 8,372 | 11,341 | 32,373* *USD	4 mm Bed Height: Flow Through 8 mm Bed Height: Bind and Elute	1 M NaOH for one cycle (30 min)	Capsule: Spiral-Wound
	ReadyToProcess Adsorber S†††	CEX (Strong)	RC membrane > 3 µm pores Sulfonic acid ligands	HCP (+)	Lysozyme: > 29 mg/mL			1 | 75 | 200 | 400 | 600 | 2,500 10 | 400 | 760 | 1,300 | 1,900 | 16kg 676 /4 251 /1 | 3,595 (/4) | 2,704 | 5,107 | 6,614 | 20,723* *USD 3 | 150 | 400 | 800 | 1,200 | 5,000 10 | 400 | 760 | 1,300 | 1,900 | 16kg 676 (/4) | 2,265 | 5,107 | 8,372 | 11,341 | 32,373* *USD	4 mm Bed Height: Flow Through 8 mm Bed Height: Bind and Elute	1 M NaOH for one cycle (30 min)	Capsule: Spiral-Wound
	ReadyToProcess Adsorber Phen†††	HIC	RC membrane > 3 µm pores Phenyl as ligands	Aggregates, HCP, viruses, endotoxins, lipids, leached ligands	IgG: 14.6 mg/mL (at 0.9 M $(NH_4)_2SO_4$)		5 CV/min	3 | 150 | 400 | 800 | 1,200 | 5,000 10 | 400 | 760 | 1,300 | 1,900 | 16kg	8 mm Bed Height: Bind and Elute, Flow Through	1 M NaOH for one hour.	Capsule: Spiral-Wound

*Note: An integrity test is performed by the diffusion test method with Sartocheck 4 Plus. *Note: Sartorius provided prices on March-19-2021. **MilliporeSigma compares the BSA and DNA binding performance (under varying salt conditions) of the Natrix Q AEX membrane to PES and RC AEX membranes in their application note. †Sartobind Q cassettes are available with validated sterility for aseptic products that cannot be sterile filtered, i.e. large viruses.††Sartobind Q and STIC PA are utilized to purify Adenovirus in bind-elute mode for initial virus capture and flow-through mode for polishing, respectively. Overall, DNA was reduced from 176 ng/dose to 1.2 ng/dose. Virus recovery was 75% and 81% for capture and polish, respectively.†††Sartobind membrane technology.

Table E2. OG per batch breakdown for MA scenario assuming dosage of 1×10^{12} PT/dose

Unit Operation	(N-4) Seed	(N-3) Seed	(N-2) Seed	(N-1) Seed	Fed-batch culture	Cell harvest	Disrup. DNA digest.	Clarification	Chrom (B&E)	Chrom (FT polish)	Buffer exch.	Sterile filtr.
						COG per batch (USD)						
Capital Charge	**3,971**	**3,971**	**4,016**	**4,016**	**16,991**	**5,955**	**5,243**	**7,044**	**5,693**	**5,424**	**1,507**	**102**
Materials	**105**	**106**	**112**	**1,762**	**5,058**	**0**	**9,525**	**6,600**	**7,049**	**7,048**	**6,948**	**8,958**
Media	0	1	7	34	1,947	0	0	0	0	0	0	0
Buffer	0	0	0	0	0	0	0	5	1	0	5	0
Direct RM	0	0	0	0	1,150	0	2,582	0	0	0	0	0
Bought WFI & PW	0	0	0	0	0	0	0	0	0	0	0	0
CIP	0	0	0	0	0	0	0	0	0	0	0	0
QC tests	105	105	105	1,729	1,961	0	6,943	6,595	7,048	7,048	6,943	8,958
Consumables	**146**	**146**	**150**	**162**	**4,567**	**1,883**	**912**	**2,094**	**634**	**645**	**722**	**25**
Resins/MA	0	0	0	0	0	0	0	0	226	237	0	0
Bags	136	136	136	136	4,382	1,698	912	1,675	408	408	137	1
Filters	0	0	0	0	185	185	0	419	0	0	585	24
Packages	0	0	0	0	0	0	0	0	0	0	0	0
Other	11	11	14	27	0	0	0	0	0	0	0	0
Labour	**2,494**	**2,494**	**3,244**	**3,244**	**8,393**	**3,651**	**2,540**	**1,485**	**5,650**	**3,332**	**3,004**	**1,036**
Process	1,105	1,105	1,437	1,437	3,719	1,618	1,126	658	2,504	1,476	1,331	459
Quality	969	969	1,260	1,260	3,260	1,418	987	577	2,195	1,294	1,167	403
Indirect	420	420	546	546	1,413	615	428	250	952	561	506	175
Other	**1,020**	**1,021**	**1,032**	**1,033**	**4,405**	**1,537**	**1,349**	**1,817**	**1,465**	**1,395**	**389**	**26**
Insurance/ other	230	230	232	232	983	344	303	407	329	314	87	6
Waste mgmt	0.54	0.54	0.54	0.54	1.22	1.01	0.38	1.13	1.88	1.87	1.14	0.31
Maintenance	199	199	201	201	850	298	262	352	285	271	75	5
Utilities	592	592	599	599	2,572	893	783	1,056	849	808	225	15
Total (USD/batch)	**7,737**	**7,738**	**8,553**	**10,217**	**39,413**	**13,026**	**19,570**	**19,040**	**20,491**	**17,843**	**12,569**	**10,147**
Total (USD/dose)	**135.6**	**135.7**	**150.0**	**179.1**	**691.0**	**228.4**	**343.1**	**333.8**	**359.2**	**312.8**	**220.3**	**177.9**

Table E3. COG per batch breakdown for MA scenario assuming dosage of 1×10^{13} PT/dose

Unit Operation	(N-4) Seed	(N-3) Seed	(N-2) Seed	(N-1) Seed	Fed-batch culture	Cell harvest	Disrup. DNA digest.	Clarification	Chrom (B&E)	Chrom (polish.)	Buffer exchan.	Sterile filtr.
						COG per batch (USD)						
Capital Charge	**2,422**	**2,481**	**3,848**	**3,850**	**21,513**	**5,847**	**5,868**	**3,579**	**13,936**	**12,232**	**3,745**	**70**
Materials	**107**	**118**	**171**	**2,058**	**32,256**	**4**	**32,203**	**6,642**	**7,070**	**7,050**	**6,988**	**8,958**
Media	3	13	66	329	19,046	0	0	0	0	0	0	0
Buffer	0	0	0	0	0	4	4	47	22	2	44	1
Direct RM	0	0	0	0	11,250	0	25,255	0	0	0	0	0
Bought WFI & PW	0	0	0	0	0	0	0	0	0	0	0	0
CIP	0	0	0	0	0	0	0	0	0	0	0	0
QC tests	105	105	105	1,729	1,961	0	6,943	6,595	7,048	7,048	6,943	8,958
Consumables	**147**	**154**	**809**	**958**	**8,096**	**3,598**	**1,025**	**2,163**	**3,070**	**2,010**	**2,156**	**131**
Resins/MA	0	0	0	0	0	0	0	0	773	1,602	0	0
Bags	136	136	765	778	6,466	1,968	1,025	1,744	2,297	408	766	1
Filters	0	0	0	0	1,630	1,630	0	419	0	0	1,390	130
Packages	0	0	0	0	0	0	0	0	0	0	0	0
Other	12	18	43	181	0	0	0	0	0	0	0	0
Labour	**2,425**	**2,425**	**3,171**	**3,171**	**16,365**	**7,224**	**4,304**	**2,506**	**4,859**	**3,224**	**2,832**	**1,001**
Process	1,035	1,035	1,353	1,353	6,984	3,083	1,837	1,069	2,074	1,376	1,209	427
Quality	997	997	1,304	1,304	6,728	2,970	1,769	1,030	1,998	1,326	1,164	411
Indirect	393	393	514	514	2,654	1,171	698	406	788	523	459	162
Other	**619**	**634**	**983**	**984**	**5,557**	**1,502**	**1,501**	**918**	**3,561**	**3,125**	**958**	**18**
Insurance/ other	136	140	216	217	1,210	329	330	201	784	688	211	4
Waste mgmt	0.54	0.54	0.57	0.60	2.31	1.26	0.38	1.14	2.03	1.93	1.17	0.37
Maintenance	121	124	192	192	1,076	292	293	179	697	612	187	4
Utilities	361	370	574	575	3,269	880	878	536	2,078	1,823	559	11
Total (USD/batch)	**5,720**	**5,812**	**8,982**	**11,022**	**83,788**	**18,176**	**44,901**	**15,809**	**32,496**	**27,641**	**16,679**	**10,179**
Total (USD/dose)	**102.5**	**104.1**	**161.0**	**197.5**	**1501.5**	**325.7**	**804.7**	**283.3**	**582.3**	**495.4**	**298.9**	**182.4**

Table E4. COG per batch breakdown for resin scenario assuming dosage of 1×10^{12} PT/dose

Unit Operation	(N-4) Seed	(N-3) Seed	(N-2) Seed	(N-1) Seed	Fed-batch culture	Cell harvest	Disrup. DNA digest.	Clarification	Chrom (B&E)	Chrom (polish.)	Buffer exchan.	Sterile filtr.
						COG per batch (USD)						
Capital Charge	**3,250**	**3,250**	**3,329**	**7,078**	**14,002**	**4,184**	**4,178**	**4,285**	**9,916**	**10,185**	**4,820**	**83**
Materials	**105**	**107**	**118**	**1,795**	**8,020**	**1**	**11,995**	**6,605**	**7,077**	**7,070**	**7,377**	**8,958**
Media	1	3	13	66	3,809	0	0	0	0	0	0	0
Buffer	0	0	0	0	0	1	1	9	29	22	86	0
Direct RM	0	0	0	0	2,250	0	5,051	0	0	0	0	0
Bought WFI & PW	0	0	0	0	0	0	0	0	0	0	0	0
CIP	0	0	0	0	0	0	0	0	0	0	0	0
QC tests	105	105	105	1,729	1,961	0	6,943	6,595	7,048	7,048	7,291	8,958
Consumables	**146**	**147**	**154**	**809**	**4,875**	**2,079**	**932**	**2,107**	**4,014**	**959**	**3,869**	**25**
Resins/MA	0	0	0	0	0	0	0	0	15	49	0	0
Bags	136	136	136	765	4,507	1,711	932	1,688	3,999	910	779	1
Filters	0	0	0	0	368	368	0	419	0	0	3,090	24
Packages	0	0	0	0	0	0	0	0	0	0	0	0
Other	11	12	18	43	0	0	0	0	0	0	0	0
Labour	**2,398**	**2,398**	**3,119**	**3,137**	**8,198**	**3,609**	**2,443**	**1,056**	**9,040**	**4,817**	**2,635**	**994**
Process	983	983	1,279	1,286	3,362	1,480	1,002	433	3,707	1,975	1,080	408
Quality	1,041	1,041	1,354	1,362	3,559	1,567	1,060	458	3,924	2,091	1,144	432
Indirect	374	374	486	489	1,277	562	381	164	1,409	751	411	155
Other	**834**	**834**	**854**	**1,815**	**3,623**	**1,078**	**1,073**	**1,103**	**2,549**	**2,616**	**1,243**	**22**
Insurance/ other	186	186	191	405	802	240	239	245	568	583	276	5
Waste mgmt	0.54	0.54	0.54	0.57	1.31	1.10	0.38	1.13	2.52	0.30	1.17	0.31
Maintenance	163	163	166	354	700	209	209	214	496	509	241	4
Utilities	484	484	496	1,055	2,120	628	624	642	1,483	1,523	725	12
Total (USD/batch)	**6,733**	**6,737**	**7,573**	**14,634**	**38,718**	**10,951**	**20,621**	**15,155**	**32,596**	**25,647**	**19,945**	**10,082**
Total (USD/dose)	**118.8**	**118.8**	**133.6**	**258.1**	**683.0**	**193.2**	**363.8**	**267.3**	**575.0**	**452.4**	**351.8**	**177.8**

Table E5. COG per batch breakdown for resin scenario assuming dosage of 1×10^{13} PT/dose

Unit Operation	(N-4) Seed	(N-3) Seed	(N-2) Seed	(N-1) Seed	Fed-batch culture	Cell harvest	Disrup. DNA digest.	Clarification	Chrom (B&E)	Chrom (polish.)	Buffer exchan.	Sterile filtr.
						COG per batch (USD)						
Capital Charge	**2,163**	**2,163**	**3,397**	**3,401**	**20,019**	**4,351**	**4,444**	**3,274**	**17,207**	**17,873**	**8,176**	**55**
Materials	**110**	**131**	**234**	**2,376**	**61,475**	**9**	**56,564**	**6,688**	**7,358**	**7,231**	**8,196**	**8,958**
Media	5	26	129	647	37,414	0	0	0	0	0	0	0
Buffer	0	0	0	0	0	9	9	93	311	183	905	1
Direct RM	0	0	0	0	22,100	0	49,613	0	0	0	0	0
Bought WFI & PW	0	0	0	0	0	0	0	0	0	0	0	0
CIP	0	0	0	0	0	0	0	0	0	0	0	0
QC tests	105	105	105	1,729	1,961	0	6,943	6,595	7,048	7,048	7,291	8,958
Consumables	**150**	**162**	**886**	**1,154**	**10,184**	**5,433**	**1,128**	**2,511**	**5,229**	**1,309**	**9,953**	**131**
Resins/MA	0	0	0	0	0	0	0	0	165	399	0	0
Bags	136	136	765	793	6,924	2,173	1,128	2,092	5,064	910	1,093	1
Filters	0	0	0	0	3,260	3,260	0	419	0	0	8,860	130
Packages	0	0	0	0	0	0	0	0	0	0	0	0
Other	14	27	120	361	0	0	0	0	0	0	0	0
Labour	**2,193**	**2,193**	**2,867**	**2,867**	**15,180**	**6,490**	**3,914**	**2,564**	**13,854**	**4,456**	**2,666**	**893**
Process	921	921	1,204	1,204	6,377	2,726	1,644	1,077	5,820	1,872	1,120	375
Quality	922	922	1,205	1,205	6,380	2,728	1,645	1,078	5,823	1,873	1,121	375
Indirect	350	350	458	458	2,423	1,036	625	409	2,211	711	426	142
Other	**551**	**552**	**866**	**868**	**5,179**	**1,120**	**1,136**	**838**	**4,398**	**4,564**	**2,095**	**15**
Insurance/ other	120	120	189	189	1,115	242	248	182	958	996	455	3
Waste mgmt	0.54	0.54	0.58	0.65	3.21	1.59	0.51	1.28	3.01	0.38	1.53	0.37
Maintenance	108	108	170	170	1,001	218	222	164	860	894	409	3
Utilities	322	322	507	508	3,060	659	666	491	2,576	2,675	1,229	8
Total (USD/batch)	**5,166**	**5,200**	**8,250**	**10,666**	**112,037**	**17,403**	**67,185**	**15,875**	**48,046**	**35,433**	**31,087**	**10,052**
Total (USD/dose)	**92.8**	**93.4**	**148.2**	**191.6**	**2012.2**	**312.6**	**1206.7**	**285.1**	**862.9**	**636.4**	**558.3**	**180.5**

Table E6. COG/dose as a function of target throughput for MA and resin scenarios at the dosages of 1×10^{12} and 1×10^{13} PT/dose

Scenario	Target throughput (doses/year)	COG/dose (USD) assuming 1×10^{12} PT/dose	COG/dose (USD) assuming 1×10^{13} PT/dose
MA	500	11,732	15,733
	1000	6,052	8,693
	1500	4,318	6,196
	2000	3,267	5,039
	2500	2,742	4,324
	3000	2,447	3,819
	3500	2,095	3,454
	4000	1,847	3,179
	4500	1,718	2,978
	5000	1,573	2,817
Resin	500	12,473	18,220
	1000	6,719	10,677
	1500	4,816	8,114
	2000	3,694	6,581
	2500	3,238	6,067
	3000	2,734	5,479
	3500	2,380	5,073
	4000	2,155	4,697
	4500	1,940	4,423
	5000	1,822	4,472

Table E7. Sensitivity analysis results for the MA scenario targeting the production of 2,000 doses/year

Parameter	Input parameter values			COG/dose (USD) – MA scenario, 1×10^{12} PT/dose			COG/dose (USD) – MA scenario, 1×10^{13} PT/dose		
	Worst-case	**Base-scenario**	**Best-case**	**Base-scenario**	**Worst-case**	**Best-case**	**Base-scenario**	**Worst-case**	**Best-case**
Titer in bioreactor (PT/L)	9.0×10^{12} PT/L	1.0×10^{13} PT/L	1.1×10^{12} PT/L	$ 3,266.82	$ 3,568.37	$ 3,162.15	$ 5,039.37	$ 5,168.29	$ 4,998.62
Capacity utilization of the plant	72%	80%	88%		$ 3,231.16	$ 3,392.72		$ 4,842.93	$ 5,259.08
Virus yield in the cell disruption/DNA digestion step	54%	60%	66%		$ 3,348.35	$ 3,243.98		$ 5,168.29	$ 4,998.62
Virus yield in the chromatography bind and elute step	63% (MA) 36% (Resin)	70% (MA) 40% (Resin)	77% (MA) 44% (Resin)		$ 3,513.49	$ 3,243.98		$ 5,168.29	$ 4,998.62
QC cost (USD/batch)	52,293	47,539	42,785		$ 3,350.17	$ 3,183.48		$ 5,124.56	$ 4,954.17
Benzonase cost (USD/kU)	4.66	3.73	2.80		$ 3,278.10	$ 3,255.54		$ 5,152.17	$ 4,926.57
Culture media cost (USD/kg)	2,834	2,267	1,700		$ 3,275.25	$ 3,258.40		$ 5,123.59	$ 4,955.15
Virus seed stock cost (USD/10^{12} PT)	6,250	5,000	3,750		$ 3,271.86	$ 3,261.78		$ 5,089.77	$ 4,988.97

Table E8. Sensitivity analysis results for the resin scenario targeting the production of 2,000 doses/year

Parameter	Input parameter values			COG/dose (USD) – Resin scenario, 1×10^{12} PT/dose			COG/dose (USD) – Resin scenario, 1×10^{13} PT/dose		
	Worst-case	Base-scenario	Best-case	Base-scenario	Worst-case	Best-case	Base-scenario	Worst-case	Best-case
Titer in bioreactor (PT/L)	9.0×10^{12} PT/L	1.0×10^{13} PT/L	1.1×10^{12} PT/L	$ 3,693.82	$ 3,715.80	$ 3,772.78	$ 6,580.54	$ 6,802.46	$ 6,408.65
Capacity utilization of the plant	72%	80%	88%		$ 3,543.75	$ 3,946.99		$ 6,348.92	$ 6,935.74
Virus yield in the cell disruption/DNA digestion step	54%	60%	66%		$ 3,715.80	$ 3,772.78		$ 6,802.46	$ 6,408.65
Virus yield in the chromatography bind and elute step	63% (MA) 36% (Resin)	70% (MA) 40% (Resin)	77% (MA) 44% (Resin)		$ 3,715.80	$ 3,772.78		$ 6,802.46	$ 6,408.65
QC cost (USD/batch)	52,293	47,539	42,785		$ 3,778.30	$ 3,609.35		$ 6,666.54	$ 6,494.53
Benzonase cost (USD/kU)	4.66	3.73	2.80		$ 3,716.03	$ 3,671.61		$ 6,802.61	$ 6,358.46
Culture media cost (USD/kg)	2,834	2,267	1,700		$ 3,710.40	$ 3,677.24		$ 6,746.34	$ 6,414.73
Virus seed stock cost (USD/10^{12} PT)	6,250	5,000	3,750		$ 3,703.74	$ 3,683.90		$ 6,679.77	$ 6,481.31

Appendix F: Standard operating procedure (SOP) for determining DNA fragment size via qPCR assay

Materials

DNA Cleaning and Concentration

- Genomic DNA Clean & Concentrator®-25 kit

qPCR Reactions

- Forward Primer 123 bp Amplicon: 5'-GCAATTATTCCCCATGAACG -3'
- Forward Primer for 254 bp Amplicon: 5'-AACAGGTCTGTGATGCCCTT-3'
- Reverse Primer for both amplicons - 5'-GGCCTCACTAAACCATCCAA-3'
- FAM-TAMRA probe - 5'-AAGTCCCTGCCCTTTGTACACACCG-3
- TaqMan Fast Advanced Master Mix (Applied Biosystems 4444556)
- TaqMan Control Genomic DNA (Human) – 10 ng/µL (Applied Biosystems 4312660)

Equipment and consumables

- Applied Biosystems StepOne™ Real-time PCR System
- qPCR reaction plate (Applied Biosystems catalogue #4346907)
- Cover for reaction plate (Applied Biosystems catalogue #436095

DNA sample preparation

1. Prepare the DNA samples using the Genomic DNA Clean & Concentrator®-25 to concentrate 60 µl of digested sample to 35 µl of samples following the kit's instructions

a. Mix 60 µL of sample with 300 µL of binding buffer

b. Load the DCC column and centrifuge at 10,000×g for 30 s

c. Add 400 µL of wash buffer and centrifuge at 10000×g for 1 min

d. Add 400 µL of wash buffer and centrifuge at 10000×g for 2 min

e. Add 35 µL of hot TE or elution buffer, let sit for 5 min and centrifuge at 10000×g for 30 s

f. Re-load the elute onto the column to improve DNA recovery, and centrifuge at 10000×g for 30 s

Note: TE or elution buffer should be warmed to >70 °C to help with the eluting of the DNA

Primer Preparation

1. Using the dry supply or primers, add nuclease-free ultrapure water to make a solution with 100,000 nM of primer

- i.e. for the 10,000 pmol dry primers, add 100 µL of ultrapure water
- Vortex well for mixing and briefly centrifuge the tube for 30 s so all the liquid stays at the bottom

Template DNA serial dilution for calibration curve preparation

A serial dilution must be performed on the template DNA (human genomic DNA standard) prepared in ultrapure water for the calibration curve. 5 dilutions must be carried out as well as a negative control of only nuclease free water. Dilutions: 50 ng/PCR reaction, 5 ng/PCR reaction, 0.5 ng/PCR reaction, 0.05 ng/PCR reaction, 0.005 ng/PCR reaction. Additionally, negative controls should be included (i.e. 0 ng/PCR reaction).

Preparation of samples of unknown concentration

If desirable, the samples to be analyzed should be diluted in ultrapure water. The dilution factor should later be accounted for when determining the concentrations based on the calibration curve.

Preparation of reaction plates for the qPCR run

1. Add 5 µL of the samples to each well (calibration curve, negative controls, and samples of unknown composition)
2. In a separate tube, prepare the reaction mixture using the following proportions for each reaction well:
    a. 0.1 µL of Forward Primer (final concentration: 500 nM)
    b. 0.1 µL of Reverse Primer (final concentration: 500 nM)
    c. 0.04 µL of FAM-TAMRA probe (final concentration: 0.2 µM)
    d. 10 µL TaqMan Fast Advanced Master Mix (final concentration: 1×)
    e. 4.76 µL of ultrapure water
3. Gently vortex the mixture (avoid foaming)

4. Add 15 µL of the mixture to each well – the final volume will be 20 µL
5. Cover the reaction plate with the film – make sure all wells are sealed to avoid evaporation
6. Briefly centrifuge the plate (750 rpm, 30 s) to ensure all liquid is at the bottom of the wells

Note: This procedure should be performed twice: once with the Forward Primer for 123 bp amplicons and once for the Forward Primer for 254 bp amplicons.

qPCR Cycle Parameters

1. In the qPCR machine, select the general settings according to the experiment
    a. Reporter: FAM
    b. Quencher: TAMRA
    c. Master Mix: Fast advanced
2. Define the cycle parameters (as per Andre, et al. 2016):
    a. Initial enzyme activation at 95°C for 10 min
    b. 45 cycles of:
        i. 95°C for 10 s
        ii. 60°C for 30 s
        iii. 72°C for 10 s – Fluorescence signal acquisition after this 72°C extension phase, for each cycle
    c. Cooling step at 40°C for 30 s

Data Analysis

1. For each primer, generate a calibration curve by plotting CT as a function of the log of the amount of DNA. Use the slope and intercept of this linear curve to obtain the DNA concentration in the unknown samples – remember to consider the sample dilution factor

2. Calculate the ratio 254/123 bp by diving the amount of DNA obtained based on the 254 bp amplicon by the amount of DNA obtained based on the 123 bp amplicon

References

1. André, M., Reghin, S., Boussard, E., Lempereur, L. & Maisonneuve, S. Universal real-time PCR assay for quantitation and size evaluation of residual cell DNA in human viral vaccines. Biologicals 44, 139–149 (2016).

2. Zymo Research - Genomic DNA Clean & Concentrator®-25 https://files.zymoresearch.com/protocols/_d4064_d4065_genomic_dna_clean_concentrator-25.pdf

1. Applied Biosystems StepOne™ Real-time PCR System - https://www.thermofisher.com/order/catalog/product/4376600